Higher order corrections to Semi-Inclusive Hadron Production Processes

Dissertation
der Mathematisch-Naturwissenschaftlichen Fakultät
der Eberhard Karls Universität Tübingen
zur Erlangung des Grades eines
Doktors der Naturwissenschaften
(Dr. rer. nat.)

vorgelegt von
Daniele Paolo Anderle
aus Trient, Italien

Tübingen 2017

Gedruckt mit Genehmigung der Mathematisch-Naturwissenschaftlichen Fakultät der Eberhard Karls Universität Tübingen.

Tag der mündlichen Qualifikation:	03.08.2017
Dekan:	Prof. Dr. Wolfgang Rosenstiel
1. Berichterstatter:	Prof. Dr. Werner Vogelsang
2. Berichterstatter:	Prof. Dr. Thomas Gutsche

Hiermit versichere ich, dass ich die vorliegende Arbeit selbstständig verfasst und keine anderen als die angegebenen Quellen und Hilfsmittel verwendet habe.

Tübingen
1. Juli 2017

.....
Daniele Paolo Anderle

A mamma e papà

Diese Arbeit auf einer Seite

Auf den folgenden Seiten werde ich die wichtigsten Ergebnisse meiner Promotionsforschung vorstellen. Der Schwerpunkt meiner Arbeit liegt auf der Verbesserung der Präzision für Berechnungen, die für das Verständnis der Struktur von Hadronen relevant sind. In den veröffentlichten Arbeiten, die in dieser Promotionsarbeit vorgestellt werden, haben wir vor allem Prozesse mit identifizierten Hadronen im Endzustand betrachtet. Unsere Studien beruhen auf dem bewährten Rahmen der perturbativen Quantenchromodynamik (pQCD) und sind daher relevant für die Beschreibung von hochenergetischen Experimenten von Teilchen die der starke Wechselwirkung unterliegen.

In diesem Rahmen stellen Faktorisierungstheoreme sicher, dass in Prozessen mit Hadronen der niederenergetische (nicht-perturbative) Anteil und der hochenergetische (perturbative) Anteil der Wechselwirkung zwischen den Teilchen in der theoretischen Beschreibung formal getrennt werden können. Der erste Teil kann durch universelle, nicht-perturbative Funktionen beschrieben werden, die in globalen Analysen von Daten extrahiert werden, während der zweite grundsätzlich (analytisch) mit perturbativen Techniken berechnet werden kann. Daher ist die Anwendbarkeit dieser Herangehensweise stark mit der Präzision sowohl des perturbativen als auch des nicht-perturbativen Anteils verbunden. Die Verbesserung der Genauigkeit verursacht auf der einen Seite eine bessere Beschreibung von Wirkungsquerschnitten in bereits untersuchten kinematischen Regionen des Phasenraums, während auf der anderen Seite eine verbesserte Vorhersagekraft in extremen kinematischen Bereichen erreicht werden kann, in denen die Präzision bisheriger Rechnungen nicht ausreichend ist.

Aufgrund der perturbativen Herangehensweise, liegt eine Möglichkeit die theoretische Berechnung zu verbessern darin höhere Beiträge der perturbativen Entwicklung mit einzubeziehen.

Dies ist zum Beispiel unser Ansatz, um die Präzision der Fragmentationsfunktionen zu verbessern. Sie beschreiben die Fragmentation eines hochenergetischen Teilchens in ein beobachtetes Hadron und wurden zuvor über eine globale Analysen extrahiert, die bislang bis zu einer “next-to leading order” Genauigkeit durchgeführt wurden. Wir haben “next-to-next-to leading order” Korrekturen für die Elektron-Positron-Annihilation mit einbezogen und eine erste Analyse von Fragmentationsfunktionen für diese Genauigkeit durchgeführt.
In einer anderen Studie haben wir eine erste Berechnung der neuen Beiträge zur longitudinalen Strukturfunktion der semi-inklusiven tief inelastischen Streuung durchgeführt. Diese Beiträge kommen zum ersten Mal in der “next-to-next-to leading order” der Störungsreihe vor und wurden als ersten Schritt zu einer vollständigen Berechnung für diesen Prozess bei dieser Genauigkeit berechnet.
Eine andere Strategie, um die Präzision der perturbativen Berechnungen voranzutreiben, ist die Anwendung von Resummations Techniken. Wiederkehrende Strukturen in der Störungsreihe, die mit bestimmten kinematischen Konfigurationen verknüpft sind, können zu allen Ordnungen "wieder aufsummiert"werden. Wir haben zwei verschiedene Arten von Resummationen betrachtet. Auf der einen Seite haben wir die Effekte von small-z Resummation in unseren bereits erwähnten Fragmentationsfunktionen berücksichtigt. Sie beeinflussen den kinematischen Bereich von extrem kleinen Impulsbruchteilen z. Das heisst, dass das beobachtete Hadron nur einen kleinen Bruchteil des Impulses des fragmentierenden Teilchens hat. Auf der anderen Seite haben wir für die polarisierte semi-inklusive tief inelastische Streuung “threshold Resummation” berechnet. Diese Art der Resummation betrifft die sogenannten threshold” Logarithmen, die mit der Abstrahlung von weichen Gluonen verbunden sind. In einer weiteren Arbeit haben wir auch das Zusammenspiel zwischen threshold Resummationünd Korrekturen aufgrund der Massen von Hadronen analysiert. Es ist in der Tat eine gute Annäherung für die meisten Prozesse, Hadronen als masselose Teilchen zu betrachten, da die Energien, bei denen Experimente durchgeführt werden, meist gross genug sind. Es gibt jedoch Fälle, in denen diese Näherung nicht ausreichend ist um eine gute Beschreibung der Daten zu bekommen. Wenn man die Masse der Hadronen in Prozessen mit beruücksichtigt, wie z. B. für Elektron-Positron-Annihilation oder tief inelastische Streuung, muss man auch den möglichen Einfluss von verschiedenen Korrekturen betrachten, die dieselbe Kinematik beeinflussen. Dies haben wir am Beispiel tief inelastischer Prozesse beobachtet, wenn man gleichzeitig threshold Resummationäls auch Hadronen Massen Effekte berücksichtigt.

The Thesis in one page

In the following pages I am going to present the main results of my PhD research activity. The main focus of my work has been directed towards the improvement of the precision in calculations relevant for understanding the structure of hadrons. More specifically, in the published papers presented in this thesis, we have mainly considered processes with identified hadrons in the final state. Our studies rely on the well established framework of perturbative Quantum Chromodynamics (pQCD) and, as such, are of interest for the description of high energy experiments involving particles interacting through means of the strong force.

In this framework, factorization theorems guarantee that in most processes involving hadrons the low energy (non-perturbative) part at which hadrons are observed and the high energy (perturbative) one where particles interact strongly with each others can be formally separated in their theoretical description. The first can be described by universal non perturbative functions which are extracted from fits of global data, whereas the second can be in principle calculated analytically with perturbative techniques. As it can be inferred, the applicability of this framework is strongly correlated to the precision of both the perturbative and the non-perturbative part. Extending their accuracy directly translates on one side into a better description of observables in the already studied kinematic regions of the phase space whereas on the other into an improved prediction power in the extreme kinematic regions where the reliability of the framework itself starts to be questionable at the previously given precision.

Due to the perturbative nature of the framework, a way of improving a theoretical calculation is to advance in the perturbative series and to include higher orders in the fixed order

expansion, where the expansion parameter considered is the strong coupling constant. This has been our approach, for example, in order to improve the precision of fragmentation functions. They describe the fragmentation of a particle into the observed final sate hadron and have been previously extracted via a global analysis performed at most up to a next-to-leading order accuracy. We have considered next-to-next-to-leading order corrections to the single-inclusive electron-positron annihilation and presented a first fit of fragmentation functions at this accuracy.

In another study, we have performed a first calculation of new contributions to the longitudinal structure function of the semi-inclusive deep inelastic scattering. They appear for the first time at next-to-next-leading order and were calculated as a first step toward a complete calculation for this process at this accuracy.

A different strategy to advance the precision of perturbative calculations is through the means of resummation techniques. Recurring structures in the perturbative series related with determined kinematical configurations can be "resummed" to all orders. We have considered two different type of resummations. On one side, we have studied the effects of small-z resummations in our already mentioned fragmentation functions' fit. They affect the extreme low momentum fraction z region, i.e. where the observed hadron carries a small fraction of the fragmenting particle momentum. On the other end, we have included "threshold resummation" in the description of the polarized semi-inclusive deep inelastic scattering. This type of resummation addresses the so called "threshold logarithms" which are connected with the presence of soft gluon emissions. In a further work we have also studied the interplay between the corrections to the fixed order calculation coming from "threshold resummation" and a more kinematical type of corrections generated by the presence of a hadron mass. It is in fact a good approximation to consider hadrons as massless particles for most processes since the scales of energies at which experiments are carried out are usually big enough. There are however cases in which this approximation can not be considered trustworthy for a good description of data. When including the mass of the hadrons in processes such as single-inclusive electron-positron annihilation or deep inelastic scattering, one has to also carefully consider the possible entangled game between different type of corrections affecting the same kinematical regions. This is what we have observed, for example, in the high momentum fraction region for the deep inelastic process when considering both "threshold resummation" and hadron mass effects.

List of Notations

c.m.s. Center of Mass reference System . . . 22

DIS Deep Inelastic Process . . . 20

FF Fragmentation Function . . . 20

FFNS Fixed Flavor Number Scheme . . . 78

LL Leading Logarithm . . . 82

MLLA Modified Leading Logarithmic Approximation . . . 67

MS Minimal Subtraction scheme . . . 14

$\overline{\text{MS}}$ modified Minimal Subtraction scheme . . . 14

NLL Next-to-Leading Logarithm . . . 82

NNLL Next-to-Next-to-Leading Logarithm . . . 66

NNLO Next-to-Next-to-Leading Order . . . 63

NPIS Non-Perturbative Input Scheme . . . 78

NS Non Singlet . . . 71

PDF Parton Distribution Function 20

pPDF polarized Parton Distribution Function 156

pQCD Perturbative Quantum ChromoDynamics 12

QCD Quantum Chromodynimics 63

QED Quantum ElectroDynamics 69

S Singlet 71

SIA Single-Inclusive electron-positron Annihilation 64

SIDIS Semi-Inclusive Deep Inelastic Scattering 156

TMD Transverse Momentum Dependent 32

UV Ultra Violet 38

VFNS Variable Flavor Number Scheme 78

List of publications

Journal Papers

[J1] Daniele P. Anderle, Felix Ringer, and Werner Vogelsang. "QCD resummation for semi-inclusive hadron production processes". In: *Phys. Rev.* D87.3 (2013), p. 034014. DOI: 10.1103/PhysRevD.87.034014. arXiv: 1212.2099 [hep-ph].

[J2] Daniele P. Anderle, Felix Ringer, and Werner Vogelsang. "Threshold resummation for polarized (semi-)inclusive deep inelastic scattering". In: *Phys. Rev.* D87 (2013), p. 094021. DOI: 10.1103/PhysRevD.87.094021. arXiv: 1304.1373 [hep-ph].

[J3] Alberto Accardi, Daniele P. Anderle, and Felix Ringer. "Interplay of Threshold Resummation and Hadron Mass Corrections in Deep Inelastic Processes". In: *Phys. Rev.* D91.3 (2015), p. 034008. DOI: 10.1103/PhysRevD.91.034008. arXiv: 1411.3649 [hep-ph].

[J4] Daniele P. Anderle, Felix Ringer, and Marco Stratmann. "Fragmentation Functions at Next-to-Next-to-Leading Order Accuracy". In: *Phys. Rev.* D92.11 (2015), p. 114017. DOI: 10.1103/PhysRevD.92.114017. arXiv: 1510.05845 [hep-ph].

[J5] Daniele P. Anderle et al. "Fragmentation Functions Beyond Fixed Order Accuracy". In: *Phys. Rev.* D95.5 (2017), p. 054003. DOI: 10.1103/PhysRevD.95.054003. arXiv: 1611.03371 [hep-ph].

[J6] Daniele Anderle, Daniel de Florian, and Yamila Rotstein Habarnau. "Towards semi-inclusive deep inelastic scattering at next-to-next-to-leading order". In: *Phys. Rev.* D95.3 (2017), p. 034027. DOI: 10.1103/PhysRevD.95.034027. arXiv: 1612.01293 [hep-ph].

[J7] Daniele P. Anderle et al. "Using hadron-in-jet data in a global analysis of D^* fragmentation functions". In: *ArXiv* (2017). arXiv: 1706.09857 [hep-ph].

Conference Proceedings

[C1] Daniele P. Anderle, Felix Ringer, and Werner Vogelsang. "QCD resummation in hadron production". In: *Nuovo Cim.* C036.05 (2013), pp. 153–157. DOI: 10.1393/ncc/i2013-11596-0. arXiv: 1307.0701 [hep-ph].

[C2] Daniele Paolo Anderle et al. "Fragmentation Functions beyond Next-To-Leading Order". In: *PoS* DIS2016 (2016), p. 063.

[C3] Daniele Paolo Anderle et al. "Fragmentation functions at NNLO and their small-z logarithmic corrections". In: *Proceedings, Parton Radiation and Fragmentation from LHC to FCC-ee: CERN, Geneva, Switzerland, November 22-23, 2016.* 2017, pp. 37–43. URL: http://inspirehep.net/record/1512992/files/1512294_37-43.pdf.

Contents

CHAPTER 1

Theoretical Framework

In this first chapter we are going to outline the key concepts of perturbative Quantum ChromoDynamics (pQCD) relevant to the work presented throughout the rest of this thesis. The aim is to provide the reader with the basic aspects of the framework within which the results of the next chapters will be presented. We refrain here from discussing those matters which are not strictly connected to the subjects of interest of this thesis and rather refer to more comprehensive reviews such as [1] or [2] and references therin.
We introduce the theory of strong interaction by briefly remembering some historical milestones of its development and then move to the description of its modern lagrangian formulation. We discuss fundamental concepts of perturbative QCD such as asymptotic freedom, factorization and evolution, crucial to the theoretical description of measurable observables. We conclude by presenting the main aspects of two types of resummation technique which will be used in our analyses of chapters 2, 3 and 5.

1.1 QCD

The first mention of a possible existence of a strong force holding together the components of an atomic nucleus is attributed to J.Chadwick and E.S.Bieler in their article of 1921 [3]. The experiments they conducted on hydrogen nuclei scattered by alpha particle brought them

to conclude that a simple coulomb interaction was not able to explain the observed angular distribuion of the project H particles in the case of high energy striking alpha particles, but a new form of interaction had to be implied. This is the very reason for which this work is considered to be the first evidence of a strong nuclear force as a distinct force of nature. The same J.Chadwick is responsible for the discovery of the neutron a decade later in 1932. It appeared mandatory, then, to assume the existence of a new force binding neutrons and protons together in the nucleus: *the nuclear force* or *the strong force*. Since then, understanding the nature of this force has been a central problem in modern physics.
A first fundamental attempt to describe the strong force in a consistent field theory manner was made by a young japanese scientist, H.Yukawa, in 1935 [4]. He suggested that a new particle with "intermediate" mass about 200 times the mass of the electron, later on called *meson*, could be responsible for the interaction energy between nucleons. The very simple nature of this first theory followed the lines suggested by the simple mathematical structures of the well-known interactions at that time, namely the coulomb interaction and the gravitational force. From this point, it would have taken more than 30 years for the community to formulate the theory that we know today as QCD. The first experimental findings didn't help steering history in the right direction. In 1937 a particle with mass about the size of the one predicted by Yukawa was discovered in cosmic rays by two independent groups [5, 6]. It was wrongly interpreted as the searched "meson". Only much later it would have been understood that the observed particles were instead leptons (i.e. *muons*) [7]. Nonetheless, this gave rise to a zoology of meson theories which latest for about a decade until the first discovery in 1947 of the lightest muon, the *pion* [8, 9]. The two decades that followed were marked by a series of exciting discoveries made possible by the invention of bubble and spark chambers. Hundreds of new particles (i.e. *hadrons*) were observed and a consistent theory that could explain such spectrum was yet to be found. M.Gell-Mann believed that one could find a pattern in the variety of particles based on underling fundamental symmetries with a rigorous mathematical group structure. The concept of isospin symmetry was already formulated by W.Heisenberg in 1932 and dubbed by E.Wigner in 1937. A new quantum number called strangeness, which was observed to be conserved in strong interaction decays, was introduced by the same M.Gell-Mann and K.Nishijima indipendently [10, 11]. The so-called *eightfold way* classification introduced by M.Gell-Mann and Yuval Ne'eman in 1961 [12, 13] was the natural extension of those concepts. Here, the particles were organized in families of different spin-parity J^P and plotted according to their charge Q and strangeness S. See Fig.1.1. The great success of this classification came

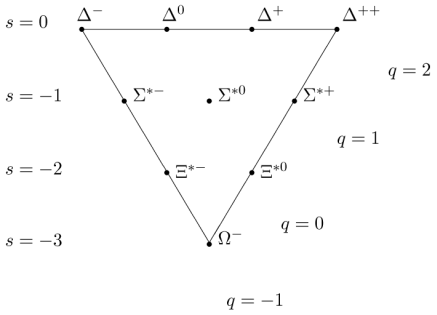

(a) Baryon-decuplet with $J^P = \frac{3}{2}^+$.

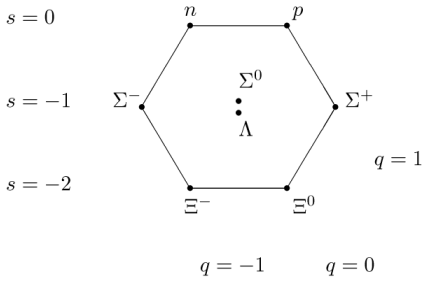

(b) Baryon-octet with $J^P = \frac{1}{2}^+$.

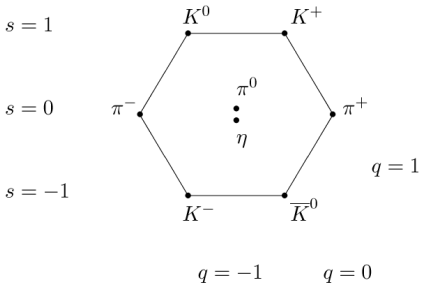

(c) Meson-octet with $J^P = 0^-$.

Figure 1.1: Eightfoldfold way diagrams for baryons $J^P = \frac{3}{2}^+$, baryons $\frac{1}{2}^+$ and mesons 0^-.

few months after its publication when the missing particle η needed to complete the pattern was discovered experimentally. Few years after, in 1964, M.Gell-Mann and G.Zweig showed independently how the large spectrum of hadrons and its classification could be understood in terms of symmetry property of more fundamental coupled $\frac{1}{2}$-spin particles called *quarks* [14–16]. In the so called *quark model* each hadron is a composite quantum state of either one quark and one anti-quark (*mesons*) or a composite quantum state of three quarks (*baryons*) and the binding between the quarks is provided by the strong force. To classify the hadrons it was necessary to assume the existence of three different quarks, each of which was identify by a new quantum number called *flavour*: up u, down d, strange s (according to the current SM it is believed that the correct number of flavours present in nature is six: up, down, strange, charm c, top t, bottom b). Moreover, it was necessary to assume that the strong force is invariant under interchange of flavours. Such assumption translates in mathematical terms by saying that the strong force has a flavour $SU(3)$ ($\equiv SU(3)_f$) symmetry. See Appendix A. The quarks lie in the fundamental representation of the $SU(3)_f$ group while the antiquarks in the corresponding

conjugate representation of it

$$q \to Uq \qquad q \equiv \begin{pmatrix} u \\ d \\ s \end{pmatrix}, \; U = \exp\left(i\frac{\lambda^a}{2}\theta^a\right) \in SU(3)_f. \tag{1.1}$$

The λ^a are the so-called Gell-Mann matrices whose explicit expression can be found in A.14. Mesons and baryons can then be classified according to the irreducible representation in which we can decompose the product between the representations of the constituting quarks. As shown in A.21 a meson can lie either in a singlet representation or in a octet representation. The corresponding mesons for the octet representation are shown in Fig.1.1c. In the same way, (see A.22) baryons can lie in a singlet representation, in two different octet representations or in a decuplet representation. Fig.1.1b and Fig.1.1a show the baryon-octet and the baryon-decuplet respectively.

The quark model soon appeared to be just a very useful periodic table of the hadrons rather than a consistent theory of the strong interaction. According to this model, some hadrons would turn out to follow the wrong statistic. The Δ^{++} baryon was discovered years before in 1951 by K.A.Brückner [17]. In its the fundamental state it is expected to have angular momentum $L = 0$. Since the third component of the total angular momentum is $J_3 = +\frac{3}{2}$, the three up quarks forming this baryon should have their spins all align in the same direction and no angular momentum component ($u^\uparrow u^\uparrow u^\uparrow$). The Δ^{++} state, therefore, would be a symmetric state, which means that this fermion would have to obey the wrong statistic. The problem was resolved independently by O.W.Greenberg [18] (1964) and M.Y.Han together with Y.Nambu [19] (1965), by assuming that the quarks have an extra quantum number called *color* and each quark state can present itself in a different color state q_α. At least at least three color quantum numbers are necessary in order to build an antisymmetric state for the $\Delta^{++} \sim \epsilon^{\alpha\beta\gamma} |u^\uparrow_\alpha u^\uparrow_\beta u^\uparrow_\gamma\rangle$. Furthermore, since no color charge and no free quark was ever observed, to avoid the existence of non-observed colored extra states, one has to postulate that all asymptotic states of the hadrons are colorless (or more precisely, singlet representations of the color symmetry transformation). This request is known as the *confinement hypothesis*, since it implies that quarks can present themselves only "confined" within colour-singlet bound states. Baryons and mesons can be

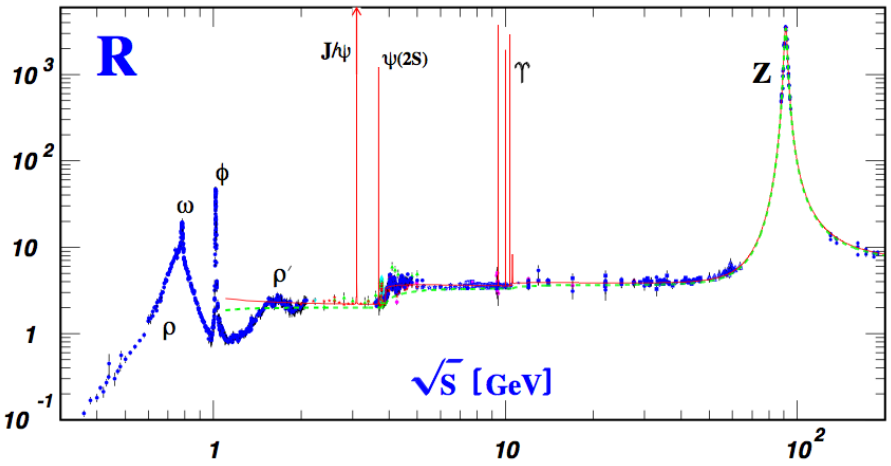

Figure 1.2: World data on the ratio $R_{e^+e^-}$. The broken lines show the simple quark model approximation with $N_C = 3$ while the solid curve is a perturbative QCD prediction [20].

then described as colour-singlet bound states as follows:

$$\text{Baryon} \equiv \frac{1}{\sqrt{6}}\epsilon^{\alpha\beta\gamma}\left|q_\alpha q_\beta q_\gamma\right\rangle, \qquad \text{Meson} \equiv \frac{1}{\sqrt{3}}\delta^{\alpha\beta}\left|q_\alpha \bar{q}_\beta\right\rangle. \tag{1.2}$$

The right number of colors N_C was found to be 3: red, green and blue. A strong experimental evidence of that comes from the measurement of the ratio

$$R_{e^+e^-} \equiv \frac{\sigma(e^+e^- \to \text{hadrons})}{\sigma(e^+e^- \to \mu^+\mu^-)} \approx N_C \sum_{f=1}^{N_f} Q_f^2 = \begin{cases} \frac{2}{3}N_C = 2, & (N_f = 3 : u, d, s) \\ \frac{10}{9}N_C = \frac{10}{3}, & (N_f = 4 : u, d, s, c) \\ \frac{11}{9}N_C = \frac{11}{3}, & (N_f = 5 : u, d, s, c, b) \end{cases} \tag{1.3}$$

where Q_f is the electric charge for a quark with flavour f. Ignoring the region around the Z peak and the low-energy region, the best choice for the number of colors which better agrees with the experimental data shown in Fig.1.2 is indeed $N_C = 3$.

The question whether or not the introduced quarks were just useful mathematical constructs instead of elementary particles describable by a proper quantum field theory lasted until the first observations in 1969 at SLAC, where deep inelastic scattering experiments showed point-like structures inside hadrons. The formulation of a quantum field theory for the strong interaction followed short after based on some key passages. The extension of gauge theories form abelian

groups to general compact, semi-simple Lie groups was done by C.N.Yang and R.Mills already in 1954 [21]. Thence, the modern approach of particle physics was to formulate a gauge field theory for the strong interaction that could be consistent with the below highlighted characteristics:

1. the strong force should be flavour-conserving and flavour-indepenent,
2. the colors should be the charge associated with the strong interaction and the quarks are color-charged particles,
3. $N_C = 3$ so that the quarks and antiquarks belong to the triplet representation $\underline{3}$ and $\underline{3}^*$ of the color symmetry group respectively,
4. quarks and antiquarks are different particles. Thus, $\underline{3} \neq \underline{3}^*$,
5. hadronic states should be colorless, hence color singlets (confinement hypothesis),
6. although we haven't discussed it yet, to complete the list of characteristics coming from empirical evidence, we have to mention that the coupling constant should be *asymptotic free*. See sections 1.2 and 1.2.2

The only possible compact Lie group surviving all requirements is the $SU(3)$. The $SO(3) \simeq SU(2)$, for example, has only a real triplet representation $\underline{3}$, that leads to the violation of point 4. Moreover, according to the already mentioned decomposition of $SU(3)$ representations' product (see A.21 and A.22), the only possible bound states of quarks that could origin colorless hadrons (point 5) are indeed the ones predicted by the quark model. In 1973, H.Fritzsch, H.Leutwyler and M.Gell-Mann [22] formulate the theory that we know today as Quantum Chromodynamcs. The same year D.Gross, F.Wilczek [23] and H.D.Politzer [24] discovered a crucial property of QCD: *the asymptotic freedom*, the property of the strong coupling to vanish at infinite energy scale. This key feature of QCD allowed for high precision predictions using perturbative methods at high energy experiments. The great success of perturbative QCD, earned D.Gross, F.Wilczek and H.D.Politzer the 2004 Nobel Price.

1.1.1 QCD Lagrangian

Following the discussion above, the modern theory for the strong interaction is a non-Abelian gauge theory with local symmetry being the $SU(3)_C$ color group. Proceeding in a similar way

to the QED, the QCD can be constructed starting from the free Dirac Lagrangian for quarks fields q_f^α with flavour $f(\in \{u, d, s, c, t, b\})$ and color α $(\in \{1, 2, 3\})$

$$\mathcal{L}_0 = \sum_f \bar{q}_f (i\gamma^\mu \partial_\mu - m_f) q_f. \tag{1.4}$$

The q_f are vectors defined as $q_f^T \equiv (q_f^1, q_f^2, q_f^3)$. 1.4 is invariant under global $SU(3)_C$ transformation

$$q_f^\alpha \to (q_f^\alpha)' = U^\alpha{}_\beta q_f^\beta, \qquad U = \exp\left\{-ig_s \frac{\lambda^a}{2}\theta_a\right\} \in SU(N) \tag{1.5}$$

where g_s is a factor taken out from the arbitrary parameters θ_a that will turn out to be the so-called *strong coupling constant*. The λ^a are the Gell-Mann matrices, the generators of the fundamental representation of $SU(3)_C$. According to the gauge principle, we require the $SU(3)_C$ symmetry to be *local*, $\theta_a = \theta_a(x)$. This yields a redefinition of the derivative into a new covariant object

$$D^\mu q_f \equiv [\partial^\mu - ig_s G^\mu(x)] q_f \tag{1.6}$$

where the matrix G^μ is defined by

$$[G^\mu(x)]_{\alpha\beta} \equiv \left(\frac{\lambda^a}{2}\right)_{\alpha\beta} G_a^\mu(x) \tag{1.7}$$

and the $G_a^\mu(x)$ are the gauge boson fields. In order to preserve the local gauge invariance of the Lagrangian, $D^\mu q_f$ has to transform in the same way as q_f. Therefore, the transformations rules for D^μ and G^μ become

$$\begin{aligned} D^\mu &\to (D^\mu)' = U D^\mu U^\dagger \\ G^\mu &\to (G^\mu)' = U G^\mu U^\dagger - \frac{i}{g_s}(\partial^\mu U) U^\dagger. \end{aligned} \tag{1.8}$$

The infinitesimal local transformations of the two fields are

$$q_f^\alpha \to (q_f^\alpha)' = q_f^\alpha - ig_s \left(\frac{\lambda^a}{2}\right)_{\alpha\beta} \delta\theta_a(x) q_f^\beta \tag{1.9}$$

$$G_a^\mu \to (G_a^\mu)' = G_a^\mu - \partial^\mu(\delta\theta_a(x)) + g_s f^{abc} \delta\theta_b(x) G_c^\mu. \tag{1.10}$$

The last term in equation 1.10 involves the gauge field itself. This is a general consequence of the non-commutativity of the $SU(N)_C$ matrices for $N > 2$. The f^{abc} are called *structure constants* and the fact that we can express the transformation of the gauge fields in terms of these constants implies that such fields belong to the *adjoint* representation of $SU(3)_C$. See Appendix A.

In analogy to what happens for the photon γ in QED, the local gauge invariance gives rise to 8 new boson gauge fields G^μ_a. In order for those to be propagating fields, hence to be able to describe physical particles, we have to add a gauge-invariant kinetic term for the G^μ_a to the free Lagrangian. We start by defining the corresponding field strength tensor

$$\begin{aligned} G^{\mu\nu}(x) &\equiv \frac{i}{g_s}[D^\mu, D^\nu] = \partial^\mu G^\nu - \partial^\nu G^\mu - ig_s[G^\mu, G^\nu] \equiv \frac{\lambda^a}{2} G^{\mu\nu}_a(x), \\ G^{\mu\nu}_a(x) &= \partial^\mu G^\nu_a - \partial^\nu G^\mu_a + g_s f^{abc} G^\mu_b G^\nu_c, \end{aligned} \tag{1.11}$$

which transforms

$$G^{\mu\nu} \to (G^{\mu\nu})' = U G^{\mu\nu} U^\dagger, \tag{1.12}$$

and we construct the corresponding Yang-Mills term

$$\mathcal{L}_{kinetic} \equiv -\frac{1}{2}\mathrm{tr}[G^{\mu\nu} G_{\mu\nu}] = -\frac{1}{4} G^{\mu\nu}_a G^a_{\mu\nu}. \tag{1.13}$$

The gauge fields describe massless spin 1 boson fields which, after quantization, will describe the so-called *gluons*. The total QCD Lagrangian is

$$\begin{aligned} \mathcal{L}_{QCD} =& \mathcal{L}_{kinetic} + \sum_f \bar{q}_f (i\gamma^\mu D_\mu - m_f) q_f \\ =& -\frac{1}{4}(\partial^\mu G^\nu_a - \partial^\nu G^\mu_a)(\partial_\mu G^a_\nu - \partial_\nu G^a_\mu) + \sum_f \bar{q}^\alpha_f (i\gamma^\mu \partial_\mu - m_f) q^\alpha_f \\ &+ g_s G^\mu_a \sum_f \bar{q}^\alpha_f \gamma_\mu \left(\frac{\lambda^a}{2}\right)_{\alpha\beta} q^\beta_f \\ &- \frac{g_s}{2} f^{abc} (\partial^\mu G^\nu_a - \partial^\nu G^\mu_a) G^b_\mu G^c_\nu - \frac{g_s^2}{4} f^{abc} f_{ade} G^\mu_b G^\nu_c G^d_\mu G^e_\nu. \end{aligned} \tag{1.14}$$

The second line of equation 1.14 contains the kinetic terms for the different fields, which will originate the two propagators of the quantized version of those fields; the third line describes the interaction between gauge and Dirac fields, which is proportional to the *strong coupling*

constants g_s; and the fourth line is responsible for the cubic and quadratic gluon self-interaction, which is also proportional to the same g_s. The presence of gauge field self-interacting terms is a common characteristic of non-Abelian gauge theories.
Although the classical formulation of the theory runs straight forward without many problems, the quantization procedure for non-Abelian theories in general encounters some technical issues. Due to the gauge invariance of the classical Lagrangian, physical observables cannot uniquely determine the gauge fields, leaving the latter subject to an infinite number of possible gauge choices. Applying quantization to the Lagrangian, however, requires the elimination of those unphysical degrees of freedom [25]. In order to overcome this issue, a gauge fixing term can be added directly to the Lagrangian. The covariant gauge $\partial_\mu G^\mu_a = 0$ is a common choice since it preserves the Lorentz invariance of the Lagrangian. The covariant-gauge fixing term for this specific case reads

$$\mathcal{L}_{GF} = -\frac{1}{2\xi}(\partial^\mu G^a_\mu)(\partial_\nu G^\nu_a) \tag{1.15}$$

where ξ sets the chosen gauge and is called the *gauge parameter*. Since physical observables are independent of the gauge choice, the value of ξ is arbitrary. One talks about Feymann gauge if $\xi = 1$, whereas the Landau gauge is commonly referred to for $\xi \to 0$. For QED, this procedure would be enough to assure that the resulting quantized fields do not contribute with unphysical degrees of freedom to scattering amplitudes. The condition $\partial_\mu A^\mu = 0$ on the photon, in fact, leaves a residual gauge invariance under transformation satisfying $\Box\psi = 0$ which guarantees the conservation of the electromagnetic current and, consequently, of the unitarity of scattering amplitudes. The same argument doesn't hold for non-Abelian theory where the non commutativity destroys the residual gauge invariance and the conservation of the current. The consequence is that the covariant scattering amplitudes calculated from the quantized Lagrangian $\mathcal{L}_{QCD}+\mathcal{L}_{GF}$ will take into account unphysical gluon contributions leading to violation of unitarity. A mathematical trick to solve this problem was given by L.D.Faddev and V.N.Popov in 1967 [26]: one can insert artificially into the theory *ghost* fields that cancel the unphysical degrees of freedom. The corresponding Lagrangian piece to add is

$$\mathcal{L}_{FP} = -\partial_\mu \bar{\Phi}_a D^\mu \Phi^a \tag{1.16}$$

where $\Phi^a, \bar{\Phi}^a$ is a set of anticommutating, massless, hermitian scalar fields and the covariant derivative is expressed in the adjoint representation

$$D^\mu \Phi^a \equiv \partial^\mu \Phi^a - g_s f^{abc} \Phi^b G_c^\mu. \tag{1.17}$$

The total QCD Lagrangian density in the covariant gauge takes the end form $\mathcal{L}_{QCD}+\mathcal{L}_{GF}+\mathcal{L}_{FP}$. The corresponding Feynman rules listed in Fig. 1.3 can be deduced from the resulting action defined as

$$S_{\mathrm{QCD}} \equiv i \int d^4x \mathcal{L}_{QCD} \tag{1.18}$$

Alternative choices of gauges more suitable for some specific applications can be found in the literature. Among non-covariant gauges, worth of mention are the Coulomb gauge and axial gauges. In particular, axial gauges, $n^\mu G_\mu^a = 0$, do not require the introduction of ghost fields. The gauge fixing term in this case reads

$$\mathcal{L}_{GF} = -\frac{1}{2\xi}(n^\mu G_\mu^a)^2 \,, \tag{1.19}$$

where n^μ is the so-called *gauge vector*. The case where the square of n^μ is taken to be positive, i.e. $n^2 > 0$, is called a *temporal gaguge*. When $n^2 = 0$ is called a *light-cone gauge*, whereas for $n^2 < 0$ we talk about a *pure axial gauge*. The drawback in this gauge is the resulting increased complexity of the gluon propagator, c.f. Fig. 1.3:

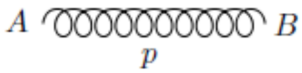

$$= \delta^{AB} \frac{-i}{p^2 + i\varepsilon} \left(g_{\mu\nu} - \frac{n_\mu p_\nu + n_\nu p_\mu}{n \cdot p} + \frac{(n^2 + \xi p^2) p_\mu p\nu}{(n \cdot p)^2} \right) \tag{1.20}$$

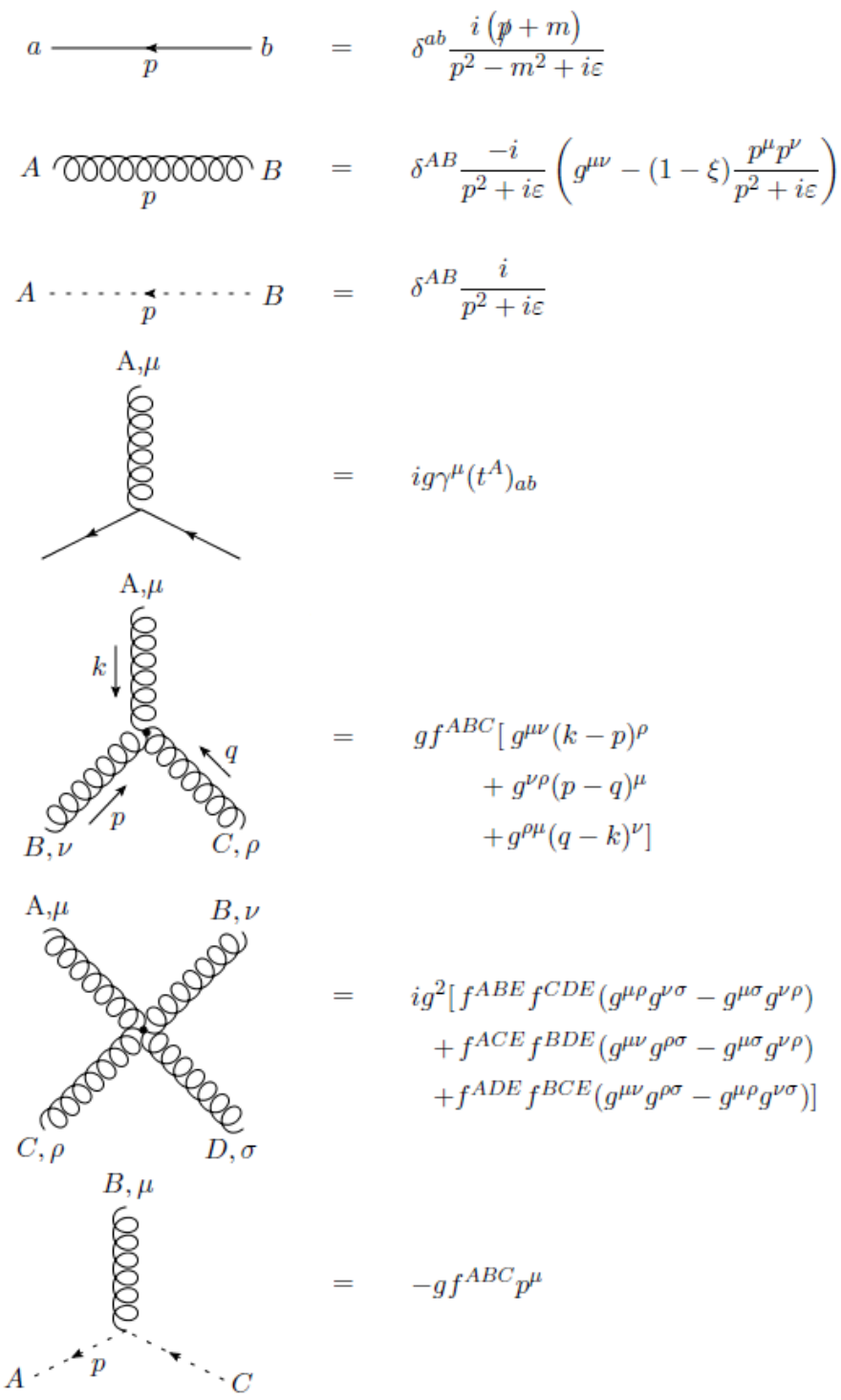

$$a \xrightarrow[p]{} b \quad = \quad \delta^{ab}\frac{i\left(\not{p}+m\right)}{p^2-m^2+i\varepsilon}$$

$$A \overset{p}{\sim\sim} B \quad = \quad \delta^{AB}\frac{-i}{p^2+i\varepsilon}\left(g^{\mu\nu}-(1-\xi)\frac{p^\mu p^\nu}{p^2+i\varepsilon}\right)$$

$$A \overset{p}{\cdots} B \quad = \quad \delta^{AB}\frac{i}{p^2+i\varepsilon}$$

$$= \quad ig\gamma^\mu(t^A)_{ab}$$

$$= \quad gf^{ABC}[\,g^{\mu\nu}(k-p)^\rho + g^{\nu\rho}(p-q)^\mu + g^{\rho\mu}(q-k)^\nu]$$

$$= \quad ig^2[\,f^{ABE}f^{CDE}(g^{\mu\rho}g^{\nu\sigma}-g^{\mu\sigma}g^{\nu\rho}) + f^{ACE}f^{BDE}(g^{\mu\nu}g^{\rho\sigma}-g^{\mu\sigma}g^{\nu\rho}) + f^{ADE}f^{BCE}(g^{\mu\nu}g^{\rho\sigma}-g^{\mu\rho}g^{\nu\sigma})]$$

$$= \quad -gf^{ABC}p^\mu$$

Figure 1.3: Feynman rules for QCD. The solid line indicates quarks, the curly gluons and the dashed ghosts [27].

1.2 Perturbative QCD

As for any theory in physics, the success of QCD is strictly connected with its ability to make phenomenological predictions for relevant observables. In this respect, under the name *perturbative* QCD (pQCD) we collect the practical instruments to calculate measurable quantities describing some process in which the strong interaction involved can be considered as a small perturbation. Crucial to any perturbative approach in field theory is the fact that, to be applied reliably, the coupling between fields has to be "small enough" at the energies involved in the described process. On the other end, the QCD coupling has to be "large enough" in order to be consistent with the *confinement* hypothesis, i.e. to be consistent with the lack of observations of free color charges in nature. As we will discuss in Sec. 1.2.1, the strong coupling constant exhibit a remarkable property called *asymptotic freedom*, which guarantees that the magnitude of the interaction decreases asymptotically to zero when the energy scale of the process increases to infinity. The affirmation of QCD in its early days was made possible by the fact that perturbative QCD turned out to be applicable at the energies accessible to experiments of that time and produced straight away satisfying descriptions of the data. A well-established framework able to describe more and more observables at high precision has developed since then. In the next sections of this chapter we are going to present key aspects of the pQCD framework making use of the deep inelastic process as an example. We focus on concepts such as *factorization* and *resummation* relevant for or discussion in the next chapters. For a more didactical treatment of the subject we refer to [1] and [2].

1.2.1 The Running of the Coupling Constant

Up until now, we have looked into the structure of the Lagrangian without properly justifying the validity of a perturbative approach to QCD. As we shall discuss in this section, the answer lies in the so-called *asymptotic freedom* of the strong coupling, i.e. in the behaviour of the strong interaction at high energy scales (or equivalently, at short distances). QCD is a quantum field theory and as such it naturally exhibit divergent integrals when calculating Green's functions with loops. This implicitly spoils our ability to identify parameters of the theory directly with physical observables. *Renormalization* is the systematic way of redefining the parameters in order to get rid of divergences and, hence, to be able to describe the physical world. As a remnant of this procedure on is left with a dependence of the parameters on a dimensionful arbitrary variable, the *renormalisation scale* μ_R. The last fact is referred in the literature as

the *running of the constants* and it can be used to inspect the quantum structure of a theory. In high energies processes the quarks can be treated as massless particles and the only remaining parameter in QCD is the coupling constant g_s. In analogy to the fine structure constant in QED, it is common to define

$$\alpha_s \equiv \frac{g_s^2}{4\pi}. \tag{1.21}$$

To renormalize the strong coupling constant one needs to proceed as usual choosing a *regularization scheme*, in order to isolate the divergences, and a *renormalization scheme*, that specifies which finite factors in addition to the divergent parts will be included in the redefinition of the constant. Among all possible regularization schemes, for the type of calculations presented in this thesis the normal choice is the *dimensional regularization* which is Lorentz and gauge invariant. Since it is a standard subject of every QFT course, we won't discuss the details of this technique. We want, however, to bring to attention the fact that each regularization scheme introduces itself an arbitrary *regularization scale* μ which, fortunately, cancels at some point of the calculations. In our case, for example, to be able to perform the dimensional regularization, hence to rewrite the divergent loop integrals in a different dimension $d = 4 - 2\epsilon$, where ϵ is an arbitrary small constant, we have to make sure that we work with dimensionless objects. Thus, to prevent the coupling constant from acquiring a dimension when $d \neq 4$, we have to introduce a regularization scale μ and define a dimensionless coupling constant $\alpha_s(\mu)$

$$\alpha_s = \alpha_s^{(d)} \mu^{-2\epsilon}. \tag{1.22}$$

The d symbol stands for "dimensionful". Once we have regularized the divergences, we end up with terms that can directly be absorbed in a redefinition of the coupling constant. For example, in a one-loop calculation those terms will manifest $1/\epsilon$ singularities. By redefining (i.e. renormalizing) the coupling constant at one-loop order as

$$\alpha_s(\mu_R^2) = \alpha_s + \beta_0 F(\epsilon) \left(\frac{\mu^2}{\mu_R^2} \right)^{\epsilon} \frac{1}{\epsilon} \alpha_s^2, \tag{1.23}$$

the ϵ poles produced by this expression exactly cancels those of the one-loop calculation. The arbitrary regularization scale μ will cancel at this point too. The renormalization scale μ_R had to be introduced here to keep the renormalized coupling constant $\alpha_s(\mu_R)$ dimensionless. β_0 is a constant that is defined in Eq.1.35. The arbitrary $F(\epsilon) = 1 + \mathcal{O}(\epsilon)$ defines the renormalization

scheme. For the so-called *minimal subtraction scheme* MS

$$F_{\mathrm{MS}}(\epsilon) = 1. \tag{1.24}$$

For the *modified minimal subtraction scheme* $\overline{\mathrm{MS}}$ the function F(ϵ) is defined as

$$F_{\overline{\mathrm{MS}}}(\epsilon) = \frac{(4\pi)^{\epsilon}}{\Gamma(1-\epsilon)} = 1 + (\ln 4\pi - \gamma_E)\epsilon + \mathcal{O}(\epsilon^2) \tag{1.25}$$

in order to get rid of some other constant terms coming from the analytical continuation of the angular integration of the one-loop integrals. Γ is the Euler gamma function and $\gamma_E \approx 0.577216$ is the Euler-Mascheroni constant.

We have explicitly kept track of the regularization scale μ for discussion purposes. It is however common to set $\mu = \mu_R$ from start when performing renormalization since, as we have seen, the dependence on μ drops out. The running of α_s is in fact a consequence of the renormalization scale independence of the renormalization process itself. The "bare" parameter g_s appearing in the Lagrangian 1.14 knows nothing about μ_R:

$$\frac{dg_s^{\mathrm{bare}}}{d\mu_R} = 0\ . \tag{1.26}$$

The running coupling is defined from the bare quantity g_s^{bare} through the renormalization constant Z_g as $g_s^{\mathrm{bare}} = \mu_R^{\epsilon} Z_g g_s$. Thus, from Eq. 1.26 and using definition 1.21 we obtain

$$\beta(\alpha_s) \equiv \mu_R^2 \frac{\partial \alpha_s(\mu_R^2)}{\partial \mu_R^2} = \frac{-\epsilon\alpha_s}{1 + 2\frac{\alpha_s}{Z_g}\frac{dZ_g}{d\alpha_s}}. \tag{1.27}$$

In the previous equation we used the fact that Z_g depends on the renormalization scale μ_R only via the presence of α_s. At one loop, for example,

$$Z_g = 1 - \frac{\beta_0}{2\epsilon}\alpha_s\ , \tag{1.28}$$

with the same β_0 defined in Eq.1.35. The introduced *beta function* $\beta(\alpha_s)$ contains all information regarding the behavior of the running coupling constant α_s and can be computed directly from the renormalization constant Z_g. Using Eq. 1.27 and expanding Eq. 1.27 in powers of α_s,

at one loop we obtain

$$\beta(\alpha_s) = -\beta_0 \alpha_s^2 + \mathcal{O}(\alpha_s^2, \epsilon) \tag{1.29}$$

As long as $\beta_0 > 0$, the magnitude of the coupling constant is predicted to diminish increasing μ_R. Hence, there should be some value of the renormalization scale above which the running coupling becomes smaller than 1. In this case, the above expansion is fully legitimate and we can solve the equation analytically in order to get the famous *running* of α_s:

$$\alpha_s(\mu_R^2) = \frac{1}{\beta_0 \ln(\mu_R^2/\Lambda_{QCD})}. \tag{1.30}$$

The parameter Λ_{QCD} is the boundary condition of the first order differential equation, and corresponds to the scale at which $\alpha_s \to \infty$.
So far, the running of the coupling has been introduced has a consequence of the renormalization procedure without any connection to the real physical world. Nonetheless, we shall see that the behaviour of the running coupling has to be such that physical observables are insensitive to the arbitrary choice of the artificial scale μ_R. In a more formal way, we would say that all physical observable should be invariant under transformations of the renormalization scale

$$\mu_R \to e^S \mu_R \,, \tag{1.31}$$

where S is a free parameter. These transformations form a group called the *renormalization group*. The requirement of invariance of a physical observable under such transformations translates itself in a set of differential equations called the *renormalization group equation*, one for each renormalized parameter in the theory. In our case the only renormalized constant is the coupling constant and the corresponding renormalization group equation for it can be easily derived. Let's take a dimensionless physical observable R like, for example, the ratio seen in Eq.1.3. Since R is dimensionless and we are neglecting the quark masses, it can be only a function of some set of dimensionless physical variables that we will denote collectively as x (angles, Bjorken variables and so on), the renormalized coupling constant $\alpha(\mu_R^2)$ and the ratio Q^2/μ_R^2 between the renormalization scale μ_R and, now, the physical scale Q^2 at which the observable is measured. In order for $R(x, Q^2/\mu_R^2, \alpha_s(\mu_R^2))$ to be independent from the choice of

μ_R the following differential equation has to be satisfied

$$\mu_R^2 \frac{\mathrm{d}}{\mathrm{d}\mu_R^2} R(x, {}^{Q^2}/_{\mu_R^2}, \alpha_s(\mu_R^2)) = 0 = \left[\mu_R^2 \frac{\partial}{\partial \mu_R^2} + \mu_R^2 \frac{\partial \alpha_s(\mu_R^2)}{\partial \mu_R^2} \frac{\partial}{\partial \alpha_s(\mu_R^2)}\right] R \equiv \left[\mu_R^2 \frac{\partial}{\partial \mu_R^2} + \beta(\alpha_s) \frac{\partial}{\partial \alpha_s(\mu_R^2)}\right] R. \tag{1.32}$$

If we set the renormalization scale equal to the physical scale, we obtain $R = R(x, 1, \alpha_s(Q^2))$, which is a solution of the above equation. This means that a physical solution of Eq.1.32 will manifest its Q-dependance only through the Q-dependence of the running coupling constant, i.e. only because of the renormalization we had to make of the latter.
The *beta function* explicitly appears in Eq. 1.32 connecting, de facto, the behaviour of α_s to the real physical world. Eq.1.27 is generally referred as the *renormalization group equation* for the running coupling since its solution describes how α_s must change under a transformation of the renormalization scale in order for R to remain invariant. From Eq.1.32 we obtain

$$\beta(\alpha_s) = -\frac{\mu_R^2 \frac{\partial R}{\partial \mu_R^2}}{\frac{\partial R}{\partial \alpha_s}}. \tag{1.33}$$

Let's suppose now that at some value of Q the coupling constant α_s becomes smaller than 1 and hence we are able to write R in a perturbative series with order parameter being α_s. As we have seen, this is a perfectly legitimate approach as long as $\beta_0 > 0$. Due to Eq.1.33 the beta function will be also perturbatively calculable. At present day the $\beta(\alpha_s)$ for the QCD is known up to four-loop accuracy [28]

$$\beta(\alpha_s) = -\alpha_s \sum_{n=0}^{\infty} \beta_n \left(\frac{\alpha_s}{4\pi}\right)^{n+1} = -\alpha_s^2(\beta_0 + \beta_1 \alpha_s + \beta_2 \alpha_s^2 + \beta_3 \alpha_s^3 + \ldots), \tag{1.34}$$

where in the $\overline{\mathrm{MS}}$ scheme

$$\begin{aligned} \beta_0 &= \frac{1}{4\pi}\left[11 - \frac{2}{3}N_f\right] \\ \beta_1 &= \frac{1}{(4\pi)^2}\left[102 - \frac{38}{3}N_f\right] \end{aligned} \tag{1.35}$$

$$\begin{aligned}\beta_2 =& \frac{1}{(4\pi)^3}\left[\frac{2857}{2} - \frac{5033}{18}N_f + \frac{325}{54}N_f^2\right] \\ \beta_3 =& \frac{1}{(4\pi)^4}\left[\left(\frac{149753}{6} + 3564\zeta_3\right) - \left(\frac{1078361}{162} + \frac{6508}{27}\zeta_3\right)N_f \right. \\ & \left. + \left(\frac{50065}{162} + \frac{6472}{81}\zeta_3\right)N_f^2 + \frac{1093}{729}N_f^3\right]\end{aligned}$$

and ζ_ν is the Riemann zeta-function, $\zeta_3 \approx 1.202057$. The N_f are the number of active flavours. If we observe the first coefficient of the expansion β_0, we note that it is a positive quantity. Therefore, according to Eq.1.34, unlike the $\beta(\alpha)$ for QED, in QCD $\beta(\alpha_s) < 0$. This change of sign in the beta function has a drastic consequence on the real physical world. Eq.1.27 obligates the running coupling constant α_s to decrease as the energy of the interaction increases, or equivalently as the distance of the interaction becomes shorter and shorter. This is what is called *the asymptotic freedom*. Although it is somewhat counterintuitive to think that an interaction builds stronger and stronger as we increase the distance between two particles, it is a consequence of the non-Abelian structure of the theory which produces self interaction terms between the gauge gluon fields (see Eq.1.14). As the scale gets smaller and smaller, the contributions of those terms will be more and more important. To have an intuitive vision of it, we could say that the quark will get surrounded by more and more charged gluons, building up from self interactions, as it moves apart from the other quarks. The color charge the quark experiences will grow rather than being screened from other quarks (as it happens in QED for the electrons). This "anti-screening" phenomenon is responsible for the asymptotic freedom. Since no free quarks are observed, a *confinement hypothesis* has to be assumed. There should be a breaking point where it is more likely for a quark to be in a hadronic state with other nearby quarks than to experience an enormous interaction with faraway quarks.
To better understand how the real world comes into play in the determination of α_s, let's solve Eq.1.27 this time by imposing a boundary condition on α_s at some physical reference scale μ_0, i.e. by solving

$$\ln\frac{Q^2}{\mu_0^2} = \int_{\alpha_s(\mu_0^2)}^{\alpha_s(Q^2)} \frac{\mathrm{d}\alpha}{\beta(\alpha)}. \tag{1.36}$$

At one-loop, the solution equivalent to Eq. 1.30 reads

$$\alpha_s(Q^2) = \frac{\alpha_s(\mu_0^2)}{1 + \beta_0\alpha_s(\mu_0^2)\ln(Q^2/\mu_0^2)} = \alpha_s(\mu_0^2)\sum_{n=0}^{\infty}\left(-\beta_0\alpha_s(\mu_0^2)\ln\frac{Q^2}{\mu_0^2}\right)^n. \tag{1.37}$$

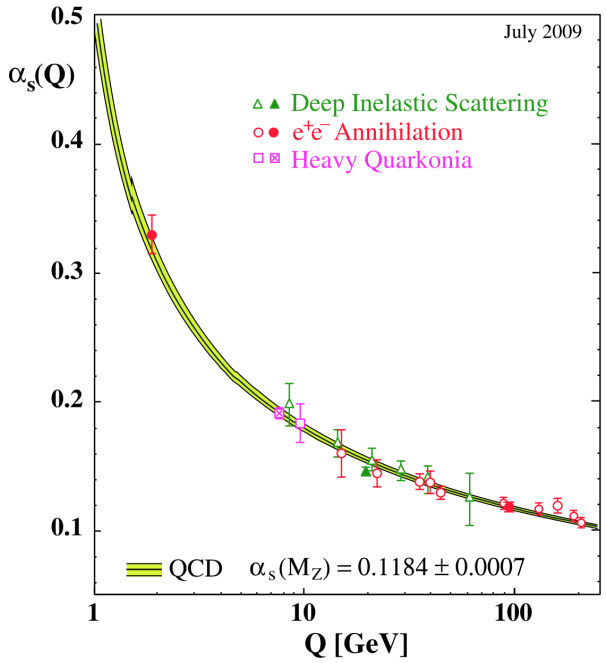

(a) Measurements of $\alpha_s(Q^2)$ as a function of the energy scale.

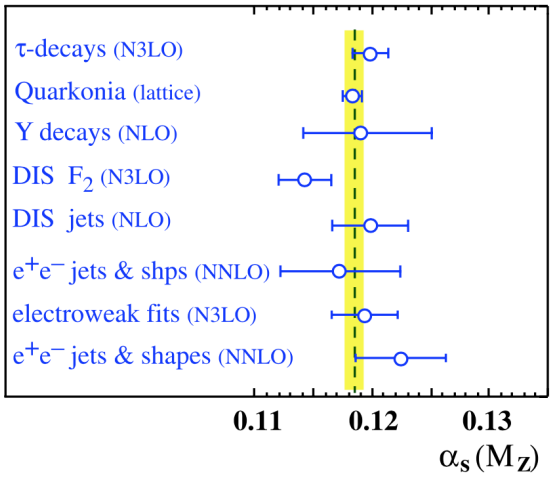

(b) Measurements of $\alpha_s(M_Z)$ at the scale M_Z. The vertical yellow stripe shows the 2009 word average $\alpha_s(M_Z) = 0.1184 \pm 0.0007$

Figure 1.4: Collection of world measurements of α_s. Pictures taken from [29].

The remarkable thing here is that the value of $\alpha_s(\mu_0^2)$ can be extracted from data. By convention μ_0 is chosen to be the mass scale of the Z boson (≈ 90GeV) and the $\overline{\text{MS}}$ scheme is taken to be the standard renormalization scheme. See [29] and Fig.1.4 for the 2009 word average of α_s. Comparing Eq. 1.37 and Eq. 1.30, the introduced renormalization group invariant Λ_{QCD} can be now interpreted in terms of the experimentally extracted parameter $\alpha_s(\mu_0^2)$:

$$\Lambda^2_{QCD} \equiv \mu_0^2 \exp\left[-\frac{1}{\beta_0}\frac{1}{\alpha_s(\mu_0^2)}\right]. \tag{1.38}$$

Moreover, Eq. 1.37 clearly shows how a change of scale induces a reorganization of the perturbative expansion of any observable. By solving the renormalization group equation for the strong coupling, one effectively *resumms* logarithms of the type $(\beta_0\alpha_s(\mu_0^2)\ln(Q^2/\mu_0^2))^n$. Including higher n-loop corrections proportional to β_n coefficients in the solution increases the accuracy of said resummation. However, beyond 1-loop, Eq. 1.36 yields no exact analytical

solution. The three loop solution, for example, can be only written implicitly through the expression

$$\alpha_s(Q^2) = \frac{\alpha_s(\mu_0^2)}{X}\left[1 - \frac{\beta_1}{\beta_0}\alpha_s(\mu_0^2)\frac{\log X}{X} + \alpha_s^2(\mu_0^2)\left(\frac{\beta_2}{\beta_0}\frac{1-X}{X^2} + \frac{\beta_1^2}{\beta_0^2}\frac{\log^2 X - \log X + X - 1}{X^2}\right)\right] \tag{1.39}$$

with

$$X = 1 + \beta_0\alpha_s(\mu_0^2)\log(Q^2/\mu_0^2) \tag{1.40}$$

As a last remark of this section, we want to point out the fact that despite the suitable behaviour of α_s at large scales, perturbation theory could still produce wrong results. A physical observable R might not be described uniquely by its series expansion $\sum_{n=0}^{\infty} R^{(n)}\alpha_s^n$, even for $\alpha_s \to 0$. The factorial growth of the perturbative coefficients $R^{(n)}$, and, hence, its $n!$-type divergence, may spoil the validity of the perturbative approach even if α_s is taken to be very small. A fundamental assumption within pQCD is, therefore, that the expansion in α_s is *asymptotic*. A series is asymptotic to a function $f(\alpha_s)$ if

$$\left| f - \sum_{n=0}^{N} f^{(n)}\alpha_s^n \right| \leq C_{N+1}\alpha_s^{N+1} \tag{1.41}$$

for all integer N when $\alpha_s \to 0$. Thus, the best approximation of an observable $R(\alpha_s)$ may be achieved truncating the series at the Nth order for which C_{N+1} is the smallest. In practice, only few orders in the perturbative expansion are shown to be necessary for the description of most of the studied high energy reaction in colliders and fixed target experiments. This ceases to be true for specific kinematical regimes where higher order contributions become large and the perturbative series is not under control. We shall see in the last section of this chapter how to account for them in two specific cases at all orders through the use of a resummation techniques. Those procedures allow us to stretch the applicability of pQCD to regions of the phase space where non-perturbative effects start to become the predominant contribution.

1.2.2 Deep Inelastic Process: from Parton Model to Factorization

Up until now we have justified the validity of the perturbative approach based on a fundamental feature of QCD: the asymptotic freedom. In our following chapters, we will be presenting results for processes involving hadrons in the initial and/or in the final state. As we have discussed

previously, the confinement hypothesis relegates hadronic states to highly non-perturbative regimes. The key connection between the perturbative description of the high momentum transfer interactions between quarks and gluons and the non-perturbative final/initial state hadrons lies in a property of some observables called *factorization*. Factorization relies on the incoherence of long distance and short distance effects in hadronic processes. It allows us to write scattering amplitudes involving high energy hadrons as a product of a "hard" scattering (short distance) piece, which only contains high energy and momentum components, and a "soft" reminder which includes all informations about the physics of low energy (long distance). Due to asymptotic freedom, the former can be computed in perturbation theory, whereas the latter can be described by process independent distribution functions. Initial state and final state distribution functions describe conceptually the distribution of the constituting fundamental elements inside an initial state hadron, *parton distribution functions* (PDFs), and the probability for them to hadronize after the scatter into a specific type of final state hadron, *fragmentation functions* (FFs). They are usually extracted through fits of global data and used as inputs when making further predictions in high energy hadronic processes.
Hereinafter, we consider the inclusive cross-section for deep inelastic proton-lepton scattering (DIS) as an exemplary observable to discuss factorization in more detail. We start by presenting the *parton model*, whose success in the 70's came from its ability to explain the observed approximate scaling property of the DIS structure function: the *Bjorken scaling*. We shall see that the parton model can be understood as the lowest order result of a more general structure and discuss how a factorized expression can be achieved at first order in perturbation theory. We are not going to extend this to higher orders as we are not interested here in presenting a formal proof of a factorization theorem. On the other end, the first order result will be useful to introduce the concepts of PDFs, FFs and *evolution* relevant to our discussions in the next chapters.

DIS in the parton model

Let's consider a lepton-hadron scattering process and label with $Q^2 = -q^2$ the momentum loss of the lepton transferred to the proton via an exchange of a virtual photon of momentum q. In order to gain better information over the structure of the hadron one may progressively improve the spatial resolution by increasing the transferred momentum, i.e. the momentum of the virtual photon. Intuitively, this is show in Fig. 1.5. If we define with W the invariant mass of the final state and with M_{hadron} the mass of the initial hadron, the condition $W^2 \gg M^2_{\text{hadron}}$

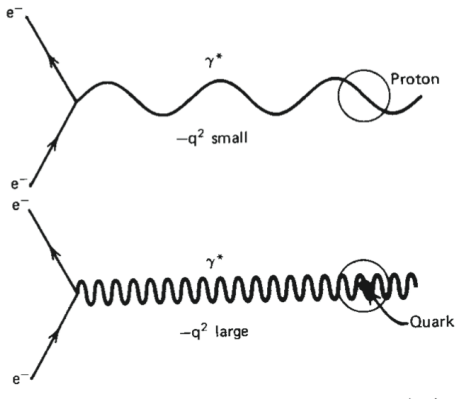

Figure 1.5: Relation between resolution and $-q^2$ [30].

identifies the inelastic regime of this process. The transition between the elastic and the inelastic regime appears clear in Fig. 1.6 where the cross section for electron-proton collision is shown. The first peak corresponds to the elastic regime where $W^2 \approx M_p^2$. The second peak takes place when $W^2 \approx M_\Delta^2$ and corresponds to the reaction $ep \to e\Delta^+ \to ep\pi^0$ where the proton brakes up and is excited to a Δ^+ state. Less and less structures are seen for higher invariant masses. The inelastic regime is said to be "deep" if, together with the inelasticity condition, the condition $Q^2 \gg M^2_{\text{hadron}}$ is satisfied. In this regime we are effectively scanning over the constituents of the hadron which are collectively called *partons*. The main idea of the parton model is to take advantage of the different time scales at which the elastic scattering between the virtual photon and the partons, and the subsequent interaction between the partons happen. Without loss of generality, let's move the reasoning in a Lorentz frame where the $|\boldsymbol{p}|_{\text{hadron}} \gg M_{\text{hadron}}$

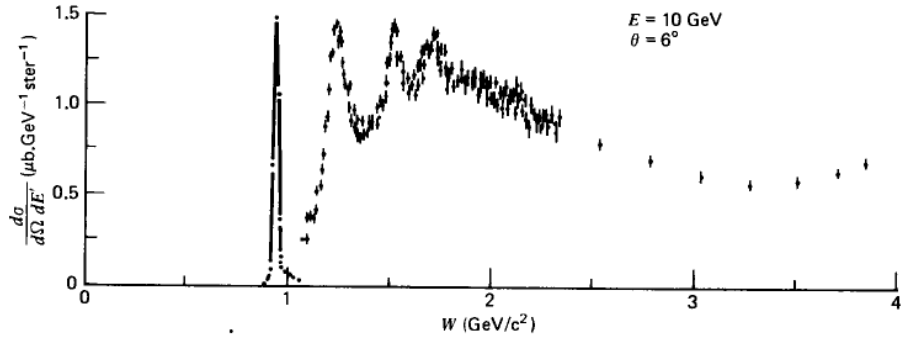

Figure 1.6: SLAC measurements for the $e^- p \to e^- X$ cross section as a function of the invariant mass W [30].

(*infinite momentum frame*). This can be done since $Q^2 \gg M^2_{\text{hadron}}$, and an example of such frame could be the center of mass frame (c.m.s.). In this system of reference, the hadron moves ultra-relativistically and both the masses of the partons m and the mass of the hadron M_{hadron} can be neglected. Moreover, due to Lorentz contraction of space the hadron will look like a disk of collinear moving partons, which allows us to neglect the transversal momenta of the partons $p_T^{\text{parton}} = 0$ in both initial and final state. On the other hand, from the point of view of a striking lepton going through the hadron, time dilatation "freezes" the partons in their virtual states. The time scale at which the hard scattering between lepton and parton occurs is much smaller than the time needed for the partons to interact with each others. For example, if we consider a transferred momentum of 100 GeV, the first reaction happens in about 0.67×10^{-26}s whereas the subsequent series of interactions take place in about 0.67×10^{-22}s after considering the time dilatation in transferring from the hadron inertial frame to the laboratory frame. Based on this considerations, one might write a cross section where this two parts of the DIS process are well separated. The conceptual picture for the parton model was firstly introduced by R.P.Feynman (1969)[31] and then formally developed by J. D. Bjorken and E. A.Paschos (1969)[32]. We can schematically summarize this picture as follows

$$d\sigma(x) = \sum_i \int_x^1 \frac{dy}{y} f_i(y) d\hat{\sigma}\left(\frac{x}{y}\right) = \sum_i \int_x^1 \frac{dz}{z} f_i\left(\frac{x}{z}\right) d\hat{\sigma}\left(z\right) = \sum_i f_i \otimes d\hat{\sigma}, \tag{1.42}$$

where σ is the measured cross section, the $\hat{\sigma}$ denotes the cross section of the hard scattering between the lepton and the parton i and $f_i(y)$ is the parton distribution function describing the probability for the virtual photon to find a parton of momentum $p_{\text{parton}_i} = yP_{\text{hadron}}$, or vice-versa, the probability for the struck parton i to carry a fraction $0 \leq y \leq 1$ of the hadron's momentum P_{hadron}. The convolution of two function is defined as

$$g(\tau) \equiv \int_0^1 dx \int_0^1 dz f(z)\delta(\tau - xz)h(x) = \int_\tau^1 \frac{dz}{z} f(z) h\left(\frac{\tau}{z}\right) = f \otimes h. \tag{1.43}$$

On the other side, the cross section of DIS can be constructed directly from the general scattering theory. For an unpolarized cross section the general expression is

$$d\sigma = \frac{\overline{|\mathcal{M}|^2}}{\text{initial flux}} dPS \tag{1.44}$$

where dPS is the Lorentz invariant phase space factor and $\overline{|\mathcal{M}|^2}$ is the *invariant amplitude*

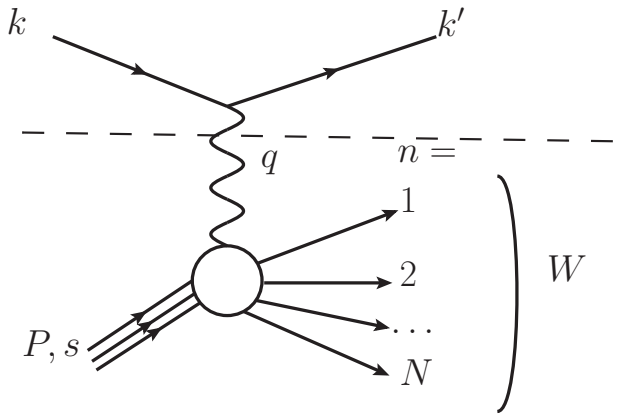

Figure 1.7: Deep inelastic scattering $l(k) + h(P) \to l(k') + X$. W is the invariant mass of the unobserved final state X and with s we indicate the spin state of the incoming hadron. q is the momentum of the virtual photon. The dashed line serves as an intuitive separation between the leptonic and the hadronic part of the process.

squared $\mathcal{M}$, summed over all outgoing spin states and averaged over the incoming ones:

$$\overline{|\mathcal{M}|^2} = \left(\prod_{\substack{i=1 \\ \text{spin ½-particles}}}^{\substack{n \\ \text{incoming}}} \frac{1}{2s_i + 1} \right) \left(\prod_{\substack{j=1 \\ \text{spin 1-particles}}}^{\substack{n \\ \text{incoming}}} \frac{1}{2s_j} \right) \sum_{\substack{\text{all outgoing} \\ \text{spin states}}} |\mathcal{M}|^2. \tag{1.45}$$

The invariant amplitude for the DIS process shown in Fig. 1.7 is given by

$$\mathcal{M} = e\bar{u}(k')\gamma^\mu u(k) \frac{1}{q^2} \langle X | J_\mu(0) | P, s \rangle \ , \tag{1.46}$$

where $J_\mu(0)$ is the electromagnetic current. We are not considering here electroweak currents since they don't add any relevant information to the discussion in this chapter. It turns out that the cross section constructed from this amplitude according to Eq. 1.45 can be separated into a leptonic part and and a hadronic part

$$d\sigma \sim L_{\mu\nu} W^{\mu\nu} \ . \tag{1.47}$$

In Fig. 1.7 the dashed line serves as an intuitive separation between the leptonic and the hadronic part of the process. The leptonic part can be calculated from first principles in QED

and gives

$$L^{\mu\nu} = \frac{1}{2} \sum_{\substack{\text{lepton} \\ \text{spins}}} [\bar{u}(k')\gamma^{\mu}u(k)][\bar{u}(k')\gamma^{\nu}u(k)]^{*} = 2(k'^{\mu}k^{\nu} + k'^{\nu}k^{\mu} - (k' \cdot k - m^2)g^{\mu\nu}) \,, \tag{1.48}$$

where m is the lepton mass, which in the deep inelastic limit can be neglected. The hadronic tensor, on the other end, has a more complicated structure and is defined as

$$\begin{aligned} W_{\mu\nu} =& \frac{1}{4\pi M} \sum_{N} \left(\frac{1}{2} \sum_{s} \right) \int \prod_{n=1}^{N} \left(\frac{d^3 P'_n}{(2\pi)^3 2E'_n} \right) \sum_{s_n} \langle P, s| \, J^{\dagger}_{\mu} \, |X\rangle \\ & \times \langle X| \, J_{\nu} \, |P, s\rangle \, (2\pi)^4 \delta^{(4)} \left(P + q - \sum_{n} P'_n \right) \,, \end{aligned} \tag{1.49}$$

where the sum runs over all possible final N-particle state X and $\sum_n P'_n = P_X$ is the momentum of the final state X. Using $\delta^4(P+q-P_X) = \int d^4z \exp(iP\cdot z + iq\cdot z - iP_X \cdot x)$, using the tranlation relation $J^{\mu}(z) = \exp(iP_{op}\cdot z) J^{\mu} \exp(-iP_{op}\cdot z)$ and using the completeness for the intermediate states, the hadron tensor can be written as the Fourier transform of the product $J^{\mu}(z)J^{\nu}(0)$ expectation value

$$W_{\mu\nu} = \frac{1}{4\pi M} \int d^4 z e^{iqz} \, \langle P| \, J^{\mu}(z) J^{\nu}(0) \, |P\rangle \,, \tag{1.50}$$

where summation and averaging over spins is left implicit. As we shall see later in this section, the hadron tensor is related to the total cross section for virtual photoabsorption. As such, the hadronic tensor is related to the forward virtual Compton amplitude through the optical theorem

$$W_{\mu\nu} = \frac{1}{\pi} \text{Im} \, T_{\mu\nu} \,, \tag{1.51}$$

where

$$2MT_{\mu\nu} = i \int d^4 z e^{iqz} \, \langle P| \, \mathcal{T} J^{\mu}(z) J^{\nu}(0) \, |P\rangle \,. \tag{1.52}$$

Although we cannot calculate $W^{\mu\nu}$ from first principles due to the non-perturbative nature of the hadronic states, we can derive its tensor structure from the properties of the strong and electromagnetic interaction. For unpolarized cross sections the most general covariant rank-2 tensor will contain only symmetric terms in μ and ν. Thus, the general form of $W^{\mu\nu}$ in this

case would be

$$W^{\mu\nu} = -W_1 g^{\mu\nu} + \frac{W_2}{M^2} P^\mu P^\nu + \frac{W_4}{M^2} q^\mu q^\nu + \frac{W_5}{M^2}(P^\mu q^\nu + q^\mu P^\nu). \tag{1.53}$$

Using the fact that J^μ is a conserved quantity, $q_\mu W^{\mu\nu} = 0$. As a consequence we obtain

$$\begin{aligned} W_5 &= -\frac{P\cdot q}{q^2} W_2 \\ W_4 &= \left(\frac{P\cdot q}{q^2}\right)^2 W_2 + \frac{M^2}{q^2} W_1, \end{aligned} \tag{1.54}$$

and inserting W_4 and W_5 into 1.53 gives us

$$W^{\mu\nu} = W_1\left(-g^{\mu\nu} + \frac{q^\mu q^\nu}{q^2}\right) + W_2 \frac{1}{M^2}\left(P^\mu - \frac{P\cdot q}{q^2} q^\mu\right)\left(P^\nu - \frac{P\cdot q}{q^2} q^\nu\right). \tag{1.55}$$

W_1 and W_2 are called the *structure functions* and depend on the two Lorentz scalar variables

$$\begin{aligned} Q^2 &\equiv -q^2 \\ \nu &\equiv \frac{P\cdot q}{M}. \end{aligned} \tag{1.56}$$

The invariant mass W of the final hadronic system can be expressed in terms of the scalars Q^2 and ν as follows

$$W^2 = (P+q)^2 = M^2 + 2M\nu - Q^2. \tag{1.57}$$

Furthermore, the variables of Eq.1.56 can be replaced by the dimensionless

$$\begin{aligned} x &\equiv \frac{Q^2}{2P\cdot q} = \frac{Q^2}{2M\nu} && 0 \le x \le 1 \\ Y &\equiv \frac{P\cdot q}{P\cdot k} && 0 \le Y \le 1. \end{aligned} \tag{1.58}$$

x is called the *Bjorken scaling variable*. The dimensionless structure functions $F_1(x)$ and $F_2(x)$ are defined from $W_1(\nu, Q^2)$ and $W_2(\nu, Q^2)$ as

$$\begin{aligned} F_1(x, Q^2) &= M W_1(\nu, Q^2) \\ F_2(x, Q^2) &= \nu W_2(\nu, Q^2). \end{aligned} \tag{1.59}$$

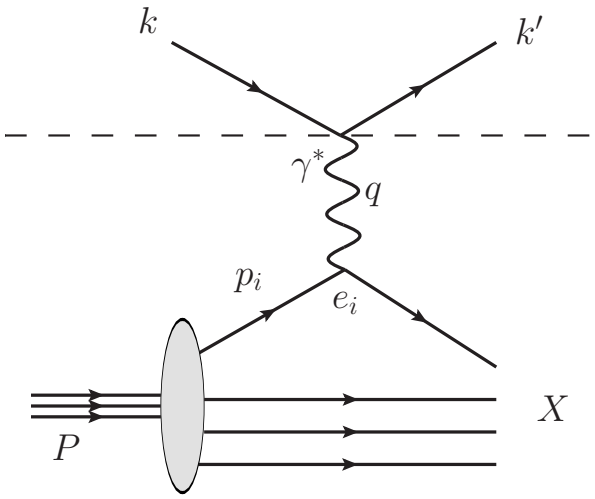

Figure 1.8: Parton model for DIS $l(k) + h(P) \to l(k') + X$.

Written as a function of F_1 and F_2, Eq. 1.55 takes the form

$$\begin{aligned} MW^{\mu\nu} &= (\frac{q^\mu q\nu}{q^2} - g^{\mu\nu})F_1(x,Q^2) + \frac{1}{P\cdot q}\left(P^\mu - q^\mu\frac{P\cdot q}{q^2}\right)\left(P^\nu - q^\nu\frac{P\cdot q}{q^2}\right) \\ &= -g_\perp^{\mu\nu}F_1(x,Q^2) + \hat{t}^\mu\hat{t}^\nu\left(-F_1 + \frac{\kappa}{2x}F_2\right), \end{aligned} \tag{1.60}$$

where

$$\kappa = 1 + \frac{4M^2x^2}{Q^2}, \quad \hat{t}^\mu = \frac{1}{Q\sqrt{\kappa}}(q^\mu + 2xP^\mu) \quad \text{and} \quad g_\perp^{\mu\nu} = g^{\mu\nu} + \frac{1}{Q^2}q^\mu q^\nu - \hat{t}^\mu\hat{t}^\nu. \tag{1.61}$$

With those definitions and ignoring hadron mass corrections $\propto M^2/Q^2$, the inclusive cross section for DIS, $l(k) + h(P) \to l(k') + X$, written in terms of the structure functions reads

$$\frac{d\sigma}{dx\,dY} = \frac{2\pi\alpha^2}{x\,Y\,Q^2}\left[\left[1 + (1-Y)^2\right]2x\,F_1 + (1-Y)\,2\,F_L\right], \tag{1.62}$$

where $F_L = F_2 - 2xF_1$.

As we discussed at the beginning of this section, the idea of the parton model is to approximate the process shown in Fig. 1.7 to a sum of incoherent scatters between the virtual photon and the individual partons, whose momentum distribution may be described by the parton distribution functions $f_i(y)$. Diagrammatically, this is show in Fig. 1.8. The hadron tensor is related to

the total cross section of the lower part of the proccess, i.e. to the virtual photon absorption $\gamma^*(q)h(P) \to X$. Since the flux for a virtual photon beam is not a well-defined quantity and can be chosen arbitrary, let's use here the so called *Hand convention* and set the flux factor for the virtual photon equal to the one of a real photon with $q^2 = 0$ and energy $q^0 = \nu \equiv K$. In this case the flux factor is $4MK$ and K has to satisfy the following equality:

$$K = \frac{W^2 - M^2}{2M} = \nu + \frac{q^2}{2M}. \tag{1.63}$$

The cross section reads

$$\sigma_\lambda^{\text{tot}} = \frac{4\pi^2\alpha}{K}\varepsilon_\lambda^{\mu*}\varepsilon_\lambda^\nu W_{\mu\nu} \equiv \sigma_0 2M\varepsilon_\lambda^{\mu*}\varepsilon_\lambda^\nu W_{\mu\nu}, \tag{1.64}$$

where $\sigma_0 = \frac{4\pi^2\alpha}{2MK}$. Taking the z axis in the same direction as $\boldsymbol{q}$, the photon polarization vectors ε_λ^μ for the different helicities λ are defined as

$$\begin{aligned} \varepsilon_\pm &= \mp\sqrt{\frac{1}{2}}(0, 1, \pm i, 0) && \text{for } \lambda = \pm 1, \\ \varepsilon_0 = \varepsilon_L &= \frac{1}{\sqrt{-q^2}}\left(\sqrt{\nu^2 - q^2}, 0, 0, \nu\right) && \text{for } \lambda = 0. \end{aligned} \tag{1.65}$$

The completeness relation for a massive photon yields

$$\sum(-1)^{\lambda+1}\varepsilon_\lambda^{\mu*}\varepsilon_\lambda^\nu = \sum_{T=\pm1}\varepsilon_T^{\mu*}\varepsilon_T^\nu + \varepsilon_L^{\mu*}\varepsilon_L^\nu = -g^{\mu\nu} + \frac{q^\mu q^\nu}{q^2}, \tag{1.66}$$

where with T and L we indicate the transversal and longitudinal components respectively.
In the deep inelastic limit, i.e. ignoring corrections of order M^2/Q^2, Eq 1.64 together with 1.55 yield

$$M(-g^{\mu\nu}W_{\mu\nu}) \equiv \frac{\sigma_T}{\sigma_0} = 2F_1(x, Q^2) \tag{1.67}$$

$$2M\left(\frac{q^\mu q^\nu}{q^2}W_{\mu\nu}\right) \equiv \frac{\sigma_L}{\sigma_0} = \frac{F_L(x, Q^2)}{x}. \tag{1.68}$$

Following the prescription of the parton model (see Eq. 1.42), the structure functions may be

written as

$$2F_1 = \frac{\sigma_T(x)}{\sigma_0} = \sum_i \int_x^1 \frac{dy}{y} f_i(y) \frac{\hat{\sigma}_T(x/y)}{\hat{\sigma}_0} = \sum_i \int_x^1 \frac{dy}{y} f_i(y) \hat{\mathcal{F}}_1 \left(\frac{x}{y}\right)$$
$$\frac{F_L}{x} = \frac{\sigma_L(x)}{\sigma_0} = \sum_i \int_x^1 \frac{dy}{y} f_i(y) \frac{\hat{\sigma}_L(x/y)}{\hat{\sigma}_0} = \sum_i \int_x^1 \frac{dy}{y} f_i(y) \hat{\mathcal{F}}_L \left(\frac{x}{y}\right) \tag{1.69}$$

where $\hat{\sigma}_0 = \frac{4\pi^2\alpha}{\hat{s}}$ and $\hat{s} = (p_i + q)^2$ is the partonic c.m. energy squared. $\hat{\sigma}$ identifies the quark-parton elastic process $\gamma^* q \to q$:

$$\hat{\sigma}(\gamma^* q) = \frac{4\pi\alpha^2}{2p_i \cdot q} \varepsilon_\lambda^{\mu *} \hat{W}_{\mu\nu} \varepsilon_\lambda^\nu. \tag{1.70}$$

Hence, the partonic structure functions $\hat{F}$ can be calculated from the partonic hadron tensor $\hat{W}_{\mu\nu}$. Similarly to Eqs.1.67 and 1.68 we can define [33]

$$M\left(-g^{\mu\nu}\hat{W}_{\mu\nu}\right) = \hat{\mathcal{F}}_2(z) - \frac{3}{2}\hat{\mathcal{F}}_L(z) \tag{1.71}$$
$$M\left(p_i^\mu p_i^\nu \hat{W}_{\mu\nu}\right) = \frac{Q^2}{8z^2}\hat{\mathcal{F}}_L(z), \tag{1.72}$$

where $z \equiv \frac{Q^2}{2p_i \cdot q}$, $\mathcal{F}_2 = \mathcal{F}_L + \mathcal{F}_1$ and the partonic hadron tensor takes the form

$$\begin{aligned}\hat{W}_{\mu\nu} &= \frac{1}{4\pi M}\frac{1}{2}\int \frac{d^3p_i'}{(2\pi)^3 2p_i'^0}(2\pi)^4\delta^{(4)}(p_i + q - p_i') \sum_s \langle p_i, s|\, \hat{J}_\mu^\dagger \,|p_i', s'\rangle \langle p_i', s'|\, \hat{J}_\nu \,|p_i, s\rangle \\ &= \frac{1}{M} e_i^2 [p_i^\mu p_i^\nu + p_i^\nu p_i^\mu + p_i^\mu q^\nu + p_i^\nu q^\mu - (p \cdot q) g^{\mu\nu}] \delta\left((p_i + q)^2\right). \end{aligned} \tag{1.73}$$

From Eq.1.72 it can be shown that $\hat{\mathcal{F}}_L \propto \frac{1}{Q^2}$ which in the deep inelastic limit $Q^2 \to \infty$ implies

$$\hat{\mathcal{F}}_L(z) \to 0 \Longrightarrow F_L(x) \to 0 \Longrightarrow\ 2xF_1(x) \approx F_2(x). \tag{1.74}$$

The expression above is better known as the *Callan-Gross relation* [34] and is a consequence of the $\frac{1}{2}$-spin nature of quarks. Let's express the momenta in light-cone components, $v = [v^-, v^+, \boldsymbol{v}_\perp]$ where $v^\pm = (v^0 \pm v^3)/\sqrt{2}$ or $v = v^- n_- + v^+ n_+ + v_T$ in terms of light-like vectors satisfying $n_-^2 = n_+^2 = 1$ and $n_+ \cdot n_- = 0$ (thus $v^\pm = v \cdot n_\mp$). This will be useful later to understand the operator definition of the parton distribution function. The relevant momenta

in the frame where P and q are collinear read in light-cone coordinates

$$\begin{aligned} q &= \left[\frac{Q^2}{A\sqrt{2}}, -\frac{A}{\sqrt{2}}, \mathbf{0}_\perp\right] \\ p_i &= \left[p^-, \frac{A}{z\sqrt{2}}, \boldsymbol{p}_\perp\right] = \left[p^-, yP^+, \boldsymbol{p}_\perp\right] \\ P &= \left[\frac{xM^2}{A\sqrt{2}}, \frac{A}{x\sqrt{2}}, \mathbf{0}_\perp\right] \ , \end{aligned} \tag{1.75}$$

where $z = -q^+/p^+ = Q^2/(2p_i \cdot q)$, $x = -q^+/P^+ = Q^2/(2P \cdot q)$. We introduce also the variable $y = p^+/P^+ = x/z$ which is called the *lightcone momentum fraction*. A defines the boost along the z-axis. For example, $A \to \infty$ for the *infinite momentum frame* mentioned before and $A = xM$ in the target rest frame. Let's consider now the frame where $|\boldsymbol{q}|^2 = Q^2$, thus $A = Q$. Since in this case $P^- = xM^2/(Q\sqrt{2})$ and $P^+ = Q/(x\sqrt{2})$, when Q^2 becomes large $P^- \ll q^-$ and the nucleon momentum is on the scale Q, i.e. becomes light-like. Also the parton momentum p_i is light-like if compared to the hard scale Q. We don't need to put it on-shell ($p_i^2 = m^2$ which implies $p^- = (m^2 + \boldsymbol{p}_T^2)/(2p^+)$) for it to be true. For a quark in a hadron we have

$$\begin{aligned} p^- &= \frac{2p_i \cdot P - yM^2}{2P^+} \\ p_T^2 &= y(1-y)M^2 - y(P-p_i)^2 - (1-y)p_i^2. \end{aligned} \tag{1.76}$$

As long as all invariants $p \cdot P \sim (P - p_i)^2 \sim p_i^2 \sim P^2 = M^2$, then $p^+ \sim P^+ \sim Q$, while $p^- \sim P^- \sim M^2/Q$ and $p_T^2 \sim M^2$. Those assumptions are well verified in the deep inelastic limit. For large enough transferred momentum Q, *minus* components of P and p_i can be neglected. This is sufficient to derive the parton model result. A more comprehensive discussion of those matters can be found in [35].

With this considerations, we may write now Eq.1.71 using Eq.1.73 and obtain

$$2\hat{\mathcal{F}}_1(z) = e_i^2 \delta(1-z). \tag{1.77}$$

Placing Eq.1.77 in Eq.1.69 gives the main result of the parton model:

$$2F_1(x) = \frac{F_2(x)}{x} = \sum_i e_i^2 f_i(x). \tag{1.78}$$

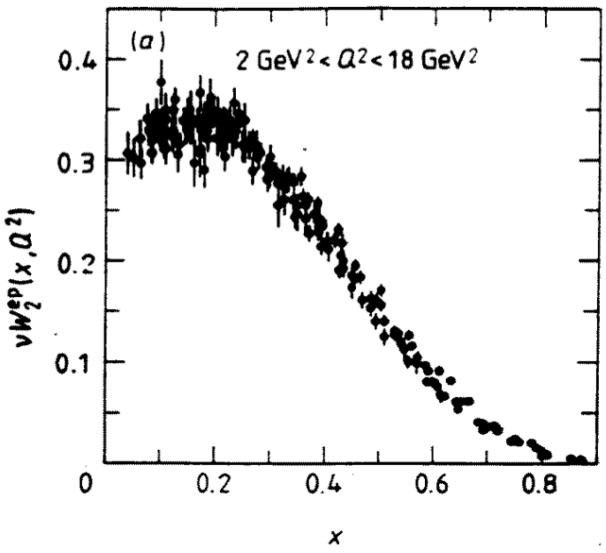

Figure 1.9: Experimental data on νW_2 as function of x for different values of Q^2 [37].

Eq. 1.78 is independent of the scale Q^2. This property is known as the *Bjorken scaling* [36] and was experimentally verified by a series of experiments at SLAC around 1980. See Fig. 1.9 [37]. Although such scaling is broken when considering gluon contributions to the process (see later), the observation of the Bjorken scaling was the first "proof" that *point-like* structures existed inside the hadron.

Parton distribution functions

In the parton model the distribution functions $f_i(z)$ are convoluted with the partonic process in a *ad hoc* manner based on the intuitive physical picture described at the beginning of the previous section. To understand the very essence of PDFs we may find an operator definition in terms of quark (strength tensor gluon) fields $\psi(x)$ ($G_a^{\mu\nu}$). To do this, we can calculate the hadronic tensor directly form the *handbag* diagram shown in Fig. 1.10 describing the incoherent scattering of the photon off an individual parton inside the hadron. The lower blob pictures the so called quark correlator defined as a Fourier transform of an hadronic matrix element

$$\Phi(p,P,s) = \frac{1}{(2\pi)^2}\int d^4\xi e^{ip\cdot\xi}\,\langle P,s|\,\overline{\psi}_j(0)\psi_i(\xi)\,|P,s\rangle\,. \tag{1.79}$$

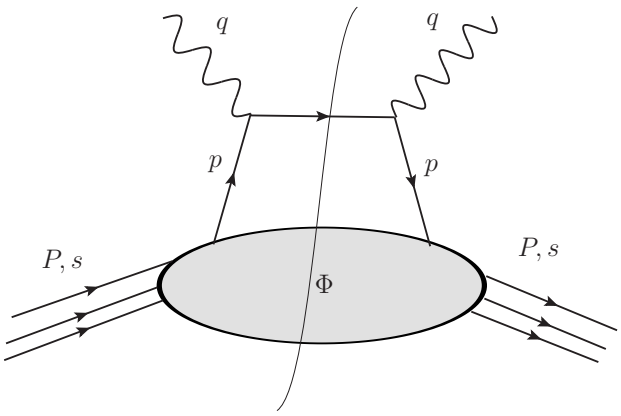

Figure 1.10: The handbag diagram for DIS. The cut identifies final state on shell particles.

The hadronic tensor restricted to the quark part only and expressed in the light-cone coordinates reads

$$\begin{aligned} 2MW^{\mu\nu}(P,q) &= \sum_q e_q^2 \int dp^- dp^+ d^2\boldsymbol{p}_\perp \mathrm{tr}[\Phi(p)\gamma^\mu(\not{p}+\not{q}+m)\gamma^\nu]\delta((p+q)^2-m^2) \\ &\approx \sum_q e_q^2 \int dp^- dp^+ d^2\boldsymbol{p}_\perp \mathrm{tr}\left(\Phi(p)\gamma^\mu \frac{\not{q}}{2q^-}\gamma^\nu\right)\delta(p^+ + q^+) \\ &\approx -g_\perp^{\mu\nu}\frac{1}{2}\sum_q e_q^2 \int dp^- d^2\boldsymbol{p}_\perp \mathrm{tr}(\gamma^+\Phi(p))\Big|_{p^+=xP^+} + \text{other tensor structures}\dots\ . \end{aligned} \tag{1.80}$$

In the second line we have ignored the minus components of p and set $p^+ = xP^+$. This approximation defines a framework called *collinear factorization* which is justified in the deep inelastic process by the considerations made at the end of the previous section. Comparing Eq. 1.80 with Eq. 1.60, and using the result of the parton model 1.78 together with the definition of the quark correlator, we can read off the definition of the "collinear" parton distribution function

$$q(x) = \frac{1}{4\pi}\int d\xi^- e^{(+ixP^+\xi^-)}\left\langle P,s\right|\overline{\psi}(0)\gamma^+\psi(\xi)\left|P,s\right\rangle\Big|_{\xi^+=\boldsymbol{\xi}_\perp=0}. \tag{1.81}$$

In the above equation the integral over dp^- and $d\boldsymbol{p}_\perp$ was carried out leaving two delta functions $\delta(\xi^+)$ and $\delta(\boldsymbol{\xi}_\perp)$. This is perfectly fine as long as $p_\perp^2 \sim M^2$ and corrections to the collinear picture are of order M^2/Q^2, which in DIS are negligible. If we do not perform the integration

over $d\boldsymbol{p}_\perp$ and keep the dependence on the transverse momentum in the definition 1.81, we define what are called transverse momentum dependent (TMD) PDFs. TMD PDFs are used in the framework of TMD *factorization* relevant for processes where corrections of order $1/Q^2$ are not anymore negligible.
In chapter 5 we will consider the case where the spin polarization of the target is taken into account. The definition of "polarized" PDF reads

$$s_L \Delta q(x) = \frac{1}{4\pi} \int d\xi^- e^{(+ixP^+\xi^-)} \langle P,s| \overline{\psi}(0)\gamma^+\gamma^5\psi(\xi) |P,s\rangle \Big|_{\xi^+=\boldsymbol{\xi}_\perp=0}, \tag{1.82}$$

where $s_L \equiv M(s\cdot q)/(P\cdot q)$ and s is the spin vector of the target hadron with momentum P. Eq. 1.81 and 1.82 are gauge dependent. In order to define PDFs in a gauge independent way one has to introduce a path ordered exponential of the gluon field

$$\mathcal{G} = \mathcal{P}\exp\left(-ig_s \int_0^{\xi^-} d\omega\; n\cdot G_a(\omega\, n) t^a\right), \tag{1.83}$$

where t^a are the colour group generators in the fundamental representation (see Appendix A). In the axial gauge $n\cdot G = 0$ it reduces to 1. The gauge invariant definition of a quark PDF is then

$$q(x) = \frac{1}{4\pi} \int d\xi^- e^{(+ixP^+\xi^-)} \langle P,s| \overline{\psi}(0)\gamma^+\mathcal{G}\psi(\xi) |P,s\rangle \Big|_{\xi^+=\boldsymbol{\xi}_\perp=0}. \tag{1.84}$$

For completeness, the definition of a gluon PDF is given by

$$g(x) = \frac{1}{2\pi\, xP^+} \int d\xi^- e^{(+ixP^+\xi^-)} \langle P,s| G_a^{+,\nu}(0)\mathcal{G}^{ab} G_{b,+\nu}(\xi) |P,s\rangle \Big|_{\xi^+=\boldsymbol{\xi}_\perp=0}, \tag{1.85}$$

where $G^{\mu\nu}$ is the gluon field strength operator and in $\mathcal{G}$ we use the adjoint representation for the color group generators.
To complete the parton model picture we need to understand PDFs as parton momentum densities. From definition 1.81 is however straight forward to obtain this interpretation. Given $\psi(0)\gamma^+\psi(\xi) = \sqrt{2}\psi_+^\dagger(\xi)\psi_+(0)$, where $\psi_\pm = P_\pm\psi_\pm$ are projections obtained from the projection

operator $P_\pm = \frac{1}{2}\gamma^\mp\gamma\pm$, we can write the PDF for the quark as

$$\begin{aligned} q(x) &= \frac{1}{2\pi\sqrt{2}} \int d\xi^- e^{(+ip\cdot\xi)} \langle P,s| \overline{\psi}(0)\psi(\xi) |P,s\rangle \Big|_{\xi^+=\boldsymbol{\xi}_\perp=0} \\ &= \frac{1}{\sqrt{2}} \sum_n |\langle P_n| \psi_+ |P\rangle|^2 \delta(P_n^+ - (1-x)P^+). \end{aligned} \tag{1.86}$$

This represents the probability that a quark is annihilated from $|P\rangle$ giving a state $|n\rangle$ with $P_n^+ = (1-x)P^+$.
In light of our discussion so far, we can view a PDF f_i graphically as

$$f_i(x) = \frac{d\mathcal{P}_i}{dx} =$$

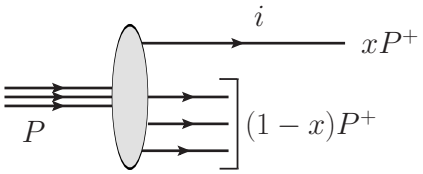

. (1.87)

where the letter $\mathcal{P}$ denotes a probability. As such, a general property that has to be satisfied is

$$\sum_{i'} \int dy\, y f_i(y) = 1. \tag{1.88}$$

The summation is carried out over all parton i', not only over the charged ones i interacting with the virtual photon. Using Eq.1.87, we can understand the parton model diagrammatically as follows:

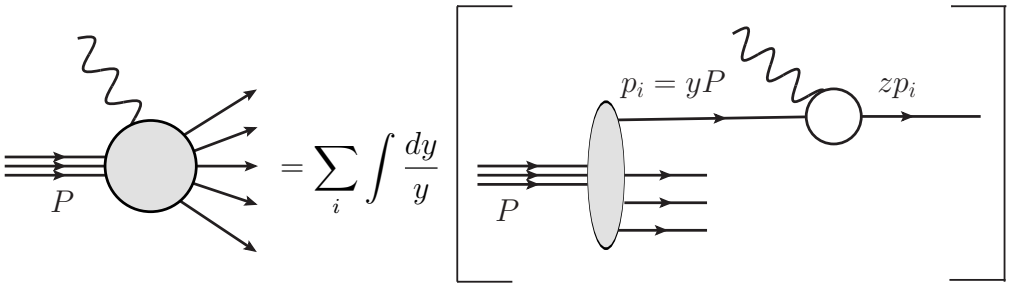

, (1.89)

where the white blob

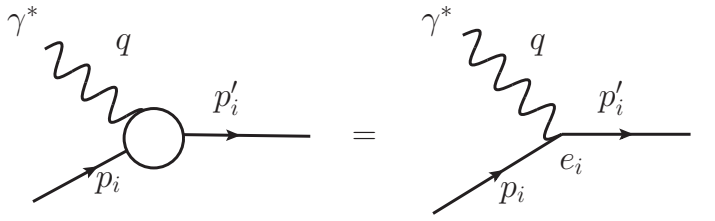

(1.90)

From this diagrams, it is now clear how the parton model can be seen as the lowest order approximation of a more general *factorization theorem*, which, for DIS [38–40], holds also in the case when gluon emission corrections are take into account in 1.90. We will discuss *factorization* for DIS in the next section.
We have derived the parton model for DIS. With analogous reasonings we could derive the parton model for other processes. For example, for the hadron-hadron process $h_1(P_1)+h_2(P_2) \to l(k_1)+l(k_2)+X$ (Drell-Yan process) the parton model gives

$$\begin{aligned}\frac{d\sigma}{dQ^2}(\tau) &= \sum_i \int_\tau^1 \frac{d\xi_1}{\xi_1} \int_{\tau/\xi_1}^1 \frac{d\xi_2}{\xi_2} \left[f_i^{h_1}(\xi_1) f_{\bar{i}}^{h_2}(\xi_2) + f_{\bar{i}}^{h_1}(\xi_1) f_i^{h_2}(\xi_2) \right] \frac{d\hat{\sigma}}{dQ^2}\left(\tau/(\xi_1\xi_2)\right) \\ &= \sum_i [f_i^{h_1} \otimes f_{\bar{i}}^{h_2} + 1 \leftrightarrow 2] \otimes \frac{d\hat{\sigma}}{dQ^2},\end{aligned} \tag{1.91}$$

where $\tau = \frac{Q^2}{s}$ is the *Drell-Yan scaling variable* and represent the fraction of momentum of the initial state transferred to the virtual photon γ^*. The great feature of definitions 1.81 and 1.85 is that they are process independent. The PDFs $f_i^{h_{1,2}}$ in Eq.1.91 are the same as the f_i for DIS and depend only on the hadron we consider for the scattering. In this sense we say that the PDFs are "universal". As a consequence of their universality, the distribution functions have to satisfy some relations connected with the conservation of the charge. Let's consider a proton. From the quark model we know that the quantum numbers of the proton should come from the combination of three quarks: *uud*. These are the so-called *valence* quarks. Within the confinement region, however, quark and antiquark pairs are constantly created and annihilated with roughly the same frequency and momentum distribution for each flavour type. Those are known as the *sea* quarks. See Fig.1.11. Considering only the lightest flavour quarks u, d and

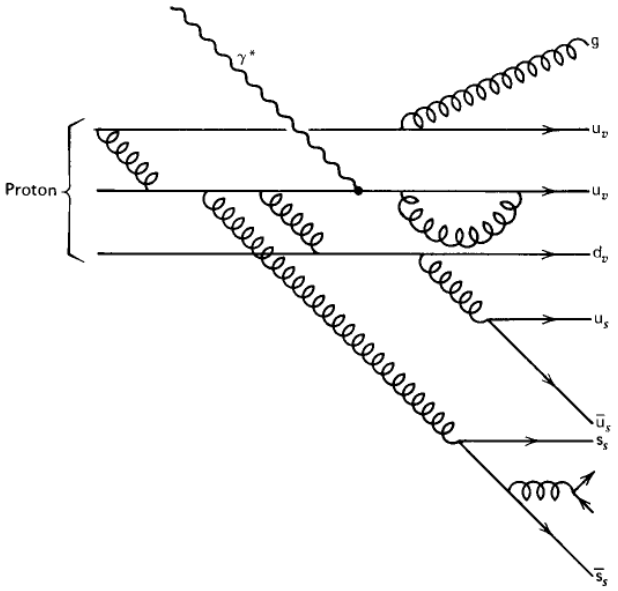

Figure 1.11: Proton's scheme of valence and sea quarks [30].

s, the following relations must hold

$$\begin{aligned} & f_{\text{see}} = u_s(x) = \bar{u}_s(x) = d_s(x) = \bar{d}_s(x) = s_s(x) = \bar{s}_s(x) \\ & \bar{u}_v(x) = \bar{d}_v(x) = 0 \\ & u(x) = u_v(x) + u_s(x) \\ & d(x) = d_v(x) + d_s(x). \end{aligned} \tag{1.92}$$

It follows that

$$f_i - f_{\bar{i}} = f_i - f_{\bar{i}\,\text{sea}} = f_i - f_{i\,\text{sea}} = f_{i\,\text{valence}}. \tag{1.93}$$

From the conservation of the charge, the valence quark distribution functions should then sum to the valence value v_i. For the proton it follows that

$$\begin{aligned} & \int_0^1 [u(x) - \bar{u}(x)]dx = v_u^{\text{proton}} = 2, \\ & \int_0^1 [d(x) - \bar{d}(x)]dx = v_d^{\text{proton}} = 1. \\ & \int_0^1 [s(x) - \bar{s}(x)]dx = v_s^{\text{proton}} = 0. \end{aligned} \tag{1.94}$$

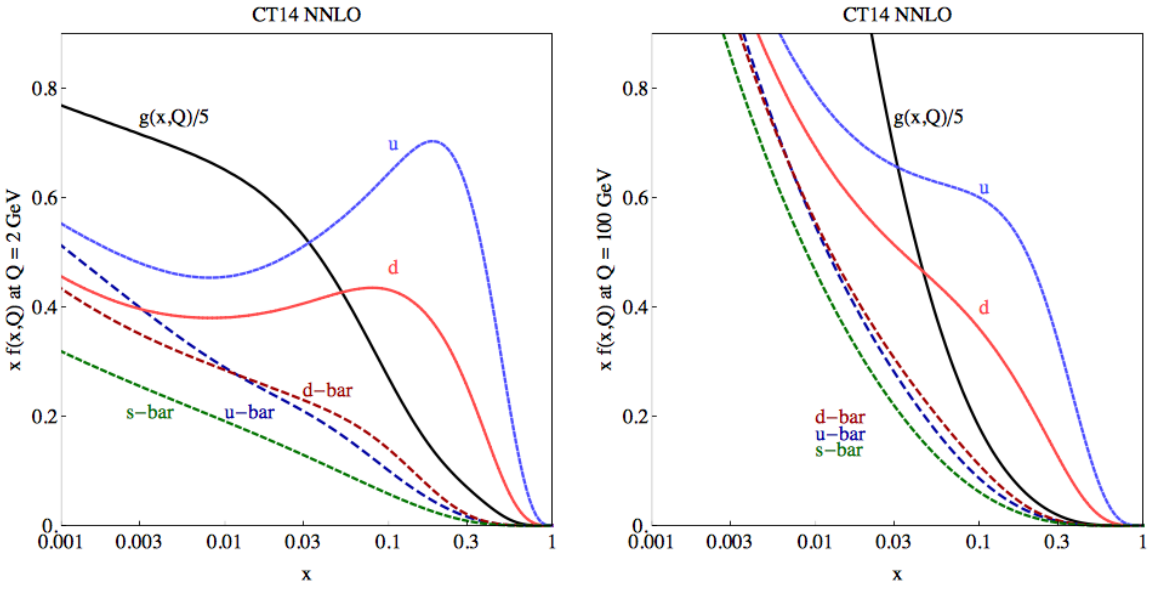

Figure 1.12: Parton distribution functions for the CT14 at $Q = 2$ and 100 GeV [41].

Eq.1.94 together with Eq.1.88 are called the *sum rules* for the PDFs. They can be derived also from their operator definition:

$$\int_{-1}^{1} dx q(x) = \int_{0}^{1} [q(x) - \bar{q}(x)] = \frac{\langle P| \overline{\psi}(0)\gamma^{+}\psi(0) |P\rangle}{2P^{+}} = n_q, \tag{1.95}$$

where n_q is the coefficient of the expectation value $\langle P| \overline{\psi}(0)\gamma^{\mu}\psi(0) |P\rangle = 2n_q P^{\mu}$, which is precisely the quark number.

Being universal, PDFs can be extracted from data of different processes through the means of fitting techniques. The CTEQ (Coordinated Theoretical-Experimental Project on QCD), for example, is a multi-institutional collaboration which, among other projects, provides the high-energy community of physicists with sets of PDFs coming from the analysis of different processes (DIS, vector boson production and single-inclusive jet production)[41]. An overview of the set of PDFs released in 2014 (CT14) is shown in Fig.1.12. In the following chapter we will consider the time-like counter part of PDFs, the fragmentation functions, which describe the momentum distributions of fragmenting partons. Similarly to what we have discuss here

we can give an operator definition for this objects

$$D_q^h(z) = \sum_X \int \frac{d\xi^+}{(2\pi)^3} e^{ip^-\xi^+} \langle 0| \mathcal{W}(\infty^+, \xi^+)\psi(\xi^+) |P_h, s_h\rangle \langle P_h, s_h| \overline{\psi}(0)\mathcal{W}(0, \infty^+) |0\rangle \Big|_{\xi^- = \boldsymbol{\xi}_\perp = 0}, \tag{1.96}$$

where the Wilson line is defined as

$$\mathcal{W}(a, b) = \mathcal{P} \exp\left(-ig_s \int_a^b d\omega \; n \cdot G_a(\omega\, n) t^a\right), \tag{1.97}$$

At the parton model level they can be interpreted as the probability density of a parton with momentum fraction $z = P_h^-/p^-$ to fragment into the observed hadron h. As such the normalization condition for FFs is given by

$$\sum_h \int dz \; z \; D_q^h = 1 \tag{1.98}$$

As we will extensively discuss in the following chapters, FFs are also extracted from data through global fits.

1.2.3 Factorization

In the previous section we introduced the concept of "factorization" which, intuitively, denotes the ability to construct a formalism that separates short- from long-distance behavior. As a starting point for the parton model, we justified Eq.1.42 by assuming that quarks do not interact at short-distant scale. However, this approximation cannot be taken for granted when QCD corrections are taken into account. Thus, Eq.1.42 and 1.91 will no longer describe the correct factorization theorems for higher-order perturbative calculations. The question if a factorization theorem for every perturbative order calculation and for every process exists at all is nowadays still a issue to be resolved. At the time of this thesis a formal proof of factorization exists only for some processes like the DIS and the Drell-Yann mentioned above, whereas a factorization theorem is simply assumed for other processes[1, 38–40, 42]. For those processes, the match between predictions and experimental data is taken to be the best proof for now. In this section we start by considering only NLO QCD corrections to the DIS process and show how it is possible to express the structure functions in an equivalent factorized form as in Eq. 1.69.

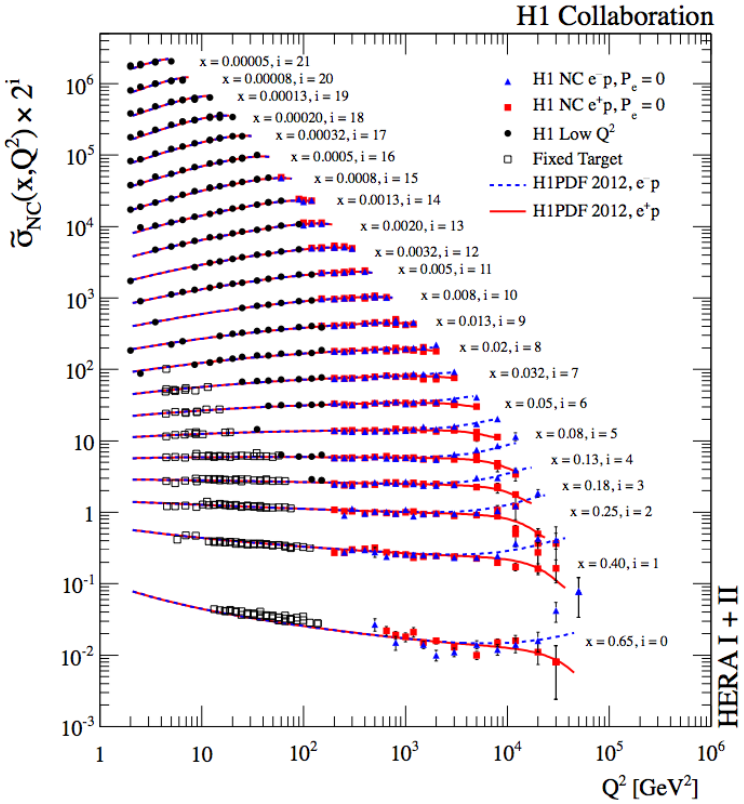

Figure 1.13: Measurements of unpolarized cross section for e^-p (solid trangles) and e^+p (solid squares) at various fixed x [43].

It turns out that divergent contributions coming from configurations when a gluon is emitted collinear to the parton can be handled in a similar way as the ultra violet (UV) divergences in the case of the running coupling. The parton distribution functions as defined in the previous section can be viewed as the "bare" unphysical quantities which can be related to "physical" PDFs through a procedure called *factorization* and equivalet to renormalization. Similarly to the renormalization procedure discussed in Sec. 1.2.1, factorization introduces a factorization scale μ and a set of renormalization group equations called DGLAP equations regulating the *evolution* (i.e. the "running") of PDFs. Since physical PDFs become then scale dependent, the *Bjorken scaling* is violated. The precise prediction of this violation in DIS was one of the greatest achievements of pQCD. Fig. 1.13 shows an example of such predictions.

Continuing the discussion from last section, one can try to rewrite the parton model for DIS

including the $\mathcal{O}(\alpha_s)$ corrections by substituting Eq.1.90 for the hard scattering with

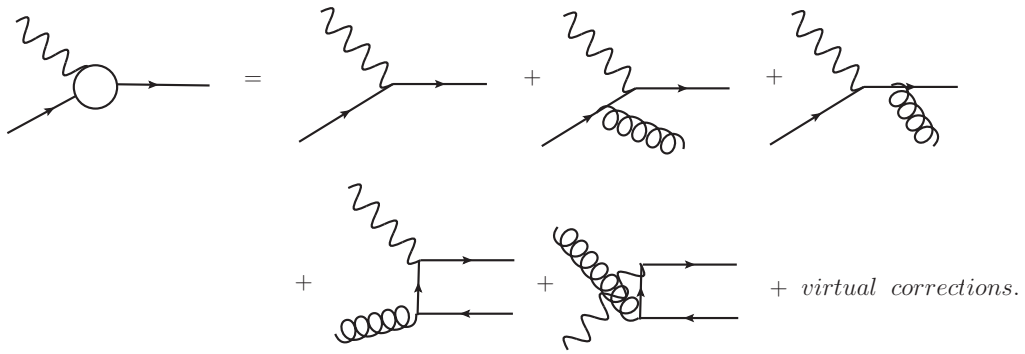

(1.99)

However, diagrams of the type shown in Fig.1.14 are affected by two kinds of divergences: the so-called *soft* and *collinear* divergences. They are a direct consequence of the emission of a *real* gluon. The fermion line connecting the two vertices is described by a propagator of the form

$$G \sim \frac{1}{(p_i - k)^2}. \tag{1.100}$$

Because both incoming quark and outgoing gluon are real particles, their on-shell property allows us to write

$$(p_i - k)^2 = -2p_i k = -2|p_i||k|(1 - \cos\theta), \tag{1.101}$$

where θ is the angle between the quark and the emitted gluon. According to the KLN theorem [44, 45], the soft divergence (i.e for $|k| = 0$) does not constitute a problem, since it is cancelled after adding real and virtual correction together. On the other side, the remaining collinear divergence (i.e. for $\theta = 0$) has to be treated in a similar way as the UV loop divergences are treated by renormalization. We follow a similar procedure to the one used to renormalize the coupling constant, wherein this time the quantities to be redefined are the PDFs. To regularize the divergences we use the dimensional regularization scheme, thus we introduce an arbitrary scale μ and we make the substitution $\alpha_s \to \alpha_s(\mu)^{2\epsilon}$. Moreover, Eq.1.102 has to be modified to

$$M(-g^{\mu\nu}\hat{W}_{\mu\nu}) = (1 - \epsilon)\hat{\mathcal{F}}_2(z) - \left(\frac{3}{2} - \epsilon\right)\hat{\mathcal{F}}_L(z). \tag{1.102}$$

The complete NLO QCD contributions to the hard process, include both virtual and real

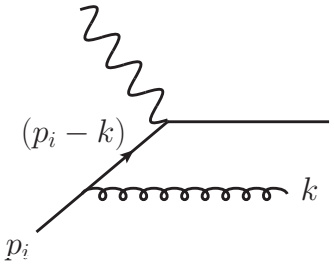

Figure 1.14: Example of Feynman diagram affected by soft and collinear divergences.

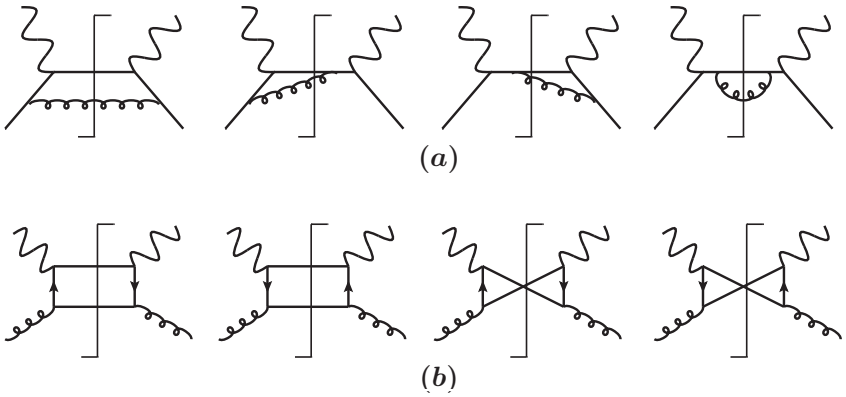

Figure 1.15: Cut diagrams for the real contributions to the NLO DIS hard process.

corrections of order $\mathcal{O}(\alpha_s)$. In Fig.1.15 the cut diagrams for the real contributions are shown whereas the virtual contributions are shown in Fig. 1.16. To understand how factorization works at NLO, let's consider explicit results [33] for the contributions to the to the partonic structure function $\hat{\mathcal{F}}_2$ given by the process $\gamma^*(q)q(p_i) \to q(p_i')g(k)$ shown in Fig.1.15a. The $\mathcal{O}(\alpha_s)$ corrections to the longitudinal partonic structure function $\hat{\mathcal{F}}_L$ are finite and hence do not require regularization of divergences and are not of interest for the discussion of this section. The explicit calculation follows straightforward from Eq.1.72 without any particular problem and can be found for example in [46]. The result is the following:

$$\begin{aligned}
&\hat{\mathcal{F}}_L(z) = \hat{\mathcal{F}}_L^{(0)}(z) + \frac{\alpha_s}{2\pi}\hat{\mathcal{F}}_L^{(1)}(z) + \mathcal{O}(\alpha_s^2) \\
&\hat{\mathcal{F}}_L^{(0)}(z) = 0 \quad \text{(see last section)} \\
&\hat{\mathcal{F}}_L^{(1)}(z) = e_i^2 C_F 2z.
\end{aligned} \tag{1.103}$$

To be noticed is the fact that the *Callan-Gross relation* doesn't hold beyond LO.

With the definitions

$$\begin{aligned}
\hat{s} &= (p_i + q)^2 \approx 2p_i \cdot q - Q^2, \\
\hat{t} &= (p_i - k)^2 \approx 2p_i \cdot k, \\
\hat{u} &= (p_i - p_i')^2 \approx 2p_i \cdot p_i', \\
y &= \frac{1}{2}(1 + cos\theta)
\end{aligned} \tag{1.104}$$

the averaged amplitude squared summed over the transverse polarization states (i.e. contracted with $-g^{\mu\nu}$, see Eq. 1.66) reads

$$\sum_{\varepsilon} \overline{|\mathcal{M}_{\gamma^* q \to gq}|^2} = 4\alpha_s e_i^2 C_F (1-\epsilon)(\mu^2)^\epsilon \left\{ (1-\epsilon)\left(\frac{\hat{s}}{-\hat{t}} + \frac{-\hat{t}}{\hat{s}}\right) - \frac{2\hat{u}q^2}{\hat{s}\hat{t}} + 2\epsilon \right\}, \tag{1.105}$$

whereas the phase space $PS = \int dPS$ for two outgoing particles reads

$$PS = \frac{1}{8\pi}\left(\frac{4\pi}{\hat{s}}\right)^\epsilon \frac{1}{\Gamma(1-\epsilon)} \int_0^1 dy (y(1-\epsilon))^{-\epsilon}. \tag{1.106}$$

In the c.m.s. $p_i + q = (\sqrt{\hat{s}}, 0, 0, 0)$ we define

$$\hat{s} = \frac{Q^2(1-z)}{z}, \qquad \hat{t} = \frac{-Q^2}{z}(1-y), \qquad \hat{u} = \frac{-Q^2}{z}y, \tag{1.107}$$

and putting together Eq.1.105, 1.106 and 1.103 in Eq.1.102, we obtain:

$$\begin{aligned}
\hat{\mathcal{F}}_2\Big|_{\text{real}} =& \frac{\alpha_s}{2\pi} e_i^2 C_F \left(\frac{4\pi\mu^2}{Q^2}\right)^\epsilon \frac{1}{\Gamma(1-\epsilon)} \Bigg\{ \overbrace{3z}^{\substack{\textbf{longitudinal} \\ \textbf{contribution}}} + z^\epsilon (1-z)^{-\epsilon} \int_0^1 dy (y(1-y))^{-\epsilon} \\
& \times \left[\left(\frac{1-z}{1-y} + \frac{1-y}{1-z} \right)(1-\epsilon) + \frac{2zy}{(1-z)(1-y)} \right] \Bigg\} \\
=& \frac{\alpha_s}{2\pi} e_i^2 C_F \left(\frac{4\pi\mu^2}{Q^2}\right)^\epsilon \frac{\Gamma(1-\epsilon)}{\Gamma(1-2\epsilon)} \left\{ \frac{2}{\epsilon^2}\delta(1-z) \frac{1}{\epsilon} \left(\frac{1+z^2}{(1-z)_+} \right) + \frac{3}{2\epsilon}\delta(1-z) \right. \\
& \left. + \left[(1+z^2) \left(\frac{\ln(1-z)}{1-z} \right)_+ - \frac{3}{2} \frac{1}{(1-z)_+} - \frac{1+z^2}{1-z} \ln z + 3 + 2z + \frac{7}{2}\delta(1-z) \right] \right\}.
\end{aligned} \tag{1.108}$$

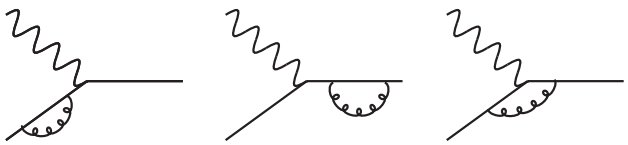

Figure 1.16: Virtual contributions to the NLO DIS hard process.

In the last equality we have defined the *plus distribution* as

$$g_+[h] = \int_0^1 dz h(z) g_+(z) \equiv \int_0^1 dz (h(z) - h(z_0)) g(z), \tag{1.109}$$

where z_0 is a singular point of the parent $g(z)$ function and $h(z)$ is a smooth test function. To go from the first to the second equality in Eq. 1.108 the following identity was used:

$$z^\epsilon (1-z)^{-1-\epsilon} \equiv -\frac{1}{\epsilon}\delta(1-z) + \frac{1}{(1-z)_+} - \left(\frac{\ln(1-z)}{1-z}\right)_+ + \epsilon \frac{\ln z}{1-z} + \mathcal{O}(\epsilon^2). \tag{1.110}$$

To calculate the virtual corrections we have to take into account the two possible self-energy corrections and the vertex correction shown in Fig.1.16. Choosing the *Landau gauge*, i.e. setting $\xi = 0$ in the gluon propagator (see Fig.1.3), not only both self energy and vertex corrections are individually UV finite (hence, there is no need for a quark-wave function renormalization), but also in the dimensional regularization the self energy vanishes at $\mathcal{O}(\alpha_s)$ for massless quarks [47]. Thus, the only virtual contribution to the invariant amplitude squared comes from the vertex correction:

$$\overline{|\mathcal{M}|^2}\Big|_{\text{virtual}} = \sum_\sigma 2\Re \left| \quad \cdot \quad \right|^2 + \mathcal{O}(\alpha_s^2). \tag{1.111}$$

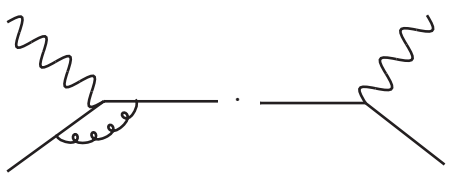

The calculation is similar to the one made for the real correction and the result is the following:

$$\hat{\mathcal{F}}_2\Big|_{\text{virtual}} = e_i^2 \delta(1-z) \left\{ 1 + \frac{\alpha_s}{2\pi} C_F \left(\frac{4\pi\mu^2}{Q^2}\right)^\epsilon \frac{\Gamma(1-\epsilon)}{\Gamma(1-2\epsilon)} \left[-\frac{2}{\epsilon^2} - \frac{3}{\epsilon} - 8 - \frac{1}{3}\pi^2 \right] \right\}. \tag{1.112}$$

Using the expansion of the Γ function

$$\Gamma(\epsilon) = \frac{1}{\epsilon} - \gamma_E \epsilon + \frac{\epsilon}{2}\left(\gamma_E^2 + \frac{\pi^2}{6}\right) + \dots \tag{1.113}$$

and the expansion of the exponential $a^\epsilon = e^{\epsilon \ln a} \approx 1 + \epsilon \ln a$, we can write

$$\left(\frac{4\pi\mu^2}{Q^2}\right)^\epsilon \frac{\Gamma(1-\epsilon)}{\Gamma(1-2\epsilon)} \approx 1 + \epsilon\left(\ln 4\pi - \gamma_E - \ln\frac{Q^2}{\mu^2}\right). \tag{1.114}$$

We can now add together the virtual and real contributes:

$$\begin{aligned}\hat{\mathcal{F}}_2 = \hat{\mathcal{F}}_2\Big|_{\text{real}} + \hat{\mathcal{F}}_2\Big|_{\text{virtual}} &= \delta(1-z) + \frac{\alpha_s}{2\pi}P_{qq}(z)\left(\ln\frac{Q^2}{\mu^2} - \frac{1}{\epsilon} + \gamma_E - \ln 4\pi\right) \\ &+ \frac{\alpha_s}{2\pi}C_F\left[(1+z^2)\left(\frac{\ln(1-z)}{1-z}\right)_+ - \frac{3}{2}\frac{1}{(1-z)_+}. - \frac{1+z^2}{1-z}\ln z + 3 + 2z - \left(\frac{9}{2} + \frac{1}{3}\pi^2\right)\delta(1-z)\right].\end{aligned} \tag{1.115}$$

The term in $\mathcal{O}(1/\epsilon^2)$ has cancelled in the summation. This is the anticipated cancellation of soft singularities.

$$P_{qq}(z) = C_F\left(\frac{1+z^2}{(1-z)_+} + \frac{3}{2}\delta(1-z)\right) = C_F\tilde{P}_{qq}(z) \tag{1.116}$$

is an *Altarelli-Parisi splitting function* and describes the probability to find a "quark into a quark", i.e. the probability for a quark to emit a gluon and become a quark with momentum reduced by a fraction z. We will leave the discussion of splitting functions for the conclusion of this section.

The complete NLO calculation incorporates also the $\gamma^* g \to q$ hard process (see Fig.1.15b), which we are not going to explicitly calculate. Using the corresponding version of Eq.1.69 for F_2 together with the result 1.115 and the gluon-absorption corrections, the conclusive LO+NLO

result for the DIS structure function $\mathcal{F}_2$ yields

$$\frac{F_2(x,Q^2)}{x} = \int_x^1 \frac{dz}{z} \sum_{i=q,\bar{q}} e_i^2 \Bigg\{ \left[\delta(1-z) + \frac{\alpha_s}{2\pi} P_{qq}(z) \left(\ln \frac{Q^2}{\mu^2} - \frac{1}{\epsilon} + \gamma_E - \ln 4\pi \right) + \frac{\alpha_s}{2\pi} C_q'^2(z) \right] f_i^0 \left(\frac{x}{z}\right) + \left(\sum_{i=q,\bar{q}} e_i^2 \right) \left[\frac{\alpha_s}{2\pi} P_{qg}(z) \left(\ln \frac{Q^2}{\mu^2} - \frac{1}{\epsilon} + \gamma_E - \ln 4\pi \right) + \frac{\alpha_s}{2\pi} C_g'^2(z) \right] f_g^0 \left(\frac{x}{z}\right) \Bigg\}. \tag{1.117}$$

The second line of the above equation comes from the $\gamma^* g \to q$ contribution which appears only starting from $\mathcal{O}(\alpha_s)$. $C_q'^2(z)$ and $C_g'^2(z)$ are finite function which are listed below:

$$\begin{aligned} C_q'^2 =& C_F \left[(1+z^2) \left(\frac{\ln(1-z)}{1-z} \right)_+ - \frac{3}{2} \frac{1}{(1-z)_+} - \frac{1+z^2}{1-z} \ln z + 3 + 2z - \left(\frac{9}{2} + \frac{1}{3}\pi^2 \right) \delta(1-z) \right] \\ C_g'^2 =& P_{qg}(z) \ln \frac{1-z}{z} + 3z(1-z) \end{aligned} \tag{1.118}$$

where

$$P_{qg}(z) = T_R \left[z^2 + (1-z)^2 \right] = T_R \tilde{P}_{qg}(z) \tag{1.119}$$

is another splitting function describing the probability to "find a quark into a gluon".
The quantity F_2 expressed by Eq.1.117 is not well-defined for $\epsilon \to 0$ and cannot be used to describe a physical observable. To get rid of this divergencies we proceed, as for the renormalization, by redefining the "parameters of the theory", which in this case are represented by the "bare" parton distribution functions f_i^0 and f_g^0. To formally perform this operation at all perturbative orders, we have to introduce the *transition functions* Γ_{ik}, which are assumed to have a perturbative expansion in α_s:

$$\Gamma_{ik}(z) = \delta_{ik}\delta(1-z) + \sum_{n=1}^{\infty} \left(\frac{\alpha_s}{2\pi} \right)^n \Gamma_{ik}^{(n)}(z). \tag{1.120}$$

For DIS, the "bare" partonic structure function $\hat{\mathcal{F}}_i$ can be expressed in terms of the physical (finite) partonic structure function $\hat{\bar{\mathcal{F}}}_k$ as

$$\hat{\mathcal{F}}_i = \Gamma_{ik} \otimes \hat{\bar{\mathcal{F}}}_k. \tag{1.121}$$

Note that, due to the general nature of this discussion, we dropped the indices L, 1 or 2 denoting the type of structure function we consider. The i index refers to the parton i. Furthermore, according to Eq.1.69 the structure function can be written in terms of the "bare" PDFs:

$$F = \sum_i f_i^0 \otimes \hat{\mathcal{F}}_i \tag{1.122}$$

Using Eq.1.121 in the above equation, we obtain

$$F = \sum_i f_i^0 \otimes \Gamma_{ik} \otimes \hat{\bar{\mathcal{F}}}_k = \sum_k f_k \otimes \hat{\bar{\mathcal{F}}}_k, \tag{1.123}$$

where $f_k = f_i^0 \otimes \Gamma_{ik}$ is the "renormalized" PDF. The DIS factorization theorem, as expressed in Eq.1.123, is well defined for all perturbative orders. The existence of such a transition function Γ_{ik} is a technical issue that we are not going to discuss. For further details refer to the citations mentioned in the introduction of this section. Using Eq.1.120, at first order Eq.1.121 becomes

$$\hat{\mathcal{F}}_i^{(0)} + \frac{\alpha_s}{2\pi}\hat{\mathcal{F}}_i^{(1)} = \hat{\bar{\mathcal{F}}}_i^{(0)} + \frac{\alpha_s}{2\pi}\left[\hat{\bar{\mathcal{F}}}_i^{(1)} + \Gamma_{ik}^{(1)} \otimes \hat{\bar{\mathcal{F}}}_k^{(0)}\right], \tag{1.124}$$

where the following perturbative expansions for the partonic structure function were taken:

$$\begin{aligned} \hat{\bar{\mathcal{F}}}_i &= \sum_{n=1}^{\infty} \left(\frac{\alpha_s}{2\pi}\right)^n \hat{\bar{\mathcal{F}}}_i^{(n)} \\ \hat{\mathcal{F}}_i &= \sum_{n=1}^{\infty} \left(\frac{\alpha_s}{2\pi}\right)^n \hat{\mathcal{F}}_i^{(n)}. \end{aligned} \tag{1.125}$$

From Eq.1.124 it follows that the "physical" NLO correction to the hard process is

$$\hat{\bar{\mathcal{F}}}_i^{(1)} = \hat{\mathcal{F}}_i^{(1)} - \Gamma_{ik}^{(1)} \otimes \hat{\mathcal{F}}_k^{(0)}. \tag{1.126}$$

Although Eq.1.123 correspond now to the right factorization theorem for DIS, the explicit expression at a given fixed-order calculation depends on the chosen transition function, i.e. on the specific *factorization scheme* used. For example, in the DIS scheme all corrections to the the structure functions are absorbed in the PDF so that the simple expression for the parton model (Eq.1.78) holds at all orders in pQCD. Using Eq.1.117 it is easy to see that in the DIS

scheme at NLO the PDFs have to be redefined as follows

$$f_i^{DIS}\left(x,\frac{Q^2}{\mu_F}\right) = f_i^0(x) + \int_x^1 \frac{dz}{z}\Bigg\{ \left[\frac{\alpha_s}{2\pi}P_{qq}(z)\left(\ln\frac{Q^2}{\mu_F^2} - \frac{1}{\epsilon} + \gamma_E - \ln 4\pi\right) + \frac{\alpha_s}{2\pi}C_q'^2(z)\right] f_i^0\left(\frac{x}{z}\right) + \left[\frac{\alpha_s}{2\pi}P_{qg}(z)\left(\ln\frac{Q^2}{\mu_F^2} - \frac{1}{\epsilon} + \gamma_E - \ln 4\pi\right) + \frac{\alpha_s}{2\pi}C_g'^2(z)\right] f_g^0\left(\frac{x}{z}\right)\Bigg\}, \tag{1.127}$$

where, as it happens for the renormalization, μ_F is an arbitrary mass scale introduced by the the factorization scheme. In the above equation the factorization scale was set equal to the regularization scale, i.e. $\mu = \mu_F$. Compare also with [33].
A more used scheme is the $\overline{\text{MS}}$, where, as explained in section 1.2.1, in addition to the singularities in ϵ, the $-\gamma_E + \ln 4\pi$ factor is absorbed in the redefinition of the PDFs at all orders in pQCD. In this scheme the factorization theorem for DIS can be written as

$$F_i(x,Q^2) = \sum_f \int_x^1 \frac{dy}{y}\mathcal{C}_f^i\left(\frac{x}{y},\frac{Q^2}{\mu^2},\frac{\mu_F^2}{\mu^2},\alpha_s(\mu^2)\right) f\left(y,\mu_F^2,\mu^2\right), \tag{1.128}$$

where $f\left(y,\mu_F^2,\mu^2\right)$ is the redefined PDF for a parton $f = q,\bar{q},g$ and $i = 1,2,L$ denotes either one of the two transversal structure functions ($T = 1,2$) or the longitudinal one (L). The expression 1.128 holds for any fixed-order calculation in pQCD up to corrections that are suppressed by the power $\frac{1}{Q^2}$ when Q^2 is large enough. The $\mathcal{C}_f^i = C_f^{i,(0)} + \frac{\alpha_s}{2\pi}C_f^{i,(1)} + \mathcal{O}(\alpha_s^2)$ are perturbatively calculable and are called *the coefficient functions* of the hard process. For each order they are independent from the soft process, i.e. from the hadron considered in the scattering. The complete set of coefficient functions for the DIS can be found in [48]. To be consistent with the logic of this section, we list the two coefficient functions $C_q^{2,(1)}$ and $C_g^{2,(1)}$ for the NLO correction to F_2/x:

$$\begin{aligned} C_q^{2,(1)}\left(z,\frac{Q^2}{\mu_F^2}\right) &= e_q^2\left[C_F\tilde{P}_{qq}(z)\ln\left(\frac{Q^2}{\mu_F^2}\right) + C_q'^2(z)\right] \\ C_g^{2,(1)}\left(z,\frac{Q^2}{\mu_F^2}\right) &= e_q^2\left[T_R\tilde{P}_{qg}(z)\ln\left(\frac{Q^2}{\mu_F^2}\right) + C_g'^2(z)\right], \end{aligned} \tag{1.129}$$

where we implicitly took $\mu_F = \mu$.

As it is shown in Eq 1.128, both the "renormalized" parton functions and the coefficient func-

tions will be μ_F scale dependent. Referring to the $\overline{\text{MS}}$ scheme, it is easy to see that imposing $\mu_F = Q^2$ we transfer most of the μ_F dependence to the PDFs. In NLO, for example, this condition cancels completely the μ_F dependence from the coefficient functions (see Eq.1.129). As it happens for the renormalization of the coupling constant, the logic requirement that a physical observable is not dependent on the arbitrary factorization scale, in our case

$$\mu_F^2 \frac{d}{d\mu_F^2} F_i(x, Q^2) = 0, \tag{1.130}$$

translates itself in a set of coupled equations for the PDFs ruling their μ_F dependance. As anticipated, those *evolution equations* are called DGLAP (*Dokshitzer-Gribov-Lipatov-Altarelli-Parisi equations*)[49, 50] and can be written in a integro-differential form:

$$\mu_F^2 \frac{d}{d\mu_F^2} f_i(x, \mu_F^2) = \sum_{j=f,\bar{f},g} \int_x^1 \frac{dy}{y} \mathcal{P}_{ij}\left(\frac{x}{y}, \alpha_s(\mu_R^2 = \mu_F^2)\right) f_j(y, \mu_F^2), \tag{1.131}$$

where the $\mathcal{P}_{ij}$ are the Altarelli-Parisi evolution kernels (or splitting functions) which can be perturbative expanded in α_s

$$\mathcal{P}_{ij} = P_{ij}^{(0)} + \frac{\alpha_s}{2\pi} P_{ij}^{(1)} + \mathcal{O}(\alpha_s^2) \tag{1.132}$$

Eqs.1.116 and 1.119 show the null order expansion terms for the $\mathcal{P}_{qq}$ and $\mathcal{P}_{qg}$ respectively.
Within the $\overline{\text{MS}}$ approach, Eq.1.131 corresponds to the he renormalization-group equation for the parton densities and hence, we can obtain the splitting functions directly from the transition function Γ_{ij}:

$$\sum_{j'} \mathcal{P}_{jj'} \otimes \Gamma_{j'k} = \frac{d}{d \ln \mu_F} \Gamma_{jk}. \tag{1.133}$$

Introducing the following notation for the "non-singlet" (f^{NS}) and "singlet" (Σ) PDFs

$$f^{NS} = f_i - f_{\bar{i}}, \qquad \Sigma = \sum_i (f_i + f_{\bar{i}}), \tag{1.134}$$

Eq.1.131 can be written as

$$\frac{\partial f^{NS}}{\partial \ln \mu_F^2} = \frac{\alpha_s(\mu_F^2)}{2\pi} \mathcal{P}_{qq} \otimes f^{NS}$$
$$\frac{\partial}{\partial \ln \mu_F^2} \begin{pmatrix} \Sigma \\ f_g \end{pmatrix} = \frac{\alpha_s(\mu_F^2)}{2\pi} \begin{pmatrix} \mathcal{P}_{qq} & 2N_f\mathcal{P}_{qg} \\ \mathcal{P}_{gq} & \mathcal{P}_{gg} \end{pmatrix} \otimes \begin{pmatrix} \Sigma \\ f_g \end{pmatrix}, \tag{1.135}$$

where N_f is the number of chosen quark flavours.
For the sake of completeness, in addition to Eq.1.116 and 1.119 we list also the LO expansion terms $P_{gq}^{(0)} \equiv P_{gq}$ and $P_{gg}^{(0)} \equiv P_{gg}$

$$\begin{aligned} P_{gq}(z) =& C_F \left(\frac{1 + (1-z)^2}{z} \right) \\ P_{gg}(z) =& 2C_A \left(\frac{1-z}{z} + z(1-z) + \frac{z}{(1-z)_+} \right) + \left(\frac{11}{6} C_A - \frac{2}{3} T_R N_f \right) \delta(1-z). \end{aligned} \tag{1.136}$$

We refrain here from discussing evolution of fragmentation functions since it will be extensively treated in the next chapter. As we shall see they undergo the same type of evolution, where, in this case, the evolution kernels will be a time-like version of the discussed splitting functions.

1.2.4 Two examples of soft gluon resummation

Threshold resummation for DIS

In the last section we have presented explicit NLO-result for the DIS structure function F_2. If we take a close look on the expression for the hard process (see Eq.1.115), we note that contributions of type

$$\alpha_s \left(\frac{\ln(1-z)}{1-z} \right)_+, \qquad \alpha_s \frac{1}{(1-z)_+} \tag{1.137}$$

are present. In general it can be shown that at $\mathcal{O}(\alpha_s^n)$ contributions proportional to

$$\alpha_s^n \left(\frac{\ln^m(1-z)}{1-z} \right)_+, \qquad m \leq 2n-1 \tag{1.138}$$

are always present [51–53]. Independently from the scale Q^2 we choose, at the phase space boundary where $z \to 1$ (*threshold limit*) those terms can spoil the validity of the perturbative expansion, even when $\alpha_s \ll 1$. To be able to get reliable results, a standard procedure is to sum to all orders the most important contributions of the type 1.138 and add them to the fixed-order perturbative calculation made for the specific hard process. Such an operation is called *resummation*. There are many ways to approach the problem. Among the most used ones, we list "the renormalization group approach" [54], "the resummation from strong factorization properties"[51], "the resummation from effective field theory"[55, 56] and "the eikonal approach"[52]. For the work of this thesis only the last one was is relevant. Because the proof of the resummation's formulas is a technical issue that lies outside the aims of this thesis, in this section we just give an idea of how the eikonal approach works for the QED case and then only sketch the generalization for the QCD case. We follow closely Section 2.3 of [57].

Let's consider in the DIS hard process the case where n extra partons are emitted. All outgoing impulses will be denoted with k_i, where $i \in \{1, \ldots, n+1\}$ and $k_{n+1} = p'$ is the LO outgoing parton. From the conservation of the impulse it follows that

$$\hat{s} = (p+q)^2 = (k_1 + \ldots + k_{n+1}) \tag{1.139}$$

which, using Eq.1.107, becomes

$$\frac{Q^2(1-z)}{z} = \sum_{i,j=1}^{n+1} k_i^0 k_j^0 (1 - \cos\theta_{ij}), \tag{1.140}$$

where θ_{ij} is the angle between $\boldsymbol{k}_i$ and $\boldsymbol{k}_j$. The above relation states that for $z \to 1$ only soft partons and sets of partons collinear to each others can be emitted. However, with a more careful analysis of the DIS kinematics and phase space, one could show that the k_i^0s are always proportional to $\frac{\sqrt{\hat{s}}}{2}$ and, hence, also in the collinear case the emitted partons turn out to be soft (see Section 3.2 of [57]). In the Drell-Yann case Eq.1.140 becomes

$$\begin{aligned} \hat{s} = (p_1 + p_2)^2 = \frac{Q^2(1-z)}{z} &= (Q + k_1 + \ldots + k_n)^2 \\ &= \sum_{i,j=1}^{n} k_i^0 k_j^0 (1 - \cos\theta_{ij}) + 2\sum_{i,j}^{n} k_i^0 \sqrt{Q^2 + |\boldsymbol{Q}|^2} - |\boldsymbol{Q}| \cos\theta_i, \end{aligned} \tag{1.141}$$

where θ_i is the angle between $\boldsymbol{k}_i$ and $\boldsymbol{Q}$. Since $(p_1 + p_2)^2$, $\sqrt{Q^2 + |\boldsymbol{Q}|^2} - |\boldsymbol{Q}| \cos\theta_i$ and

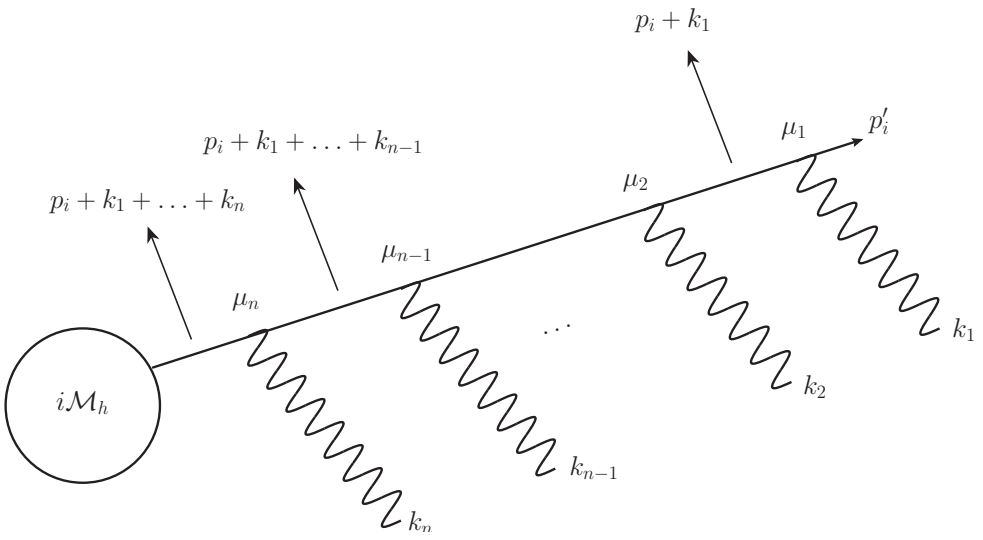

Figure 1.17: An external fermion line with n extra photon emitted. The white blob indicates the hard scattering amplitude ($i\mathcal{M}_h$) without one external fermion line.

$\sum_{i,j=1}^{n} k_i^0 k_j^0 (1 - \cos\theta_{ij})$ are positive defined quantities, also here for $z \to 1$ only soft partons ($k_i \to 0$) can be emitted.

In the eikonal approach we take the soft limit as a starting point to calculate the contribution of n emitted extra partons. Let's consider the diagram of Fig.1.17 where, together with the parton p', n soft photons are emitted. In the *eikonal approximation* (also called *soft approximation*) we neglect every $(k_1 + ... + k_i)^2$ contribution in the denominator of all propagators and every $\not{k}_i$ in the numerator. In this approximation, the amplitude of the diagram shown in Fig.1.17 can be written as follows:

$$\bar{u}(p')(-ie\gamma^{\mu_1})\frac{i\not{p}'}{2p'\cdot k_1}(-ie\gamma^{\mu_2})\frac{i\not{p}'}{2p'\cdot(k_1+k_2)}\cdots(-ie\gamma^{\mu_n})\frac{i\not{p}'}{2p'\cdot(k_1+\ldots+k_n)}i\mathcal{M}_h. \qquad (1.142)$$

Using the Dirac equation $\bar{u}(p')\not{p}' = 0$ and the anti-commutation relation of the γ-matrices we can rearrange the factors in the numerator in the following way:

$$\bar{u}(p')\gamma^{\mu_1}\not{p}'\gamma^{\mu_2}\not{p}'\ldots\gamma^{\mu_n}\not{p}' = \bar{u}(p')2p'^{\mu_1}\gamma^{\mu_2}\not{p}'\ldots\gamma^{\mu_n}\not{p}' = \bar{u}(p')2p'^{\mu_1}2p'^{\mu_2}\ldots 2p'^{\mu_n}. \qquad (1.143)$$

Hence Eq.1.142 becomes

$$e^n\bar{u}(p')\left(\frac{p'^{\mu_1}}{p'\cdot k_1}\right)\left(\frac{p'^{\mu_2}}{p'\cdot(k_1+k_2)}\right)\ldots\left(\frac{p'^{\mu_n}}{p'\cdot(k_1+\ldots+k_n)}\right)i\mathcal{M}_h \qquad (1.144)$$

To obtain the total amplitude, we should sum over the set of diagrams resulting from all $n!$ possible permutation $P(i)$ of the momenta $k_1 \dots k_n$. To do that we can use the so-called *eikonal identity*

$$\sum_P \frac{1}{p \cdot k_{P(1)}} \frac{1}{p \cdot (k_{P(1)} + k_{P(2)})} \cdots \frac{1}{p \cdot (k_{P(1)} + \cdots + k_{P(n)})} = \frac{1}{p \cdot k_1} \cdots \frac{1}{p \cdot k_n}, \tag{1.145}$$

which combined with Eq.1.144 gives us

$$e^n \bar{u}(p') \left(\frac{p'^{\mu_1}}{p' \cdot k_1} \right) \left(\frac{p'^{\mu_2}}{p' \cdot k_2} \right) \cdots \left(\frac{p'^{\mu_n}}{p' \cdot k_n} \right) i\mathcal{M}_h. \tag{1.146}$$

Let's now consider an initial fermion line with momentum p. In this case Eq.1.142 becomes

$$\bar{u}(p)(-ie\gamma^{\mu_1}) \frac{i\not{p}}{2p \cdot (-k_1)} (-ie\gamma^{\mu_2}) \frac{i\not{p}}{2p \cdot (-k_1 - k_2)} \cdots (-ie\gamma^{\mu_n}) \frac{i\not{p}}{2p \cdot (-k_1 - \ldots - k_n)} i\mathcal{M}_h. \tag{1.147}$$

We can generalize Eq.1.146 for the case where we sum over all possible diagrams containing n soft photons connected in any possible order to j initial and final fermion lines:

$$e^n i\mathcal{M}_0 \prod_{i=1}^{n} \sum_j \frac{\eta_j p^{\mu_j}}{p_j \cdot k_i}. \tag{1.148}$$

where

$$\eta_j = \begin{cases} 1 & \text{for a final fermion line} \\ -1 & \text{for an initial fermion line} \end{cases} \tag{1.149}$$

and $i\mathcal{M}_0$ is the remaining matrix elements without ingoing and outgoing fermion lines. Let's consider now the case where only one real photon is emitted, thus we set $n = 1$ in equation 1.148. To obtain the cross section in this case we have to add the corresponding polarization vector for the real photon, sum over the possible polarizations and integrate over the phase space:

$$Y = \int \frac{d^3k}{(2\pi)^2 2k^0} e^2 \left(\sum_j \frac{\eta_j p_j}{p_j \cdot k} \right)^2 \delta \left(\sum_j \eta_j p_j - k \right). \tag{1.150}$$

The phase space factorizes the Mellin space (see Appendix B) since the delta function can be written as the inverse Mellin transform of 1. Thus, the whole expression 1.150 factorizes in Mellin space. Recalling Eq.1.148, we obtain that in Melling space the total cross section

("resummed") for the emission of any number of soft photon is

$$\sigma^{(N)}_{\text{resummed}} = \sigma^{(N)}_0 \sum_{n=0}^{\infty} \frac{Y^{(N)n}}{n!} = \sigma^{(N)}_0 e^{Y^{(N)}}, \tag{1.151}$$

where the index (N) denote the Mellin moments of the respective quantities and σ_0 is the hard cross section for the process without extra soft emission. The factor $\frac{1}{n!}$ comes from the symmetry of the n identical boson in the final state.
Y still contains the collinear and soft divergences that we encountered in the last section. Adding the virtual corrections and subtracting the collinear divergences, we obtain

$$\sigma^{(N)}_{\text{resummed}} = \sigma^{(N)}_0 e^{\sigma^{(N)}_1}, \tag{1.152}$$

where $\sigma^{(N)}_1$ is the Mellin moment of the cross section of the hard process where only one extra soft emission in taken into account. In technical jargon we say that the *eikonal hard scattering functions* σ_1 exponentiate in Mellin space, leading to the resummed result. The higher is the fixed-order at which we can calculate σ_1, the more accurate will be the resummed result.
The generalization to the QCD case is a non-trivial issue since the presence of three-gluon vertices between soft gluons complicates the above sketched factorization of the terms. The exponentiation of soft emission still works, but the eikonal hard scattering functions will in general be different from σ_1 of the fixed-order calculation since only a subset of the eikonal diagrams appear in the exponent with *modified color factors*. The *non-abelian eikonal exponentiation* was discovered and proven in [58–60]. Hereinafter we highlight the main concepts of this proof following closely [61].
The theorem states that a given cross section X with two external colored fermion lines exponentiates in the eikonal approximation similarly to the QED case, i.e.

$$\sigma^{\text{eik, }(N)} \equiv X = e^Y. \tag{1.153}$$

However, the exponent Y has the following properties:

- it can be recursively defined and can be expressed as perturbative series of terms, each of which corresponds to a Feynman diagram;
- only a subset of diagrams contributing to X and called *webs* contribute to the exponent Y ;

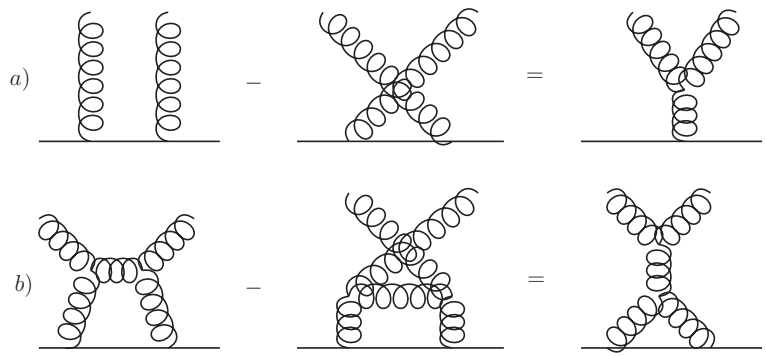

Figure 1.18: The commutation relation a) and the Jacobi identity b) for color-weight diagrams

- the diagrams appearing in Y are dressed with a "modified" *color-weights* which can be calculated recursively and are in general different from the ones in X;

- the phase space must be symmetric in the real gluon momenta.

In order to define the *color-weight* diagrams, one uses the fact that the colour part may be separated from the rest of a QCD diagram. The rules for evaluating colour-weight diagrams follow directly from the color part of the QCD Feynmann rules and can be summarized as follows: every vertex contributes with a color matrix $(t^A)_{ab}$ or a structure function if^{ABC}, whereas a factor δ_{ab} and δ_{AB} is given for every quark and gluon line respectively. Here $a, b \in \{1, 2, 3\}$ and $A, B \in \{1, 2, \ldots, 8\}$. By using the Lie commutator $[t^A, t^B] = if^{ABC}t^C$ and the Jacobi identity $f^{ADE}f^{EBC} + f^{BDE}f^{AEC} + f^{CDE}f^{ABE} = 0$ different diagrams can be related with each others. See Fig. 1.18 for a graphical representation of those relations in the language of color-weight diagrams.

On the other end, the *web* diagrams are defined in [59, 60] as a set of gluon lines, which cannot be partitioned without cutting at least one of its lines. At higher order *c-webs* (connected webs) appear. They are defined as a connected set of gluon lines. Examples of this definitions is given graphically in Fig. 1.19. Moreover, webs can be separated into a Feynmann integral part $\mathcal{F}$ containing all internal eikonal propagators and a modified color-weight $\bar{C}$. For the final result to exponentiate, both parts needs to factorize. For the $\mathcal{F}$-part a non-abelian analogue of the eikonal identity Eq. 1.145 is sufficent for this to happen. The main point of the proof of the theorem lies in the ability of writing each Feynman diagram as a sum of products of c-webs. It can be shown that this can happen once the following definition of a "modified" color weight $\bar{C}$

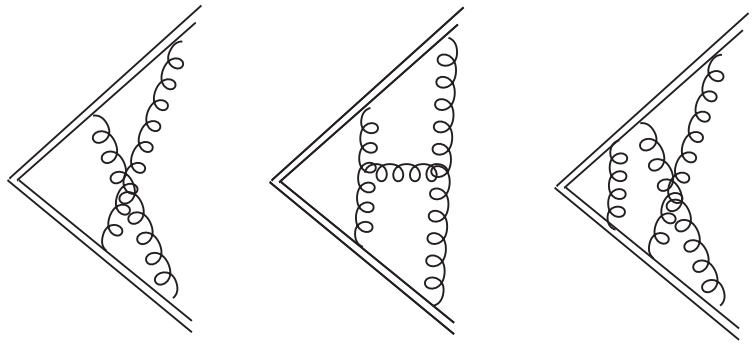

Figure 1.19: Examples of web diagrams: a) is web of $\mathcal{O}(\alpha_s^2)$, b) is a c-web of $\mathcal{O}(\alpha_s^3)$ c) is not a web but a product of a $\mathcal{O}(\alpha_s)$ web and a $\mathcal{O}(\alpha_s^2)$ web. The eikonal lines are indicated by a double line.

is introduced:

$$\begin{aligned}\bar{C}(W^{(m)}) &= \frac{1}{\mathrm{tr}\mathbb{1}} C(W^{(m)}) - \sum_d \prod_{d_i} \bar{C}(W^{(i)}_{n_i}),\\ \bar{C}(W^1) &= \frac{1}{\mathrm{tr}\mathbb{1}} C(W^{(1)}),\end{aligned} \tag{1.154}$$

where $W^{(m)}$ is a web of $\mathcal{O}(\alpha_s^m)$, $C(W^{(m)})$ is a non-modified color weight diagram and $\frac{1}{\mathrm{tr}\mathbb{1}}$ is just a normalization factor. The sum runs over all set of non-trivial decompositions d of $W^{(m)}$ obtained by using the identities in Fig. 1.18. The multiplication is done for all n_i webs of order $i < m$. The final factorization of the Feynmann diagrams is proven by induction and at $\mathcal{O}(\alpha_s^n)$ reads

$$F^n = \sum_{\{n_i\}, \sum_i i\, n_i = n} \prod_i \frac{1}{n_i!} \left(\sum_{\text{webs of order } i} \bar{C}(W^{(i)}) \mathcal{F}(W^{(i)})^{n_i} \right), \tag{1.155}$$

where $\{n_i\}$ is a set of integer with the constraint $\sum_i i\, n_i = n$. The cross section is obtained summing over all possible $F^{(n)}$

$$\begin{aligned} X = \sum_{n=0}^{\infty} F^{(n)} &= \prod_i \exp\left(\sum_{\text{webs of order } i} \bar{C}(W^{(i)}) \mathcal{F}(W^{(i)})^{n_i} \right) \\ &= \exp\left(\sum_i \sum_{\text{webs of order } i} \bar{C}(W^{(i)}) \mathcal{F}(W^{(i)})^{n_i} \right) = e^Y \end{aligned} \tag{1.156}$$

As an example, we report the resummed result for DIS that can be also found in section 3.2.2, written in terms of the resummed transversal coefficient function

$$\begin{aligned}\mathcal{C}_q^{T,\mathrm{res}}(N) &= e_q^2 H_q\left(\alpha_s(Q^2), \frac{Q^2}{\mu^2}\right)\exp\left[\int_0^1 d\xi \frac{\xi^N - 1}{1-\xi}\right. \\ &\left.\times\left\{\int_{Q^2}^{(1-\xi)Q^2}\frac{dk_\perp^2}{k_\perp^2}A_q(\alpha_s(k_\perp^2)) + \frac{1}{2}B_q\left(\alpha_s((1-\xi)Q^2)\right)\right\}\right],\end{aligned} \tag{1.157}$$

where the three functions A_q, B_q and H_q are perturbative calculable. They are listed in section 3.2.2 together with further specific details. Here, we just want to observe how the threshold-limit logarithms coming from the fixed order calculation are connected with Eq.1.157. Let us consider the Mellin transformations of the terms shown in Eq.1.137 when $z \to 1$ (i.e. when $N \to \infty$ in Mellin space; see AppendixB)

$$\begin{aligned}\left(\frac{\ln(1-z)}{1-z}\right)_+ &\longrightarrow \frac{1}{2}\left(\ln^2\bar{N} + \frac{\pi^2}{6}\right) + \mathcal{O}(\ln\bar{N}), \\ \frac{1}{(1-z)_+} &\longrightarrow -\ln\bar{N} + \mathcal{O}\left(\frac{1}{N}\right),\end{aligned} \tag{1.158}$$

where $\bar{N} = Ne^{\gamma_E}$. From Eq.1.158 we deduce that in Mellin space the large threshold logarithms are represented by $\sim \ln^m N$ logarithms, where $m \leq 2k$ for every $\mathcal{O}(\alpha_s^k)$ fixed-order calculation. In Table 1.1 a schematic overview of the soft large logarithms is shown.

LO	1			
NLO	$\alpha_s \ln^2 N$	$\alpha_s \ln N$		
NNLO	$\alpha_s^2 \ln^4 N$	$\alpha_s^2 \ln^3 N$	$\alpha_s^2 \ln^2 N$	$\dots$
$\dots$	$\dots$	$\dots$	$\dots$	$\dots$
$\mathbf{N^kLO}$	$\alpha_s^k \ln^{2k} N$	$\alpha_s^k \ln^{2k-1} N$	$\alpha_s^k \ln^{2k-2} N$	$\dots$
	$\downarrow$ **LL**			

Table 1.1: Threshold logarithms for every fixed-order $\mathrm{N^kLO}$ ($\mathcal{O}(\alpha_s^k)$) calculation.

Let's now consider Eq.1.157 and neglect for simplicity the B_q function since we are not interested in the explicit result but rather in the discussion of more general aspects. The term in the exponent reads then

$$\log \Delta_q^{(N)} \equiv \left[\int_0^1 dx \frac{\xi^N - 1}{1-\xi} \int_{Q^2}^{(1-\xi)^2 Q^2} \frac{dk_\perp^2}{k_\perp^2} A_q(\alpha_s(k_\perp^2)) \right]. \tag{1.159}$$

If we take only the lowest order term in α_s for A_q (see Eq.5.16) together with a fixed value for $\alpha_s = \alpha_s(Q^2)$ the above equation becomes

$$\log \Delta_{q,\,LL}^{(N)} \approx \frac{\alpha_s C_F}{\pi} \int_0^1 dx \frac{\xi^N - 1}{1-\xi} \int_{Q^2}^{(1-\xi)^2 Q^2} \frac{dk_\perp^2}{k_\perp^2} \approx \frac{\alpha_s C_F}{\pi} \ln^2 \bar{N} + \mathcal{O}\left(\frac{1}{N}\right). \tag{1.160}$$

It is easy to see that after expanding the exponent $\Delta_q^{(N)}$, all the terms laying in the first column of Table 1.1 are recovered. Those logarithms are the so-called *leading-logs* (LL). Taking in addition the $\mathcal{O}(\alpha_s^2)$ term for A_q, we resum also the NLL (next-to-leading logs) and so on. Moreover, for the NLL result the two-loop expansion of the strong coupling constant has to be taken into account:

$$\begin{aligned}\alpha_s(k^2) =& \frac{\alpha_s(\mu_0^2)}{1+\beta_0 \alpha_s(\mu_0^2)\ln(k^2/\mu_0^2)} \left[1 - \frac{\beta_1}{\beta_0} \frac{\alpha_s(\mu_0^2)}{1+\beta_0\alpha_s(\mu_0^2)\ln(k^2/\mu_0^2)} \ln(1+\beta_0\alpha_s(\mu_0^2)\ln(k^2/\mu_0^2)) \right. \\ & \left. + \mathcal{O}(\alpha_s^2(\mu_0^2)(\alpha_s(\mu_0^2)\ln(k^2/\mu_0^2))^n) \right],\end{aligned} \tag{1.161}$$

where the β_0 and β_1 coefficient are specified in Eq.1.35. In this case, Eq.1.159 can be written as

$$\log \Delta_{q,\,NLL}^{(N)} \approx \ln \bar{N} h_q^{(1)}(\lambda) + h_q^{(2)}\left(\lambda, \frac{Q^2}{\mu^2}, \frac{Q^2}{\mu_F^2}\right), \tag{1.162}$$

where $\lambda \equiv \beta_0 \alpha_s(\mu^2) \log \bar{N}$. The $\ln \bar{N} h_q^{(1)}(\lambda)$ term collects the "generator" of the leading logarithms $\ln^2 \bar{N}$ of Eq.1.160 plus all logarithms of the form $\alpha_s^k \ln^{k+1} \bar{N}$, which, after expanding the exponent, generate $\alpha_s^{ik} \ln^{i(k+1)} \bar{N}$ ($i \in \{0, \ldots, \infty\}$) logs of the fixed order calculation. The $h_q^{(2)}(\lambda)$ collects all logarithms of the form $\alpha_s^k \ln^k \bar{N}$, thus $\alpha_s^{ik} \ln^{ik} \bar{N}$ logs of the fixed order calculation.

Small-z resummation in single-inclusive e^+e^- annihilation

In the next chapter we will discuss another type of resummation which can be traced back to soft gluon emissions as well. We shall see that in the electron-positron process $e^+e^- \to \gamma/Z(q) \to h(P_h)X$ mediated by an intermediate virtual photon γ or Z and with an observed hadron h in the final state, double logarithmic contributions of type

$$\left(\frac{\alpha_s}{4\pi}\right)^n \frac{1}{z}\log^{2n-l}(z), \tag{1.163}$$

appear both in the time-like splitting functions, regulating the evolution of the FF, and in the coefficient functions. In Eq. 1.163, l is an integer number which depends on the logarithmic accuracy considered and on the type of coefficient function or splitting function in which the logarithm appears (see section 2.3.1 in the next chapter). The scaling variable z is defined in terms of the four momenta P_h and q of the observed hadron and γ/Z boson, respectively, as $z \equiv 2P_h \cdot q/Q^2$.

At LL accuracy, defined in Tabs. 2.1 and 2.2, the double logarithmic contributions can be understood as a specific configuration of the partonic sub process $e^+e^- \to \gamma/Z(q) \to \mathcal{Q}(p) + \bar{\mathcal{Q}}(\bar{p}) + g(k) + X$ in the case the observed hadron is generated by the "observed" gluon g with momentum k. More specifically, leading small-z double logarithm contributions are generated whenever g is soft and the unobserved part consists of $m \to \infty$ soft gluons with momenta $k_1, k_2, \ldots, k_m$, whose three-momenta and angles in respect to the hard quark $\mathcal{Q}$ with momentum p are strongly ordered [62]

$$\begin{aligned} &|\boldsymbol{k}| \ll |\boldsymbol{k}_1| \ll |\boldsymbol{k}_2| \ll \cdots \ll |\boldsymbol{k}_m| \ll \frac{Q^2}{2} \\ &\theta \ll \theta_1 \ll \theta_2 \ll \cdots \ll \theta_m, \end{aligned} \tag{1.164}$$

where $Q^2 \approx (p+\bar{p})^2$ is the process hard scale and $\bar{p}$ is the momentum of the recoiling hard anti-quark $\bar{\mathcal{Q}}$ necessary for momentum conservation since all gluons are assumed to be soft.

By using again the *eikonal* approximation for the soft gluons, it can be shown that the partonic cross section describing this specific configuration factorizes (e.g. see [63, 64])

$$d\hat{\sigma}_{m+1}(p,\bar{p},k) = \sum_{m=0}^{\infty} d\hat{\sigma}_{m+1}(p,\bar{p},k,k_1,k_2,\ldots,k_m)$$

$$= \sum_{m=0}^{\infty} d\hat{\sigma}_B(p,\bar{p}) dw_g(k) dw_g(k_1) dw_g(k_2) \dots dw_g(k_{m-1}) dw_{\mathcal{Q}}(k_m), \tag{1.165}$$

where $dw_I(k)$ describes the probability of emission of a soft gluon from a parton $I = g, \mathcal{Q}, \bar{\mathcal{Q}}$, and $d\hat{\sigma}_B(p,\bar{p})$ is the partonic Born cross section for the $e^+ e^-$ annihilation. In dimensional regularization with $d = 4 - 2\epsilon$

$$dw_I(k_\alpha) = dw_I(y_\alpha, t_\alpha) = \frac{\alpha_s}{\pi} \left(\frac{\mu^2}{Q^2}\right)^{\epsilon} \frac{(4\pi)^\epsilon}{\Gamma(1-\epsilon)} K_I \frac{dy_\alpha}{y_\alpha^{1+2\epsilon}} \frac{dt_\alpha}{t_\alpha^{1+\epsilon}}, \tag{1.166}$$

where $K_{\mathcal{Q}/\bar{\mathcal{Q}}} = C_F = 4/3$ and $K_g = C_A = 3$, and

$$t_\alpha = \frac{p \cdot k_\alpha}{\bar{p} \cdot k_\alpha}, \quad y_\alpha = \frac{\bar{p} \cdot k_\alpha}{\bar{p} \cdot p}. \tag{1.167}$$

Integrating out the unobserved degrees of freedom, fixing the momentum fraction of the "observed gluon" as the experimentally measured momentum fraction (i.e. substituting $dw_g(k) = dw_g(y,t) \to \delta(z-y) dw_g(y,t)$ in Eq. 1.165) and normalizing with the Born partonic cross section we obtain

$$\frac{1}{d\sigma_B(p,\bar{p})} \frac{d\sigma}{dz}(p,\bar{p},z) = \frac{C_F X z^{-1-2\epsilon}}{C_A} \int_z^1 \frac{dy}{y} y\, G(y,X,\epsilon), \tag{1.168}$$

where

$$X = C_A \frac{\alpha_s}{\pi} \frac{(4\pi)^\epsilon}{\Gamma(1-\epsilon)} \left(\frac{\mu^2}{Q^2}\right)^{\epsilon}, \tag{1.169}$$

and

$$\begin{aligned} G(y,X,\epsilon) = \delta(1-y) + y^{-1-2\epsilon} \sum_{m=1}^{\infty} X^m \int_y^1 \frac{dy_1}{y_1^{1+2\epsilon}} \int_{y_1}^1 \frac{dy_2}{y_2^{1+2\epsilon}} \dots \int_{y_{m-2}}^1 \frac{dy_{m-1}}{y_{m-1}^{1+2\epsilon}} \\ \times \int_0^1 \frac{dt_1}{t_1^{1+\epsilon}} \int_{t_1}^1 \frac{dt_2}{t_2^{1+\epsilon}} \dots \int_{t_{m-1}}^1 \frac{dt_m}{t_m^{1+\epsilon}} \end{aligned}$$

$$= \delta(1-y) + \frac{1}{y} \sum_{m=1}^{\infty} X^m \frac{(-1)^m y^{-2\epsilon} (y^{-2\epsilon} - 1)^{m-1}}{m!(m-1)! 2^{m-1} \epsilon^{2m-1}}. \tag{1.170}$$

Taking the Mellin transform of Eq. 1.170 one ends up with

$$G^{(N)}(N,X,\epsilon) = \int_0^1 dy\, y^{N-1} G(y,X,\epsilon) = {}_0F_1\left(;\, 1 - \frac{N-1}{2\epsilon};\, \frac{X}{2\epsilon^2}\right), \tag{1.171}$$

where ${}_pF_q(a_1, a_2, \ldots, a_p;\ b_1, b_2, \ldots, b_q;\ z)$ is the generalized hypergeometric function. This quantity is divergent for $\epsilon \to 0$.

According to what we have discussed in Sec. 1.2.3, we can use factorization to get rid of collinear divergences and define a finite quantity $C^{(N)}$ from $G^{(N)}$ through means of a time-like transition function $\Gamma^{T,(N)}$ collecting all collinear divergences appearing as poles in ϵ:

$$G^{(N)}(N, X, \epsilon) = C^{(N)}\left(N, \alpha_s(\mu_F^2, \epsilon), \frac{Q^2}{\mu_F^2}, \epsilon\right) \Gamma^{T,(N)}\left(N, \alpha_s(\mu_F^2, \epsilon), \epsilon\right). \tag{1.172}$$

For the precision needed at LL, corrections of $\mathcal{O}(\alpha_s^2)$ and $\mathcal{O}(\epsilon^2)$ to the running coupling $\alpha_s(\mu_R)$ can be dropped. Moreover we have set $\mu_R = \mu_F$ and also used the fact that convolutions become normal products in Mellin space (c.f. Eq. 1.121 and Appendix B). Using the time-like equivalent of Eq. 1.133, where for now only the case of the "observed" gluon is taken into account,

$$\mathcal{P}_{gg}^{T,(N)}(N, \alpha_s(\mu_F^2, \epsilon)) = \frac{d}{\ln \mu_F} \ln \Gamma^{T,(N)}(N, \alpha_s(\mu_F^2, \epsilon), \epsilon) \tag{1.173}$$

together with the definition of the *beta function* in d dimension,

$$\frac{d\alpha_s(\mu_R^2, \epsilon)}{d \ln \mu_R^2} = -\epsilon \alpha_s(\mu_R^2, \epsilon) - \sum_{n=0}^{\infty} \beta_n \alpha_s^{n+2}(\mu_R^2, \epsilon), \tag{1.174}$$

and ignoring corrections of $\mathcal{O}(\alpha_s^2)$ and $\mathcal{O}(\epsilon^2)$, the transition function has the solution

$$\Gamma^{T,(N)}(N, \alpha_s, \epsilon) = \exp\left[-\frac{1}{\epsilon} \int_0^{\alpha_s} \frac{d\alpha_s}{\alpha_s} \mathcal{P}_{gg}^{T,(N)}(N, \alpha_s)\right]. \tag{1.175}$$

In order to calculate the finite coefficient function $C^{(N)}$ and time-like splitting function $\mathcal{P}_{gg}^{T,(N)}$ describing the partonic configuration that we are investigating with its correct evolution, one would simply need to expand Eq. 1.171 in powers of ϵ and perform a coefficient comparison in Eq. 1.172. However, expanding Eq. 1.171 is not possible with the mathematical knowledge at the time of writing of this thesis. Nonetheless, we can use the fact that Eq. 1.171 satisfies

$$\frac{\ddot{G}^{(N)} - \frac{N-1}{2\epsilon}\dot{G}^{(N)}}{G^{(N)}} = \frac{X}{2\epsilon^2}, \tag{1.176}$$

where

$$\dot{f}(X) = X \frac{df}{dX}. \tag{1.177}$$

Let's set for simplicity and without loss of information $\mu_R = \mu_F = Q$, so that $X = \frac{\alpha_s(Q^2,\epsilon)\, C_A}{\pi}[1+O(\epsilon^2)] + O(a_s^2)$. From Eq. 1.175, the transition function satisfies

$$\dot{\Gamma}^{T,(N)} = -\frac{\mathcal{P}_{gg}^{T,(N)}}{\epsilon}\Gamma^{T,(N)}. \tag{1.178}$$

Putting Eq. 1.172 into 1.176 and using the above equation, we obtain

$$\frac{1}{\epsilon^2}\left(\left(\mathcal{P}_{gg}^{T,(N)}\right)^2 + \frac{(N-1)\mathcal{P}_{gg}^{T,(N)}}{2}\right) - \frac{1}{\epsilon}\left(\left[2\mathcal{P}_{gg}^{T,(N)} + \frac{N-1}{2}\right]\frac{\dot{C}^{(N)}}{C^{(N)}} + \dot{\mathcal{P}}_{gg}^{T,(N)}\right) + \frac{\ddot{C}^{(N)}}{C^{(N)}} \stackrel{!}{=} \frac{X}{2\epsilon^2}. \tag{1.179}$$

Comparing the ϵ^{-2} coefficients on both sides gives

$$\left(\mathcal{P}_{gg}^{T,(N)}\right)^2 + \frac{(N-1)\mathcal{P}_{gg}^{T,(N)}}{2} - \frac{X}{2} = 0, \tag{1.180}$$

and its solution gives the *resummed* splitting function [65, 66] at LL accuracy

$$\mathcal{P}_{gg}^{T,res,(N)}(N,\alpha_s) = \frac{1}{4}\left(-(N-1) + \sqrt{(N-1)^2 + 8C_A\frac{\alpha_s}{\pi}}\right). \tag{1.181}$$

Comparing the ϵ^{-1} coefficients on both sides gives

$$\frac{\partial \ln C^{(N)}}{\partial \mathcal{P}_{gg}^{T,(N)}} = -\frac{1}{2}\frac{1}{\mathcal{P}_{gg}^{T,(N)} + \frac{N-1}{4}}, \tag{1.182}$$

whose solution is

$$C^{(N)} = \frac{A(N)}{\sqrt{\mathcal{P}_{gg}^{T,(N)} + \frac{N-1}{4}}}, \tag{1.183}$$

where $A(\omega)$ is an unknown constant of integration which can be determined by the condition $C^{(N)}(N,0) = 1$ from perturbation theory. Using Eq. 1.181, the *resummed* coefficient function reads

$$C^{res,(N)}(N,\alpha_s) = \frac{1}{\left(1 + 8C_A\frac{a_s}{\pi(N-1)^2}\right)^{\frac{1}{4}}}. \tag{1.184}$$

In Eqs. 1.173 and 1.172 we have neglected the contributions coming from inclusive quark production, i.e. when the same process is considered but instead of a gluon g being the "observed" parton we consider a quark with the same momentum. In the complete calculation [63], the two

contributions get entangled via factorization due to the DGLAP equations (c.f. Eq. 1.135). If we call $\boldsymbol{g}$ the unfactorized coefficient function for the process in which the gluon is the "observed" particle and $\boldsymbol{q}$ the one where the quark is "observed", the correct factorization yields

$$(\boldsymbol{q}, \mathbf{g}) = (C_q^{(N)}, C_g^{(N)})\hat{\Gamma}, \tag{1.185}$$

where at the considered accuracy $\boldsymbol{q} = C_q^{(N)} = 1$ and

$$\hat{\Gamma} = \begin{pmatrix} 1 & \frac{2C_F}{C_A}(\Gamma^{T,(N)} - 1) \\ 0 & \Gamma^{T,(N)} \end{pmatrix}. \tag{1.186}$$

Due to the introductory nature of this first chapter and since the subject will be dealt in great detail in the next chapter, we refrain here from performing the complete calculation. The *resummed* coefficient function free of collinear singularities for the gluon inclusive process in e^+e^- annihilation turns out to be

$$C_g^{res,(N)}(N, \alpha_s) = 2\frac{C_F}{C_A}\left[C^{res,(N)}(N, \alpha_s) - 1\right], \tag{1.187}$$

whereas the quark-gluon resummed splitting function reads

$$\mathcal{P}_{gq}^{T,res,(N)}(N, \alpha_s) = \frac{C_F}{C_A}\mathcal{P}_{gg}^{T,res,(N)}(N, \alpha_s). \tag{1.188}$$

All Eqs. 1.181, 1.187 and 1.188 reproduce the correct LL small-z logarithms appearing in the known fixed order results [67–71]. As we shall see in the next chapter, they are mapped to $N = 1$ poles in the Mellin N-moment space. By expanding Eqs. 1.181, 1.187 and 1.188 around $\alpha_s \to 0$ one recovers the leading power of $1/(N-1)^{n-l}$ for each α_s^n coefficient. By performing the Mellin inversion then, we can easily recover all leading small-z contributions to each fixed order calculation. In the next chapter we will discuss how to extend this type of resummation to NNLL accuracy.

CHAPTER 2

Fragmentation functions beyond NLO

In this chapter we present a first analysis of parton-to-pion fragmentation functions beyond next-to-leading order accuracy in QCD based on single-inclusive pion production in electron-positron annihilation. We extend previous fixed order analyses (e.g. see [72–79]) up to NNLO accuracy. A second analysis is performed including all-order resummations of logarithmically enhanced contributions at small momentum fraction of the observed hadron in order to estimate their phenomenological relevance. Special emphasis is put on the technical details necessary to perform the QCD scale evolution and cross section calculation in Mellin moment space. The formalism to perform resummations in Mellin moment space is briefly reviewed, and all relevant expressions up to next-to-next-to-leading logarithmic order are derived, including their explicit dependence on the factorization and renormalization scales. We discuss the details pertinent to a proper numerical implementation of fixed order NNLO and resummed results comprising the solution to the time-like evolution equations, the matching to known fixed-order expressions, and the choice of the contour in the Mellin inverse transformation. We demonstrate how the description of the data and the theoretical uncertainties are improved when such higher order QCD corrections are included. This chapter is based on the published works [J4, J5].

2.1 Introduction

Fragmentation functions (FFs) $D_i^h(z, Q^2)$ are an integral part of the theoretical framework describing hard-scattering processes with an observed hadron in the final-state in perturbative QCD (pQCD) as they can be convoluted with perturbatively calculable hard-scattering coefficient functions to describe cross sections. The underlying theoretical foundations have been established in factorization theorems (see for example [80]). In an analogous manner to PDFs, FF parametrize in a process-independent way the non-perturbative transition of a parton with a particular flavor i into a hadron of type h and depend on the fraction z of the parton's longitudinal momentum taken by the hadron and a large scale Q inherent to the process under consideration [81, 82]. The prime example is single-inclusive electron-positron annihilation (SIA), $e^-e^+ \to hX$, at some center-of-mass system (c.m.s.) energy $\sqrt{S} = Q$, where X is some unidentified hadronic remnant. Precise data on SIA [83–91], available at different $\sqrt{S}$, ranging from about 10 GeV up to the mass M_Z of the Z boson, reveal important experimental information on FFs that is routinely used in theoretical extractions, i.e., fits of FFs [J4, 72, 75–79, 92, 93]. Processes other than SIA are required, however, to gather the information needed to fully disentangle all the different FFs D_i^h for $i = u, \bar{u}, d, \bar{d}, \ldots$ quark and antiquark flavors and the gluon. Specifically, data on semi-inclusive deep-inelastic scattering (SIDIS), $e^{\pm}p \to hX$, and the single-inclusive, high transverse momentum (p_T) production of hadrons in proton-proton collisions, $pp \to hX$, are utilized, which turn extractions of FFs into global QCD analyses [77–79, 92]. Most recently, a proper theoretical framework in terms of FFs has been developed for a novel class of processes, where a hadron is observed inside a jet [94–100]. It is expected that corresponding data [101–107] will soon be included in global analyses, where they will provide additional constraints on, in particular, the gluon-to-hadron FF.

The ever increasing precision of all these probes sensitive to the hadronization of (anti-)quarks and gluons has to be matched by more and more refined theoretical calculations, which crucially depend on the precise knowledge of FFs and their uncertainties.

One way of advancing QCD calculations is the computation of higher order corrections in the strong coupling α_s. Here, next-to-leading order (NLO) results are available throughout for all ingredients needed for a global QCD analysis of FFs as outlined above. Specifically, they comprise the partonic hard scattering cross sections for inclusive hadron production in SIA [48, 108, 109], SIDIS [48, 108–111], and pp collisions [112–114] and the evolution kernels or time-like parton-to-parton splitting functions P_{ij}^T [67, 68, 115–118], which govern the scale Q dependence

of the FFs through a set of integro-differential evolution equations [49, 50, 119, 120]. Such type of NLO global analyses of FFs represent the current state-of-the-art in this field.

Here, SIA data are of utmost importance, similar to the singular role played by deep-inelastic scattering (DIS) measurements in determinations of PDFs. Recently, results from the BELLE [83] and BABAR [84] collaborations have complemented the existing suite of SIA data mainly from the CERN-LEP experiments taken at a center-of-mass system (c.m.s.) energy of $\sqrt{S} = 91.2\,\text{GeV}$. Thanks to the unprecedented precision of the new data sets, where the statistical uncertainties are mainly at the sub-percent level despite their fine binning, and the lower $\sqrt{S}$, global QCD analyses can now utilize the energy dependence of the SIA data in the range from about 10.5 GeV to 91.2 GeV [79] to extract FFs also from scaling violations, a key prediction of pQCD. For instance, a recent extraction of parton-to-pion FFs D_i^π at NLO accuracy including those data can be found in Ref. [79]. Moreover, contrary to the case of hadron production in SIDIS or in pp collisions, with SIA data fits of FFs can be carried out already at the next-to-next-leading order (NNLO) level thanks to the available SIA coefficient functions [67, 68, 70, 121] and kernels P_{ij}^T at NNLO [122–124]. In this chapter we will present the main results of our first determination of parton-to-pion FFs from SIA data at NNLO accuracy performed recently in [J4].

In our phenomenological study there, we adopt the technical framework used in the DSS global analyses [77–79] which we extend to NNLO accuracy. As we shall discuss in some detail below, we apply efficient Mellin space techniques in order to both solve the evolution equations and compute the SIA cross section at NNLO. As it turns out, the numerical implementation of the Mellin inverse transformation, needed to compare to data, requires special attention in case of the time-like scale evolution of FFs. Global fits to SIA data at leading order (LO), NLO, and NNLO accuracy are performed to demonstrate the anticipated reduction in theoretical uncertainties inherent to the truncation of the perturbative calculation at a given fixed order in α_s. In [J4] we refrain from including other sources of hadron production data used in the DSS global analyses at NLO accuracy [77–79], such as hadron multiplicities in semi-inclusive DIS and high transverse momentum hadron production in proton-proton collisions, due to the lack of corresponding NNLO partonic cross sections. As a consequence, our fits use less free parameters than in the DSS global analyses. Nonetheless, the quality of the fit is observed to gradually improve by including higher order terms in the global analysis. We note that first reference results for the scale evolution of FFs at $\mathcal{O}(\alpha_s^3)$ were obtained in [125] with which we compare.

Another important avenue for systematic improvements in the theoretical analysis of data sensitive to FFs, which we have pursued in [J5] and present here in this chapter, concerns large logarithms present in each fixed order of the perturbative series in α_s for both the evolution kernels P_{ij}^T and the process-dependent hard scattering coefficient functions. They may become large in the limit of small momentum fractions z and, in this way, can spoil the convergence of the expansion in α_s even when the coupling is very small. As we shall see, two additional powers of $\log^{2k}(z)$ can arise in each fixed order α_s^k, which is numerically considerably more severe than in the space-like case relevant to deep-inelastic scattering (DIS) and the scale evolution of parton density functions (PDFs) and completely destabilizes the behavior of cross sections and FFs in the small-z regime.

To mitigate the singular small-z behavior imprinted by these logarithms, one needs to resum them to all orders in perturbation theory, a well-known procedure (see for instance [66, 126–128]). Knowledge of the fixed-order results up to N^{m}LO determines, in principle, the first $m + 1$ "towers" of logarithms to all orders. Hence, thanks to the available NNLO results, small-z resummations have been pushed up to the first three towers of logarithms for SIA and the time-like splitting functions P_{ij}^T recently, which is termed the next-to-next-to-leading logarithmic (NNLL) approximation [129, 130]. Based on general considerations on the structure of all-order mass factorization, as proposed and utilized in Ref. [129, 130], we re-derive the resummed coefficient functions for SIA and the evolution kernels P_{ij}^T and compare them to the results available in the literature. Next, we extend these expressions by restoring their dependence on the factorization and renormalization scales μ_F and μ_R, respectively, which allows us to estimate the theoretical uncertainties related to the choice of μ_F/Q. It is in fact expected that the scale ambiguity shrinks the more higher order corrections are included. We note that large logarithms also appear in the limit $z \to 1$. Their phenomenological implications have been addressed in the case of SIA in Ref. [J1, 131–135], and we shall not consider here focussing mainly on the small-z regime.

Resummations are most conveniently carried out in Mellin-N moment space, which also gives the best analytical insight into the solution of the coupled, matrix-valued scale evolution equations obeyed by the quark singlet and gluon FFs. We discuss in some detail how we define a solution to these evolution equations beyond the fixed-order approximation, i.e., based on resumed kernels P_{ij}^T. We also explain how we match the resummed small-z expressions to a given fixed-order result defined for all z, thereby avoiding any double-counting of logarithms and also maintaining the validity of the momentum sum rule. As for the NNLO case, we also address

in our following discussions the proper numerical implementation of the resummed expressions in Mellin N space, in particular, the structure of singularities and the choice of the integration contour for the inverse Mellin transformation back to the physical z space.

So far, resummations in the context of FFs have been, to the best of our knowledge, exclusively studied for the first five integer N moments of the z-integrated hadron multiplicities, in particular, their scale evolution and the shift of the peak of the multiplicity distribution with energy [63, 66, 126–128, 136–139]. At fixed order, multiplicities are ill-defined due to the singularities induced by the small-z behavior. In the "modified leading logarithmic approximation" (MLLA) and beyond, i.e., upon including resummed expressions, these singularities are lifted, and one finds a rather satisfactory agreement with data, which can be used to determine, e.g., the strong coupling α_s in SIA [63, 136–139].

In [J5], however, we apply resummations in the entire z range, i.e., for the first time, we extract FFs from SIA data with identified pions up to NNLO+NNLL accuracy, including a proper matching procedure. We investigate the phenomenological relevance of small-z resummations in achieving the best possible description of the SIA data. This is done by comparing the outcome of a series of fits to data both at fixed order accuracy and by including up to three towers of small-z logarithms. We also compare the so obtained quark singlet and gluon FFs and estimate the residual theoretical uncertainty due to the choice of μ_F/Q in each case. An important phenomenological question that arises in this context is how low in z one can push the theoretical framework outlined above before neglected kinematic hadron mass corrections become relevant. Hadron mass effects in SIA is investigated to some extent in Chapter 3 (see also corresponding published article [J3]) but so far there is no fully consistent way to properly include them in a general process, i.e., ultimately in a global analysis of FFs. See for example [140, 141]. Therefore, one needs to determine a lower value of z, largely on kinematical considerations, below which fits of FFs make no sense. We discuss this issue as well in the phenomenological section of this chapter. In general, it turns out, that in the range of z where SIA data are available and where the framework can be applied, a fit at fixed, NNLO accuracy already captures most of the relevant small-z behavior needed to arrive at a successful description of the data, and resummations add only very little in a fit.

In Sec. 2.2, we outline all the necessary technical ingredients for the extension of the pQCD framework for SIA to NNLO, specifically, those related to the proper Mellin space implementation and the Mellin inverse transformation. This framework is extended in Sec 2.3 in order to include resummations corrections for the small z region In Sec. 2.4, we briefly recall the DSS

global analysis framework and discuss the results of our fits of SIA data up to NNLO accuracy. In particular, we demonstrate the reduction of the scale uncertainty when increasing the perturbative order from LO and NLO to NNLO. In addition, we compare the resulting fragmentation functions to those obtained by DSS [79] and Kretzer [72]. Analogouly, in Sec. 2.5.1 we present and discuss various fits to semi-inclusive annihilation data at different fixed-orders in perturbation theory and levels of small-z resummations. We summarize our main results in Sec. 2.6, where we also discuss potential further improvements of the presented analysis framework for fragmentation functions.

2.2 Semi-inclusive e^+e^- annihilation up to NNLO accuracy

In this Section we review the necessary technical aspects to compute SIA cross sections up to NNLO accuracy. Special emphasis is put on the transformation from momentum to Mellin moment space and the additional subtleties appearing beyond NLO. To set the stage, we first recall in Sec. 2.2.1 the general structure of the SIA cross section. Next, we discuss some relevant features of the NNLO coefficient functions. In Sec. 2.2.2 we review the time-like evolution equations at NNLO and their truncated and iterated solutions, which we shall compare numerically in Sec. 2.4. Section 2.2.3 is devoted to a detailed discussion of the numerical implementation of the Mellin space expressions and the proper choice of contour for the Mellin inverse transformation. We will also compare to the results of the MELA evolution code presented in Ref. [125].

2.2.1 Cross Section and Coefficient Functions

We consider the SIA process $e^+e^- \to \gamma/Z \to hX$ mediated by an intermediate virtual photon γ or Z boson at a c.m.s. energy $\sqrt{S}$, more specifically, hadron multiplicities defined as

$$\frac{1}{\sigma_{\text{tot}}}\frac{d\sigma^h}{dz} = \frac{1}{\sigma_{\text{tot}}}\left[\frac{d\sigma_T^h}{dz} + \frac{d\sigma_L^h}{dz}\right] . \tag{2.1}$$

Since we have already integrated over the scattering angle θ of the produced hadron h in (2.1), parity-violating interference terms vanish, and the cross section $d\sigma^h/dz$ can be decomposed only into a transverse (T) and a longitudinal (L) part, where T, L refer to the γ/Z polarizations (see

for instance [109]). The scaling variable z is defined in terms of the four momenta P_h and q of the observed hadron and γ/Z boson, respectively, as

$$z \equiv \frac{2P_h \cdot q}{Q^2} \overset{\text{c.m.s.}}{=} \frac{2E_h}{Q}\,, \tag{2.2}$$

where $Q^2 \equiv q^2 = S$. As indicated in Eq. (2.2), z reduces to the hadron's energy fraction in the c.m.s. and is often also labeled as x_E [109].

Up to NNLO accuracy, i.e., $\mathcal{O}(\alpha_s^2)$ in the strong coupling, the total hadronic cross section σ_{tot} in Eq. (2.1) is given by [67, 142–144]

$$\begin{aligned}\sigma_{\text{tot}} &= \sigma_0 N_c \sum_q \hat{e}_q^2 \left[1 + 3C_F\, a_s + a_s^2 \left(-\frac{3}{2}C_F^2 + C_A C_F \left(-11 \log\left(\frac{Q^2}{\mu_R^2}\right) - 44\,\zeta(3) + \frac{123}{2}\right)\right.\right. \\ &\quad \left.\left. + N_f C_F T_f \left(4 \log\left(\frac{Q^2}{\mu_R^2}\right) + 16\,\zeta(3) - 22\right)\right)\right]\,,\end{aligned} \tag{2.3}$$

where $\sigma_0 = 4\pi\alpha^2/(3Q^2)$ is the lowest order QED cross section for $e^+e^- \to \mu^+\mu^-$, α denotes the electromagnetic fine structure constant, $\hat{e}_q$ are the electroweak quark charges, and $N_c = 3$ is the number of colors. In addition, we have introduced the usual QCD color factors $C_A = 3$, $C_F = 4/3$, and $T_f = 1/2$. The sum in (2.3) runs over N_f active massless quark flavors. Here and throughout this chapter, we use the definition $a_s = \alpha_s(\mu_R^2)/4\pi$, where μ_R is the renormalization scale. We refrain from reproducing the well-known expressions for the electroweak quark charges which can be found, e.g., in Ref. [67].

The NNLO QCD corrections to the transverse and longitudinal cross sections $d\sigma_k^h/dz$, $k = T, L$, in Eq. (2.1) were calculated in [67, 68, 70]. Adopting the same notation, they can be expressed in factorized form as a convolution of appropriate combinations of quark and gluon fragmentation functions $D_{l=q,g}^h(z,\mu^2)$ and calculable coefficient functions $\mathbb{C}_{k,l}^{\text{S,NS}}(z, Q^2/\mu^2)$ [67, 121]:

$$\begin{aligned}\frac{d\sigma_k^h}{dz} &= \sigma_{\text{tot}}^{(0)} \left[D_{\text{S}}^h(z,\mu^2) \otimes \mathbb{C}_{k,q}^{\text{S}}\left(z, \frac{Q^2}{\mu^2}\right) + D_g^h\left(z,\mu^2\right) \otimes \mathbb{C}_{k,g}^{\text{S}}\left(z, \frac{Q^2}{\mu^2}\right)\right] \\ &\quad + \sum_q \sigma_q^{(0)}\, D_{\text{NS},q}^h(z,\mu^2) \otimes \mathbb{C}_{k,q}^{\text{NS}}\left(z, \frac{Q^2}{\mu^2}\right)\,,\end{aligned} \tag{2.4}$$

where, for simplicity, we have set the renormalization scale μ_R equal to the factorization scale μ_F, i.e., $\mu_R = \mu_F \equiv \mu$. The symbol $\otimes$ denotes the standard convolution integral defined as

$$f(z) \otimes g(z) \equiv \int_0^1 dx \int_0^1 dy\, f(x)\, g(y)\, \delta(z - xy)\,. \tag{2.5}$$

$\sigma_q^{(0)}$ in Eq. (2.4) is the total quark production cross section for a given flavor q at LO, $\mathcal{O}(\alpha_s^0)$, and $\sigma_{\rm tot}^{(0)}$ is the corresponding sum over all N_f active flavors. They read $\sigma_q^{(0)} = \sigma_0 N_c \hat{e}_q^2$ and $\sigma_{\rm tot}^{(0)} = \sum_q \sigma_q^{(0)}$. With this notation, the transverse and longitudinal cross sections are related to the usual longitudinal and transverse structure functions [68] according to

$$\begin{aligned} F_k \equiv \frac{1}{3\sigma_0}\frac{d\sigma_k^h}{dz} &= \left(\sum_q \hat{e}_q^2\right)\left[D_{\rm S}^h(z,\mu^2) \otimes \mathbb{C}_{k,q}^{\rm S}\left(z, \frac{Q^2}{\mu^2}\right) + D_g^h\left(z,\mu^2\right) \otimes \mathbb{C}_{k,g}^{\rm S}\left(z, \frac{Q^2}{\mu^2}\right)\right] \\ &\quad + \sum_q \hat{e}_q^2\, D_{{\rm NS},q}^h(z,\mu^2) \otimes \mathbb{C}_{k,q}^{\rm NS}\left(z, \frac{Q^2}{\mu^2}\right) \\ &= \sum_{l=q,\bar{q},g} D_l^h(z,\mu^2) \otimes \mathbb{C}_{k,l}\left(z, \frac{Q^2}{\mu^2}\right)\,. \end{aligned} \tag{2.6}$$

Factorization in Eq. (2.4) holds in general only in the presence of a hard scale, in this case Q. SIA is a one-scale process, and the hard scale should be chosen to be of $\mathcal{O}(Q)$. The power corrections for SIA are much less well understood than in DIS, perhaps due to the lack of an operator product expansion in the time-like case. One source, which we will get back to later on, is of purely kinematic origin. Instead of the energy fraction z, SIA data are often given in terms of the hadron's three-momentum fraction in the c.m.s., $x_p = 2p/Q$, which leads to $1/Q^2$ corrections when converted back to proper scaling variable: $x_p = z - 2m_h^2/(zQ^2) + \mathcal{O}(1/Q^4)$ [109]. m_h is the produced hadron's mass and is neglected in the factorized formalism outlined above. Other sources of power corrections arise in the non-perturbative formation of a hadron from quarks or gluons and are expected to behave like $1/Q$ from model estimates [109]. Higher-twist corrections to Eq. (2.4), that are suppressed by inverse powers of the hard scale, can be usually safely neglected as long as Q is large enough. We do not consider them in this study.

The non-perturbative but universal FFs $D_i^h(z,\mu^2)$ have a formal definition as bilocal operators [81, 82] and parametrize the hadronization of a massless (anti)quark or gluon, $i = q, \bar{q}, g$, into the observed hadron h as a function of its fractional momentum z. The fragmentation process is assumed to be independent of any other colored particles produced in a hard scattering.

The scale dependence of the FFs is calculable in pQCD and governed by renormalization group equations similar to those for PDFs. The SIA cross section in Eq. (2.4) depends on the gluon-to-hadron FF $D_g^h(z,\mu^2)$ and the quark singlet (S) and non-singlet (NS) combinations that are defined as

$$D_{\rm S}^h(z,\mu^2) = \frac{1}{N_f}\sum_q \left[D_q^h(z,\mu^2) + D_{\bar{q}}^h(z,\mu^2)\right] \tag{2.7}$$

and

$$D_{{\rm NS},q}^h(z,\mu^2) = D_q^h(z,\mu^2) + D_{\bar{q}}^h(z,\mu^2) - D_{\rm S}^h(z,\mu^2) \tag{2.8}$$

respectively, in terms of the quark plus antiquark FFs $D_q^h(z,\mu^2) + D_{\bar{q}}^h(z,\mu^2)$ for each flavor q.

The corresponding $i = {\rm S}, {\rm NS}$ coefficient functions in Eq. (2.4) can be calculated perturbatively in pQCD as a series in a_s,

$$\mathbb{C}_{k,l}^i = \mathbb{C}_{k,l}^{i,(0)} + a_s\,\mathbb{C}_{k,l}^{i,(1)} + a_s^2\,\mathbb{C}_{k,l}^{i,(2)} + \dots\,, \tag{2.9}$$

where we have suppressed the arguments $(z, Q^2/\mu^2)$ in (2.9). Results are available up to $\mathcal{O}(a_s^2)$ [67, 68, 70] which is NNLO for the $\mathbb{C}_{T,l}^{\rm S,NS}$ but formally only of NLO accuracy for the subleading longitudinal coefficient functions $\mathbb{C}_{L,l}^{\rm S,NS}$. The latter coefficients vanish at $\mathcal{O}(a_s^0)$, and their perturbative series is hence shifted by one power in the strong coupling a_s. The situation is completely analogous to DIS but, unlike in DIS [145], the $\mathcal{O}(a_s^3)$ NNLO contributions have not been calculated yet for SIA. In our phenomenological studies in Sec. 2.4, we will therefore resort, for the time being, to the approximation where the perturbative orders for $\mathbb{C}_{L,l}^{\rm S,NS}$ are counted as for $\mathbb{C}_{T,l}^{\rm S,NS}$, i.e., we treat the $\mathcal{O}(a_s^2)$ longitudinal coefficients as NNLO. In that case, the gluon FFs does not contribute directly in SIA at LO as also $\mathbb{C}_{T,g}^{i,(0)} = 0$, again, similar to DIS. In addition, we note that up to NLO accuracy, the relation $\mathbb{C}_{k,q}^{\rm S} = \mathbb{C}_{k,q}^{\rm NS}$ holds, which can be used to simplify Eq. (2.4) as was done, e.g., in Ref. [48, 108].

Numerically, in particular, when fitting a large number of data in a global QCD analysis, it is advantageous to work in complex Mellin N moment space rather than with expressions like Eq. (2.4) containing one or several time-consuming convolution integrals. In general, the Mellin transform $f(N)$ of a function $f(z)$ is defined by

$$f(N) = \int_0^1 dz\, z^{N-1} f(z) \equiv \mathcal{M}[f(z)]\,. \tag{2.10}$$

It has the well-known property that convolutions of two functions factorize into ordinary

products, i.e., both the transverse and longitudinal cross section $d\sigma_k^h/dz$ in Eq. (2.4) can be schematically written as products of the Mellin N moments of FFs and coefficient functions, $D_l^h(N,\mu^2)\cdot\mathbb{C}_{k,l}(N,Q^2/\mu^2)$. See Appendix B.

The Mellin moments of the NNLO coefficient functions $\mathbb{C}_{k,l}^{i,(2)}$ in (2.9) were computed in both Ref. [70] and [121]. We analytically checked the consistency of the two results, which are presented using somewhat different notations, by independently calculating the Mellin moments from scratch starting from the z-space expressions given in Appendix C of Ref. [70]. To this end, two MATHEMATICA [146] packages [147, 148] were employed. The z-space results in [70] are given in terms of harmonic polylogarithms expressed in the notation $H_{m_1,\ldots,m_w}$, $m_j = 0,\pm 1$ introduced in [149]. Their Mellin transform can be written in terms of harmonic sums

$$S_{a_1,\ldots,a_n}(N) = \sum_{k_1=1}^{N}\sum_{k_2=1}^{k_1}\ldots\sum_{k_n=1}^{k_{n-1}}\frac{\mathrm{sign}(a_1)^{k_1}}{k_1^{|a_1|}}\ldots\frac{\mathrm{sign}(a_n)^{k_n}}{k_n^{|a_n|}}\,, \tag{2.11}$$

where the a_k are positive or negative integers, and N is a positive integer. The number n of a_k indices indicates the so-called depth, whereas $w = \sum_{k=1}^{n}|a_k|$ is called the weight of the function. At NNLO accuracy one ends up dealing with harmonic sums of weight up to $w = 4$.

In order to perform the Mellin inverse transformation to z-space along a contour in the complex N plane at the very end, see Sec. 2.2.3 below, one needs to know all functions not only for discrete integers but for any complex value of N. This is achieved by proper analytical continuation of the harmonic sums in Eq. (2.11). As it is well known [115, 150, 151], there is no analytical continuation for all integer values of N due to the presence of terms $\propto (-1)^N$, and a choice $(-1)^N \to \pm 1$ has to be made based on physical considerations. For instance, the analytical continuation of all the coefficient functions $\mathbb{C}_{k,l}^{\mathrm{S,NS}}$ appearing in Eq. (2.4) has to correctly reproduce only even integer N moments.

To compare our results for the Mellin moments of the NNLO coefficients obtained with the help of the MATHEMATICA packages [147, 148] with those given for even values of N in [70], special care needs to be taken for factors $\propto S_{-2}(N-2)/(N-2)$ since the zero in the denominator for $N = 2$ suggests the presence of a pole. However, this is a spurious pole as can be seen by making use of its the integral representation [152]

$$S_{-2}(N) \;=\; -\int_0^1 dz\,\log(z)\frac{(-z)^N-1}{1+z}\,. \tag{2.12}$$

The existence of this spurious pole for $N = 2$ at NNLO is the reason for the notation adopted in [70], where the Mellin moments of the coefficient functions are written proportional to $\theta(N-3)$ and $\delta(N-2)$, representing the finite $N \to 2$ limit. Note that the limit in Eq. (2.12) has to be taken for even N to obtain the correct sign. This can be made manifest by rewriting Eq. (2.12) in terms of the digamma function which is defined as the derivative of the Euler Gamma function $\psi(x) \equiv d\log[\Gamma(x)]/dx$. The harmonic sum in Eq. (2.12) then reads [153]

$$S_{-2}(N) = (-1)^{N+3}\beta'(N+1) - \frac{1}{2}\zeta(2)\,, \tag{2.13}$$

where

$$\beta(N) = \frac{1}{2}\left[\psi\left(\frac{N+1}{2}\right) - \psi\left(\frac{N}{2}\right)\right]. \tag{2.14}$$

We fully reproduce both the $\theta(N-3)$ pieces and the $N \to 2$ limits of the NNLO coefficients $\mathbb{C}^{\mathrm{S,NS}}_{k,l}(N)$ listed in Ref. [70]. Note that the subtleties concerning the spurious pole for $N = 2$ first appear at the NNLO level. We also completely agree with the results given in Ref. [121] as long as we do not use their definitions of the functions $A_3(N)$, $A_5(N)$, $A_{18}(N)$, $A_{21}(N)$, and $A_{22}(N)$ in Eq. (14) of [121] but, instead, define them as the Mellin transforms of the functions $g_3(x)$, $g_5(x)$, $g_{18}(x)$, $g_{21}(x)$, and $g_{22}(x)$ specified in the ANCONT package [153].
In our numerical code we implement the Mellin N space expressions for the NNLO coefficient functions in the way as they are presented in [121]. The proper analytical continuations of all the harmonic sums and special functions are taken from [121, 152–154]. In addition, we are making use of some of the routines provided in the ANCONT package [153].

2.2.2 Time-like Evolution Equations

The factorization procedure invoked in Eq. (2.4) introduces an arbitrary scale μ_F which conceptually separates the high-energy perturbative regime from the low-energy, non-perturbative region. Both the hard coefficient functions and the FFs depend on μ_F in such a way that at $\mathcal{O}(a_s^n)$ in pQCD any residual dependence of a physical cross section on μ_F is of order $\mathcal{O}(a_s^{n+1})$. Similar to the case of PDFs, this leads to a set of $2N_f + 1$ coupled renormalization group equations (RGE) governing the scale μ_F dependence of the gluon and N_f quark and antiquark FFs into a given hadron species h. Schematically, these time-like evolution equations read

$$\frac{\partial}{\partial \ln \mu^2} D_i^h(z,\mu^2) = \sum_j P_{ji}^T(z,\mu^2) \otimes D_j^h\left(z,\mu^2\right)\,, \tag{2.15}$$

$i, j = q, \bar{q}, g$, and where, for simplicity, we have set $\mu_R = \mu_F = \mu$ as in Sec. 2.2.1. The $j \to i$ splitting functions $P_{ji}^T(z, \mu^2)$ can be calculated perturbatively as a series in a_s,

$$P_{ji}^T = a_s P_{ji}^{T,(0)} + a_s^2 P_{ji}^{T,(1)} + a_s^3 P_{ji}^{T,(2)} + \dots , \tag{2.16}$$

suppressing all arguments z, μ^2 in (2.16). They are known up to NNLO accuracy [122–124], i.e., $\mathcal{O}(a_s^3)$, as is the case for their space-like counterparts P_{ij}^S [71, 155] needed for the scale evolution of PDFs. In fact, there is still a small uncertainty left concerning the off-diagonal splitting kernel $P_{qg}^{T,(2)}$ which could not be completely determined by the crossing relations to the space-like results employed in [122–124]. Presumably, this remaining ambiguity is numerically irrelevant for all phenomenological applications; see, however, Ref. [156] for the status of an ongoing direct calculation of the NNLO time-like kernels. To implement the time-like evolution equations (2.15) numerically up to NNLO accuracy, we closely follow the strategies and framework developed for the public, space-like PDF evolution code PEGASUS [157]. In general, the structure and solutions of the space-like and time-like evolution equations are completely analogous apart from replacing PDFs by FFs and the kernels P_{ij}^S by P_{ji}^T. Hence, for completeness, we repeat here only the most important aspects, in particular, those features appearing for the first time at NNLO. Instead of working directly with the system of $2N_f + 1$ coupled equations in (2.15) it is convenient to recast the quark sector into a flavor singlet

$$D_\Sigma^h \equiv \sum_q^{N_f} (D_q^h + D_{\bar{q}}^h) , \tag{2.17}$$

which evolves along with the gluon FF D_g^h,

$$\frac{d}{d \ln \mu^2} \begin{pmatrix} D_\Sigma^h \\ D_g^h \end{pmatrix} = \begin{pmatrix} P_{qq}^T & 2N_f P_{gq}^T \\ \frac{1}{2N_f} P_{qg}^T & P_{gg}^T \end{pmatrix} \otimes \begin{pmatrix} D_\Sigma^h \\ D_g^h \end{pmatrix} , \tag{2.18}$$

and $2N_f - 1$ non-singlet combinations

$$D_{\mathrm{NS},l}^{h,\pm} \equiv \sum_{i=1}^{k} (D_{q_i}^h \pm D_{\bar{q}_i}^h) - k(D_{q_k}^h \pm D_{\bar{q}_k}^h) , \tag{2.19}$$

$$D_{\mathrm{NS},v}^h \equiv \sum_q^{N_f} (D_q^h - D_{\bar{q}}^h) , \tag{2.20}$$

reflecting the properties of the (anti)quark to (anti)quark splitting functions and which all evolve independently. In Eq. (2.19) $l = k^2 - 1$, $k = 1, \ldots, N_f$, and the subscripts i, k were introduced to distinguish different quark flavors. After the evolution is performed, the individual D_q^h and $D_{\bar{q}}^h$ can be recovered from Eqs. (2.17), (2.19), and (2.20), and any combination relevant for a cross section calculation can be computed, such as those used in the factorized expression for SIA given in Eq. (2.4).

More specifically, the three NS combinations in Eq. (2.19) and (2.20) evolve with the following NS splitting functions [122–124]

$$\begin{aligned} P_{\rm NS}^{T,\pm} &= P_{qq}^{T,v} \pm P_{q\bar{q}}^{T,v}\,, \\ P_{\rm NS}^{T,v} &= P_{\rm NS}^{T,-} + P_{\rm NS}^{T,s}\,, \end{aligned} \tag{2.21}$$

respectively, and the singlet P_{qq}^T in (2.18) obeys

$$P_{qq}^T = P_{\rm NS}^{T,+} + P^{T,ps}\,. \tag{2.22}$$

Similarly to the space-like case, $P_{q\bar{q}}^{T,v} = P_{\rm NS}^{T,s} = P^{T,ps} = 0$ and $P_{\rm NS}^{T,s} = 0$ in LO and NLO, respectively, such that three independently evolving NS quark combinations appear for the first time at NNLO accuracy [122–124]. We note that $P_{\rm NS}^{T,s} \neq 0$ can lead to a perturbatively generated, albeit small strange-quark asymmetry for FFs, i.e., $D_s^h(z,\mu^2) - D_{\bar{s}}^h(z,\mu^2) \neq 0$, even if the input D_s^h and $D_{\bar{s}}^h$ are symmetric; see Ref. [158] for a detailed discussion of a similar effect in the context of PDFs. For pion FFs such a charge asymmetry is expected to be further suppressed since the effect is driven by a non-zero $D_{{\rm NS},v}^h$ in Eq. (2.20). This combination vanishes when exact charge conjugation and isospin symmetry is imposed on the u and d quark and antiquark FFs as is the case in many of the available sets of pion FFs [72–76].

As mentioned already, we choose to solve the set of time-like evolution equations in Mellin N space, which not only has the benefit of turning all integro-differential equation into ordinary differential equations but also makes them amenable to further analytical studies, such as the inclusion of those resummation corrections presented later on in this chapter. Solutions of the evolution equations in N space, as well as their numerical implementation, are well known and were treated extensively in, e.g., Ref. [157] in the space-like case relevant for PDFs. Since the procedure for FFs is essentially the same, we will in the following only sketch some aspects of the solution at NNLO important for our discussions later on. The needed NNLO kernels $P_{ji}^{T,(2)}(N)$ can be found in [122–124]. As for the SIA coefficient functions presented in Sec. 2.2.1,

we have verified the expressions for $P_{ji}^{T,(2)}(N)$ starting from z-space and find full agreement.

We start our discussions by recalling the Mellin transformed time-like evolution equations. Adopting the notations used in the PEGASUS code [157], one finds

$$\frac{\partial \boldsymbol{D}^h(N,a_s)}{\partial a_s} = -\frac{1}{a_s}\left[\boldsymbol{R}_0(N) + \sum_{k=1}^{\infty} a_s^k \boldsymbol{R}_k(N)\right]\boldsymbol{D}^h(N,a_s)\,, \tag{2.23}$$

where the bold characters indicate that we are dealing in general with 2×2 matrix-valued equations, cf. Eq. (2.18). For the NS combinations (2.19) and (2.20), Eq. (2.23) reduces to a set of single partial differential equations which are straightforward to solve, and we do not consider them here any further.

The $\boldsymbol{R}_k$ in (2.23) are defined recursively as

$$\boldsymbol{R}_0 \equiv \frac{1}{\beta_0}\widetilde{\boldsymbol{P}}^{T,(0)}\,, \quad \boldsymbol{R}_k \equiv \frac{1}{\beta_0}\widetilde{\boldsymbol{P}}^{T,(k)} - \sum_{i=1}^{k} b_i \boldsymbol{R}_{k-i}\,, \tag{2.24}$$

where $\widetilde{\boldsymbol{P}}^{T,(k)}(N)$ is the k-th term in the perturbative expansion of the 2×2 matrix of singlet splitting functions as it shows in Eq. (2.18)

$$\widetilde{\boldsymbol{P}}^{T}(N) = \begin{pmatrix} P_{qq}^T(N) & 2N_f P_{gq}^T(N) \\ \frac{1}{2N_f}P_{qg}^T(N) & P_{gg}^T(N) \end{pmatrix}. \tag{2.25}$$

In addition, $b_i \equiv \beta_i/\beta_0$ with β_k denoting the expansion coefficients of the QCD β-function; see Ref. [159, 160] for explicit expressions up to NNLO, i.e, β_2. Also note that Eq. (2.23) is now written in terms of ∂a_s rather than $\partial \log \mu^2$ used in Eq. (2.15). This convenient change of variables is possible as long as factorization and renormalization scales are related by a constant, i.e., $\mu_R = \kappa\mu_F$, in numerical studies; see Ref. [157] for a detailed discussion. For simplicity, we have so far only considered the case $\mu = \mu_R = \mu_F$. Expressions for $\kappa \neq 1$ can be easily recovered both for the coefficient functions (2.9) and the splitting functions (2.16) by re-expanding a_s in powers of $\log(\mu_F^2/\mu_R^2)$. The general expressions are implemented in our numerical code.

Due to the matrix-valued nature of Eq. (2.23), no unique closed solution exists beyond LO. Instead, it can be written as an expansion around the LO solution, $(a_s/a_0)^{-\boldsymbol{R}_0(N)}\boldsymbol{D}^h(N,a_0)$, where a_0 is the value of a_s at the initial scale μ_0 where the non-perturbative input $\boldsymbol{D}^h(N,a_0)$

is specified from a fit to data. This expansion reads

$$\boldsymbol{D}^h(N,a_s) = \left[1+\sum_{k=1}^{\infty} a_s^k\,\boldsymbol{U}_k(N)\right]\left(\frac{a_s}{a_0}\right)^{-\boldsymbol{R}_0(N)}\left[1+\sum_{k=1}^{\infty} a_s^k\,\boldsymbol{U}_k(N)\right]^{-1}\boldsymbol{D}^h(N,a_0)\;. \tag{2.26}$$

The evolution matrices $\boldsymbol{U}_k$ are recursively defined by the commutation relations

$$[\boldsymbol{U}_k,\boldsymbol{R}_0] = \boldsymbol{R}_k + \sum_{i=1}^{k-1}\boldsymbol{R}_{k-1}\boldsymbol{U}_i + k\boldsymbol{U}_k\;. \tag{2.27}$$

Based on (2.26), it is now possible to define several solutions at order $\mathrm{N^mLO}$ which are all equivalent up to the accuracy considered, i.e., up to subleading higher-order terms. Any numerical differences between two different choices should be treated as a source of theoretical uncertainty in the determination of FFs or PDFs, and it is expected that the inclusion of NNLO corrections reduces this type of ambiguity as compared to NLO. We highlight two possible solutions which we pursue further in our phenomenological studies in Sec. 2.4. Suppose the perturbatively calculable quantities $\boldsymbol{P}^{T,(k)}$ and β_k are available up to a certain order $k=m$. One possibility is to expand Eq. (2.26) in a_s and strictly keep only terms up to a_s^m. This defines what is usually called the *truncated solution* in Mellin moment space, and, unless stated otherwise, will be used in all our phenomenological applications.

However, given the iterative definition of the $\boldsymbol{R}_k$ in Eq. (2.24), one may alternatively calculate the $\boldsymbol{R}_k$ and, hence the $\boldsymbol{U}_k$ in Eq. (2.27), for any $k>m$ from the known results for $\boldsymbol{P}^{T,(k)}$ and β_k up to $k=m$. Any higher order $\boldsymbol{P}^{T,(k)}$ and β_k with $k>m$ are simply set to zero. Taking into account all the thus constructed $\boldsymbol{U}_k$ in Eq. (2.26) defines the so-called *iterated solution*. This solution is important as it mimics the results that would be obtained by solving Eq. (2.15) directly in z-space by some numerical iterative method. Both choices are equally valid as they only differ by terms that are of order $\mathcal{O}(a_s^{m+1})$ and are implemented in our numerical code; see Ref. [157] for a more detailed discussion in the context of space-like evolution equations. We shall illustrate the numerical differences between the truncated and iterated solution in Sec. 2.4.

2.2.3 Numerical Implementation: NNLO analysis

We base the development of our new NNLO evolution code for FFs on the well-tested PEGASUS package [157] which provides different numerical solutions to the space-like evolution of PDFs up to NNLO accuracy in Mellin N space and the necessary routines for the subsequent Mellin

inverse transformation back to momentum space. It also solves the RGE for the strong coupling $a_s(\mu_R^2)$ in the required order in pQCD. In addition to extending PEGASUS to handle also time-like evolution, we also add packages to compute the SIA cross section in N-space and to determine the parameters of the FFs at some input scale μ_0 from a fit to existing SIA data at LO, NLO, and NNLO accuracy.

In Sec. 2.2.2 we have omitted how we deal with heavy quark flavors, i.e., charm and bottom, in the time-like scale evolution apart from defining the relevant $2N_f - 1$ NS combinations of FFs in Eqs. (2.19) and (2.20). In PEGASUS [157] both a fixed flavor-number scheme (FFNS) and a variable flavor-number scheme (VFNS) evolution are implemented. For the latter, matching coefficients between the space-like evolution for N_f and N_f+1 are provided for both PDFs [161] and the RGE for a_s [162, 163] up to NNLO accuracy. Similar time-like matching coefficients for FFs are only known up to NLO and can be found in Ref. [164]. They are implemented in our evolution code. In practice, however, all fits of FFs performed so far [72–79], have used a different approach for the charm and bottom-to-light hadron FFs. Once the scale μ in the evolution crosses the heavy quark pole mass $Q = m_{c,b}$, a new non-perturbative input distribution is introduced at that scale $D^h_{c,b}(z, m^2_{c,b})$ and $N_f \to N_f + 1$. The parameters describing these input distributions $D^h_{c,b}(z, m^2_{c,b})$ are also determined by a fit to, usually flavor-tagged, data taken at scales $\mu \gg m_{c,b}$. We will also adopt this non-perturbative input scheme (NPIS) in all our phenomenological studies below. We note that as one of the many cross-checks for our new time-like evolution code, we have implemented the input parameters and $a_s(\mu_0)$ value of the NLO NPIS fit to SIA data performed in Ref. [72]. We obtain an excellent numerical agreement with the FFs of [72] for all z and μ values.

As the last technical issue, we would like to comment on the numerical implementation of the Mellin inverse transformation. To this end, one needs to perform a numerical integration in complex N-space along a suitably chosen contour $\mathcal{C}_N$ in order to recover expressions in z-space which can be compared to data. In case of the SIA cross section, this transformation schematically reads

$$D(z) \otimes \mathbb{C}(z) = \frac{1}{2\pi i} \int_{\mathcal{C}_N} dN\, z^{-N}\, D(N)\, \mathbb{C}\,(N)\ , \tag{2.28}$$

where we have omitted any scale μ and flavor dependence in Eq. (2.28). In practice, one chooses a tilted contour $\mathcal{C}_N$ which can be parametrized in terms of a real variable x as $N = c + x\, e^{i\phi}$, see Fig. 2.1 for an illustration of the path and Ref. [157] for more details. To ensure that the value of the integral is independent of $\mathcal{C}_N$, c has to be to the right of the rightmost pole of the

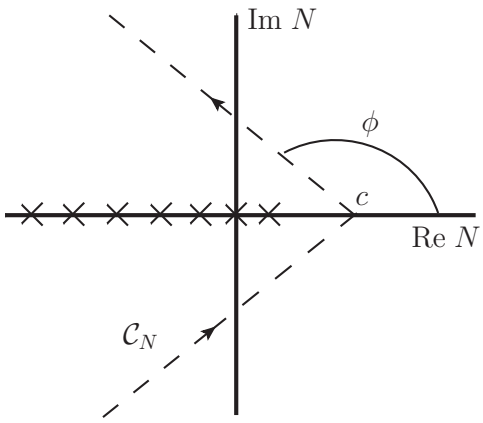

Figure 2.1: The dashed line represents the contour $\mathcal{C}_N$ in complex N-space to perform the inverse Mellin transformation (2.28). The poles of the integrand along the real axis are schematically represented by the crosses.

integrand, which, in our case, are all located along the real axis. An exponential dampening of the integrand in (2.28) is achieved for $\pi > \phi \geq \pi/2$, resulting in a smaller upper integration limit $x_{\max}$ sufficient for a numerically stable result.

However, extra care needs to be taken in choosing actual values for both c and ϕ beyond the requirements just outlined. As it turns out, the standard choice, $c = 1.9$ and $\phi = 3/4$, made for the PDF evolution in PEGASUS cannot be used in the time-like case. This is due to the fact that the time-like kernels $P^T(z)$ are more singular than their space-like counterparts $P^S(x)$ in the limit $z, x \to 0$. At NLO accuracy, one finds, for instance, that $P_{gg}^{T,(1)}(z) \propto \log^2(z)/z$ [122–124] whereas $P_{gg}^{S,(1)}(x) \propto 1/z$ [71, 155]. In Mellin space this behavior translates into $\propto 1/(N-1)^3$ and $\propto 1/(N-1)$, respectively, i.e., a leading singularity at $N = 1$. To order $\mathrm{N^mLO}$ this generalizes to $P_{gg}^{T,(m)}(N) \propto 1/(N-1)^{(2m+1)}$ [62, 126] whereas in the space-like case only one additional power of $1/(N-1)$ appears in each order (see e.g. [165] and references therin). As a result, the function that is integrated in Eq. (2.28) has potentially much stronger oscillations in the vicinity of the pole $N = 1$ than for the corresponding Mellin inverse transformations for space-like PDFs and observables, and achieving numerical convergence becomes considerably more delicate.

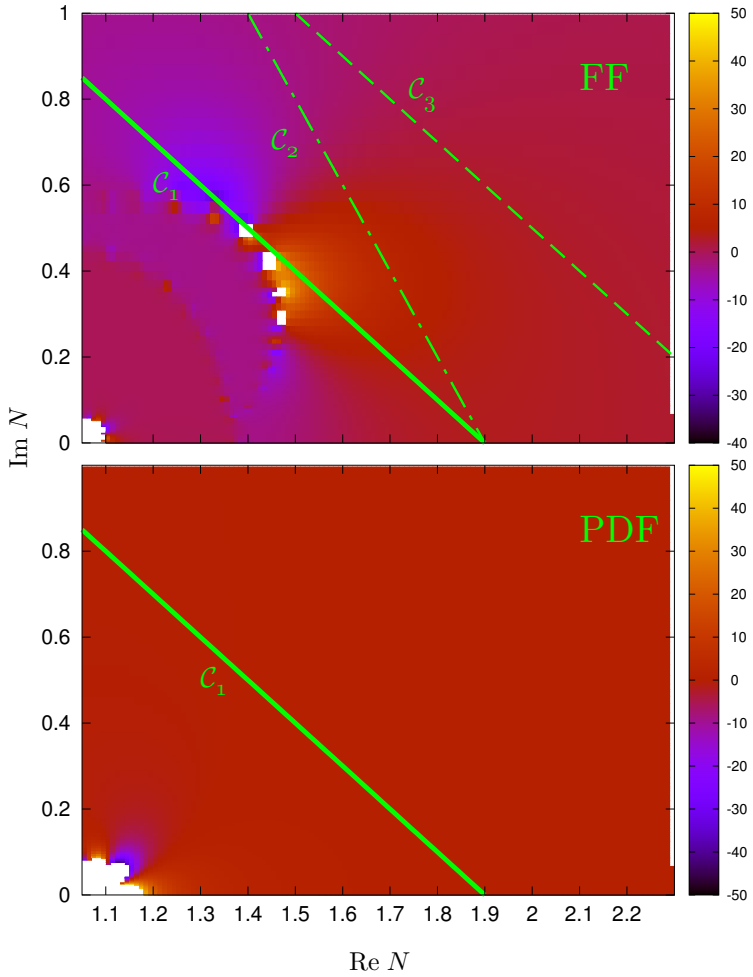

Figure 2.2: The value of the real part of $\mathcal{K}_{12}$ in Eq. (2.29) in a region of the complex N plane for both the evolution of FFs (upper panel) and PDFs (lower panel). The lines correspond to three different integration contours $\mathcal{C}_N$ in (2.28). $\mathcal{C}_1$ is the default choice in the PEGASUS package [157]; see text.

To illustrate this issue further, we schematically write the general solution in Eq. (2.26) as

$$\boldsymbol{D}^h(N, a_s) = \begin{pmatrix} \mathcal{K}_{11}^T(a_s, a_0, N) & \mathcal{K}_{12}^T(a_s, a_0, N) \\ \mathcal{K}_{21}^T(a_s, a_0, N) & \mathcal{K}_{22}^T(a_s, a_0, N) \end{pmatrix} \boldsymbol{D}^h(N, a_0) \,, \tag{2.29}$$

where the $\mathcal{K}_{ij}^T$ denote the entries of the 2×2 time-like evolution matrix on the right-hand-side of (2.26). A similar equation can be written down for the evolution of PDFs.

In Fig. 2.2 we show a comparison of the real part of the NLO singlet evolution kernel $\text{Re}\{\mathcal{K}_{12}^{T,S}\}$

for the iterated solution for both the evolution of FFs (upper panel) and PDFs (lower panel) in the relevant section of the complex N plane. As an illustrative example, we have chosen $\mu_0^2 = 1$ GeV^2 and $\mu^2 = 110$ GeV^2, the scale relevant for BELLE and BABAR, in Eq. (2.29). The line labeled as $\mathcal{C}_1$ represents the standard contour $\mathcal{C}_N$ implemented in PEGASUS [157], and $\mathcal{C}_{2,3}$ are two alternative choices.

As can be seen from the upper panel of Fig. 2.2, the contour $\mathcal{C}_1$ with $c = 1.9$ and $\phi = 3/4$ goes through a region of strong numerical oscillations of $\mathrm{Re}\{\mathcal{K}_{12}^T\}$ and, as a consequence, yields numerically unstable results for the integral in Eq. (2.28). Hence, in our code we need to choose either a different angle, e.g., $\phi = 2/3$ as in $\mathcal{C}_2$, or a different value of c, such as $c = 2.5$ adopted in $\mathcal{C}_3$. Both choices lead to numerically stable and identical results for the Mellin inverse transformation in Eq. (2.28) for all practical purposes. Figure 2.2 also shows that no such issue appears for the evolution of PDFs because of the weaker $N = 1$ singularity than in the time-like case.

Finally, we compare the results of our time-like evolution code with those obtained with the publicly available MELA [125] package, where also tables of benchmark numbers are given corresponding to input FFs taken from the fit in Ref. [76]; cf. Eq. (3.3) in [125]. Using the same input FFs, we were not able to directly reproduce their benchmark results as generated "out of the box" from the downloadable script. The RGE for $a_s(\mu_R)$ is always solved exactly in our code by means of a fourth order Runge-Kutta integration [166] (as taken from the PEGASUS package [157]), whereas in MELA the standard, expanded solution is utilized for the truncated solution of Eq. (2.26). After this small difference is accounted for, we achieve perfect numerical agreement with differences of less than 0.01% for both the truncated and iterated solution using the FFNS with $N_f = 3$ or the VFNS.

2.3 Small-z Resummation for Semi-inclusive $\mathbf{e}^+\mathbf{e}^-$ annihilation

This section covers all the relevant technical aspects of small-z resummations in SIA: in Sec. 2.3.1 we sketch the systematics of the small-z enhanced logarithmic contributions that appear in both the coefficient functions for SIA and in the time-like evolution kernels in each order of perturbation theory. The resummation of these logarithms up to NNLL accuracy is concisely reviewed in Sec. 2.3.2, where we also compare our results to those available in the

literature. In Sec. 2.3.3, we extend the currently available resummed expressions for the SIA cross section by re-introducing their dependence on the scales μ_F and μ_R, which is vital for a discussion of theoretical uncertainties later on in the phenomenological section of this chapter. In Sec. 2.3.4 we explain in some detail how the resummed kernels are used in solving the time-like evoltion equations in Mellin N space, and numerical peculiarities, in particular, those associated with the Mellin inverse transformation are covered in Sec. 2.3.5

2.3.1 Systematics of small-z logarithms

The fixed order results of the coefficient functions contain logarithms that become large for $z \to 1$ (large-z regime) and $z \to 0$ (small-z regime). Such large logarithms can potentially spoil the convergence of the perturbative expansion even for $a_s \ll 1$ and, hence, need to be taken into account to all orders in the strong coupling. The resummation of large-z logarithms in SIA has been addressed, for instance, in Refs. [J1, 131–135]. The main focus of the work [J5] is on the so far very little explored small-z regime and its phenomenology. In contrast to the space-like DIS process with its single logarithmic enhancement, one finds a double logarithmic enhancement for the time-like SIA; see, e.g., [167] and references therein. For example, for the gluon sector in Eq. (2.4) one finds

$$\begin{aligned} \mathbb{C}_{T,g}^{S,(k)} &\propto a_s^k \frac{1}{z} \log^{2k-1-a}(z)\,, \\ \mathbb{C}_{L,g}^{S,(k)} &\propto a_s^k \frac{1}{z} \log^{2k-2-a}(z)\,, \end{aligned} \tag{2.30}$$

where $a = 0, 1$, and 2 corresponds to the leading logarithmic (LL), next-to-leading logarithmic (NLL), and NNLL contribution, respectively.

Furthermore, the same logarithmic behavior at small-z is found for the time-like splitting functions that govern the scale evolution of the FFs. For example, for the gluon-to-gluon and the quark-to-gluon splitting function, one finds

$$P_{gi}^{T,(k)} \propto a_s^{(k+1)} \frac{1}{z} \log^{2k-a}(z)\,, \tag{2.31}$$

where $i = q, g$, and k denotes the perturbative order starting from $k = 0$, i.e., LO. In order to obtain a reliable prediction from perturbative QCD in the small-z regime, these large logarithmic contributions, both in the coefficient functions and in the splitting functions, need to be

	$\mathbb{C}^{S,(n)}_{T,g}$	$\mathbb{C}^{S,(n)}_{T,q}$	$\mathbb{C}^{S,(n)}_{L,g}$	$\mathbb{C}^{S,(n)}_{L,q}$
LL	$\bar{N}^{-2n}$	–	$\bar{N}^{1-2n}$	–
NLL	$\bar{N}^{1-2n}$	$\bar{N}^{1-2n}$	$\bar{N}^{2-2n}$	$\bar{N}^{2-2n}$
NNLL	$\bar{N}^{2-2n}$	$\bar{N}^{2-2n}$	$\bar{N}^{3-2n}$	$\bar{N}^{3-2n}$
	$n \geq 1$	$n \geq 2$	$n \geq 1$	$n \geq 2$

Table 2.1: The explicit $1/\bar{N}$ dependence of the coefficient functions $\mathbb{C}^S_{k,l} = \sum_n a_s^n \mathbb{C}^{S,(n)}_{k,l}$ at any given fixed order n of the perturbative expansion at the LL, NLL, and NNLL approximation. These generic structures are valid starting from $n = 1$ or $n = 2$ as indicated in the bottom row of the table. For smaller values of n, the correct $1/\bar{N}$ dependence must be extracted from the fixed order results; see text. Also, note that the entry for $\mathbb{C}^{S,(n)}_{L,g}$ at NNLL is obtained by $\mathcal{AC}$ relations; see text.

	$P^{T,(n)}_{gg}$	$P^{T,(n)}_{gq}$	$P^{T,(n)}_{qq}$	$P^{T,(n)}_{qg}$
LL	$\bar{N}^{-1-2n}$	$\bar{N}^{-1-2n}$	–	–
NLL	$\bar{N}^{-2n}$	$\bar{N}^{-2n}$	$\bar{N}^{-2n}$	$\bar{N}^{-2n}$
NNLL	$\bar{N}^{1-2n}$	$\bar{N}^{1-2n}$	$\bar{N}^{1-2n}$	$\bar{N}^{1-2n}$
	$n \geq 0$	$n \geq 0$	$n \geq 2$	$n \geq 2$

Table 2.2: Same as Tab. 2.1 but for the splitting functions $P^T_{ij} = \sum_n a_s^{n+1} P^{T,(n)}_{ij}$.

resummed to all orders. The resulting expressions are available in the literature up to NNLL accuracy [129, 130] and we will re-derive them in the next subsection. Traditionally, and most conveniently, these calculations are carried out in the complex Mellin transform space. The Mellin transform of the small-z logarithms given in Eqs. (2.30) and (2.31) reads

$$\mathcal{M}\left[\frac{\log^{2k-1}(z)}{z}\right] = (-1)^k \frac{(2k-1)!}{\bar{N}^{2k}}\,, \tag{2.32}$$

where $\bar{N} \equiv N - 1$, i.e., they give rise to singularities at $N = 1$ in Mellin space.
The structure of the $1/\bar{N}$ divergences for all quantities relevant to a theoretical analysis of SIA up to NNLL accuracy is summarized schematically in Tables 2.1 and 2.2. Note that no LL contributions appear in the quark sector, neither for the splitting nor for the coefficient functions. Moreover, the LO and NLO small-z contributions to $\mathbb{C}^S_{T/L,q}$, P^T_{qq}, and P^T_{qg} are not contained in the generic structure summarized in Tables 2.1 and 2.2. Instead, these terms have

to be extracted directly from the respective fixed order calculations. We would like to point out that there is no complete NNLO calculation (i.e., third order in a_s) for the longitudinal coefficient functions available at this time. Therefore, only the first two non-vanishing logarithmic contributions can be resummed for the time being. For this reason, the third entry for $\mathbb{C}^S_{L,g}$ in Tab. 2.1 has to be deduced using analytic continuation ($\mathcal{AC}$) relations between DIS and SIA; see Refs. [122–124, 168] for details.

2.3.2 Small-z resummations

The resummation of the first three towers of small-z logarithms, summarized in Tables 2.1 and 2.2, was performed recently in Refs. [129, 130] in a formalism based on all-order mass factorization relations and the general structure of unfactorized structure functions in SIA. Explicit analytical results can be found for the choice $\mu = Q$. The corresponding LL and NLL expressios are known for quite some time [62, 66, 126–128] and have been derived by other means. We have adopted the same framework based on mass factorization as in [129, 130] and re-derived all results from scratch up to NNLL accuracy. We are in perfect agreement with all of their expressions except for some obvious, minor typographical errors [1]. In this section, we will concisely summarize the main aspects of the calculation as we will extend the obtained results to a general choice of scale $\mu \neq Q$ in the next subsection.

One starts from the unfactorized structure functions using dimensional regularization. In our case, we choose to work in $d = 4-2\varepsilon$ dimensions. The unfactorized partonic structure functions can be written as

$$\hat{\mathcal{F}}_{k,l}(N, a_s, \varepsilon) = \sum_{i=q,g} C_{k,i}(N, a_s, \varepsilon)\Gamma_{il}(N, a_s, \varepsilon)\,, \tag{2.33}$$

with $k = L, T$ and $l = q, g$. We have introduced the d-dimensional coefficient functions $C_{k,l}$, which contain only positive powers in ε,

$$C_{k,l}(N, a_s, \varepsilon) = \delta_{kT}\delta_{l,q} + \sum_{i=1}^{\infty} a_s^i \sum_{j=0}^{\infty} \varepsilon^j c_{k,l}^{(i,j)}(N)\,, \tag{2.34}$$

[1] We noticed the following typographical errors in Ref. [129] which should be corrected as follows:
Eq. (2.12): $\left(\frac{67}{9}C_A - 4\zeta_2\right) \to \left(\frac{67}{9} - 4\zeta_2\right)$
Eq. (3.18) 1st line, last term: $-\frac{38}{9}C_A^2 C_F n_f \to -\frac{38}{9}C_A C_F^2 n_f$
Eq. (4.8) 2st line, last term: $-\frac{47}{9}C_F n_f^2 \to -\frac{47}{9}C_F^2 n_f$
Eq. (5.5) denominator: $9(N-1)^{2n-2} \to 9(N-1)^{2n-3}$

whereas the transition functions Γ_{ij} include all IR/mass singularities, which are manifest in $1/\varepsilon$ poles, i.e., they contain all negative powers of ε. The transition functions are calculable order by order in a_s by solving the equation

$$\beta_d(a_s)\frac{\partial\Gamma_{ik}}{\partial a_s}\Gamma^{-1}_{kj} = P^T_{ij}\,. \tag{2.35}$$

Here, $\beta_d(a_s) = -\varepsilon\, a_s - a_s^2\sum_{i=0}^{\infty}\beta_i a_s^i$ denotes the d-dimensional beta function of QCD. Eq. (2.35) can be derived from the time-like evolution equations and its solution reads

$$\begin{aligned}\boldsymbol{\Gamma} &= \mathbb{1} - a_s\frac{\boldsymbol{P}^{T,(0)}}{\varepsilon} + a_s^2\left[\frac{1}{2\varepsilon^2}(\boldsymbol{P}^{T,(0)}+\beta_0)\boldsymbol{P}^{T,(0)} - \frac{1}{2\varepsilon}\boldsymbol{P}^{T,(1)}\right]\\
&+ a_s^3\Bigg[-\frac{1}{6\varepsilon^3}(\boldsymbol{P}^{T,(0)}+\beta_0)(\boldsymbol{P}^{T,(0)}+2\beta_0)\boldsymbol{P}^{T,(0)} +\\
&\quad\frac{1}{6\varepsilon^2}\Big\{(\boldsymbol{P}^{T,(0)}+2\beta_0)\boldsymbol{P}^{T,(1)} + (\boldsymbol{P}^{T,(1)}+\beta_1)2\boldsymbol{P}^{T,(0)}\Big\} - \frac{1}{3\varepsilon}\boldsymbol{P}^{T,(2)}\Bigg] + \mathcal{O}(a_s^4)\end{aligned} \tag{2.36}$$

where

$$\boldsymbol{P}^T \equiv \sum_{i=0}^{\infty} a_s^{i+1}\boldsymbol{P}^{T,(i)} \equiv \sum_{i=0}^{\infty} a_s^{i+1}\begin{pmatrix} P_{qq}^{T,(i)} & P_{gq}^{T,(i)} \\ P_{qg}^{T,(i)} & P_{gg}^{T,(i)}\end{pmatrix} \tag{2.37}$$

is the 2×2 matrix that contains the time-like singlet splitting functions. Note that here, the off-diagonal entries of the matrix $\boldsymbol{P}^T$ differ from the ones of $\widetilde{\boldsymbol{P}}^T$ in Eq. (2.18) and Eq. (2.25) by factors $2N_f$ and $1/2N_f$. Since we are interested only in the small-z regime, we take the small-$\bar{N}$ limit of the known coefficient and splitting functions in Eq. (2.33).

Alternatively, one can express the unfactorized partonic structure functions in Eq. (2.33) as a series in a_s,

$$\hat{\mathcal{F}}_{k,l}(N, a_s, \varepsilon) = \sum_n a_s^n \hat{\mathcal{F}}^{(n)}_{k,l}(N, a_s, \varepsilon)\,. \tag{2.38}$$

The key ingredient to achieve the resummations of the leading small-$\bar{N}$ contributions, which is the main result of [129], is the observation that the $\mathcal{O}(a_s^n)$ contribution in Eq. (2.38) may be written as

$$\hat{\mathcal{F}}^{(n)}_{k,l}(N, a_s, \varepsilon) = \varepsilon^{\delta_{kL}+\delta_{lq}+1-2n}\sum_{i=0}^{n-1-\delta_{lq}}\frac{1}{\bar{N}-2(n-i)\varepsilon}\times\left(A^{(i,n)}_{k,l} + \varepsilon B^{(i,n)}_{k,l} + \varepsilon^2 C^{(i,n)}_{k,l} + \dots\right). \tag{2.39}$$

Each of the coefficients A, B, and C is associated with a different logarithmic accuracy of the

resummation, i.e., LL, NLL, and NNLL, respectively.

By equating Eqs. (2.33) and (2.38), one obtains a system of equations which may be solved recursively order by order in a_s. The small-z (small-$\bar{N}$) limits of the fixed order results are needed here as initial conditions for the first recursion. Since these results are only known up to NNLO accuracy, resummations are limited for the time being to the first three towers listed in Tables 2.1 and 2.2. At each order n, this procedure then yields expressions for $c_{k,l}^{(n,m)}$, $P_{ij}^{T,(n-1)}$, $A_{k,l}^{(m,n)}$, $B_{k,l}^{(m,n)}$, and $C_{k,l}^{(m,n)}$.

Note that up to NNLL accuracy only β_0 is needed in Eq. (2.36). All terms proportional $\beta_{i\geq 1}$ will generate subleading contributions and, hence, can be discarded. For instance, when initiating the recursive solution, $\boldsymbol{P}^{T,(0)}$ and $\boldsymbol{P}^{T,(1)}$ are known from fixed order calculations, and $\boldsymbol{P}^{T,(2)}$, that appears at $\mathcal{O}(a_s^3)$ in Eq. (2.36), is the unknown function that is being determined. The NNLL contribution for, say, $P_{gg}^{T,(2)}$ is $\propto 1/\bar{N}^2$, cf. Table 2.2, whereas the highest inverse power of $\bar{N}$ in the term $\beta_1 P_{gg}^{T,(0)}$ appearing in the curly brackets of Eq. (2.36) is $\propto 1/\bar{N}$ and, thus, beyond NNLL accuracy.

After solving the system of equations algebraically using MATHEMATICA [146], we find expressions for $c_{k,l}^{(n,0)}$, and $P_{ij}^{T,(n)}$. Since the coefficient functions and the splitting functions both have a perturbative expansion in a_s,

$$P_{ij}^{T} = \sum_{n=0}^{\infty} a_s^{n+1} P_{ij}^{T,(n)} \tag{2.40}$$

and

$$\mathbb{C}_{k,l}^{\mathrm{S}} = \sum_{n=0}^{\infty} a_s^{n} c_{k,l}^{(n,0)} \tag{2.41}$$

one can eventually deduce a closed expression for resummed splitting functions and coefficient functions as listed in [130]. As mentioned above, we fully agree with these results up to the typographical errors listed in the footnote.

2.3.3 Resummed scale dependence

All calculations presented so far in this chapter, including Refs. [129, 130], have been performed by identifying, for simplicity, the renormalization and factorization scales with the hard scale Q, i.e., by setting $\mu_F = \mu_R = \mu = Q$. However, it is well known that the resummation procedure should not only yield more stable results but should also lead to a better control of the residual dependence on the unphysical scales μ_F and μ_R that arises solely from the truncation of the

perturbative series. Hence, for our subsequent studies of the phenomenological impact of the small-z resummations on the extraction of FFs from SIA data it is imperative to reintroduce the dependence on the scales μ_F and μ_R in the resummed expressions. This is the goal of this section. In what follows, we reinstate the scale dependence with two different, independent methods. We find full agreement between the two approaches.

Firstly, we consider a renormalization group approach; see also Ref. [169]. The dependence of the coefficient functions on the factorization scale μ_F can be expressed as

$$\mathbb{C}^{\mathrm{S}}_{k,l}(N, a_s, L_M) = \sum_{i=0}^{\infty} a_s^i \left(c^{(i)}_{k,l}(N) + \sum_{m=1}^{i} \tilde{c}^{(i,m)}_{k,l}(N) L_M^m \right) , \tag{2.42}$$

with $L_M \equiv \log \frac{Q^2}{\mu_F^2}$. The coefficients $c^{(i)}_{k,l} \equiv \tilde{c}^{(i,0)}_{k,l}$ are the finite (i.e., ε independent) coefficients as given in Eq. (2.34). The $\tilde{c}^{(i,m)}_{k,l}$ can be calculated order by order in a_s by solving a set of renormalization group equations (RGEs). These equations can be obtained by requiring that $\frac{d}{d\log\mu_F^2} F_k \stackrel{!}{=} 0$, where $F_k \equiv \sum_l \mathbb{C}_{k,l} D_l$ (see Eq. (2.6) for the definition of these structure functions in z space), which leads to

$$\left[\left\{ \frac{\partial}{\partial \log \mu_F^2} + \beta(a_s) \frac{\partial}{\partial a_s} \right\} \delta_{lm} + P^T_{lm}(N) \right] \mathbb{C}^{\mathrm{S}}_{k,m}(N, a_s, L_M) = 0 \, . \tag{2.43}$$

Here, the sum over $m = q, g$ is left implicit. For the sake of better readability, we drop the arguments of all functions for now. From (2.43), the following recursive formula can be obtained

$$\tilde{c}^{(i,m)}_{k,l} = \frac{1}{m} \sum_{w=m-1}^{i-1} \tilde{c}^{(w,m-1)}_{k,j} \left(P^{T,\,(i-w-1)}_{lj} - w \beta_{i-w-1} \delta_{jl} \right) . \tag{2.44}$$

Again, the sum over $j = q, g$ is implicitly understood. Up to NNLO accuracy, we obtain the same results as given in [67].

If one now plugs in the small-$\bar{N}$ results for the splitting and coefficient functions, one can compute the coefficients $\tilde{c}^{(n,m)}_{k,l}$ up to any order n and identify the leading three towers of $1/\bar{N}$ in Eq. (2.42), i.e., the LL, NLL, and NNLL contributions. At order n we find at LL accuracy

$$\mathbb{C}^{\mathrm{S,LL},(n)}_{k,g} = c^{\mathrm{LL},(n)}_{k,g} \, . \tag{2.45}$$

Thus, no improvement of the scale dependence is achieved by a LL resummation (recall that

resummation in the quark sector only starts at NLL accuracy). The full L_M dependence is given by the fixed-order expressions, which have to be matched to the resummed result for all practical purposes. As usual, the matching of a resummed observable $T^{\rm res}$ to its N$^\kappa$LO fixed-order expression $T^{\rm N^\kappa LO}$ is performed according to the prescription schematically given by

$$T^{\rm matched} = T^{\rm N^\kappa LO} + T^{\rm res} - T^{\rm res}|_{\mathcal{O}(a_s^\kappa)} \,. \tag{2.46}$$

Here, $T^{\rm res}|_{\mathcal{O}(a_s^\kappa)}$ denotes the expansion in a_s of $T^{\rm res}$ up to order $\mathcal{O}(a_s^\kappa)$. Likewise, at NLL accuracy one obtains the following results

$$\mathbb{C}_{T,g}^{\rm S,NLL,(n)} = c_{T,g}^{\rm NLL,(n)} + L_M \left\{ P_{gq}^{T\ \rm LL,(n-1)} + \sum_{j=0}^{n-2} c_{T,g}^{\rm LL,(n-1-j)} P_{gg}^{T\ \rm LL,(j)} \right\}, \tag{2.47}$$

$$\mathbb{C}_{L,g}^{\rm S,NLL,(n)} = c_{L,g}^{\rm NLL,(n)} \quad + \quad L_M \sum_{j=0}^{n-2} c_{L,g}^{\rm LL,(n-1-j)} P_{gg}^{T\ \rm LL,(j)} \tag{2.48}$$

and

$$\mathbb{C}_{T,q}^{\rm S,NLL,(n)} = c_{T,q}^{\rm NLL,(n)} \,, \tag{2.49}$$

$$\mathbb{C}_{L,q}^{\rm S,NLL,(n)} = c_{L,q}^{\rm NLL,(n)} \,. \tag{2.50}$$

The scale dependent terms $\propto L_M$ enter here for the first time in the gluonic sector, Eqs (2.47) and (2.48), and are expressed in terms of LL quantities. Due to the fact that the quark coefficient functions are subleading, they still do not carry any scale dependence at NLL. Finally, at NNLL accuracy one finds

$$\begin{aligned} \mathbb{C}_{T,g}^{\rm S,NNLL,(n)} \;=\; & c_{T,g}^{\rm NNLL,(n)} + L_M \Bigg\{ P_{gq}^{T\ \rm NLL,(n-1)} - (n-1)\beta_0 c_{T,g}^{\rm LL,(n-1)} + \sum_{j=0}^{n-3} c_{T,q}^{\rm NLL,(n-1-j)} P_{gq}^{T\ \rm LL,(j)} \\ & + \sum_{j=0}^{n-2} \left(c_{T,g}^{\rm LL,(n-1-j)} P_{gg}^{T\ \rm NLL,(j)} + c_{T,g}^{\rm NLL,(n-1-j)} P_{gg}^{T\ \rm LL,(j)} \right) \Bigg\} \end{aligned}$$

$$+\frac{L_M^2}{2}\left[\sum_{j=0}^{n-2} P_{gq}^{T\,\mathrm{LL},(n-2-j)} P_{gg}^{T\,\mathrm{LL},(j)} + \sum_{i=0}^{n-3}\sum_{j=0}^{n-2-i} c_{T,g}^{\mathrm{LL},(n-2-i-j)} P_{gg}^{T\,\mathrm{LL},(i)} P_{gg}^{T\,\mathrm{LL},(j)}\right], \tag{2.51}$$

$$\begin{aligned}\mathbb{C}_{L,g}^{\mathrm{S,NNLL},(n)} &= c_{L,g}^{\mathrm{NNLL},(n)} + L_M\Bigg\{ -(n-1)\beta_0 c_{L,g}^{\mathrm{LL},(n-1)} \\ &+ \sum_{j=0}^{n-2}\left(c_{L,g}^{\mathrm{LL},(n-1-j)} P_{gg}^{T\,\mathrm{NLL},(j)} + c_{L,g}^{\mathrm{NLL},(n-1-j)} P_{gg}^{T\,\mathrm{LL},(j)}\right) + \sum_{j=0}^{n-2} c_{L,q}^{\mathrm{NLL},(n-1-j)} P_{gq}^{T\,\mathrm{LL},(j)}\Bigg\} \\ &+ \frac{L_M^2}{2}\sum_{i=0}^{n-3}\sum_{j=0}^{n-3-i} c_{L,g}^{\mathrm{LL},(n-2-i-j)} P_{gg}^{T\,\mathrm{LL},(i)} P_{gg}^{T\,\mathrm{LL},(j)}\,,\end{aligned} \tag{2.52}$$

$$\mathbb{C}_{T,q}^{\mathrm{S,NNLL},(n)} = c_{T,q}^{\mathrm{NNLL},(n)} + L_M\left\{P_{qq}^{T\,\mathrm{NLL},(n-1)}(1-\delta_{n,2}) + \sum_{j=0,j\neq 1}^{n-1} c_{T,g}^{\mathrm{LL},(n-1-j)} P_{qg}^{T\,\mathrm{NLL},(j)}\right\}, \tag{2.53}$$

and

$$\mathbb{C}_{L,q}^{\mathrm{S,NNLL},(n)} = c_{L,q}^{\mathrm{NNLL},(n)} + L_M \sum_{j=0,j\neq 1}^{n-2} c_{L,g}^{\mathrm{LL},(n-1-j)} P_{qg}^{T\,\mathrm{NLL},(j)} \tag{2.54}$$

It should be noticed that by the subscripts LL, NLL, and NNLL in Eqs. (2.45) and (2.47)-(2.54), we denote *only* those contributions in $1/\bar{N}$ specific to the tower at LL, NLL, or NNLL accuracy, respectively. This means, for instance, that the full next-to-next-to-leading logarithmic expression at some given order n in the a_s perturbative expansion of $\mathbb{C}_{k,l}^{\mathrm{S}}$ in Eq.(2.42) will be always given by the *sum* of the individual LL, NLL, and NNLL contributions. As one may expect from the fixed-order results, the scale dependence at $\mathrm{N}^m\mathrm{LL}$ is expressed entirely in terms of the resummed expressions at $\mathrm{N}^k\mathrm{LL}$ with $k < m$. Since the resummed results are known up to NNLL accuracy, we may, in principle, extend our calculations to fully predict the scale dependent terms at $\mathrm{N}^3\mathrm{LL}$. These findings are consistent with the scale dependence of fixed-order cross sections. Finally, for all practical purposes, as we shall see below, it is numerically adequate to have explicit results for each tower up to sufficiently high order in n, say, $n = 20$, in lieu of a closed analytical expression for the resummed series as was provided for the case $\mu = Q$ in Refs. [129, 130].

We may now reintroduce the renormalization scale dependence as well by following the straightforward steps outlined in Ref. [67]. In practice, this amounts to replacing all couplings a_s in the expressions given above according to

$$a_s(\mu_F^2) = a_s(\mu_R^2)\left(1 + a_s(\mu_R^2)\beta_0 \log\frac{\mu_R^2}{\mu_F^2} + \mathcal{O}(a_s^2)\right) . \tag{2.55}$$

In a second step one needs to re-expand all results in terms of $a_s(\mu_R^2)$ which leads to additional logarithms of the type $L_R \equiv \log(\mu_R^2/\mu_F^2)$. In our phenomenological studies below we will study, however, only the case $\mu_F = \mu_R \neq Q$ and, hence, we do not pursue the L_R dependence any further.

The second approach we adopt to recover the scale dependence of the SIA coefficient functions obtained in Sec. 2.3.2 is based on the all-order mass factorization procedure. After removing the ultraviolet (UV) singularities from the bare partonic structure functions $\hat{\mathcal{F}}_{k,l}$ (which have been computed directly from Feynman diagrams) by a suitable renormalization procedure, the remaining final-state collinear/mass singularities have to be removed by mass factorization

$$\tilde{\mathcal{F}}_{k,l} = \mathbb{C}_{k,i} \otimes \tilde{\Gamma}_{li} . \tag{2.56}$$

Here, all singularities are absorbed into the transition functions $\tilde{\Gamma}_{li}$ while the coefficient functions $\mathbb{C}_{k,i}$ are finite. We have labeled the quantities in Eq. (2.56) with a tilde to show that they contain the full dependence on all scales.

We may thus proceed in the following way: first, we "dress" the transition functions and partonic structure functions in Eq. (2.33) with the appropriate scale dependence, i.e., we substitute $a_s \to a_s \cdot (\mu_F^2/\mu^2)^{-\varepsilon}$ in the Γ_{ij} and $a_s \to a_s \cdot (Q^2/\mu^2)^{-\varepsilon}$ in the $\hat{\mathcal{F}}_{k,l}$, where the mass parameter μ stems from adopting dimensional regularization. As a next step, we go back to the unrenormalized expressions, where we assume that the renormalization was performed at the scale μ_F^2 and Q^2, respectively. Afterwards, we perform renormalization again, but now at a different scale μ_R^2. Schematically, this amounts to

$$\tilde{\Gamma}_{ij} = R_{\mu^2}^{\mu_R^2}\left[(R_{\mu^2}^{\mu_F^2})^{-1}\left[\Gamma_{ij}(a_s \to a_s \cdot (\mu_F^2/\mu^2)^{-\varepsilon})\right]\right] \tag{2.57}$$

and

$$\tilde{\mathcal{F}}_{k,l} = R_{\mu^2}^{\mu_R^2}\left[(R_{\mu^2}^{Q^2})^{-1}\left[\mathcal{F}_{k,l}(a_s \to a_s \cdot (Q^2/\mu^2)^{-\varepsilon})\right]\right] . \tag{2.58}$$

Here, we are using the following notation: with $R_{\mu^2}^{\mu_R^2}[\hat{f}(\hat{a}_s)] = f[a_s(\mu_R^2)]$ we denote the renormalization of a bare quantity $\hat{f}(\hat{a}_s)$ which, as indicated, depends on the unrenormalized, bare coupling $\hat{a}_s$. This procedure yields a renormalized quantity $f[a_s(\mu_R^2)]$, which now depends on the physical coupling $a_s(\mu_R^2)$. The renormalization procedure $R_{\mu^2}^{\mu_R^2}$ is performed by replacing the bare coupling with

$$\hat{a}_s = a_s(\mu_R^2) Z(\mu_R^2, \mu^2) \tag{2.59}$$

where we have introduced the renormalization constant

$$Z(\mu_R^2, \mu^2) \equiv \left[1 - a_s(\mu_R^2) \cdot \left(\frac{\mu_R^2}{\mu^2}\right)^{-\varepsilon} \frac{\beta_0}{\varepsilon} + \mathcal{O}(a_s^2)\right] . \tag{2.60}$$

Analogously, $(R_{\mu^2}^{\mu_R^2})^{-1}[f[a_s(\mu_R^2)]] = \hat{f}(\hat{a}_s)$ performs the inverse operation, i.e., it translates the renormalized quantity $f(a_s(\mu_R^2))$ back to the corresponding bare quantity $\hat{f}(\hat{a}_s)$. This is achieved by replacing the renormalized coupling with

$$a_s(\mu_R^2) = \hat{a}_s \hat{Z}(\mu_R^2, \mu^2) , \tag{2.61}$$

where the "inverse" renormalization constant reads

$$\hat{Z}(\mu_R^2, \mu^2) \equiv \left[1 + \hat{a}_s \cdot \left(\frac{\mu_R^2}{\mu^2}\right)^{-\varepsilon} \frac{\beta_0}{\varepsilon} + \mathcal{O}(\hat{a}_s^2)\right] . \tag{2.62}$$

The latter can be obtained from Eq. (2.60) by a series reversion. After substituting Eqs. (2.57) and (2.58) into Eq. (2.56) one can solve the latter equation for the coefficients $\mathbb{C}_{k,i}$, which now exhibit the full dependence on μ_R and μ_F.

In order to generate the renormalization constant Z in Eq. (2.60) at each order n in an expansion in a_s with the maximal precision available at this time (i.e., up to terms proportional to β_i, $i \leq 2$), we adopt renormalization group techniques. The general form of the renormalization constant reads

$$Z = 1 + \sum_{k=1}^{\infty} a_s^k \sum_{l=1}^{k} \frac{f_{k,l}}{\varepsilon^l} \tag{2.63}$$

and may also be written as

$$Z = 1 + \sum_{l=1}^{\infty} \frac{g_l(a_s)}{\varepsilon^l} \tag{2.64}$$

where $g_l(a_s) = \sum_{k=l}^{\infty} a_s^k f_{k,l}$ is a power series in a_s with l being the lowest power. Using the RGE it is possible to derive a recursive formula for this power series,

$$g'_{k+1}(a_s) = g'_1(a_s)\frac{d(a_s g_k(a_s))}{da_s}\,. \tag{2.65}$$

Here the prime denotes a derivative with respect to a_s. Hence, we obtain $g_{k+1}(a_s)$ by integration of Eq. (2.65). From the expression of the renormalization constant up to a_s^3, see, for example Ref. [170], we obtain as initial conditions

$$f_{1,1} = -\beta_0, \qquad f_{2,1} = -\frac{\beta_1}{2}, \qquad f_{3,1} = -\frac{\beta_2}{3}\,. \tag{2.66}$$

As already stated above, only terms proportional to β_0 are relevant up to NNLL accuracy.

2.3.4 Solution to the time-like evolution equation with a resummed kernel

As discussed above, small-z resummations are carried out in Mellin space. It is therefore of most convinience to use the developed framework for the NNLO solution to the time-like evolution (see Sec. 2.2.2) and extend it to define a resummed solution.

Instead of the fixed-order expressions defined in Eq. (2.16) for the kernels, we shall now consider the resummed results for the splitting functions $P_{jl}^{T\,\mathrm{N^\kappa LL}}$ as discussed in Sec. 2.3.2 and listed in Ref. [129, 130]. They obey a similar expansion in a_s as in Eq.(2.16), which reads

$$P_{ji}^{T\,\mathrm{N^\kappa LL}} = \sum_{n=0}^{\infty} a_s^{n+1} P_{ji}^{T\,\mathrm{N^\kappa LL},(n)}\,, \tag{2.67}$$

where each term $P_{ji}^{T\,\mathrm{N^\kappa LL},(n)}$ in (2.67) is, in principle, known up to NNLL accuracy, i.e., for $\kappa = 0$, 1, and 2.

The simplest way of extending the fixed-order framework outlined above to the resummed case is to take the *iterated solution* as defined in Sec. 2.2.2. However, instead of setting contributions beyond the fixed order to zero, we use the resummed expressions. One can define a $\mathrm{N^mLO{+}N^\kappa LL}$ resummed "matched solution" by defining the k-th term of the splitting matrix

which appears in Eq. (2.24) as follows:

$$\widetilde{\boldsymbol{P}}^{T,(k)} \equiv \begin{cases} \widetilde{\boldsymbol{P}}^{T\,\mathrm{FO},(k)} & k \leq m \\ \widetilde{\boldsymbol{P}}^{T\,\mathrm{N^\kappa LL},(k)} & k > m\,. \end{cases} \tag{2.68}$$

In other words, the full fixed-order expressions $\widetilde{\boldsymbol{P}}^{T\,\mathrm{FO},(k)}$ for $k \leq m$ are kept in $\boldsymbol{R}_k$, whereas we use the resummed expressions for $k > m$. This iterated and matched solution is the one implemented in our numerical code and will be used in Sec. 2.5 for all our phenomenological studies. For the range of z-values covered by the actual data sets considered in our analysis, only the terms up to $k = 20$ are indeed numerically relevant as we shall discuss further in Sec. 2.3.5. However, when evolving the FFs in scale with such an extended iterative solution, one finds that momentum conservation is broken to some extent due to missing sub-leading terms in the evolution kernels.

In fact, total momentum conservation for FFs is expressed by the sum rules for combinations of splitting functions, see, e.g. Ref. [49].

$$\begin{aligned} \int_0^1 dx\, x \left(P_{qq}^T(x) + P_{gq}^T(x)\right) &= 0\,, \\ \int_0^1 dx\, x \left(P_{gg}^T(x) + P_{qg}^T(x)\right) &= 0\,. \end{aligned} \tag{2.69}$$

In terms of Mellin moments, these relations read

$$P_{qq}^T(N=2) + P_{gq}^T(N=2) = 0\,, \tag{2.70}$$

$$P_{gg}^T(N=2) + P_{qg}^T(N=2) = 0\,. \tag{2.71}$$

These sum rules are satisfied, i.e., built into the kernels, at any given fixed order.

In the case of the iterated and matched solution we use in our numerical implementation, the sum rules in Eqs. (2.70) and (2.71) deviate from zero only about a few ‰ which is perfectly tolerable. We note, that in calculations of the SIA cross section, we also adopt the matching procedure for the relevant resummed coefficient functions as specified in Eq. (2.46).

However, when evaluating the sum rules without matching, the sums in (2.70) and (2.71) yield the approximate values 0.05 and 0.1, respectively, which is, of course, not acceptable.

We would like to point out that a NLO *truncated* + resummed solution has been proposed in

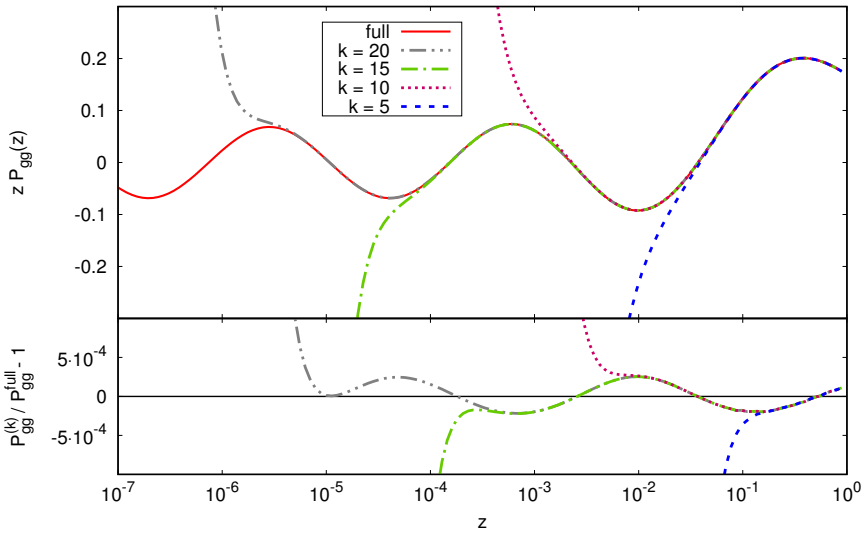

Figure 2.3: Upper panel: expansion of the splitting function $P_{gg}(z)$ times z at NNLL accuracy for different upper values of k compared to the fully resummed expression of Ref. [129, 130]. **Lower panel:** deviation of the full and $\mathcal{O}(k)$ expanded results. All functions are evaluated at $Q^2 = 110\,\text{GeV}^2$ and $N_f = 5$ active flavors.

Ref. [167]. Its extension to NNLO accuracy and the numerical comparison with its *iterated* counterpart as discussed above is not pursued here.

Given that the logarithmic contributions to the NS splitting function are subleading up to the NNLL accuracy, see Ref. [130], no small-z effects have to be considered. The usual fixed-order NS evolution equations and kernels should be used instead.

2.3.5 Numerical Implementation: including the small-z resummations

In this section, we will review how to adapt the numerical implementation of the fixed-order results up to NNLO accuracy, as discussed in Ref. [J4] and Sec. 2.2.3 to include also the small-z resummations as discussed above.

Following the discussions on the iterated solution in Sec. 2.3.4, we start with assessing the order k in $\boldsymbol{P}^{T\,\mathrm{N}^\kappa\mathrm{LL},(k)}$ that is necessary to capture the behavior of fully resummed series down to values of z relevant for phenomenological studies of SIA data in terms of scale-dependent FFs. To this end, we study the convergence of the series expansion of the resummed expressions when

evaluated up to a certain order k. This is achieved by first expanding the resummed splitting functions in Mellin N space and then using an appropriate numerical Mellin inversion, see below, to compare the expanded result with the fully resummed splitting functions in z-space given in [129, 130]. A typical example, the gluon-to-gluon splitting function, is shown in Fig. 2.3. As can be seen, $k = 20$ in the expansion is accurate at a level of less than 0.3‰ differences down to values of $z \approx 10^{-5}$. This is more than sufficient for all phenomenological studies as SIA data only extend down to about $z = 10^{-3}$ as we shall discuss later.

However, the splitting functions enter the scale evolution of the FFs in a highly non-trivial way, cf. Eqs. (2.23) and (2.24), such that this convergence property does not directly imply that the effects of truncating the expansion at $\mathcal{O}(k = 20)$ are also negligible in the solution of the evolution equations. To explore this further, we recall that the N-space version of Eq. (2.15) reads

$$\frac{\partial}{\partial \ln \mu^2} D_i^h(N, \mu^2) = \sum_j \widetilde{P}_{ji}^T(N, \mu^2) \cdot D_j^h\left(N, \mu^2\right) , \tag{2.72}$$

where $\widetilde{P}_{ji}^T$ is the ij-entry of the 2×2 singlet matrix in (2.25). One can solve this equation numerically with the fully resummed kernels, assuming some initial set of FFs, and compare the resulting, evolved distributions with the corresponding FFs obtained from the iterative solution of Eq. (2.26) at $\mathcal{O}(k = 20)$ defined in Sec. 2.3.4. Again, we find that the two results agree at a level of a few per mill for $z \gtrsim 10^{-5}$, i.e., after transforming the evolved FFs from N to z-space.

In general, the Mellin inversion of a function $f(N)$ is defined as

$$f(z) = \frac{1}{2\pi i} \int_{\mathcal{C}_N} dN\, z^{-N}\, f(N)\,, \tag{2.73}$$

where the contour $\mathcal{C}_N$ in the complex plane is usually taken parallel to the imaginary axis with all singularities of the function $f(N)$ to its left. As we have seen in Sec. 2.2.3, for practical purposes, i.e. faster numerical convergence, one chooses a deformed contour instead, which can be parametrized in terms of a real variable t, an angle φ, and a real constant c as $N(t) = c + te^{i\varphi}$; see Fig. 2.4 for an illustration of the chosen path and Ref. [157] for further details.

In order to properly choose the contour parameters c and φ, we proceed as for our NNLO analysis and analyze the pole structure of the evolution kernels $\mathcal{K}_{ij}^T$.

In complete analogy to what was found in Ref. [167] in the space-like case, the fully resummed time-like splitting functions exhibit additional singularities as compared to the fixed order

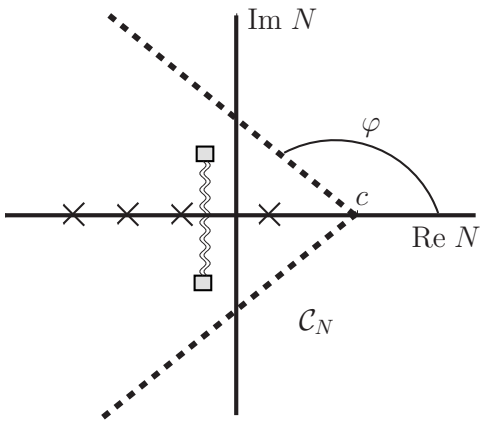

Figure 2.4: The dashed line represents the standard contour $\mathcal{C}_N$ in the complex N plane for the inverse Mellin transformation (2.28). The poles of the integrand along the real axis are schematically represented by crosses, whereas the poles lying in the complex plane away from the real axis are represented by squares. The branch cut is illustrated by the wiggly line.

expressions. Their location in the complex plane away from the real axis depends on the value of a_s. More specifically, if we consider, for instance, P_{gg}^T at NLL [130], one can identify terms proportional to $\left(\sqrt{1+32C_A a_s(\mu)/(N-1)^2}\right)^{-1}$ which lead to poles at $N = 1 \pm i\sqrt{32C_A a_s(\mu)}$ that are connected by a branch cut. If we had chosen to directly solve Eq. (2.72) numerically with the fully resummed splitting functions, the appropriate choice of contour for the Mellin inversion in Fig. 2.4 would have to be μ dependent as the position of these poles, denoted by the squares, depends on $a_s(\mu)$.

In the iterative solution, which we adopt throughout, only the expanded splitting functions $\boldsymbol{P}^{T\,\mathrm{N^\kappa LL},(k)}$ enter the $\mathcal{K}_{ij}^T$ in Eq. (2.29). Therefore, the evolution is not affected by the singularities present in the fully resummed kernels, and a unique, μ-independent choice of the contour parameters c and φ is still possible. In our numerical code, we take $c = 4$ and $\varphi = 3/4\,\pi$. This choice also tames numerical instabilities generated, in particular, by large cancellations caused by the oscillatory behavior in the vicinity of the $N = 1$ pole. This is visualized in the upper panel of Fig. 2.5. Here, we show the real part of the singlet evolution kernel $\mathrm{Re}\{\mathcal{K}_{12}^T\}$ defined in Eq. (2.29) at NLO+NNLL accuracy and $Q^2 = 110\,\mathrm{GeV}^2$. The numerical instabilities are well recognizable near the $N = 1$ pole.

Finally, in order to perform a fit of FFs based on SIA data one has to compute the multiplicities as defined in Eq. (2.4). As was mentioned above, in order to arrive at a fast but reliable

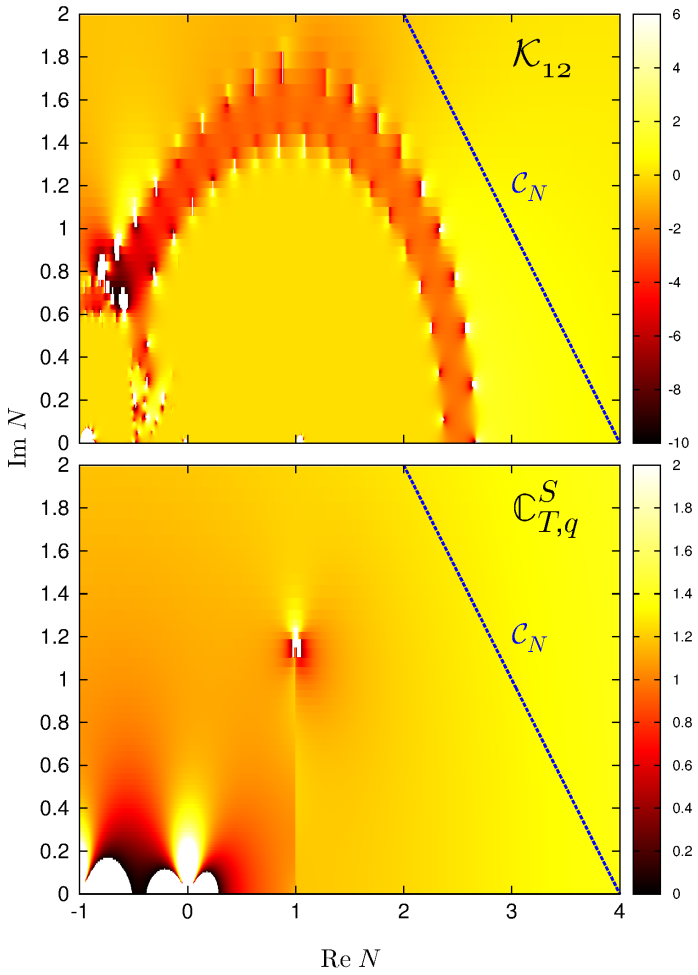

Figure 2.5: Upper panel: real part of $\mathcal{K}_{12}$ in Eq. (2.29) in a portion of the complex N plane. **Lower panel:** as above but for the coefficient function $\mathbb{C}^S_{T,q}(N)$. Both quantities are computed at NLO+NNLL accuracy for $Q^2 = 110\,\text{GeV}^2$. The line corresponds to the contour $\mathcal{C}_N$ in (2.28).

numerical implementation of the fitting procedure, we choose to evaluate the SIA cross section also in Mellin moment space and, then, perform a numerical inverse transformation to z-space.

In principle, while performing the Mellin inversion, one has to deal with the same kind of a_s-dependent singularities in the fully resummed resummed coefficient functions, cf. Ref. [130], that we have just encountered in the resummed splitting functions. In the lower panel of Fig. 2.5, we show the real part of the coefficient function $\mathbb{C}^S_{T,q}(N)$ for which the pole structure

and the branch cut are again well recognizable. However, for the typical scales relevant for a phenomenological analysis ($\mu = 10.5 - 91.2\,\text{GeV}$; see Sec. 2.5), our choice of contour $\mathcal{C}_N$ is nevertheless applicable since the position of the singularities does not change considerably in this range of energies.

2.4 Phenomenological Applications: NNLO analysis

As a first application of our time-like evolution package presented in Sec. 2.2, we will perform a fit to the available SIA data with identified pions up to NNLO accuracy in Sec. 2.4.1. The obtained sets of LO, NLO, and NNLO pion FFs will be used in Sec. 2.4.2 to demonstrate the relevance of the NNLO corrections to the SIA cross section and to estimate the residual theoretical uncertainties due to variations of the factorization scale in each order or to the choice of a truncated or iterated variant of the solution to the evolution equations given in (2.26).

2.4.1 Fit of Pion FFs up to NNLO Accuracy

Since full NNLO corrections are only available for a rather limited set of hard scattering processes, we have to restrict our first analysis of FFs at NNLO accuracy to data obtained in SIA for the time being. In addition, we focus solely on pion production where data are most abundant and precise. In any case, the main interest of this work are the general features of NNLO corrections rather than to provide a new set of FFs.
To facilitate the fitting procedure, we closely follow the framework outlined and used in the series of DSS global QCD analyses of parton-to-pion FFs at NLO accuracy [77–79]. Specifically, we adopt the same flexible functional form

$$D_i^{\pi^+}(z,\mu_0^2) = \frac{N_i\, z^{\alpha_i}(1-z)^{\beta_i}[1+\gamma_i(1-z)^{\delta_i}]}{B[2+\alpha_i,\beta_i+1]+\gamma_i B[2+\alpha_i,\beta_i+\delta_i+1]} \tag{2.74}$$

to parametrize the non-perturbative input FFs for charged pions at a scale μ_0 in the $\overline{\text{MS}}$ scheme. Here, $B[a,b]$ is the Euler Beta function used to normalize the parameter N_i in (2.74) for each flavor i to its contribution to the energy-momentum sum rule. In addition to the gluon $i = g$, we only consider FFs for the sum of a quark and an antiquark of a given flavor i, i.e., $i = u+\bar{u}$, $d+\bar{d}$, $s+\bar{s}$, $c+\bar{c}$, and $b+\bar{b}$, since SIA is only sensitive to $q+\bar{q}$ flavor combinations as can be already inferred from Eq. (2.4). Also, since all hadrons in SIA originate from the initially

produced $q\bar{q}$ pair, the rates for π^+ and π^- are the same, and data for charged pions are usually presented for the sum $d\sigma^\pi \equiv d\sigma^{\pi^+} + d\sigma^{\pi^-}$.

We assume charge conjugation and isospin symmetry and impose $D_{u+\bar{u}}^{\pi^\pm} = D_{d+\bar{d}}^{\pi^\pm}$ as is also suggested by the flavor composition of $\pi^\pm$. We note that a recent global QCD analysis of pion FFs at NLO accuracy based on SIA, SIDIS, and pp data [79] finds a breaking of this symmetry of less than 0.5%. Beyond that, we are forced to fix certain parameters in our ansatz (2.74) as they cannot be constrained by data. More specifically, we set $\alpha_{s+\bar{s}} = \alpha_{u+\bar{u}}$, $\beta_{s+\bar{s}} = \beta_{u+\bar{u}} + \delta_{u+\bar{u}}$, and $\beta_g = 8$. In addition, $\delta_{g,s+\bar{s},c+\bar{c}} = 0$ and $\gamma_{g,s+\bar{s},c+\bar{c}} = 0$. For light quark flavors and the gluon, we choose an initial scale of $\mu_0 = 1$ GeV. As in all previous fits [72–79], the charm and bottom-to-pion FFs are treated as a non-perturbative input and are turned on discontinuously at $\mu_0^c = m_c = 1.4$ GeV and $\mu_0^b = m_b = 4.75$ GeV, respectively. Their parameters are essentially determined by charm and bottom flavor-tagged SIA data. In case of $D_{b+\bar{b}}^{\pi^+}$, a good fit is only achieved with the full functional form (2.74) using all five parameters, whereas for charm only three free parameters are needed. Since the heavy quark masses are neglected throughout in the NPIS, $D_{c+\bar{c}}^{\pi^+}$ and $D_{b+\bar{b}}^{\pi^+}$ should be only used in cross sections such as Eq. (2.4) at scales well beyond their partonic thresholds $\mu = 2m_c$ and $\mu = 2m_b$, respectively.

The remaining 16 free parameters are determined by a standard χ^2 minimization procedure as described, for instance, in Ref. [79]. They are listed in Tab. 2.3 for our LO, NLO, and NNLO sets of pion FFs. For each set of experimental data we determine the optimum normalization shift analytically and assign an additional contribution to χ^2 according to the quoted experimental uncertainties; see, e.g., Eq. (5) in Ref. [79] for details.

Our fits are performed to the following sets of inclusive and flavor-tagged SIA data with identified pions: SLD [88], ALEPH [89], DELPHI [90], and OPAL [91], all taken at a c.m.s. energy of $\sqrt{S} = 91.2$ GeV, TPC [85–87] at $\sqrt{S} = 29$ GeV, and BABAR [84] and BELLE [83] both at $\sqrt{S} = 10.5$ GeV. The SLD, DELPHI and TPC experiments not only provide inclusive SIA measurements but also uds, charm and bottom-tagged data. All these sets were also used in the recent global analysis presented in Ref. [79].

As is customary [72–79], we do not include any data below a certain $z_{\min}$ in the fit where finite, but neglected hadron mass effects $\propto M_\pi/(z^2 S)$ might become relevant [J3], and potentially the large logarithmic contributions $\propto \log z$, discussed above in Sec. 2.3, need to be resumed to all orders [62, 63, 126–130, 171, 172]. For all our fits in this section, we choose $z_{\min} = 0.075$. In addition, we employ an upper cut of $z < z_{\max} = 0.95$. In this region threshold logarithms $\propto \log(1-z)$ in the coefficient functions are expected to become increasingly relevant, and,

parameter	LO	NLO	NNLO
$N_{u+\bar{u}}$	0.735	0.572	0.579
$\alpha_{u+\bar{u}}$	-0.371	-0.705	-0.913
$\beta_{u+\bar{u}}$	0.953	0.816	0.865
$\gamma_{u+\bar{u}}$	8.123	5.553	4.062
$\delta_{u+\bar{u}}$	3.854	1.968	1.775
$N_{s+\bar{s}}$	0.243	0.135	0.271
$\alpha_{s+\bar{s}}$	*-0.371*	*-0.705*	*-0.913*
$\beta_{s+\bar{s}}$	*4.807*	*2.784*	*2.640*
N_g	0.273	0.211	0.174
α_g	2.414	2.210	1.595
β_g	*8.000*	*8.000*	*8.000*
$N_{c+\bar{c}}$	0.405	0.302	0.338
$\alpha_{c+\bar{c}}$	-0.164	-0.026	-0.233
$\beta_{c+\bar{c}}$	5.114	6.862	6.564
$N_{b+\bar{b}}$	0.462	0.405	0.445
$\alpha_{b+\bar{b}}$	-0.090	-0.411	-0.695
$\beta_{b+\bar{b}}$	4.301	4.039	3.681
$\gamma_{b+\bar{b}}$	24.85	15.80	11.22
$\delta_{b+\bar{b}}$	12.25	11.27	9.908

Table 2.3: Parameters describing our optimum LO, NLO, and NNLO $D_i^{\pi^+}(z,\mu_0)$ in Eq. (2.74) at the input scale $\mu_0 = 1$ GeV. Results for the charm and bottom FFs refer to the scale $\mu_0^c = m_c = 1.4$ GeV and $\mu_0^b = m_b = 4.75$ GeV, respectively. The parameters given in italics are fixed by $\alpha_{s+\bar{s}} = \alpha_{u+\bar{u}}$, $\beta_{s+\bar{s}} = \beta_{u+\bar{u}} + \delta_{u+\bar{u}}$, and $\beta_g = 8$ but are listed for completeness.

again, all-order resummations are needed [J1, J3, 131–133].

We note that we are not fitting the initial value a_s at some reference scale in order to solve the RGE governing the running of the strong coupling but rather adopt the following boundary conditions $\alpha_s(M_Z) = 0.135$ at LO, $\alpha_s(M_Z) = 0.120$ at NLO, and $\alpha_s(M_Z) = 0.118$ at NNLO accuracy from the recent MMHT global analysis of PDFs [173].

Table 2.4 and Fig. 2.6 illustrate the quality of our fits to SIA data at LO, NLO, and NNLO accuracy in terms of the individual χ^2-values obtained for each experiment and the quantity "[data-theory]/theory", respectively. The total χ^2-penalty originating from the normalization shifts applied to each data set can be also found at the bottom of Tab. 2.4. It turns out to be small, about 7 units, and is largely independent of the perturbative order. Upon applying the cuts on the z-range discussed above, a total of 288 data points remains for the fitting

Experiment	Data	# Data	χ^2		
	type	in fit	LO	NLO	NNLO
SLD [88]	incl.	23	15.0	14.8	15.5
	uds tag	14	9.7	18.7	18.8
	c tag	14	10.4	21.0	20.4
	b tag	14	5.9	7.1	8.4
ALEPH [89]	incl.	17	19.2	12.8	12.6
DELPHI [90]	incl.	15	7.4	9.0	9.9
	uds tag	15	8.3	3.8	4.3
	b tag	15	8.5	4.5	4.0
OPAL [91]	incl.	13	8.9	4.9	4.8
TPC [85–87]	incl.	13	5.3	6.0	6.9
	uds tag	6	1.9	2.1	1.7
	c tag	6	4.0	4.5	4.1
	b tag	6	8.6	8.8	8.6
BABAR [84]	incl.	41	108.7	54.3	37.1
BELLE [83]	incl.	76	11.8	10.9	11.0
NORM. SHIFTS			7.4	6.8	7.1
TOTAL:		288	241.0	190.0	175.2

Table 2.4: The individual χ^2-values and number of points for each inclusive and flavor-tagged data set included in our fits at LO, NLO, and NNLO accuracy. At the bottom, we list the total χ^2-penalty from the normalization shifts and the total $\chi^2$for each fit.

procedure and to determine the 16 free parameters describing our parton-to-pion FFs $D_i^{\pi^+}(z,\mu_0)$ in Eq. (2.74). All fits yield a very good χ^2 per degree of freedom (d.o.f.) ranging from 0.89 in LO to 0.64 at NNLO accuracy. We note, however, that the χ^2/d.o.f. would deteriorate very significantly if the number of free fit parameters would be reduced further by setting, for instance, $\gamma_{u+\bar{u}} = 0$ or $\gamma_{b+\bar{b}} = 0$.

As can be seen from Tab. 2.4 and Fig. 2.6, nearly all SIA data sets can be described equally well in LO, NLO, and NNLO accuracy with just a few exceptions, most notably the BABAR data [84] taken at the smallest $\sqrt{S}$ which drive the differences found in the total χ^2-values of the three fits. Here, the inclusion of higher order corrections progressively leads to better fits. A closer inspection reveals that the larger χ^2 at LO, and also at NLO, stems from the data points corresponding to the lowest z values included in the fit, i.e., $0.075 \leq z \lesssim 0.12$; note that the BELLE Collaboration does not provide any data below $z = 0.2$. This result is readily understood from the fact that calculations at higher orders contain more of the

numerically important small z enhancements $\propto \log z$ mentioned above, i.e., are closer to an all-order result. From the observation that calculations at NNLO accuracy provide a significantly better description of data at small-z, one could anticipate that including all-order resummations into the analysis framework would eventually further extend the range of z amenable to pQCD. We will show in Sec. 2.5, however, that the phenomenological relevance of small-z resummations in the kinematical region of interest is very small. The neglected hadron mass is another source of potentially large corrections at small z and/or $\sqrt{S}$. In Chapter 3 [J3] it is shown, however, that hadron mass terms are relatively small for pion production in SIA in the kinematic regime relevant for the BaBar data with $z > z_{\min} = 0.075$. We also wish to recall that BaBar provides their data in two variants called "conventional" and "prompt", differing by the treatment of weak decays into pions in their event sample [84]. As in the recent global NLO analysis [79], our results are based on the latter set. We have verified that a decent fit to all SIA data can be also obtained when the "conventional" data are used instead but at the expense of a less favorable total χ^2, e.g., 236.4 rather than 190.0 units at NLO, and, more importantly, for undesirable corners of the parameter space describing the $D_i^{\pi^+}(z,\mu_0)$ in Eq. (2.74). For instance, the $u+\bar{u}$ fragmentation tends to saturate the energy-momentum sum rule, which is summed over all hadrons, already for pions.

Table 2.4 and Fig. 2.6 also reveal that some flavor-tagged data from Sld can be described best at LO but at the expense of larger χ^2-values for inclusive Aleph and Opal data. In general, the NLO and NNLO results are very similar for all data sets used in the fits except, as just discussed, for a few points from BaBar at small z. This observation also carries over to the obtained FFs at NLO and NNLO accuracy, in particular, those flavor combinations which are constrained best by the SIA data alone.

Figure 2.7 shows our fitted LO, NLO, and NNLO $D_i^{\pi^+}(z,Q^2)$ at $Q^2 = 10\,\mathrm{GeV}^2$ for $i = u+\bar{u}$, $s+\bar{s}$, g, and the flavor singlet combination in (2.17) for $N_f = 4$. As a comparison with previous NLO results, we consider the most recent global analysis of the DSS group [79], based on the same set of SIA data plus SIDIS and pp data, and the old fit by Kretzer [72]. The latter still provides a good description of all pion data, including those from SIDIS and pp, despite making use of only a small subset of the SIA data listed in Tab. 2.4 comprising Sld [88], Aleph [89], and Tpc [85–87]. To illustrate how the current experimental uncertainties typically propagate to the extraction of parton-to-pion FFs, we also show in Fig. 2.7 the 90% confidence level (C.L.) estimates of the latest DSS global QCD fit (shaded bands). As was already mentioned, we refrain from providing uncertainty bands for our fits as SIA data alone are not sufficient for

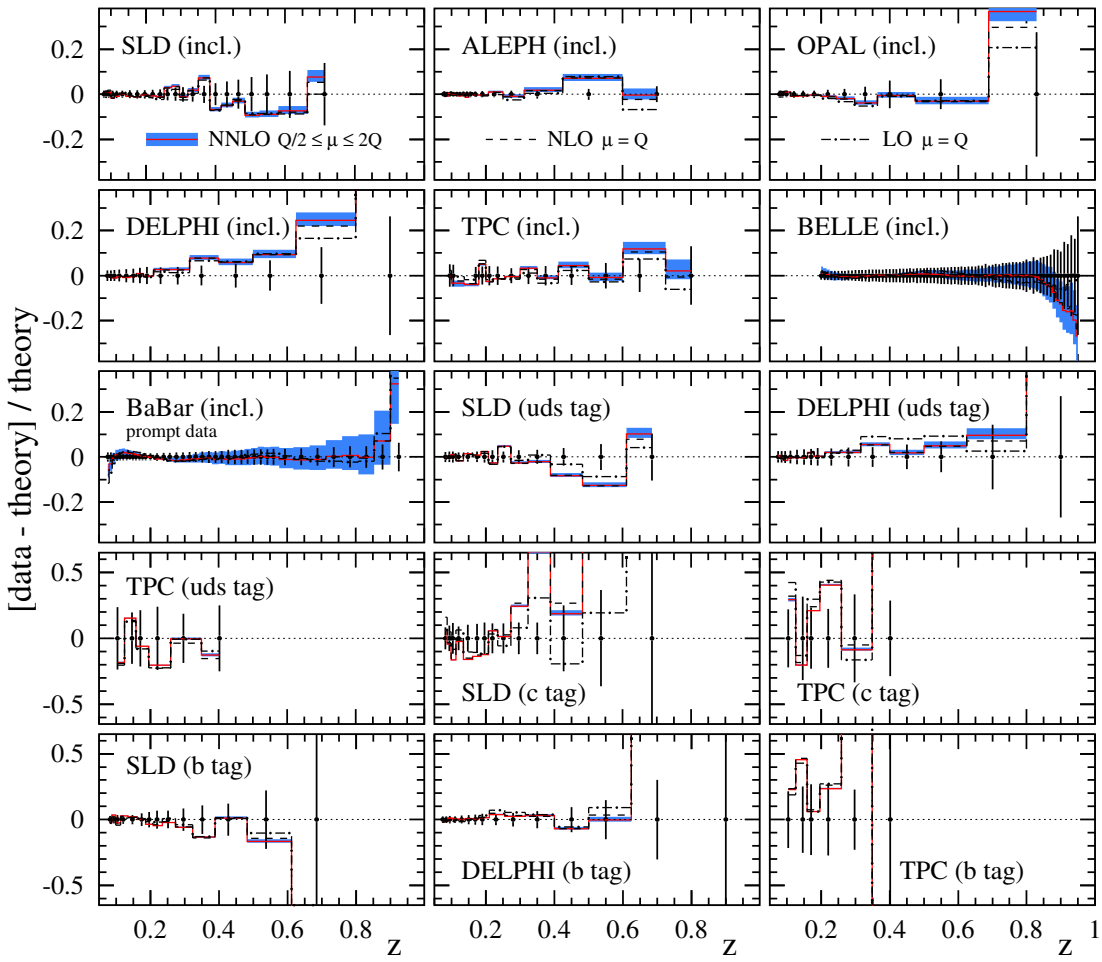

Figure 2.6: / theory for our LO (dot-dashed), NLO (dashed), and NNLO (solid lines) fits computed with the scale $\mu = Q$ for the data sets listed in Tab. 2.4"]Ratios for [data-theory]/theory for our LO (dot-dashed), NLO (dashed), and NNLO (solid lines) fits computed with the scale $\mu = Q$ for the data sets listed in Tab. 2.4. The shaded bands illustrate the remaining scale ambiguity at NNLO accuracy in the range $Q/2 \leq \mu \leq 2Q$. The points along the zero axis indicate the relative experimental uncertainty.

providing a reliable estimate due to the assumptions one has to impose on the parameter space describing the $D_i^{\pi^+}(z, \mu_0)$ in Eq. (2.74).

From Fig. 2.7 one can make the following observations: the quantity which is known to be constrained best by the SIA data alone [72–79], the flavor singlet combination $D_\Sigma^{\pi^+}$ defined in Eq. (2.17), is very similar for all the NLO results, DSS, Kretzer, and our fit, in particular, for

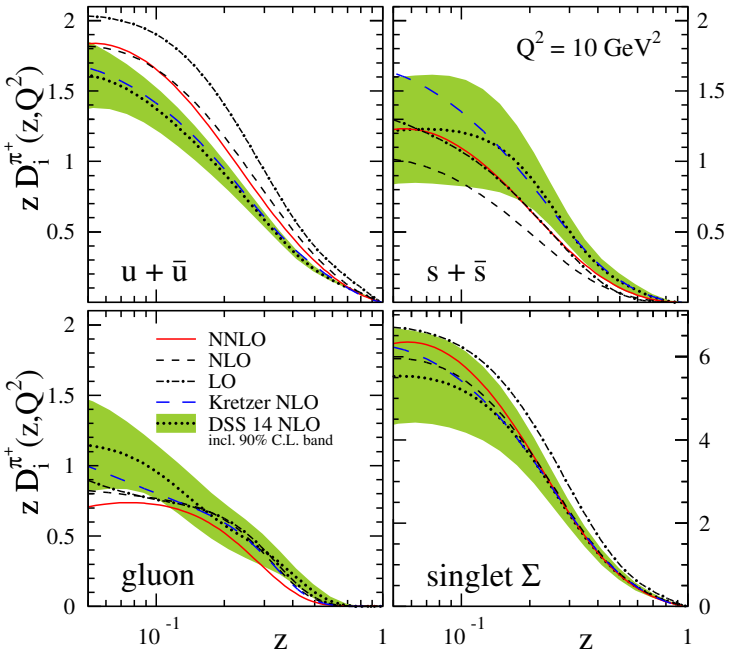

Figure 2.7: Comparison of our LO, NLO, and NNLO FFs $D_i^{\pi^+}(z, Q^2)$ at $Q^2 = 10\,\mathrm{GeV}^2$ for $i = u + \bar{u}$, $s + \bar{s}$, g, and the flavor singlet combination in (2.17) for $N_f = 4$. Also shown are the optimum NLO FFs from Kretzer [72], obtained also solely from SIA data, and the latest global analysis of the DSS group [79] based on SIA, SIDIS, and pp data. For the latter, we also illustrate their 90% C.L. uncertainty estimates (shaded bands).

$z \gtrsim 0.1$. The fact that also the singlet FF determined at NNLO accuracy is close to the NLO results gives some indication that NNLO corrections do not seem to alter results obtained at NLO accuracy too much. A similar level of agreement for $D_\Sigma^{\pi^+}$ is found also at other scales, for instance, $\mu = M_Z$.

Breaking up the singlet into FFs for individual quark flavors depends on the assumptions made in the fit, including such details as the choice for $z_{\min}$. Therefore, it is not too surprising that one finds some differences between the various fits shown in Fig. 2.7 for the favored $D_{u+\bar{u}}^{\pi^+}$ and the unfavored $D_{s+\bar{s}}^{\pi^+}$, with the latter FF, of course, being considerably less well constrained by data than the former. Another FF which is only loosely constrained by a fit to solely SIA data is the gluon $D_g^{\pi^+}$, which, despite the different assumptions, agrees rather well among all fits. Finally, one notices that for a LO fit both the singlet and the favored FFs, $D_\Sigma^{\pi^+}$ and $D_{u+\bar{u}}^{\pi^+}$, respectively, are significantly larger than the corresponding NLO estimates. In general, we find that in order to achieve a good fit to SIA data at LO accuracy, some of the parameters listed in Tab. 2.3 tend to approach extreme values, for instance, the $u + \bar{u}$ fragmentation saturates

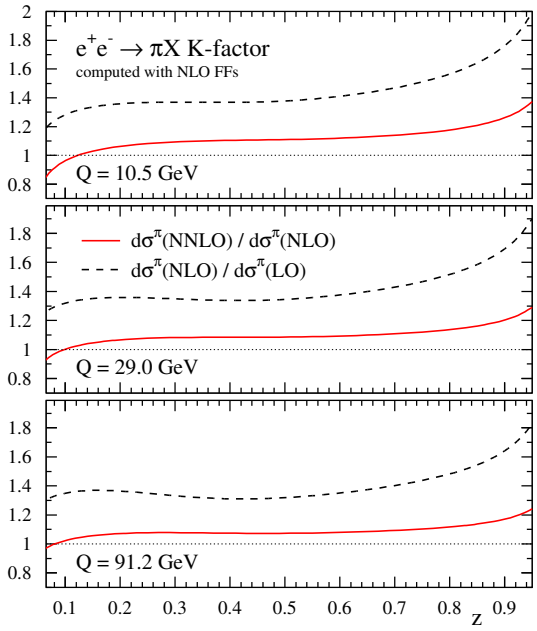

Figure 2.8: NNLO/NLO (solid) and NLO/LO (dashed lines) K-factors for the SIA process for three different c.m.s. energies. All computations are performed with our NLO set of parton-to-pion FFs; see text.

most of the energy-momentum sum rule already for pions. In any case, LO estimates are not sufficient for phenomenological applications.

2.4.2 Impact of NNLO Corrections on Theoretical Uncertainties

In this Section we analyze the relevance of the NNLO corrections for a reliable phenomenology of the SIA process. To this end, we will examine the importance of various sources of theoretical uncertainties in LO, NLO, and NNLO accuracy. We will present results for the size of the NNLO corrections in terms of the K-factor, study the residual dependence on the choice of scale μ, and investigate the uncertainties induced by choosing a particular solution, truncated or iterated, to the time-like evolution equations. All these results are largely independent of the details of fitting an actual set of FFs, and as such they represent the main numerical results of our analysis along with our newly developed code described in Sec. 2.2 and 2.3.
In Fig. 2.8, we show the K-factor for the SIA process defined as $d\sigma^\pi(\mathrm{N^mLO})/d\sigma^\pi(\mathrm{N^{m-1}LO})$ for $m = 2$ (solid) and $m = 1$ (dashed lines) for the three c.m.s. energies corresponding to the experiments included in our fit; see Tab. 2.4. To determine only the impact of the genuine

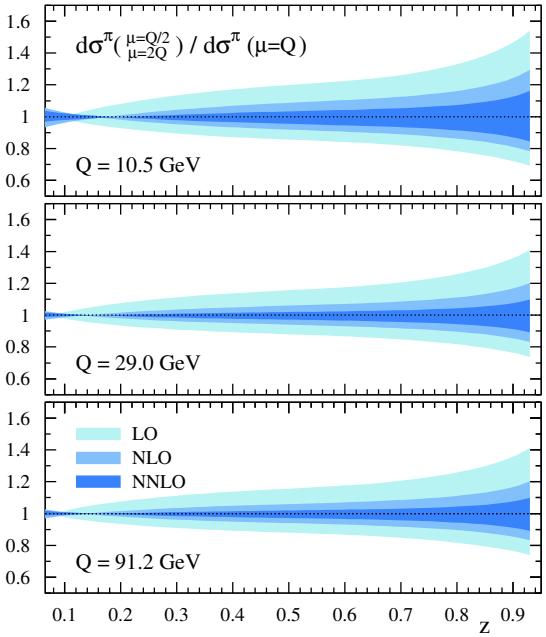

Figure 2.9: Scale dependence of the SIA cross section at LO, NLO, and NNLO accuracy in the range $Q/2 \leq \mu = \mu_R = \mu_F \leq 2Q$ normalized to the results obtained for $\mu = Q$ for three values of $\sqrt{S}$.

higher order corrections and not some numerical differences in the LO, NLO, and NNLO FFs, like those illustrated in Fig. 2.7, all calculations in Fig. 2.8 are performed with our NLO input FFs. Their evolution, the running of the strong coupling a_s, and the coefficient functions are taken consistently either at LO, NLO, or NNLO accuracy though.

As one expects, the K-factor for the NNLO/NLO results is significantly smaller than the one for NLO/LO, and for most values of z the additional NNLO corrections are at the level of about 10% or less. Both at large and small z, one finds clear indications for the presence of large logarithmic corrections to the perturbative series contained in the evolution kernels P^T and the SIA coefficient functions $\mathbb{C}$. They need to be resummed to all orders to extend the range of applicability of the presented fixed order results to both $z \to 1$ and $z \to 0$ (see Sec. 2.5). We note that the small $\sqrt{S}$ dependence of the K-factors in Fig. 2.8 is only caused by the different orders in pQCD used in the denominator and in the numerator, $d\sigma^\pi(\mathrm{N^mLO})$ and $d\sigma^\pi(\mathrm{N^{m\text{-}1}LO})$, respectively, to compute the scale evolution of FFs and the coupling a_s. There is no scale in the coefficient functions as we have set $\mu_R = \mu_F = \mu = Q$ throughout, i.e., all logarithms of the type $\log(\mu_R^2/\mu_F^2)$ or $\log(Q^2/\mu_F^2)$ vanish.

The scale dependence of the SIA cross section is illustrated in Fig. 2.9, where we show results at

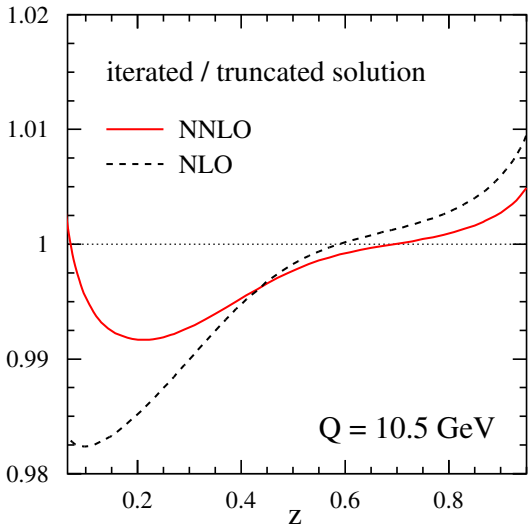

Figure 2.10: Ratio of the iterated and truncated variant of the solution (2.26) to the time-like evolution equations at NLO (dashed) and NNLO (solid line) accuracy at the scale of the BABAR and BELLE experiments.

LO, NLO, and NNLO accuracy (shaded bands) for $\mu_R = \mu_F = \mu = 2Q$ and $\mu = Q/2$ normalized in each case to our default choice $\mu = Q$. The residual dependence on the choice of the scale μ in a theoretical calculation is presumably the most important source of uncertainty and is expected to shrink progressively upon including higher and higher order corrections. This is exactly what we find. For instance, at $\sqrt{S} = 10.5\,\text{GeV}$, relevant for BABAR and BELLE, the typical scale uncertainty at $z \approx 0.5$ amounts to about 20% at LO and reduces to $\approx 10\%$ at NLO and $\approx 5\%$ at NNLO. At larger c.m.s. energies, the scale ambiguities are even smaller and reach around $1 - 2\%$ at NNLO accuracy. This is actually needed in a phenomenological analysis to roughly match the experimental uncertainties for the most precise sets of inclusive pion data as can be inferred from Fig. 2.6; note that the scale uncertainty bands are hardly visible for some of the flavor-tagged data as we had to inflate the axis of the ordinate in Fig. 2.6 to accommodate the rather sizable experimental uncertainties.

As can be seen from Fig. 2.9, all scale uncertainty bands narrow down somewhere in the range $0.1 \lesssim z \lesssim 0.15$ before they start to increase again towards $z \to 0$. This can be readily understood from fact that one has approximate "scaling" of the SIA cross section, or, alternatively, the quark FFs, for some value of z in this region, i.e., they become independent of the scale μ. This is very much similar to DIS and PDFs, where this happens somewhere near momentum fractions of about 0.2. Of course, QCD corrections always introduce some scale dependence,

and higher order cross sections never probe a FFs or a PDFs locally at one value of momentum fraction but rather over a broad range due to the presence of convolutions, like, for instance, in Eq. (2.4).

We close our discussions about the relevance of the NNLO corrections by showing the theoretical ambiguity associated with the different choices one has in defining the solution to the time-like evolution equations beyond the LO accuracy. More specifically, Fig. 2.10 gives the ratio of the iterated and truncated variant of the general solution given in Eq. (2.26) computed in NLO (dashed) and NNLO (solid line); see also the corresponding discussions in Sec. 2.2.2. In the z-range relevant for the extraction of FFs from data, this type of theoretical uncertainty is rather small, and we note that it is usually not considered or even mentioned [72–79]. As for the K-factor and the scale dependence shown in Fig. 2.8 and 2.9, respectively, including NNLO corrections reduces the residual uncertainties by about a factor of two as compared to the results obtained at NLO accuracy. For most values of z, the differences between the truncated and iterated solutions are less than 0.5% at NNLO, i.e., smaller than scale uncertainties and potentially missing higher order corrections as indicated by the K-factor for NNLO/NLO.

2.5 Phenomenological Applications: including small-z resummations

In the literature, small-z resummations have been exploited to exclusively study the fixed $N = 1$ moment of integrated hadron multiplicities in SIA, in particular, their scale evolution and the shift of the peak of the multiplicity distribution with energy [63, 136–139]. In this section, we will extend these studies to the entire z-range and present a first phenomenological analysis of SIA data with identified pions in terms of FFs up to NNLO+NNLL accuracy. More specifically, we use the same data sets as in the fixed-order fit of parton-to-pion FFs at NNLO accuracy presente in Sec. 2.4 and [J4]. In Sec. 2.5.1 we perform various fits to SIA data with and without making use of small-z resummations to quantify their phenomenological relevance. The impact of small-z resummations on the residual dependence on the factorization scale is studied in Sec. 2.5.2.

2.5.1 Fits to SIA data and the relevance of resummations

The procedures is analogous to the one presented Sec. 2.5.1 and outlined in Refs. [J4, 77–79, 92]. However, we choose $\mu_0 = 10.54$ GeV, which is equivalent to the lowest c.m.s. energy $\sqrt{S}$ of the the data sets relevant for the fit. This choice is made to avoid any potential bias in our comparison of fixed-order and resummed extractions of FFs from starting the scale evolution at some lowish, hadronic scale $\mathcal{O}(1\,\text{GeV})$ where non-perturbative corrections, i.e., power corrections, might be still of some relevance.

As for the NNLO analysis, in all our fits here, we only consider FFs for the flavor combinations $u+\bar{u}$, $d+\bar{d}$, $s+\bar{s}$, $c+\bar{c}$, $b+\bar{b}$, and g, each parametrized by the ansatz in (2.74). The treatment of heavy flavor FFs, i.e., charm and bottom quark and antiquark, proceeds also in the same, non-perturbative input scheme (NPIS) used for the NNLO case and in the global analyses of [77–79, 92] (see Sec.2.4.1 for more details). However, since we use $\mu_0 = 10.54$ GeV $> m_b$, no heavy flavour mass threshold is crossed during the evolution. In this case the NPIS corresponds to the standard FFNS. The parameters of $D^h_{c+\bar{c},b+\bar{b}}(z, m^2_{c,b})$ are determined by the fit to data according to the Eq. (2.74). We note that a general-mass variable flavor number scheme for treating the heavy quark-to-light hadron FFs has been recently put forward in Ref. [174]. Since this scheme, as well as other matching prescriptions [164], are only available up to NLO accuracy, we refrain from using them in our phenomenological analyses.

Rather than fitting the initial value of the strong coupling at some reference scale in order to solve the RGE governing its running, we proceed as in Sec 2.4.1 and adopt the boundary conditions $\alpha_s(M_Z) = 0.135$, 0.120, and 0.118 at LO, NLO, and NNLO accuracy, respectively, from the recent MMHT global analysis of PDFs [173]. When we turn on small-z resummations at a given logarithmic order N^{m}LL in our fit, we keep the α_s value as appropriate for the underlying, fixed-order calculation to which the resummed results are matched. For instance, in a fit at NLO+NNLL accuracy, we use the α_s value at NLO.

In this section, we are mainly interested in a comparison of fixed-order fits with corresponding analyses including small-z resummations to determine the phenomenological impact of the latter. We make the following selection of data to be included in our fits. First of all, as in for the NNLO alalysis, we limit ourselves to SIA with identified pions since these data are the most precise ones available so far. They span a c.m.s. energy range from $\sqrt{S} \simeq 10.5\,\text{GeV}$ at the b-factories at SLAC and KEK to $\sqrt{S} = M_Z \simeq 91.2\,\text{GeV}$ at the CERN-LEP. The second, more important selection cut concerns the lower value in z accepted in the fit. As already discussed in Sec. 2.4.1, fits of FFs introduce a minimum value z_{min} of the energy fraction z in the analyses

below which all SIA data are discarded and FFs should not be used in other processes. This rather ad hoc cut is mainly motivated by kinematic considerations, more specifically, by the finite hadron mass or other power corrections which are neglected in the factorized framework [109]. Hadron mass effects in SIA have been investigated to some extent in [J3] (see also Chapter 3) but so far there is no fully consistent way to properly include them in a general process, i.e., ultimately in a global analysis of FFs. See for example [140, 141].

In case of pion FFs, one usually sets $z_{\min} = 0.1$ [77, 79] or, as for our NNLO analysis $z_{\min} = 0.075$.

The two main assets one expects from small-z resummations, and which we want to investigate, are an improved scale dependence and an extended range towards lower values of z in which data can be successfully described. For this reason, we have systematically explored to which extent one can lower the cut $z_{\min}$ in a fit to SIA data once resummations as outlined in Sec. 2.3 are included. It turns out, that for the LEP data, taken at the highest c.m.s. energy of $\sqrt{S} = 91.2$ GeV, we can extend the z-range of our analyses from $0.075 < z < 0.95$ used in the NNLO fit [J4] to $0.01 < z < 0.95$. Unfortunately, any further extension to even lower values of z is hampered by the fact that two of the data sets from LEP, the ones from ALEPH [89] and OPAL [91], appear to be mutually inconsistent below $z \simeq 0.01$, see Fig. 2.11. Including these data at lower z, always lets the fits, i.e., the minimization in the multi-dimensional parameter space defined by Eq. (2.74), go astray and the convergence is very poor.

For the relevant data sets at lower c.m.s. energies, TPC [85–87] ($\sqrt{S} = 29$ GeV), BELLE [83] ($\sqrt{S} = 10.52$ GeV), and BABAR [84] ($\sqrt{S} = 10.54$ GeV), the above mentioned problems related to the finite hadron mass arise at small values of z not considered before in Sec. 2.4. A straightforward, often used criterion to assess the relevance of hadron mass effects is to compare the scaling variable z, i.e. the hadron's energy fraction $z = 2\,E_h/Q$ in a c.m.s. frame, with the corresponding three-momentum fraction x_p which is often used in experiments. Since they are related by $x_p = z - 2m_h^2/(zQ^2) + \mathcal{O}(1/Q^4)$ [109], i.e., they coincide in the massless limit, any deviation of the two variables gives a measure of potentially important power corrections. To determine the cut $z_{\min}$ for a given data set, we demand that z and x_p are numerically similar at a level of 10 to at most 15%. The BELLE data are limited to the range $z > 0.2$ [83], where z and x_p differ by less than 1%. BABAR data are available for $z \gtrsim 0.05$, which translates in a maximum difference of the two variables of about 14%. Concerning the TPC data, we had to place a lower cut $z_{\min} = 0.02$ to arrive at a converged fit, which corresponds to a difference of approximately 11% between z and x_p. After imposing these cuts, the total amount of data points taken into account in our fits is 436. We note that, in general, the interplay between

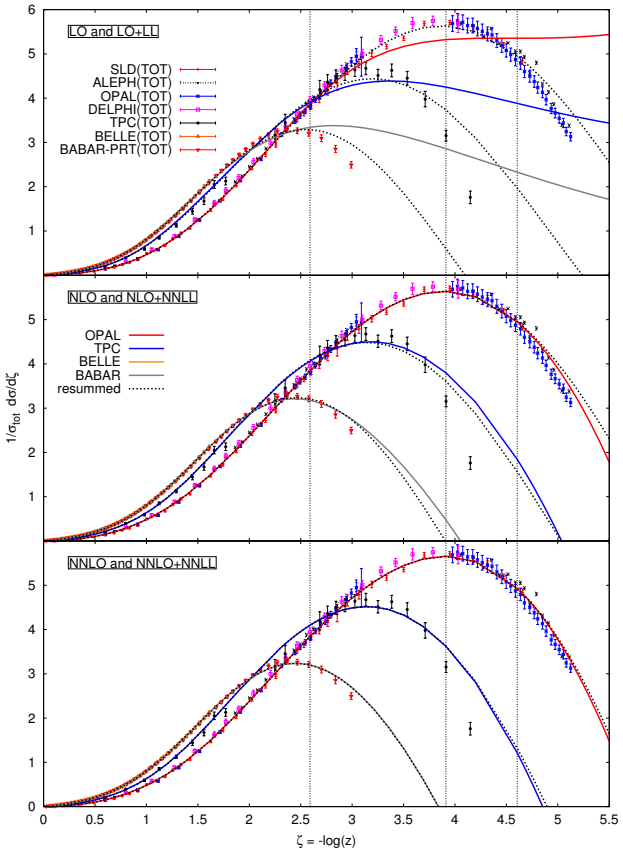

Figure 2.11: Pion multiplicity data [83–91] included in the analyses as a function of $\zeta = \log(1/z)$ compared to the results of various fits without (solid lines) and with (dotted lines) small-z resummations. All curves refer to the central choice of scale $\mu = Q$. The top, middle, and lower panel shows the results at LO and LO+LL, NLO and NLO+NNLL, and NNLO and NNLO+NNLL accuracy, respectively. The vertical dotted lines illustrate, from left to right, the lower cuts $z_{\min} = 0.075$ adopted in [J4], and $z_{\min} = 0.02$ and 0.01 used in all our fits for the TPC data and otherwise, respectively.

small-z resummations and the various sources of power corrections poses a highly non-trivial problem which deserves to be studied further in some dedicated future work.

It is also worth mentioning that with the lowered kinematic cut $z_{\min}$, we achieve a better convergence of our fits with our choice of a larger initial scale $\mu_0 = 10.54$ GeV in Eq. (2.74). Starting the scale evolution from a lower value $\mu_0 = \mathcal{O}(1)$ GeV, like in our NNLO analysis of Ref. [J4], leads, in general, to less satisfactory fits in terms of their total χ^2 value which is used to judge the quality of the fits. This could relate to the fact that other types of power

corrections have to be considered as well when evolving from such a low energy scale in order to be able to describe the shape of the differential pion multiplicities, cf. Fig. 2.11, measured in experiment. To corroborate this hypothesis is well beyond the scope of this analysis. In any case, our choice of μ_0 is certainly in a region where the standard perturbative framework can be safely applied and meaningful conclusions on the impact of small-z resummations in SIA can be drawn.

We emphasize that the choice of μ_0 is solely due to technical rather than conceptional reasons. As the evolution equations are, in principle, forward-backward symmetric, the actual choice of μ_0 should not matter in a fit. Our functional form (2.74) is presumably not flexible enough to obtain an equally good description of the data if the initial scale is chosen well below 10 GeV, which manifests itself in larger values of χ^2 and poor convergence of the fits. The main results and conclusions of our work are, however, not affected by the actual choice of μ_0.

Turning back to the choice of our flexible ansatz for the FFs, it is well known that fits based solely on SIA data are not able to constrain all of the free parameters in Eq. (2.74) for each of the flavors i. Again, we impose the constraint $D_{u+\bar{u}}^{\pi^\pm} = D_{d+\bar{d}}^{\pi^\pm}$. We further limit the parameter space associated with the large-z region by setting $\delta_{g,s+\bar{s},c+\bar{c}} = 0$ and $\gamma_{g,s+\bar{s},c+\bar{c}} = 0$. Note that in contrast to Sec 2.4.1, we are now able to keep β_g as a free parameter in the fits.

The remaining 19 free parameters are then determined by a standard χ^2 minimization procedure as described, for example, in Ref. [79] and used in Sec 2.4.1. The optimal normalization shifts for each data set are computed analytically. They contribute to the total χ^2 according to the quoted experimental normalization uncertainties; see, e.g., Eq. (5) in Ref. [79] for further details. The resulting χ^2-values, the corresponding "penalties" from the normalization shifts, and the χ^2 per degree of freedom (dof) are listed in Tab. 2.5 for a variety of fits with a central choice of scale $\mu = Q$. Results are given both for fits at fixed order (LO, NLO, and NNLO) accuracy and for selected corresponding fits obtained with small-z resummations. Here, all cross sections are always matched to the fixed order results according to the procedures described in Sec. 2.3.3 and Sec. 2.3.4. More specifically, we choose the logarithmic order in such a way that we do not resum logarithmic contributions which are not present in the fixed-order result. For this reason, we match the LO calculation only with the LL resummation as the only logarithmic contribution at LO is of LL accuracy; cf. Tabs. 2.1 and 2.2. Using the same reasoning, we match NLO with the NNLL resummed results. Finally, at NNLO accuracy five towers of small-z logarithms are present. However, the most accurate resummed result currently available is at NNLL accuracy which includes the first three towers. Thus, we can match NNLO only with

accuracy	χ^2	norm shift	χ^2/dof
LO	1260.78	29.02	2.89
NLO	354.10	10.93	0.81
NNLO	330.08	8.87	0.76
LO+LL	405.54	9.83	0.93
NLO+NNLL	352.28	11.27	0.81
NNLO+NNLL	329.96	8.77	0.76

Table 2.5: The obtained χ^2-values, the "penalties" from normalization shifts, and the χ^2/dof for the fits at fixed order and resummed accuracy as described in the text.

NNLL. It should be stressed that the results for the fixed-order fits are not directly comparable to the ones given in Sec. 2.4 since we use more data points at lower values of z, a slightly different set of fit parameters, and a different initial scale μ_0. However, the main aspects of these fits remain the same and can be read off directly from Tab. 2.5: a LO fit is not able to describe the experimental results adequately. The NLO fit already gives an acceptable result, which is further improved upon including NNLO corrections. Compared to the corresponding fixed-order results, the fits including also all-order resummations of small-z logarithms exhibit, perhaps somewhat surprisingly, only a slightly better total χ^2, except for the LO+LL fit, where resummation leads to a significant improvement in its quality. The small differences in χ^2 between fits at NNLO and NNLO+NNLL accuracy are not significant. Hence, we must conclude that in the z-range covered by the experimental results, NNLO expressions already capture most of the relevant features to yield a satisfactory fit to the SIA data with identified pions.

The same conclusions can be reached from Fig. 2.11, where we compare the used inclusive pion multiplicity data in SIA with the theoretical cross sections at different levels of fixed- and logarithmic-order obtained from the fits listed in Tab. 2.5. The theoretical curves are corrected for the optimum normalization shifts computed for each set of data. For the sake of readability, we only show a single curve for the different experiments at $\sqrt{S} = M_Z$ which is corrected for the normalization shift obtained for the OPAL data. The individual normalization shifts for the other sets are, however, quite similar. We refrain from showing the less precise flavor-tagged data which are, nevertheless, also part of the fit. The vertical dotted lines in Fig. 2.11 indicate the lower cuts in z applied for the data sets at different c.m.s. energies as discussed above. The leftmost line (corresponding to $z_{\min} = 0.075$) is the cut used in our NNLO analysis. Both, the

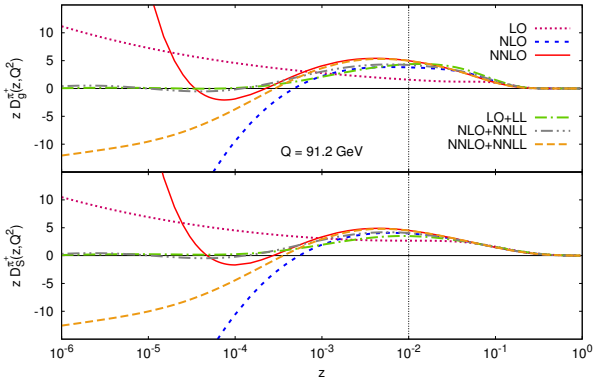

Figure 2.12: z times the obtained gluon (upper panel) and singlet (lower panel) FFs as a function of z, evaluated at $Q = 91.2$ GeV for the different fits listed in Tab. 2.5. The singlet is shown for $N_f = 5$ active flavors. The fitted z-range, $z > 0.01$, is to the right of the dotted vertical line.

data and the calculated multiplicities are shown as a function of $\zeta \equiv -\log z$.

In Fig. 2.12, we plot z times the gluon and singlet FFs for positively charged pions, $D_g^{\pi^+}(z, Q^2)$ and $D_S^{\pi^+}(z, Q^2)$, respectively, resulting from our fits given in Tab. 2.5. The FFs are computed at $Q = M_Z = 91.2\,\text{GeV}$ and in a range of z shown extending well below the $z_{\min} = 0.01$ cut above which they are constrained by data. We would like to point out that the resummed (and matched) results for which we have full control over all logarithmic powers (i.e. for LO+LL and NLO+NNLL) are well behaved at small-z and show the expected oscillatory behavior with z which they inherit from the resummed splitting functions through evolution. The latter behave like different combinations of Bessel functions when the Mellin inverse back to z-space is taken; for more details see Ref. [130]. The singlet and gluon FFs at NNLO+NNLL accuracy still diverge for $z \to 0$ (i.e. they turn to large negative values in the z-range shown in Fig. 2.12) since we do not have control over all five logarithmic powers that appear in a fixed-order result at NNLO; cf. Tabs. 2.1 and 2.2. However, the resummation of the three leading towers of logarithms, considerably tames the small-z singularities as compared to the corresponding result obtained at NNLO.

Finally, to further quantify the impact of small-z resummations in the range of z relevant for phenomenology, Fig. 2.13 shows the K-factors at scale $Q = 91.2\,\text{GeV}$ for the pion multiplicities (2.4) obtained in our fits. Schematically, they are defined as

$$K \equiv \frac{\mathbb{C}^{\text{FO + Res}} \otimes D^{\text{FO + Res}}}{\mathbb{C}^{\text{FO}} \otimes D^{\text{FO}}} \,. \tag{2.75}$$

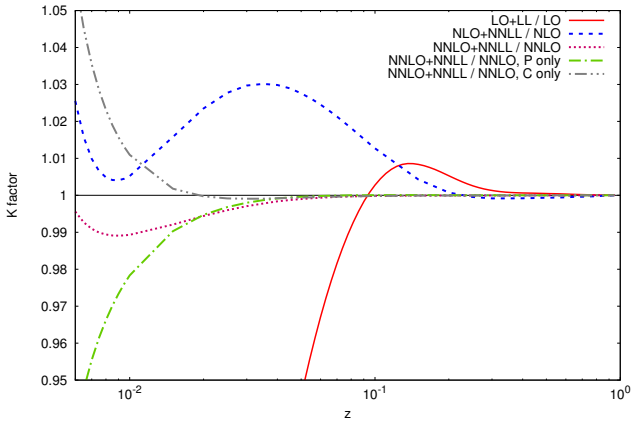

Figure 2.13: K-factors as defined in Eq. (2.75) at LO+LL, NLO+NNLL, and NNLO+NNLL accuracy at $Q = 91.2$ GeV in the range of z relevant for phenomenology. In addition, we show NNLO+NNLL results where the resummations are only performed either for the coefficient functions ("C only") or for the splitting functions ("P only").

Here, $\mathbb{C}^{\rm FO}$ and $\mathbb{C}^{\rm FO+Res}$ denote the fixed-order coefficient functions at LO, NLO, and NNLO accuracy and the corresponding resummed and matched coefficient functions, respectively. Likewise, $D^{\rm FO}$ and $D^{\rm FO+Res}$ are the FFs evolved with splitting functions at fixed order and resummed, matched accuracy, respectively. In order to assess the relevance of the small-z resummations independent of the details of the non-perturbative input for the FFs at scale μ_0, we adopt the same FFs for both calculating the numerator and the denominator. In each computation of K, we select the set of FFs obtained from the corresponding fixed-order fit and the different logarithmic orders of the resummations are chosen as discussed and given in Tab. 2.5.

By comparing the results for the K-factors at LO+LL, NLO+NNLL, and NNLO+NNLL accuracy, it can be infered that the corrections due to the small-z resummations start to become appreciable at a level of a few percent already below $z \simeq 0.1$. As one might expect, resummations are gradually less important when the perturbative accuracy of the corresponding fixed-order baseline is increased, i.e., the NNLO result already captures most of the small-z dynamics relevant for phenomenology whereas the differences between LO and LO+LL are still sizable. This explains the pattern of χ^2 values we have observed in Tab. 2.5. In addition, Fig. 2.13 also gives the K-factor at NNLO+NNLL accuracy where the small-z resummations are only performed either for the coefficient functions (labeled as "C only") *or* for the splitting functions ("P only"). By comparing these results with the full K-factor at NNLO+NNLL

accuracy, one can easily notice, that there are very large cancellations among the two.

2.5.2 Scale dependence

In this section, the remaining scale dependence of the resummed expressions is studied and compared to the corresponding fixed-order results. The scale-dependent terms are implemented according to the discussions in Sec. 2.3.3. As usual, we use the iterated solution with up to $n = 20$ terms in the perturbative expansion.

As was already observed in the NNLO analysis, the dependence on the factorization scale μ_F in SIA is gradually reduced the more higher order corrections are considered in the perturbative expansion. This is in line with the expectation that all artificial scales, μ_F and μ_R, should cancel in an all-order result, i.e. if the series is truncated at order m, the remaining dependence on, say, μ_F should be of order a_s^{m+1}. Following this reasoning, we do expect a further reduction of the scale dependence upon including small-z resummations on top of a given fixed-order calculation; see Sec. 2.3.3.

The scale dependence is studied by varying the scale μ_F by a factor of two or four around its default (central) value, $\mu_F = Q$ in case of SIA. Therefore, we introduce the parameter $\xi \equiv \mu_F^2/Q^2$; note that thoriughout this chapter we kept $\mu_F = \mu_R$ as is commonly done. Hence, $\xi = 1$ corresponds to the standard choice of scale $\mu_F = Q$. The conventional way of showing the dependence of a quantity T, like the pion multiplicity (2.4), on ξ is to plot the ratio $T(\xi)/T(\xi = 1)$ for various values of ξ; in our analyses, we will use $\xi = 2$ and $\xi = 0.5$.

However, we find that the oscillatory behavior of the resummed splitting and coefficient functions causes the SIA multiplicities to become an oscillatory function as well, which for certain small values of z, well below the cut $z_{\min}$ down to which we fit FFs to data, eventually becomes negative. Therefore, it is not feasible to utilize the common ratio plots to investigate the resummed scale dependence. Instead, we decide to study the *width* of the scale variation Δ_T for a quantity T, defined as

$$\begin{aligned} \Delta_T(z) &\equiv \max[T_{\xi=1}(z), T_{\xi=2}(z), T_{\xi=0.5}(z)] \\ &- \min[T_{\xi=1}(z), T_{\xi=2}(z), T_{\xi=0.5}(z)] \end{aligned} \tag{2.76}$$

in the range $\xi = [0.5, 2]$ as a measure of the residual dependence on μ_F.

In Fig. 2.14, we show $\Delta_{\text{SIA}}(z)$ for the pion multiplicities (2.4) at $Q = 10.54\,\text{GeV}$ for the two fixed-order fits (NLO and NNLO accuracy) as well as for resummed and matched fit at NNLO+NNLL.

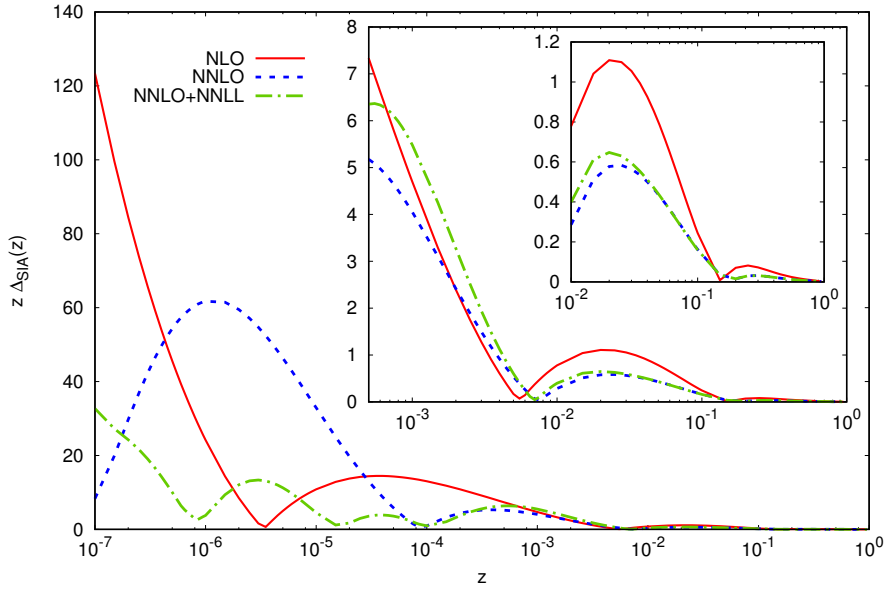

Figure 2.14: z times the width of the scale band $\Delta_{\rm SIA}$ defined in (2.76) for for three different ranges of z at NLO, NNLO and NNLO+NNLL accuracy. All results for the SIA pion multiplicities are obtained for $Q = 10.54\,\text{GeV}$; see text.

The main plot, which covers the z-range down to 10^{-7}, clearly demonstrates that the band $\Delta_{\rm SIA}$ is, on average, considerably more narrow for the NNLO+NNLL resummed cross section than for the fixed-order results, according to the expection. From the middle inset in Fig. 2.14, which shows z values relevant for experiments, i.e. $z \gtrsim 10^{-3}$, one can infer that the band $\Delta_{\rm SIA}$ is roughly of the same size for all calculations and resummations do not lead to any improvement in the scale dependence in this range. The small inset zooms into the range $z > 0.01$, where a similar conclusion can be reached.

In order to fully understand this behavior, one perhaps would have to include the yet missing N^{4}LL corrections, which would allow one to resum all five logarithmic towers present at NNLO accuracy. The observed result might be due to these missing subleading terms or it could be related to some intricate details in the structure of the perturbative series in the time-like case at small-z.

In any case, one can safely conclude that in the z-region relevant for phenomenology of SIA, the residual scale dependence of the resummed result does not differ from the fixed order calculation at NNLO accuracy. The latter is therefore entirely sufficient for extractions of FFs from SIA data as resummations neither improve the quality of the fit, cf. Sec. 2.5.1 nor do they reduce

theoretical uncertainties. Nonetheless, it important to demonstrate from a theoretical point of view that, on average, resummation does achieve smaller scale uncertainties, although for values of z that are well outside the range of currently available data. It should be also kept in mind that the study of the $N = 1$ moment of multiplicities, though not studied here, would not be possible without invoking small-z resummations as fixed-order results are singular.

2.6 Conclusions

In this chapter we have presented the results of [J4] and [J5], which extended for the first time previous FF analysis frameworks based on single-inclusive pion production in electron-positron annihilation beyond NLO. To this end, we have extended the existing space-like evolution package PEGASUS for parton distribution functions to the time-like region and fragmentation functions. The code is numerically very efficient and works throughout in Mellin N moment space, where the evolution equations can be solved analytically. It was used to conduct two separate analyses. The first one at next-to-next-to leading order whereas the second one included resummations for the small-z kinematical region. The technical details of each separate implementation were discussed in Sec 2.2 and 2.3.

First in Sec 2.2, we have studied all the relevant technical details to perform the QCD scale evolution and cross section calculation for single-inclusive hadron production in electron-positron annihilation up to next-to-next-to-leading order accuracy. We have verified all the needed expressions for the N moments of the time-like evolution kernels and the hard-scattering coefficient functions by re-deriving them from their counterparts in momentum space. We find full agreement with the results given in the literature. The results obtained with our time-like evolution code at NNLO are found to agree with the MELA package.

On the other hand in Sec 2.3, we have reviewed how to resum coefficient functions and splitting functions to all orders in perturbation theory up to next-to-next-to-leading logarithmic accuracy. The approach used here was proposed in the literature and is based on general considerations concerning all-order mass factorization. Our results agree with those presented in the literature, and we have extended them to allow for variations in the factorization and renormalization scales away from their default values. Moreover, we have shown how to properly implement the resummed expressions in Mellin moment space and how to set up a solution to the coupled, matrix-valued singlet evolution equations. The non-singlet sector is subleading and not affected by the presently available logarithmic order. For all practical purposes we

advocate an iterated solution for the scale evolution of fragmentation functions, and we have shown that keeping twenty terms in the expansion of the resummed expressions is sufficient for all applications. We have also discussed how to match the resummed towers of logarithms for both the coefficient and the evolution kernels to the known fixed-order expressions. Numerical subtleties in complex Mellin moment space related to finding a proper choice of contour for the inverse transformation despite the more complicated structure of singularities of the resummed evolution kernels and coefficient functions have been addressed as well.

For both studies a number of phenomenological results were presented and the relevance of each contribution was discussed separately. In Sec. 2.4, we have proceeded by extracting new sets of parton-to-pion fragmentation functions from a fit to electron-positron annihilation data up to next-to-next-to-leading order accuracy. We have compared our results to existing next-to-leading order fits in the literature. The flavor singlet fragmentation function, which is known to be constrained best by data, comes out very similar as in all previous fits in both our next-to-leading and next-to-next-to-leading order analyses whereas some small ambiguities remain for the fully flavor-decomposed fragmentation functions. While the quality of our fits to electron-positron annihilation data was already acceptable at leading order accuracy, it gradually improved upon including higher order corrections. In particular, the description of data at small momentum fractions z at the lowest energies Q is significantly better at next-to-next-to-leading order accuracy. In addition, leading order fits are found to explore regions in the parameter space which are at the border of becoming unphysical in order to achieve the best possible fit to data. As for the analysis of parton distributions, we expect global fits of fragmentation functions at next-to-next-to-leading order accuracy to become the new standard soon. The most important new asset in this section, however, is the found reduction of theoretical uncertainties related to the choice of the factorization scale by about a factor of two as compared to the next-to-leading order level. The uncertainties now match the precision of the data in most of the kinematic regime relevant for an analysis of fragmentation functions. A similar reduction by a factor of two was found for the size of the genuine higher order corrections relative to calculations performed one order lower in the perturbative series, i.e., in the K-factor.

The corresponding results for the analysis including small-z resummations effects was addressed in Sec. 2.5 were a first analysis of semi-inclusive annihilation data with an identified pion in terms of parton-to-pion fragmentation functions and in the presence of resummations was presented. To this end, various fits at different fixed-orders in perturbation theory and levels of small-z resummations were compared in order to study and quantify the phenomenological

impact of the latter. It turned out that for both the quality of the fit to data and the reduction of theoretical uncertainties due to the choice of the factorization scale, resummations provide only litte improvements with respect to an analysis performed at fixed, next-to-next-to-leading order accuracy. At values of the hadron's momentum well outside the range of phenomenological interest, we did observe, however, a significant improvement in the scale dependence of the inclusive pion cross section in the presence of resummations.

There are several avenues one can follow to further improve the theoretical framework for the analysis of fragmentation functions and the phenomenology of single-inclusive hadron production in electron-positron annihilation. For instance, the treatment of heavy quark to light meson fragmentation functions in global analyses certainly leaves room for improvement as, for exapmle, matching conditions for a variable flavor number scheme are only know up to next-to-leading order accuracy so far.

Moreover, as was pointed out in this chapter, a better understanding of the interplay of resummations and other sources of potentially large corrections in the region of small momentum fractions is another important avenue of future studies for time-like processes. One if not the most important source of power corrections is the hadron mass, which is neglected in the factorized framework adopted for any analysis of fragmentation functions. At variance with the phenomenology of parton distributions functions, where one can access and theoretically describe the physics of very small momentum fractions, hadron mass corrections prevent that in the time-like case. In fact, they become an inevitable part and severely restrict the range of applicability of fragmentation functions and the theoretical tools such as resummations.

As is well known and utilized in global QCD analyses of fragmentation functions at next-to-leading order already, other processes such as semi-inclusive deep-inelastic scattering or inclusive hadron production in hadron-hadron collisions provide invaluable information on the flavor decomposition and the gluon fragmentation function. Full next-to-next-to-leading order expressions for these processes are unfortunately not yet available but one can resort to results obtained with resummation techniques that contain the dominant higher order terms. Again, these expression can be most conveniently implemented numerically in terms of Mellin moments.

Possible further applications of resummations comprise revisiting the analyses of the first moment of hadron multiplicities available in the literature. Here, resummations are indispensable for obtaining a finite theoretical result. So far, the main focus was on the energy dependence of the peak of the multiplicity distribution, its width, and a determination of the strong coupling. It might be a valuable exercise to merge the available data on the first moment and the

relevant theoretical formalism with the extraction of the full momentum dependence of fragmentation functions as described in this chapter to further our knowledge of the non-perturbative hadronization process.
In addition, resummations can and have been studied for large fractions of the hadron's momentum. With more and more precise data becoming available in this kinematical regime, it would be very valuable to incorporate also these type of large logarithms into the analysis framework for fragmentation functions at some point in the future.

CHAPTER 3

Interplay of Threshold Resummation and Hadron Mass Corrections in Deep Inelastic Processes

We discuss hadron mass corrections and threshold resummation for deep-inelastic scattering $\ell N \to \ell' X$ and semi-inclusive annihilation $e^+e^- \to hX$ processes, and provide a prescription how to consistently combine these two corrections respecting all kinematic thresholds. We find an interesting interplay between threshold resummation and target mass corrections for deep-inelastic scattering at large values of Bjorken x_B. In semi-inclusive annihilation, on the contrary, the two considered corrections are relevant in different kinematic regions and do not affect each other. A detailed analysis is nonetheless of interest in the light of recent high precision data from BaBar and Belle on pion and kaon production, with which we compare our calculations. For both deep inelastic scattering and single inclusive annihilation, the size of the combined corrections compared to the precision of world data is shown to be large. Therefore, we conclude that these theoretical corrections are relevant for global QCD fits in order to extract precise parton distributions at large Bjorken x_B, and fragmentation functions over the whole kinematic range. This chapter is based upon our published work [J3].

3.1 Introduction

Predictions from QCD rely on perturbative calculations of parton-level hard scattering processes as well as on non-perturbative input in the form of parton distribution functions (PDFs) and fragmentation functions (FFs). On the one hand, PDFs contain information about the distributions of quarks and gluons in hadrons, which is relevant for processes with initial-state hadrons. On the other hand, as we have seen in Chpater 2, FFs describe the fragmentation of an outgoing parton into the observed hadron and, to some extent, may be viewed as the final-state analogue of PDFs. The applicability of this framework within perturbative QCD was established in factorization theorems [80] allowing one to absorb long-distance dynamics into these two universal non-perturbative objects. Therefore, the predictive power of QCD relies crucially on the precise knowledge of PDFs and FFs, that are nowadays extracted from a global analysis of a wide set of experimental data, see Refs. [175–177] for recent reviews.

Modern PDF fits [178–181] are available within a next-to-leading order (NLO) framework and most of them also at (partial) next-to-next-to-leading order. Key data sets for the extraction of PDFs are provided by measurements of inclusive deep-inelastic scattering (DIS) $\ell N \to \ell' X$, which is one of the two processes that we are considering in this chapter. Despite a lot of progress in the past years, large uncertainties are still present for large values of the parton momentum fraction x [182]. As it turns out, it is precisely this region that is particularly relevant at the LHC, when trying to find signals of new physics in, for example, (di-)jet measurements [183, 184]. Furthermore, the large-x region is also interesting as it can provide a window into the non-perturbative dynamics of the color confinement mechanism holding quarks and gluons inside hadrons [185, 186].

On the experimental side, improvements for the gluon PDF at large-x can be obtained from jet data taken at the Tevatron and the LHC, direct photon production in fixed target experiments, and from longitudinal DIS structure functions. Concerning quark PDFs, the present focus is mostly on low-energy experiments carried out for example at JLab [187], with important information coming from directly reconstructed W charge asymmetries at the Tevatron [182]. On the theoretical side a number of corrections to the pQCD calculations of these events are needed in order to harvest fully the available and upcoming experimental data, and extract precise large-x quark and gluon PDFs from global QCD fits. These corrections include, in particular, resummation of threshold logarithms, Target Mass Corrections (TMCs), higher-twist diagrams, and nuclear corrections when nuclear targets are considered. The last three

have been included consistently, for example, in the CTEQ-JLab collaboration PDF fits [179] and the fits by Alekhin and collaborators [188], allowing to substantially extend the range in x of the fitted DIS data. Threshold resummation has been considered in the past to estimate the theoretical errors of PDFs or was used for fits of only a subset of the data [189–191], but has not yet been fully included for all relevant data sets in a global QCD fit.

In the first part of this chapter, we consider the interplay between two major corrections to the standard NLO formalism for DIS both of which have their greatest impact at large-x, namely TMCs and higher order contributions derived from threshold resummation. Here we choose the collinear factorization TMC framework of Accardi and Qiu [192], that contrary to most other approaches [193, 194] respects the kinematic $x_B \leq 1$ bound on the Bjorken variable. Threshold resummation for QCD processes was derived in [52, 58–60] and recently revisited in [J1, J2, C1]; see also Chpater 5. Large logarithms that need to be resummed to all orders arise near the phase space boundary where gluon radiation is limited. We perform the resummation at the level of next-to-leading logarithmic (NLL) accuracy. In particular, we derive a resummation procedure that also respects the Bjorken x_B bound when a non-zero target mass is considered, and can therefore be consistently combined with the TMC calculation. We discuss the interplay of both kinds of corrections, and assess their relevance for PDF global fits by comparing them to a selection of world data on DIS scattering.

Unlike for PDFs, global fits of FFs [76, 77, 79, 92, 195, 196] are less constrained by presently existing data sets. As it is extensively discussed in Chapter 2, one of the main sources of constraints on FFs is semi-inclusive annihilation (SIA) $e^+e^- \to hX$ which we are going to consider in this chapter aswell. Recently, very precise data sets from BELLE [83] and BaBar [84] became available, where the statistical accuracy is partially in the sub one percent level. In addition, a very fine binning was applied over a wide range of the fragmentation variable $z \equiv x_E = 2E^h/\sqrt{s}$ reaching up to ≈ 0.95. Here, E^h is the energy of the observed hadron in the center-of-mass system (c.m.s.) and $\sqrt{s} = 10.5$ GeV is the energy for collisions at both experiments. This offers a new possibility for studying effects that go beyond the standard NLO framework and for learning more about QCD dynamics in fragmentation processes. On the theory side, the present day state of the art is NLO in QCD but a first NNLO FF analysis including small-z resummations effects was given in [J4, J5] and presented in Chapter 2. Several additional effects, including small-x resummation, threshold resummation and hadron mass effects have been studied in [195, 197].

In the second part of this chapter we revisit calculations of hadron mass corrections (HMCs)

and threshold resummation in analogy to our DIS analysis. We present for the first time (to our knowledge) a resummed calculation for kaon SIA events, and compare our kaon and pion production cross section to the recent BELLE and BaBar data. In contrast to the Operator Product Expansion based formalism for mass corrections, the approach in [192] may be generalized to other processes, such as semi-inclusive deep-inelastic scattering [198]. Here we extend this framework to SIA in electron-positron scattering, we perform a detailed analysis of the effects of the produced hadron mass on the parton-level kinematics, and evaluate their numerical consequences. We note that previous studies of HMCs were carried out in [195, 197], showing in particular that inclusion of these HMCs in global FF fits results in better χ^2 values. We then consider the combination with threshold resummation [131] in the framework of the so-called "crossed resummation" [199], that exploits similarities between various color-singlet QCD processes such as DIS, SIA, Drell-Yan, and semi-inclusive deep-inelastic scattering. We will again also build upon the recent threshold resummation studies in [J1, J2, C1]. Contrary to DIS, we find that HMCs are dominant at low x_E, whereas threshold resummation is again most relevant for large x_E. We analyze the crosstalk of these effects and evaluate their relevance to global FF fits by comparing these to the new data sets from BELLE and BaBar.

The following sections are organized as follows. In Sec. 3.2, we discuss TMCs and threshold resummation in DIS before we derive our prescription to combine both. We briefly review the TMC derivation of [192], and provide some basic formulas concerning threshold resummation in order to establish our notation in this chapter. Then, we analyze the numerical relevance of the corrections, and compare these to a selection of world DIS data. In Sec. 3.3, we discuss SIA following the same steps as for the DIS case before, and compare our numerical results to the recent BELLE and BaBar data on pion and kaon production. Finally, we draw our conclusions in Sec. 3.4.

3.2 Target Mass Corrections and Resummation for DIS

3.2.1 Target Mass Corrections

In DIS, a parton of momentum k belonging to a nucleon of momentum p is struck by a virtual photon of momentum q. This generates in the final state a target jet with momentum p_Y and a current jet with momentum p_j, see Fig. 3.1. We work in a "collinear" frame where the spacial components of p and q are parallel and directed along the longitudinal axis, and we parametrize

the involved the momenta p, q, k following [192]:

$$\begin{aligned} p^\mu &= p^+ \bar{n}^\mu + \frac{m_N^2}{2p^+} n^\mu \,, \\ q^\mu &= -\xi p^+ \bar{n}^\mu + \frac{Q^2}{2\xi p^+} n^\mu \,, \\ k^\mu &= x p^+ \bar{n}^\mu + \frac{k^2 + k_T^2}{2x p^+} n^\mu + \boldsymbol{k}_T^\mu \,, \end{aligned} \tag{3.1}$$

In this expression p^+ can be regarded as a parameter for boosts along the longitudinal axis. The light-cone vectors n^μ and $\bar{n}^\mu$ satisfy

$$n^2 = \bar{n}^2 = 0 \quad n \cdot \bar{n} = 1 \,, \tag{3.2}$$

and the plus- and minus- components of a general 4-vector a are given by

$$a^+ = a \cdot n \quad a^- = a \cdot \bar{n}. \tag{3.3}$$

The momenta are parametrized in terms of the external (*i.e.*, experimentally measurable) variables

$$x_B = \frac{-q^2}{2p \cdot q}, \quad Q^2 = -q^2, \quad p^2 = m_N^2 \,, \tag{3.4}$$

where m_N is the target mass and Q^2 the photon virtuality. The parton fractional light-cone momentum with respect to the nucleon is a kinematic internal (*i.e.*, non measurable) variable and is defined by

$$x = \frac{k^+}{p^+}. \tag{3.5}$$

In an analogous way we can define the virtual boson fractional momentum as

$$\xi = -\frac{q^+}{p^+} = \frac{2x_B}{1 + \sqrt{1 + 4x_B^2 m_N^2 / Q^2}}, \tag{3.6}$$

which is an external kinematic variable and coincides with the Nachtmann variable [200]. The target's mass can be neglected in the Bjorken limit $Q^2 \gg m_N^2$ at fixed x_B, and in many analysis is omitted from the outset. (This is fine for unpolarized scattering but poses problems for the definition of the nucleon's spin in the case of polarized scattering.) In this chapter we explicitly work at finite Q^2 and verify that our result correctly reproduces the "massless target" formulas

in the Bjorken limit, where $\xi \to x_B$.

In order to perform collinear factorization of the DIS structure functions, one expands the momentum k of the struck parton around its positive light-cone component $xp^+\bar{n}^\mu$, and neglects in the kinematics the transverse components, as well as (for light quarks) the negative light-cone component. This is equivalent to kinematically treating the parton as massless and collinear to the parent nucleon from the very beginning, and setting $k^2 = 0$ and $\boldsymbol{k}_T{}^\mu = 0$ in Eq. (3.1) from the beginning.

The parton's momentum fraction x then appears as an integration variable in the structure functions, that are given by a convolution integral of perturbatively calculable coefficient functions and non-perturbative PDFs [80, 201]. Following [192], we may derive limits on the dx integration by examining both the external and internal kinematics of the diagram shown in Fig. 3.1, and apply four momentum and net baryon number conservation. This latter, in particular requires that at least one baryon of mass larger than m_N be present in the final state. This can appear in either the target jet (lower right part in Fig. 3.1) or the current jet (upper right part in Fig. 3.1). Unless the rapidity difference between the current jet and the target jet is too small [202, 203], the baryon mass appears in the latter [192], so that $p_Y^2 \geq m_N^2$ and $p_j \geq 0$. Next, considering four-momentum conservation the hard-scattering vertex we find

$$0 \leq p_j^2 = (q+k)^2 = \left(1 - \frac{\xi}{x}\right) \frac{Q^2 x}{\xi}\,, \tag{3.7}$$

where we used the momenta defined in Eq. (3.1). In order to obtain another constraint on the dx integration, it is not sufficient to analyze the other vertex. Instead, we have to consider the invariant momentum squared of the whole process:

$$(q+p)^2 = (p_j + p_Y)^2 \geq (q+k)^2 + m_N^2\,. \tag{3.8}$$

where we used $p_Y^2 \geq m_N$, as previously discussed, as well as $2p_j \cdot p_Y \geq 0$ since both final state jets consist of on-shell particles. Evaluating $(q+k)^2$ as before in Eq. (3.7) we finally obtain

$$1 - \frac{1}{x_B} \leq \left(1 - \frac{x}{\xi}\right). \tag{3.9}$$

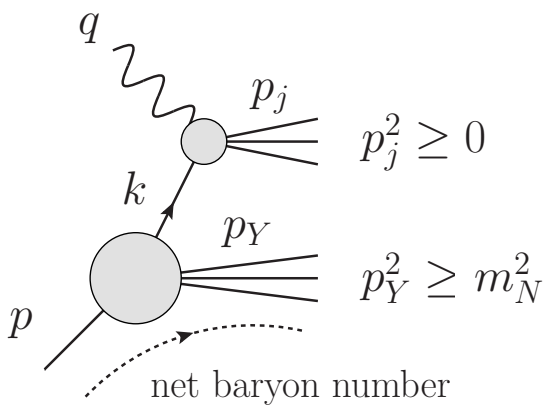

Figure 3.1: Diagram for DIS specifying all momenta. The net baryon number is shown to flow into the target jet. Figure taken from [192].

In summary, the parton's fractional momentum x is kinematically bound by

$$\xi \leq x \leq \xi/x_B\,, \tag{3.10}$$

as first discussed in [192].

The structure functions including the finite target mass kinematics we have discussed can be written in collinear factorization at leading twist as [192, 204]

$$\begin{aligned}
\mathcal{F}_1^{\rm TMC}(x_B,Q^2) &\equiv 2F_1^{\rm TMC}(x_B,Q^2) = \mathcal{F}_1(\xi,Q^2)\,,\\
\mathcal{F}_2^{\rm TMC}(x_B,Q^2) &\equiv \frac{1}{x_B}F_2^{\rm TMC}(x_B,Q^2) = \frac{1}{\rho^2}\mathcal{F}_2(\xi,Q^2)\,,\\
\mathcal{F}_L^{\rm TMC}(x_B,Q^2) &\equiv \frac{1}{x_B}F_L^{\rm TMC}(x_B,Q^2) = \mathcal{F}_L(\xi,Q^2)\,,
\end{aligned} \tag{3.11}$$

where for convenience we defined

$$\rho^2 = 1 + \frac{4x_B^2 m_N^2}{Q^2}\ . \tag{3.12}$$

Note that here we adopted the convention of Ref. [J1, 205] for the $\mathcal{F}_i^{\rm TMC}$ structure functions in terms of the customary ones appearing in the Lorentz decomposition of the hadronic tensor satisfying $\mathcal{F}_L^{\rm TMC}(x_B,Q^2) = \rho^2\mathcal{F}_2^{\rm TMC}(x_B,Q^2) - \mathcal{F}_1^{\rm TMC}(x_B,Q^2)$. On the right hand side of

Eq. (3.11), convolution integrals appear

$$\mathcal{F}_i(\xi, Q^2) = \sum_f \int_\xi^{\xi/x_B} \frac{dx}{x} f(x, \mu^2)\, \mathcal{C}_f^i \left(\frac{\xi}{x}, \frac{Q^2}{\mu^2}, \alpha_s(\mu^2) \right) , \tag{3.13}$$

where the integration over dx ranges only over the region allowed by the limits in Eq. (3.10). The notation we use implies that whenever the lower limit exceeds the upper limit the integral is zero, so that the structure functions are indeed zero in the kinematically forbidden region $x_B > 1$. The functions $f(x, \mu^2)$ denote the distribution of a parton of flavor f in the target nucleon and the sum runs over $f = q, \bar{q}, g$, with q a shorthand for all active quark flavors. The hard-scattering coefficient functions $\mathcal{C}_f^i$ encode the short-distance hard scattering of the virtual photons with partons from the nucleon target, and are independent of the mass of the latter. They can be calculated in perturbative QCD order-by-order in powers of the strong coupling constant,

$$\mathcal{C}_f^i = C_f^{i,(0)} + \frac{\alpha_s(\mu^2)}{2\pi} C_f^{i,(1)} + \mathcal{O}(\alpha_s^2) , \tag{3.14}$$

which are related by $\mathcal{C}_f^L = \mathcal{C}_f^2 - \mathcal{C}_f^1$ for massless partons. For example, at leading-order (LO) we have

$$C_{q,\bar{q}}^{2,(0)}(\hat{x}) = e_q^2 \delta(1 - \hat{x}), \quad C_g^{2,(0)}(\hat{x}) = 0, \quad C_{q,\bar{q},g}^{L,(0)}(\hat{x}) = 0 , \tag{3.15}$$

with $\hat{x} = \xi/x$. F_2^{TMC} reduces to the target mass corrected version of the parton model [206, 207] except for a step function imposing the proper kinematic bounds:

$$F_2^{\mathrm{TMC}}(x_B, Q^2) = \frac{x_B}{\rho^2} \sum_{f=q,\bar{q}} e_f^2 f(\xi, Q^2) \theta(1 - x_B) . \tag{3.16}$$

For completeness, we list all the relevant coefficient functions $\mathcal{C}_f^i$ up to NLO in Appendix C.1.

Note that in the large Q^2 limit (in which $M^2/Q^2 \to 0$), as well as in the small Bjorken-x limit $x_B \to 0$, the Nachtmann variable $\xi \to x_B$ and $\rho \to 1$, so that

$$\mathcal{F}_i^{\mathrm{TMC}}(x_B, Q^2) \to \mathcal{F}_i(x_B, Q^2) \tag{3.17}$$

and the usual massless target formulas are recovered. Conversely, in the $x_B \to 1$ limit, the

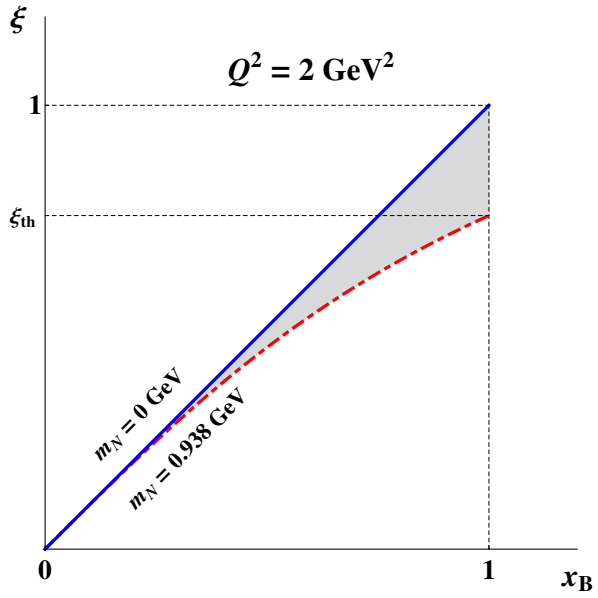

Figure 3.2: The Nachtmann variable ξ as a function of x_B with $m_N = 0$ GeV (solid blue line) and $m_N = 0.938$ GeV (dash-dotted red line) at $Q^2 = 2$ GeV^2.

Nachtmann variable $\xi \to \xi_{\rm th}$, where

$$\xi_{\rm th} = \frac{2}{1+\sqrt{1+4m_N^2/Q^2}}\,, \tag{3.18}$$

and ξ differs maximally from x_B (see Fig. 3.2). Therefore, in this limit, TMC effects are the largest. Since the integral over dx is limited to the region defined by the kinematic bounds in Eq. (3.10), the structure functions $\mathcal{F}_i^{\rm TMC}$ have support only over the physical region at $x_B \leq 1$. This is the defining characteristics of the treatment of TMCs proposed in Ref. [192] and sets this apart from most other TMC prescriptions, that in fact violate that bound and allow for non-zero structure functions also at $x_B > 1$. When combining TMCs with threshold resummation in Section 3.2.3, we will pay special attention to preserve this feature of our TMC treatment and not introduce a spurious violation of the Bjorken-x bound.

3.2.2 Threshold Resummation for DIS

The DIS coefficient functions $\mathcal{C}_f^i$ contain singular distributions. Near threshold they can get large and weaken or even violate the convergence of the perturbative expansion in the strong

coupling constant. Therefore, they have to be taken into account to all orders via threshold resummation. At NLO, singular distributions only appear in the structure function $\mathcal{F}_1$ (or equivalently $\mathcal{F}_2$) but not in $\mathcal{F}_L$. In the $\overline{\text{MS}}$ scheme, they read

$$C_{q,\text{th}}^{1,(1)}(x) = C_F \left[(1+x^2) \left(\frac{\ln(1-x)}{1-x} \right)_+ - \frac{3}{2} \frac{1}{(1-x)_+} - \left(\frac{9}{2} + \frac{\pi^2}{3} \right) \delta(1-x) \right], \quad (3.19)$$

where the plus-distribution is defined as

$$\int_0^1 dx\, f(x)[g(x)]_+ \equiv \int_0^1 dx\, (f(x) - f(1))\, g(x) \quad (3.20)$$

In general, at a given order k in the perturbative expansion, the coefficient function contains logarithms of the form

$$\alpha_s^k \left(\frac{\ln^n(1-x)}{1-x} \right)_+, \quad \text{with } n \leq 2k-1\,. \quad (3.21)$$

Performing the resummation at NLL, we fully take into account contributions down to $n = 2k-3$ at all orders. In other words, resummation at NLL accuracy sums up correctly the three most dominant towers of threshold logarithms. Results at next-to-next-to leading logarithmic accuracy were derived in [132, 133], where the next two subleading towers of threshold logarithms are also correctly taken into account. However, the main phenomenological effects are already captured at the level of NLL. In addition, the proposed prescription for combining TMC and resummation, as discussed in the next subsection, is independent of the accuracy of resummation that we are considering.

In the massless limit, $m_N^2/Q^2 \to 0$, resummation may be performed by introducing Mellin moments in x_B of the massless structure functions:

$$\mathcal{F}_1^N(Q^2) = \int dx_B\, x_B^{N-1}\, \mathcal{F}_1(x_B, Q^2) = \mathcal{C}_f^{1,N}\left(Q^2/\mu^2, \alpha_s(\mu^2)\right) \cdot f^N(\mu^2)\,, \quad (3.22)$$

where

$$\mathcal{C}_f^{1,N} = \left(\int_0^1 dx\, x^{N-1} \mathcal{C}_f^1 \left(x, Q^2/\mu^2, \alpha_s(\mu^2)\right) \right) \quad (3.23)$$

$$f^N = \left(\int_0^1 dy\, y^{N-1} f(y, \mu^2) \right) \quad (3.24)$$

and the superscript N denotes the dependence on the complex Mellin variable N. The Mellin

space expression of the NLO coefficient function up to terms that are suppressed as $\mathcal{O}(1/N)$ and choosing $\mu^2 = Q^2$ is given by

$$C_q^{1,(1),N} = C_F \left[\ln^2 \bar{N} + \frac{3}{2} \ln \bar{N} - \frac{9}{2} - \frac{\pi^2}{6} \right] , \tag{3.25}$$

where large logarithms in $\bar{N} = N e^{\gamma_E}$ correspond to large logarithms in $1 - x$ in Eq. (3.19). The resummed DIS coefficient function for the structure function $\mathcal{F}_1$ reads to NLL [J1, 52, 131, 199]:

$$\mathcal{C}_{q,\mathrm{res}}^{1,N}(Q^2/\mu^2, \alpha_s(\mu^2)) = e_q^2 H_q \left(Q^2/\mu^2, \alpha_s(\mu^2)\right) \times \Delta_q^N(Q^2/\mu^2, \alpha_s(\mu^2))\, J_q^N(Q^2/\mu^2, \alpha_s(\mu^2)) \,. \tag{3.26}$$

The radiative factor Δ_q^N describes gluon radiation from the initial quark that is both soft *and* collinear. The function J_q^N takes into account collinear (*i.e.* soft and hard) emissions from the unobserved parton in the final state. The two functions Δ_q^N and J_q^N are given by the following two exponentials

$$\begin{aligned} \log \Delta_q^N &\equiv \int_0^1 dx \frac{x^N - 1}{1 - x} \int_{Q^2}^{(1-x)^2 Q^2} \frac{dk_\perp^2}{k_\perp^2} A_q(\alpha_s(k_\perp^2)), \\ \log J_q^N &\equiv \int_0^1 dx \frac{x^N - 1}{1 - x} \left\{ \int_{(1-x)^2 Q^2}^{(1-x) Q^2} \frac{dk_\perp^2}{k_\perp^2} A_q(\alpha_s(k_\perp^2)) + \frac{1}{2} B_q(\alpha_s((1-x)Q^2) \right\} . \end{aligned} \tag{3.27}$$

The functions $A_q(\alpha_s)$ and $B_q(\alpha_s)$ can be calculated in a perturbative expansion in the strong coupling constant

$$\begin{aligned} A_q(\alpha_s) &= \frac{\alpha_s}{\pi} A_q^{(1)} + \left(\frac{\alpha_s}{\pi}\right)^2 A_q^{(2)} + \dots \,, \\ B_q(\alpha_s) &= \frac{\alpha_s}{\pi} B_q^{(1)} + \left(\frac{\alpha_s}{\pi}\right)^2 B_q^{(2)} + \dots \,. \end{aligned} \tag{3.28}$$

The relevant coefficients for resummation at NLL accuracy are given by

$$\begin{aligned} A_q^{(1)} &= C_F, \quad A_q^{(2)} = \frac{1}{2} C_F \left[C_A \left(\frac{67}{18} - \frac{\pi^2}{6} \right) - \frac{5}{9} N_f \right], \\ B_q^{(1)} &= -\frac{3}{2} C_F, \end{aligned} \tag{3.29}$$

where $C_F = 4/3$, $C_A = 3$ and N_f is the number of active flavors. Finally, the hard-scattering

coefficient H_q in Eq. (3.26) reads

$$H_q\left(Q^2/\mu^2, \alpha_s(\mu^2)\right) = 1 + \frac{\alpha_s}{2\pi} C_F \left(-\frac{9}{2} - \frac{\pi^2}{6} + \frac{3}{2}\ln\frac{Q^2}{\mu^2}\right) + \mathcal{O}(\alpha_s^2). \tag{3.30}$$

Expanding the exponents in Eq. (3.27) up to NLL accuracy, we find [J1, 208–212]

$$\begin{aligned} \log \Delta_q^N &= \ln \bar{N} h_q^{(1)}(\lambda) + h_q^{(2)}\left(\lambda, \frac{Q^2}{\mu^2}, \frac{Q^2}{\mu_F^2}\right) \\ \log J_q^N &= \ln \bar{N} f_q^{(1)}(\lambda) + f_q^{(2)}\left(\lambda, \frac{Q^2}{\mu^2}\right), \end{aligned} \tag{3.31}$$

where $\lambda = b_0 \alpha_s(\mu^2) \ln \bar{N}$. The two functions $h_q^{(1)}$, $f_q^{(1)}$ ($h_q^{(2)}$, $f_q^{(2)}$) collect all leading logarithmic (next-to-leading logarithmic) contributions in the exponent of the type $\alpha_s^k \ln^n \bar{N}$ with $n = k+1$ ($n = k+2$). The functions $h^{(1)}$ and $h^{(2)}$ for Δ_q^N are given by

$$\begin{aligned} h_q^{(1)}(\lambda) =& \frac{A_q^{(1)}}{2\pi b_0 \lambda}\left[2\lambda + (1-2\lambda)\ln(1-2\lambda)\right], \\ h_q^{(2)}\left(\lambda, \frac{Q^2}{\mu^2}, \frac{Q^2}{\mu_F^2}\right) =& -\frac{A_q^{(2)}}{2\pi^2 b_0^2}\left[2\lambda + \ln(1-2\lambda)\right] + \frac{A_q^{(1)} b_1}{2\pi b_0^3}\left[2\lambda + \ln(1-2\lambda) + \frac{1}{2}\ln^2(1-2\lambda)\right] \\ &+ \frac{A_q^{(1)}}{2\pi b_0}\left[2\lambda + \ln(1-2\lambda)\right]\ln\frac{Q^2}{\mu^2} - \frac{A_q^{(1)}}{\pi b_0}\lambda \ln\frac{Q^2}{\mu_F^2}. \end{aligned} \tag{3.32}$$

The functions $f^{(1)}$ and $f^{(2)}$ for J_q^N are given by

$$\begin{aligned} f_q^{(1)}(\lambda) &= h_q^{(1)}\left(\frac{\lambda}{2}\right) - h_q^{(1)}(\lambda), \\ f_q^{(2)}\left(\lambda, \frac{Q^2}{\mu^2}\right) &= 2h_q^{(2)}\left(\frac{\lambda}{2}, \frac{Q^2}{\mu^2}, 1\right) - h_q^{(2)}\left(\lambda, \frac{Q^2}{\mu^2}, 1\right) + \frac{B_q^{(1)}}{2\pi b_0}\ln(1-\lambda). \end{aligned} \tag{3.33}$$

Here, the b_0, b_1 are the coefficients of the QCD beta function

$$\begin{aligned} b_0 &= \frac{11 C_A - 4 T_R N_f}{12\pi}, \\ b_1 &= \frac{17 C_A^2 - 10 C_A T_R N_f - 6 C_F T_R N_f}{24\pi^2}. \end{aligned} \tag{3.34}$$

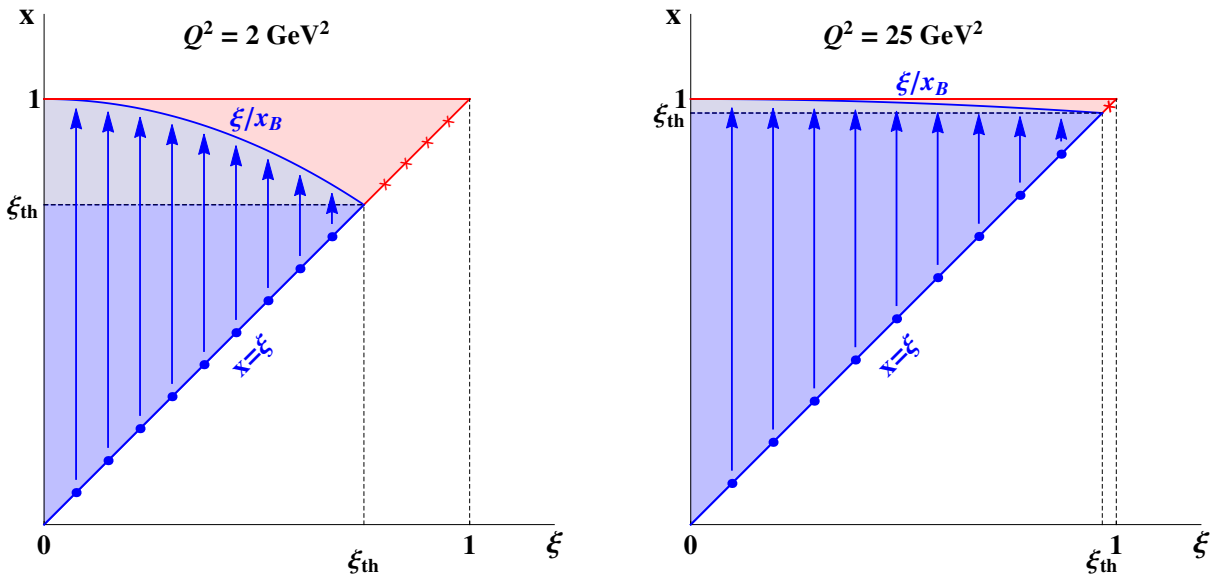

Figure 3.3: On the left (right) hand side the integration regions for $Q^2 = 2$ GeV^2 ($Q^2 = 25$ GeV^2) concerning Eq. (3.38) are shown. The blue dots denote the boundary where the threshold singularities arise and the arrows indicate the direction of integration.

In the end, we go back to x-space by numerically performing the Mellin inverse, which is given by

$$\mathcal{F}_{1,\mathrm{res}}(x_B, Q^2) = \int_{\mathcal{C}_N} \frac{dN}{2\pi i}\, x_B^{-N} \times \mathcal{C}^{1,N}_{q,\mathrm{res}}(Q^2/\mu^2, \alpha_s(\mu^2))\, f^N(\mu^2)\,. \tag{3.35}$$

The contour $\mathcal{C}_N$ is taken to run between the rightmost pole of the moments of the PDFs and the Landau pole following the minimal prescription of [213]. After the Mellin inverse is taken, we match to the full NLO which is still a good approximation away from threshold. We avoid double counting of threshold distributions at NLO by considering the matched combination

$$\mathcal{F}_{\mathrm{match}} = \mathcal{F}_{\mathrm{res}} - \mathcal{F}_{\mathrm{res}}\big|_{\mathcal{O}(\alpha_s)} + \mathcal{F}_{\mathrm{NLO}}\,. \tag{3.36}$$

3.2.3 Combining TMC and Threshold Resummation

After target mass corrections, the integration over the parton's momentum fraction in the collinear factorization formula (3.13) ranges from ξ to ξ/x_B. As a consequence, the Mellin moments of the structure function are no longer the product of the moments of the coefficient function $\mathcal{C}_1$ and the parton distribution f. One therefore may be tempted to express the structure function (3.13) as

$$\mathcal{F}_1^{\rm TMC} = \int_\xi^1 \frac{dx}{x} \mathcal{C}_f^1\left(\frac{\xi}{x}\right) f(x) - \int_{\xi/x_B}^1 \frac{dx}{x} \mathcal{C}_f^1\left(\frac{\xi}{x}\right) f(x)\,, \tag{3.37}$$

where for ease of notation we omitted any dependence of the coefficient functions and the PDFs on the scale Q^2/μ^2 and on $\alpha_s(\mu^2)$. The advantage of this reformulation is that the first term is integrated up to 1 (and differs from the Bjorken limit approximation only by a $x_B \to \xi$ replacement), so that its Mellin transform would indeed be given by the product of moments of the coefficient and parton distribution functions. However, written in this way, $\mathcal{F}_1^{\rm TMC}$ acquires support also in the unphysical region $x_B > 1$, where it actually becomes negative after crossing 0 at $x_B = 1$.

A better way to manipulate the structure function convolution in Eq. (3.13) in order to obtain a product of moments after performing its Mellin transformation, is to write

$$\mathcal{F}_1^{\rm TMC} = \int_\xi^{\xi_{\rm th}} \frac{dx}{x} \mathcal{C}_f^1\left(\frac{\xi}{x}\right) f(x) + \int_{\xi_{\rm th}}^{\xi/x_B} \frac{dx}{x} \mathcal{C}_f^1\left(\frac{\xi}{x}\right) f(x)\,. \tag{3.38}$$

In the small x_B limit only the first term on the right hand side survives, and the massless limit is recovered, as it should be. In the $x_B \to 1$ limit, each term separately tends to zero and remain zero for larger values of x_B. Therefore, the structure function as well remains zero in the unphysical region $x_B > 1$, as it happens with the original Eq. (3.13). This is then a good starting point for performing the resummation of threshold distributions in a way that respects the partonic and hadronic kinematics discussed in Section 3.2.1.

In order to get a deeper insight into the effects of TMCs on resummation, we can more closely analyze the integration region, that we depict in Fig. 3.3 for a small and a large value of Q^2. The partonic threshold for resummation is set by $x = \xi$, as indicated by the blue dots. Hence, we may view the effect of TMCs as cutting out the singularities lying at $x > \xi_{\rm th}$. As Q^2 increases, the amount of excluded singularities decreases, as can be seen from the diagram on the right.

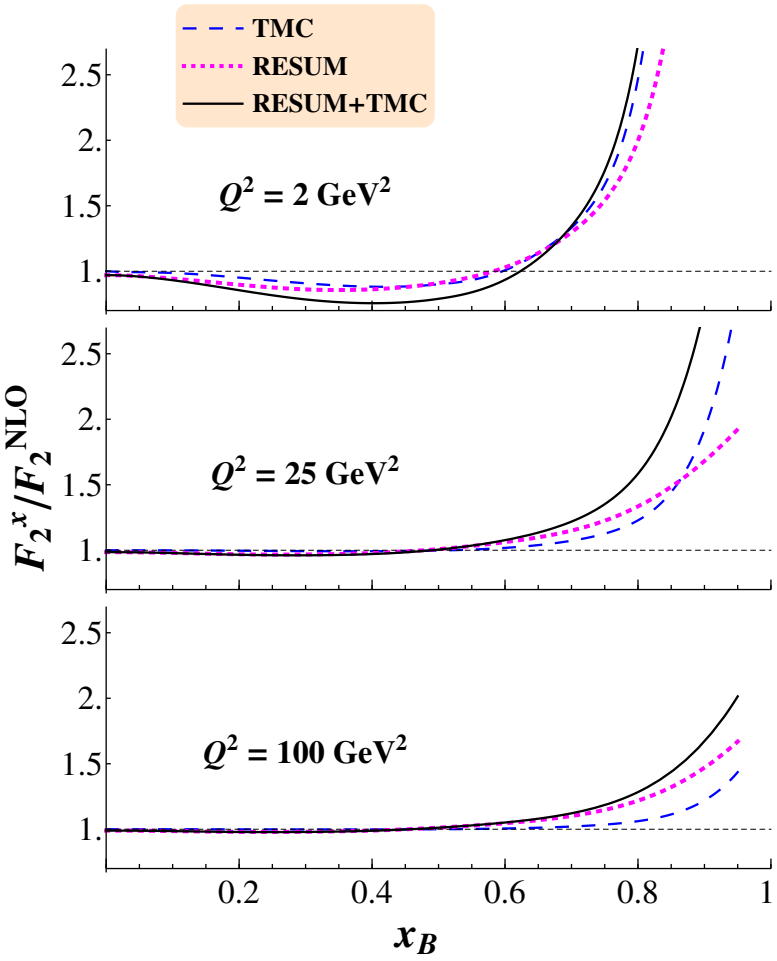

Figure 3.4: We show the effects of TMC (dashed blue), threshold resummation (dotted magenta) and the combination of both (solid black) normalized to NLO for the DIS structure function F_2 for different values of $Q^2 = 2,\ 25,\ 100$ GeV^2. The PDF set of [178] is used.

In the Bjorken limit ($Q^2 \to \infty$), ξ_{th} tends to 1, the integration region spans the whole triangle, and no singularity is excluded. Since the threshold for gluon radiation is set for $x \to \xi$ the threshold singularities appear only at the lower integration boundary of the first term, which is therefore the only one where large logarithms appear and need resummation. This can then be achieved without introducing a non-zero result for the resummed structure function in the unphysical region of $x_B > 1$ because the first term in Eq. (3.38) is zero at $x_B \geq 1$. In the second term, that also tends to zero as $x_B \to 1$, the threshold limit is not reached so that there is no need to regularize any of the terms in the coefficient function and we can treat this as part of

the matching procedure to the full NLO calculation, see Eq. (3.36).

As in the massless target approximation, we derive threshold resummation in Mellin space but taking special care of the fact that at finite Q^2 the first term in Eq. (3.38) does not have the standard convolution structure as for the massless approximation of the structure functions. Taking Mellin moments with respect to ξ of the first term in Eq. (3.38) only, we obtain

$$\begin{aligned}
\mathcal{F}_1^{\mathrm{TMC},N} &= \int_0^1 d\xi\, \xi^{N-1} \int_\xi^{\xi_{\mathrm{th}}} \frac{dx}{x} \mathcal{C}_f^1 \left(\frac{\xi}{x}\right) f(x) \\
&= \int_0^1 d\xi\, \xi^{N-1} \int_0^1 dy \int_0^{\xi_{\mathrm{th}}} dx\, \mathcal{C}_f^1(y)\, f(x)\, \delta(xy-\xi) \\
&= \left(\int_0^1 dy\, y^{N-1} \mathcal{C}_f^1(y)\right) \left(\int_0^{\xi_{\mathrm{th}}} dx\, x^{N-1} f(x)\right) \\
&= \mathcal{C}_f^{1,N}\, f_{\xi_{\mathrm{th}}}^N \,,
\end{aligned} \tag{3.39}$$

where we denoted by $f_X^N = \int_0^X dx\, x^{N-1} f(x)$ the N-th truncated moment of a function f. Hence, In Mellin space, the TMC corrected structure function $\mathcal{F}_1^{\mathrm{TMC}}$ factorizes into a product of the moments of the coefficient function $\mathcal{C}_f^{1,N}$, exactly as in the massless approximation, and of the truncated moments of parton distributions. The appearance of the latter reflects the reduced support for integration over x in Eq. (3.13) (as illustrated in Fig. 3.3). The truncation of the PDF moments increases in magnitude with the increase of x_B and the decrease of Q^2.

Using the resummed coefficient function $\mathcal{C}_{q,\mathrm{res}}^{1,N}$ in Eq. (3.26), we may perform the inverse transformation,

$$\mathcal{F}_{1,\mathrm{res}}^{\mathrm{TMC}}(x_B, Q^2) = \int_{\mathcal{C}_N} \frac{dN}{2\pi i}\, \xi^{-N}\, \mathcal{C}_{q,\mathrm{res}}^{1,N}\, f_{\xi_{\mathrm{th}}}^N \,, \tag{3.40}$$

using the same contour as in the massless target case, see e.g. [J1]. Note that this corresponds only to resummation of the first term in Eq. (3.38). We always have to calculate the second term separately and add it to the resummed result. Other than that, the matching procedure required to include the full NLO calculation is the same as that without TMCs, see Eq. (3.36).

3.2.4 Phenomenological Results

We now investigate the numerical effects of TMC and threshold resummation as well as their combination. Throughout this section we only consider a proton target. We make use of both the NLO "Martin–Stirling–Thorne–Watt" (MSTW 2008) set of parton distribution func-

tions [178] as well as the NLO CJ12 PDF set of [179] . As shown in Eq. (3.39), in order to perform numerical calculations for threshold resummation, we have to compute Mellin moments of the PDFs. Since these are provided in x space, we first fit suitable functions to the PDFs using the following parametrization

$$a_0\, x^{a_1}\,(1-x)^{a_2}\left(\sum_{j=3}^{n} a_j x^{b_j}\right), \tag{3.41}$$

where a_i are free parameters and b_j are some chosen fixed values in the range of 0 to 3. We take into account the Q^2 evolution of the PDFs by allowing a Q^2 dependence in the parameters a_i of the form

$$a_i = a_{i1} + a_{i2}\log(\log(Q^2/Q_0^2))\,. \tag{3.42}$$

The parameters $a_{i1,i2}$ are free parameters to be fitted for each different PDF and Q_0^2 is a chosen fixed scale. The truncated Mellin moments of the fitted PDFs are then taken analytically. With TMCs, we obtain a sum of incomplete Beta functions of the type

$$B_{\xi_{\rm th}}(N + a_1 + b_j, a_2 + 1). \tag{3.43}$$

The index $\xi_{\rm th}$ corresponds to the upper integration limit in the definition of the incomplete Beta function. (Without TMCs, or rather in the large Q^2 limit, where $\xi_{\rm th} = 1$, we obtain a sum regular Beta functions, B_1.)

In our code, we implement the incomplete Beta functions by making use of the identity

$$B_{\xi_{\rm th}}(N + a_1 + b_j, a_2 + 1) = \frac{\xi_{\rm th}^{N+a_1+b_j}}{N + a_1 + b_j} \times\ {}_2F_1(N + a_1 + b_j, -a_2, 1 + N + a_1 + b_j, \xi_{\rm th})\,, \tag{3.44}$$

and for the complex hypergeometric function ${}_2F_1$ we use the routine provided in [214]. In order to rule out uncertainties introduced in our calculation when using the fitted functions for the Mellin inversion, we checked the accuracy of the fits by comparing results at NLO obtained from the convolution code in x-space and the Mellin inverse. Indeed, we find very good agreement even for very large values of x_B.

The reason behind the numerical stability of our result is the following. When performing the Mellin inverse, we obtain an exponential suppression for large negative real values of N due to the factor ξ^{-N} in Eq. (3.40). When TMCs are included, this suppression is softened by the

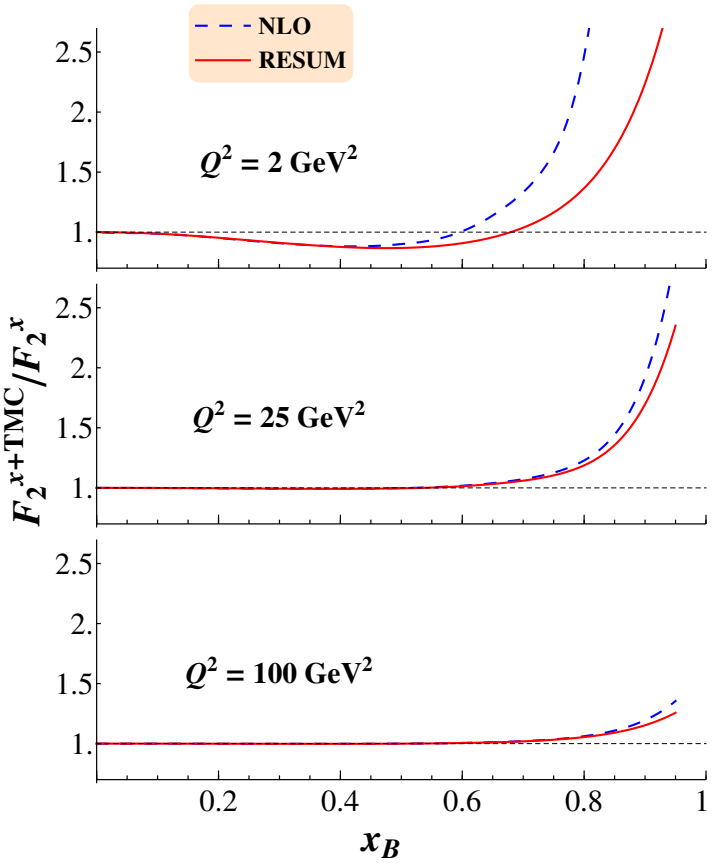

Figure 3.5: The effect of TMC is shown for the structure function F_2 on top of a NLO and a resummed calculation. We show TMC normalized to NLO (dashed blue) as well as TMC and resummation combined normalized to the resummed result (solid red). Again, we choose three representative values of $Q^2 = 2$, 25, 100 GeV^2. The PDF set of [178] is used.

factor ξ_{th}^N in Eq. (3.44). These two exponential factors originate from two different parts of the calculation: the first comes from the definition of the inverse Mellin transform, whereas the second is due to the incomplete beta function. We need to combine the two factors into one single exponential, $\exp[-N \ln(\xi/\xi_{\mathrm{th}})]$, where the cancellations between the two is made explicit and makes the numerical integration over dN well-behaved even for very large values of x_B.

In Fig. 3.4, we present our numerical results for the DIS structure function F_2 using the PDF set of [178]. All results are normalized to the massless NLO calculation. We choose to plot our results only up to $x_B = 0.95$ as non-perturbative effects are expected to set in for too large values of x_B, which is beyond the scope of this work. The two effects under consideration

are shown separately in dashed blue (TMCs) and in dotted magenta (threshold resummation) for three representative values of $Q^2 = 2$, 25, 100 GeV^2. Both TMC and resummation effects become increasingly large as x_B tends to 1, as it is clear from the kinematic analysis presented in Sec. 3.2. Both vanish at small x_B, the former because the Nachtmann variable ξ and the kinematic factor ρ tend to their massless value of x_B and 1, respectively, and the latter because the integrals are evaluated more and more far from the resummation threshold. Concerning the Q^2 dependence of the two corrections under discussion, both effects taken separately are large at small values of squared momentum transfer, and decrease with increasing Q^2. However, TMCs exhibit a power law suppression in Q^2, while resummation corrections decrease much less rapidly and become dominant, and non-negligible, at $Q^2 \gtrsim 25$ GeV. The results we find for TMCs are in agreement with numerical results in previous work such as [204] and [192] up to some prefactor conventions. Concerning the validity of our results on DIS threshold resummation one may compare to Ref. [J1, 189].

We can now turn to the combination of TMC and threshold resummation, shown by the solid black line in Fig. 3.4. We notice that the strength of the two effects does not add in a simple way. In order to understand the interplay of TMCs and threshold resummation, we analyze the plots in Fig. 3.5. Again, we use the PDF set of [178]. There, we compare the ratio of the target mass corrected F_2 structure function to the massless calculation without resummation (Dashed blue line), and the ratio of the structure function with both TMC and resummation, but normalized to the resummed result (solid red line). This way, we can see how the TMC contribution acts on top of a purely NLO calculation compared to being added to a resummed calculation. Firstly, we note that the effects remain decoupled for small values of x_B, where both ratios lie exactly on top of each other. This decoupled region extends to larger values of x_B as Q^2 increases. However, at large enough values of x_B the two functions deviate and TMC acts differently for NLO than for the resummed result.

As discussed in [182, 220], such a variation in the calculation of the F_2 structure function can lead to considerable difference in the value of the d-quark parton distribution extracted in a global fit. The theoretical description of the data crucially depends on whether resummation is included or not. In order to gauge the relevance of TMCs and resummation for the extraction of PDFs, but leaving a detailed QCD fit for future work, we present in Fig. 3.6 a comparison of our calculations to a variety of electron-proton scattering data from JLab (E94-110) [215], JLab (E00-116) [216], HERA [217], SLAC [218], and EMC [219]. Here we use the CJ12 PDF set of [179]. The data was bin-centered in Q^2 for the analysis of Nachtmann moments of the DIS

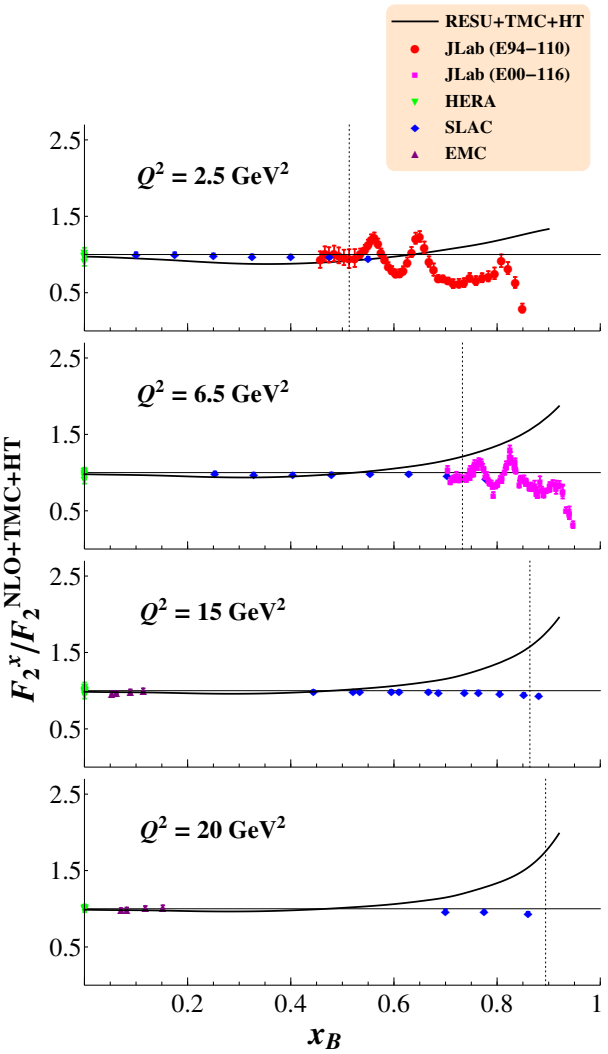

Figure 3.6: We plot ratios of data/theory for DIS structure function F_2 at several Q^2. Here "theory" denotes the NLO results with TMC and higher twist contributions based on the CJ PDF set of [179]. The data is taken from [215–219]. Due to our choice of a linear scale for the horizontal axis, the HERA data appears clustered at the vertical axis, i.e. at very small x_B. In addition, using the same normalization, we plot the theoretical prediction when resummation is included as well. The dotted line corresponds to $W^2 = 3.25\,\mathrm{GeV}^2$.

longitudinal structure function in [221] allowing a direct comparison of different experimental results [1]. The data was normalized to a calculation including TMCs only; but in order to do so we also need to add the "residual" power corrections in $1/Q^2$ not taken care of by target

[1] we thank P. Monaghan for kindly providing us with the bin-centered data points

mass corrections. These were included in the CJ12 QCD fit [179] via a multiplicative factor $1+C(x_B)/Q^2$, with C a parametrized function of Bjorken x_B with parameters fitted to a variety of DIS data. We include the same multiplicative factor in our NLO calculation, and use the parameters obtained in the CJ12 fit. The vertical dotted line in Fig. 3.6 corresponds to a value of $W^2 = (P_h + q)^2 = m_N^2 + Q^2(1 - x_B)/x_B = 3.25\,\mathrm{GeV}^2$, which is generally regarded as the end of the DIS regime and the beginning of the resonance region where fluctuations of the data around the DIS calculation are generally understood in terms of quark-hadron duality [222].
Finally, in order to gauge the relevance of resummation corrections to a global fit of parton distributions, we also plot in Fig. 3.6 the structure function F_2 with resummation, TMCs and higher twist contributions, normalized by the pure NLO calculation including TMCs and higher twists which was also used to normalize the data. Comparing the obtained deviation of this curve from one with the experimental uncertainties, we find a very significant effect which is getting larger for increasing Q^2, while at low Q^2, TMCs already capture the main effects. In fact, threshold resummation also decreases with increasing Q^2, as can be seen from both Figs. 3.4 and 3.5 above. However, as already remarked, TMCs die off rather quickly, whereas resummation remains clearly non-negligible in both the DIS and the resonance regions. Hence, resummation is likely to affect the extraction of large-x partons (quarks directly, and gluons indirectly through QCD evolution in DIS) in global PDF fits. In this respect, it is important to remark that the non power law dependence of the resummation corrections cannot be effectively included in a phenomenological higher-twist term, and needs to be instead explicitly calculated in order to obtain the correct behavior of the quark PDFs at large values of the parton momentum fraction x. In particular it would be interesting to see how the effect is on the $u-$ and d-quark PDFs, and how much the extrapolation of the d/u quark ratio to $x \to 1$ obtained in Ref. [179] would be affected.
Finally, see also the work of [223, 224] concerning TMC effects for (polarized) structure functions.

3.3 Hadron Mass Corrections and Resummation for SIA

3.3.1 Hadron Mass Corrections

Hadron level and parton level kinematics

We study the kinematics for Single Inclusive electron-positron Annihilation hadron in the $\gamma-h$ frame, where both the photon γ and the observed hadron h have no transverse momentum component. We start by parametrizing the momenta of the virtual photon q, the observed hadron in the final state P_h and the momentum of the fragmenting parton k. All momenta are also shown in Fig. 3.7. We find,

$$\begin{aligned} q^\mu &= q^+\bar{n}^\mu + \frac{Q^2}{2q^+}n^\mu\,, \\ P_h^\mu &= \xi_E q^+\bar{n}^\mu + \frac{m_h^2}{2\xi_E q^+}n^\mu\,, \\ k^\mu &= \frac{\xi_E}{z}q^+\bar{n}^\mu + \frac{(k^2+\boldsymbol{k}_T^2)z}{2\xi_E q^+}n^\mu + \boldsymbol{k}_T\,, \end{aligned} \tag{3.45}$$

where $Q^2 = q^\mu q_\mu$ denotes the virtuality of the photon, m_h is the mass of the observed hadron h, and $\xi_E = P_h^+/q^+$ its light cone momentum fraction; analogously, $z = P_h^+/k^+$ is the light-cone fractional momentum of the hadron relative to the parton that it is fragmenting from.
The external Lorenz invariants are

$$Q^2 = q^2 = s, \quad x_E = \frac{2q\cdot P_h}{q^2}, \quad P_h^2 = m_h^2\,, \tag{3.46}$$

where s is the center of mass energy of the process. Solving for the virtual boson fractional momentum, we obtain

$$\xi_E = \frac{P_h^+}{q^+} = \frac{1}{2}x_E\left(1+\sqrt{1-\frac{4}{x_E^2}\frac{m_h^2}{Q^2}}\right)\,, \tag{3.47}$$

which is a "Nachtmann-type" fragmentation variable, *cf.* Eq. (3.6). Note that the radicand is always positive due to energy conservation at the hadron level, as we derive below. Inverting Eq. (3.47) we obtain

$$x_E = \xi_E\left(1+\frac{m_h^2}{\xi_E^2 Q^2}\right)\,. \tag{3.48}$$

Concerning the unobserved parton's (internal) kinematics, we work in collinear factorization

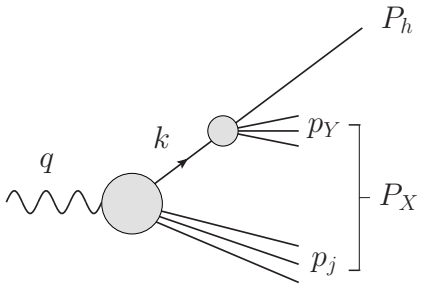

Figure 3.7: Diagram for SIA $e^+e^- \to hX$ where all momenta are specified.

but refrain from fixing the value of the parton virtuality k^2 until we analyze the effects of non-zero hadron masses on the partonic kinematic bounds. Therefore, for the time being, we only set

$$\boldsymbol{k}_T = 0\,. \tag{3.49}$$

Finally, we define the partonic fragmentation invariant $\hat{x}_E$ by

$$\hat{x}_E = \frac{2k\cdot q}{q^2} = \frac{\xi_E}{z} + \frac{zk^2}{\xi_E Q^2}\,, \tag{3.50}$$

where the parton virtuality k^2 appears explicitly for the time being.

Four momentum conservation and kinematic bounds

We consider now the kinematics at the hadron level, and derive the kinematic limits for x_E and ξ_E due to four momentum conservation. Firstly, we find a lower bound for x_E which ensures that ξ_E in Eq. (3.47) is well defined. Calculating in the e^+e^- c.m. frame with $q^+ = q^- = Q/\sqrt{2}$, we find

$$x_E = \frac{2P_h\cdot q}{Q} = \frac{\sqrt{2}}{Q}(P_h^+ + P_h^-) = \frac{2E_h}{Q} \geq \frac{2m_h}{Q} \equiv x_E^{\min}\,. \tag{3.51}$$

As a next step, we may derive an upper bound by considering the overall momentum conservation at the hadron level, $q = P_h + P_X$. We find

$$0 \leq P_X^2 = (P_h - q)^2 = m_h^2 - x_E Q^2 + Q^2\,. \tag{3.52}$$

Hence,

$$x_E \leq 1 + m_h^2/Q^2 \equiv x_E^{\max}\,, \tag{3.53}$$

which implies that x_E can become slightly larger than one. This is due to the neglect of hadron mass effects in the unobserved hadron jet shown at the bottom of Fig. 3.7. This is in analogy to what we did when analyzing the DIS kinematics. Using these two relations, we may determine the minimal and maximal values for ξ_E, which are

$$\xi_E^{\min} = \frac{x_E^{\min}}{2} = \frac{m_h}{Q}, \qquad \xi_E^{\max} = 1\,. \tag{3.54}$$

With these limits at hand, we may plot ξ_E as a function of x_E, see Fig. 3.8. Here, the effects of hadron mass corrections are large when the invariant x_E is small, contrary to the case of DIS, where target mass corrections are most relevant at large values of x_B. This can be understood as a consequence of crossing symmetry on the kinematics of the process, where now the virtual photon is time-like.

In a second step, again analogously to the procedure for DIS, we analyze the kinematics at the parton level. Firstly, we consider the hard-scattering vertex which corresponds to the lower grey circle in Fig. 3.7. Using momentum conservation at the vertex $q = k + p_j$ and neglecting any non-zero lower bound for the mass of the recoiling jet, we obtain the following constraint

$$0 \leq p_j^2 = (q-k)^2 = Q^2\left(1 - \frac{z}{\xi_E}\frac{k^2}{Q^2}\right)\frac{z-\xi_E}{z}\,. \tag{3.55}$$

Secondly, we consider the hadronization vertex which corresponds to the upper right grey circle in Fig. 3.7, and we apply again four-momentum conservation. We obtain

$$0 \leq p_Y^2 = (k - P_h)^2 = \left(zk^2 - m_h^2\right)\frac{1-z}{z}\,. \tag{3.56}$$

Interestingly, in SIA there appears no "threshold problem", as is the case in DIS, and ξ_E can range all the way up to 1. This is due to the system having no net baryon number, contrary to the case of DIS where the net baryon number is 1, and its conservation needs to be explicitly taken into account in the parton-level kinematics. It is also important to notice that while the parton virtuality k^2 in the first of these inequalities is parametrically suppressed at large Q^2, no hard scale suppresses this nor the hadron mass m_h in the second inequality. Therefore, it is

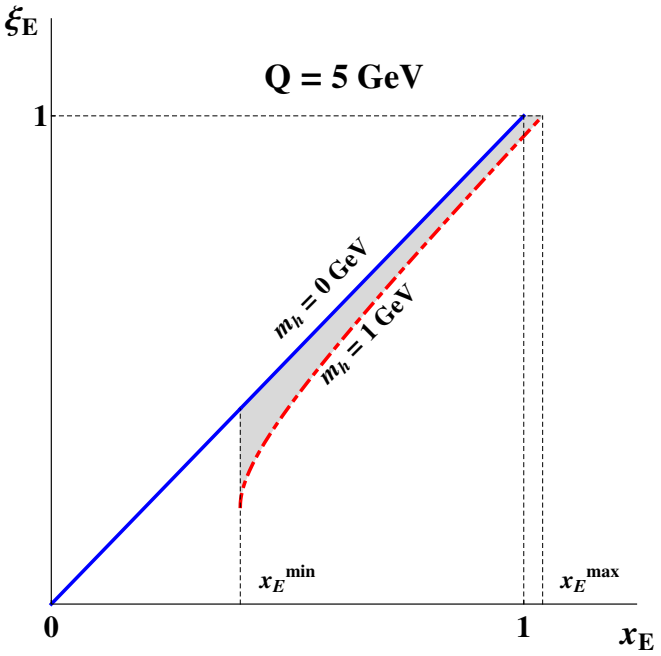

Figure 3.8: The fragmentation "Nachtmann-type" fragmentation variable ξ_E as a function of x_E at fixed $Q = 5$ GeV. For illustration purposes, we choose a fictional mass of $m_h = 1$ GeV (dash-dotted red) and compare it with a massless hadron, $m_h = 0$ GeV (solid blue line).

not possible to define a "massless hadron limit" as was done for the DIS case, where the nucleon mass, m_N, always appears divided by Q. The physical solutions of Eqs. (3.55)-(3.56) are:

$$\xi_E \leq z \leq 1 \tag{3.57}$$

$$m_h^2 \leq zk^2 \leq \xi_E Q^2 \ . \tag{3.58}$$

In particular, the quark virtuality must always be larger than m_h^2 because this value corresponds to the minimum invariant mass of the parton fragmentation products when a hadron of flavor h is detected. Following our philosophy, we should then perform the collinear expansion around an on-shell massive quark rather than around $k^2 = 0$. However, dealing with the subtleties involved in proving the factorization theorem at NLO for this case goes beyond the scope of this work and will not be treated here. Instead, we use the well known collinear factorization theorem for massless, $k^2 = 0$, fragmenting partons as in [195, 197] and we continue to explore the interplay of hadron mass corrections and threshold resummation.

Cross section at NLO

In order to compare our results to the SIA measurements from BELLE and BaBar, we need to compute hadron multiplicities in $e^+e^- \to hX$ which are defined as

$$R^h_{e^+e^-} \equiv \frac{1}{\sigma^{\rm tot}} \frac{d^2\sigma^h}{dx_E d\cos\theta} \,. \tag{3.59}$$

Here the hadron h is produced at an angle θ relative to the initial positron. $\sigma^{\rm tot}$ denotes the totally inclusive cross section for $e^+e^- \to X$. At NLO, this is given by

$$\sigma^{\rm tot} = \frac{4\pi\alpha^2}{3Q^2} N_c \sum_q e_q^2 \left(1 + \frac{\alpha_s}{\pi}\right) \,, \tag{3.60}$$

where $N_c = 3$ is the number of colors and α is the electromagnetic fine structure constant. As mentioned before, we may write the differential cross section $d^2\sigma^h/dx_E d\cos\theta$ in terms of two structure functions which we denote as $\hat{\mathcal{F}}^h_i$ (i=1,L), cf. [C1, 48, 109]. Including HMC, we find

$$\begin{aligned} \frac{d^2\sigma^h}{dx_E d\cos\theta} &= \frac{\pi\alpha^2}{Q^2} N_c \frac{1}{1-\frac{m_h^2}{\xi_E^2 Q^2}} \left[\frac{1+\cos^2\theta}{2} \hat{\mathcal{F}}^h_1(x_E,Q^2) + \sin^2\theta\, \hat{\mathcal{F}}^h_L(x_E,Q^2)\right] \\ &= \frac{1}{1-\frac{m_h^2}{\xi_E^2 Q^2}} \frac{d^2\sigma^h}{d\xi_E d\cos\theta}\bigg|_{x_E=\xi_E} \,, \end{aligned} \tag{3.61}$$

where the Jacobian factor of $1/(1-m_h^2/\xi_E^2 Q^2)$ is included in order to obtain a cross section differential in x_E instead of ξ_E [195, 197]. The structure functions $\hat{\mathcal{F}}^h_i$ with HMCs take into account the kinematic bounds on z from Eq. (3.57) and read

$$\hat{\mathcal{F}}^h_i(x_E,Q^2) = \sum_f \int_{\xi_E}^1 \frac{dz}{z} D^h_f\left(z,\mu^2\right) \hat{\mathcal{C}}^i_f\left(\frac{\xi_E}{z}, \frac{Q^2}{\mu^2}, \alpha_s(\mu^2)\right) \,, \tag{3.62}$$

where $D^h_f(z,\mu^2)$ denotes the fragmentation function for an observed hadron h in the final state resulting from a parent parton f. The $\hat{\mathcal{C}}^i_f$ are the corresponding coefficient functions which we list in Appendix C.2 for completeness up to NLO. The cross section without HMCs is obtained by replacing ξ_E with x_E in Eq. (3.62) and by setting $m_h = 0$ in Eq. (3.61). Having chosen to factorize the cross section around a parton virtuality $k^2 = 0$ this massless hadron limit can also

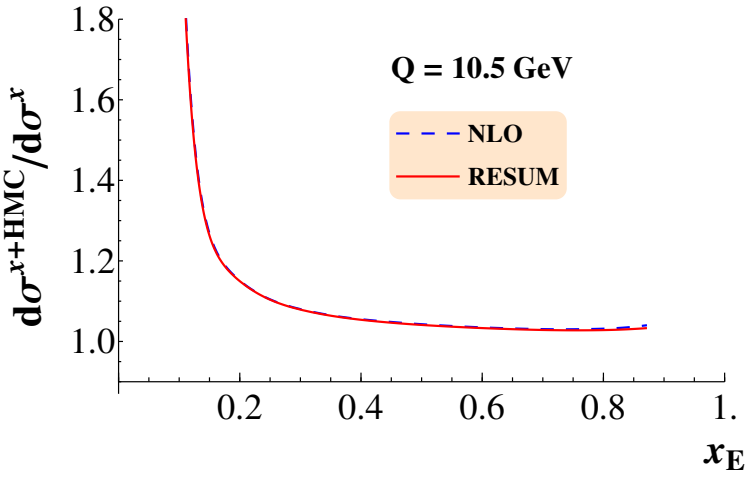

Figure 3.9: Comparison of the effect of HMC on top of NLO (dashed blue) and the resummed result (solid red) for $Q = \sqrt{s} = 10.5$ GeV and the kaon mass $m_{K^0} = 497.6$ MeV.

be achieved in the $Q^2 \to \infty$ limit.

3.3.2 Combining HMC and Threshold Resummation

In the spirit of "crossed resummation" [199], we note that the only difference concerning the resummation in SIA in comparison to DIS is that we have to adjust one term in the matching coefficient H_q in Eq. (3.30) $-\pi^2/6 \to 5\pi^2/6$, see also [J1, 131]. This similarity may be understood in the sense that both processes have one "observed" and one "unobserved" parton. Hence, the threshold resummed expression may again be written as a product of the form $H'_q \, \Delta_q^N \, J_q^N$. HMC and resummation are combined by simply replacing $x_E \to \xi_E$ in the resummed formula. There are no issues with ξ_{th} as it was the case for DIS, since the upper integration limit for z in Eqs. (3.57), (3.62) is left unchanged compared to the massless hadron calculation. Since resummation effects increase with x_E and HMC effects become large at small values of x_E, we do not expect a significant interplay of the two, contrary to the DIS case in which both effects increase at large x_B. We can numerically assess the interplay of HMC and threshold resummation similarly to what we did for DIS. In Fig. 3.9, we plot the cross section including the effect of HMCs on top of an NLO (dashed-dotted blue line) and a resummed (solid red line) calculation. These are normalized to the corresponding massless hadron calculation to highlight HMC effects. We find that both ratios match completely. Hence, there is no crosstalk between the two effects.

3.3.3 Phenomenological Results

Given the actuality of the recent BELLE [83] and BaBar [84] results, we choose to present our numerical results for HMC and threshold resummation directly in comparison to data. The BELLE experiment is operating at a c.m.s. energy of $\sqrt{s} = 10.52$ GeV and similarly BaBar at $\sqrt{s} = 10.54$ GeV, just below the lower end of the energy range of experiments typically included in FF fits, see for example Refs. [77, 195]. This way, we maximize the effect of HMC and resummation of threshold logarithms and we may directly evaluate the significance of the two corrections compared to statistical and systematic uncertainties of the data.

For the plots we discuss in this section, as well as for that in Fig. 3.9, we used the "de Florian-Sassot-Stratmann" [77] set of fragmentation functions at NLO, where the new data from BELLE and BaBar is not yet included. The goal is to show the phenomenological importance of threshold resummation and HMCs, and to qualitatively assess their relevance in global FF fits, rather than obtain a perfect description of the data. Comparing the size of HMC and threshold resummation to statistical and systematical errors, we will conclude that a fit including the two effects may yield rather different results for the extracted FFs. Whether indeed a better χ^2 can be obtained given all the other data sets used in a global fit, as the study presented in [195] indicates, will be left for future work.

Both BELLE and BaBar have an angular coverage of $-1 < \cos\theta < 1$. Hence, we integrate over the full range of $\cos\theta$ and obtain a cross section differential only in x_E. An important difference between the two data sets is that BELLE data is presented as a function of the Lorentz invariant energy fraction x_E, whereas BaBar is using the momentum fraction variable

$$x_p = \frac{2|\boldsymbol{p}_h|}{\sqrt{s}}\,. \tag{3.63}$$

Only for massless calculations are these equivalent, however, and in particular for kaons at present energies the difference between x_E and x_p is quite significant. When comparing our results to data, we multiply the BaBar data set by $J = dx_p/dx_E$ to obtain a cross section differential in x_E and compare this to measurements at BELLE.

We start by analyzing our calculations for (charge integrated) pion production, plotted in Fig. 3.10. All multiplicities $1/\sigma_{\rm tot}\, d\sigma/dx_E$ presented here are normalized to the calculation at NLO without hadron mass corrections. Our results for HMC (dashed blue line), threshold resummation (dotted magenta line) and the combination of both (solid black line) is shown. On the left (right) panels of Fig. 3.10, we show BELLE and BaBar data with statistical (systematic)

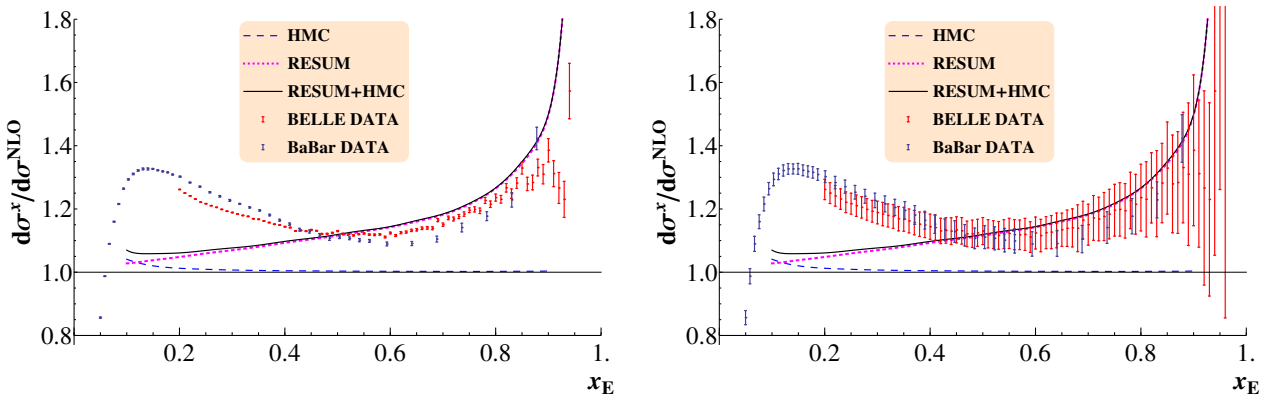

Figure 3.10: Both theory and data $1/\sigma_{\rm tot}\, d\sigma/dx_E$ are normalized to NLO for charge integrated pions at $\sqrt{s} = 10.5$ GeV. The dashed blue lines shows the HMC corrected multiplicities, magenta dotted the resummed calculation and solid black the combination of both. BELLE data (red) and BaBar data (blue) is shown along with statistical (left) and systematical uncertainties (right). The FFs of [77] are used.

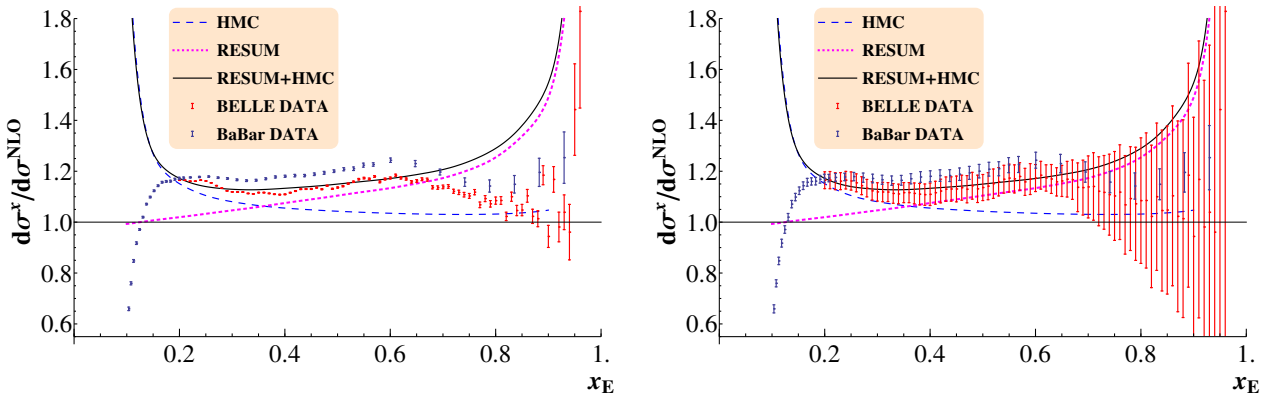

Figure 3.11: Same as Fig. 3.10 but for observed kaons.

uncertainties. As expected, the effects of threshold resummation are quite significant and most relevant at large x_E, whereas HMCs affect the calculation at small x_E, and in the measured range are not large, due to the smallness of the pion mass, $m_{\pi^0} = 135$ MeV. Nonetheless, given the statistical precision of this data, it seems important to account for HMCs in a global fit. Much of discrepancy between NLO calculations and pion data can be resolved by including the new data in a global FF fit, as it was very recently shown in Ref. [79]. Finally, we note that below $x_E = 0.1$, small-z logarithms start to become relevant and need to be resummed; see Chapter 2 and [197].

For kaons, with mass $m_{K^0} = 497.6$ MeV, HMCs are much larger than for pions, as shown in

Fig. 3.11. The combination of HMC and resummation leads to a significant increase of the cross section compared to a massless hadron NLO calculation for all values of x_E, and their inclusion in global FF fits is even more important than in the pion case. The steep rise of the HMC corrected result over the NLO calculation at small x_E is mostly due to the kinematic limit $x_E > 2m_{K^0}/Q \approx 0.1$ derived in Eq. (3.51), and in its vicinity the validity of our treatment of HMCs may come into question. This is also the region where resummation of small-x logarithms becomes important, and a proper treatment of these is likely to require a careful consideration of the interplay with HMCs. It would then be very interesting to explore the similarities and differences of this with the interplay of threshold logarithms and target mass corrections in large-x_B DIS events we have discussed in Section 3.2, but we defer this analysis to a future effort.

3.4 Conclusions

In this chapter we have presented the results of [J3]. We have investigated two phenomenologically important effects for the analysis of data in inclusive DIS and single-inclusive electron-positron annihilation, namely the corrections to NLO calculations due to a non-zero mass of the nucleon target in DIS, and of the detected hadron in SIA, as well as the resummation of threshold logarithms arising in the perturbative expansion of the hard scattering coefficients. In both cases, these lead to a non-negligible enhancement in the calculated observable compared to the precision of the currently available experimental data. Therefore, both effects are significant for precise QCD fits of PDFs as well as FFs.

In DIS, target mass corrections and threshold resummation are both most relevant at large values of x_B. In particular, we have derived a way to perform resummation respecting the parton level kinematic constraints arising from consideration of the non-zero target mass. The resulting structure functions can then be consistently combined with TMC calculations such that they remain zero in the unphysical region $x_B \geq 1$. We find that two effects are coupled especially for small values of Q^2. At large x_B, the size of the combined TMC and resummation corrections is considerably larger than the accuracy of the existing DIS data over an extended Q^2 range. Therefore, it should be taken into account for a precise extraction of large-x PDFs in global fits.

In SIA processes, hadron mass corrections are relevant at small x_E while threshold resummation is important at large x_E, and we find no interplay of the two effects. We have included both in

our calculations of cross sections for pion and kaon production, and compared these to recent data from the BELLE and BaBar collaborations. The effects are again large, and non-negligible for the extraction of FFs, given the precision of the new data sets. This is particularly true for kaons due to their bigger mass compared to observed pions. Given this large effect for kaon SIA, it becomes a topic of practical as well as theoretical interest to determine what the interplay is between the finite mass kinematics and the resummation of small-x logarithms. We leave this for future efforts.

Finally, we remark that we have performed calculations in collinear factorization around massless, on-shell partons. For SIA, we have found that this choice, however commonly made, actually violates parton-level four momentum conservation. A detailed analysis of collinear factorization with non-zero virtuality partons is a subject of future work.

CHAPTER 4

Towards semi-inclusive deep inelastic scattering at next-to-next-to-leading order

In this chapter, we present our computation of the first set of $\mathcal{O}(\alpha_s^2)$ corrections to semi-inclusive deep inelastic scattering structure functions. We start by studying the impact of the contribution of the partonic subprocesses that present itselves for the first time at this order for the longitudinal structure function. We perform the full calculation analytically, and obtain the expression of the factorized cross section at this order. Special care is given to the study of their flavour decomposition structure. We analyze the phenomenological effect of the corrections finding that, even though expected to be small a priori, it turns out to be sizable with respect to the previous order known, calling for a full NNLO calculation. This chapter is based upon our published paper [J6].

4.1 Introduction

Over the last decades, our understanding of hadron structure has remarkably improved, thanks to impressive experimental and theoretical progress. That includes the extraction of precise parton distribution functions (PDFs) from global analysis [41, 173, 181, 225–227], complemented with accurate perturbative calculations for several processes in quantum chromody-

namics (QCD). As outlined in Chapter 2, recent progress has been observed towards a better description of the hadronization process, related experimentally to observables with identified light hadrons in the final-state. Their description relies on the previous two ingredients plus the knowledge of the corresponding fragmentation functions (FFs), which are evolving following the path of PDFs. It is in fact only recently that our next-to-next-to-leading order (NNLO) analysis of FFs based on electron-positron annihilation data was presented in [J4]. This work together with [J5] is treated in detail in Chapter 2. A global analysis including also proton-proton collision's data and semi-inclusive deep inelastic scattering (SIDIS) data at this precision level is still yet to come. Therefore, the computation of NNLO corrections to the SIDIS process is an absolute requirement in order to extend existing NLO global analyses [74–76, 79, 195]. Analyses solely based on electron-positron annihilation into hadrons give no information on how the individual quark flavour fragments into hadrons, and leave a considerable uncertainty on the gluon density. The measurement of final state hadrons in SIDIS provides an excellent complementary tool for the extraction of fragmentation functions. Furthermore, SIDIS plays a very important role in understanding the spin structure of the nucleon, that can be described by the (non-perturbative) polarized parton distribution functions (pPDFs). The most complete global fit of pPDFs includes all available data taken in spin-dependent DIS, semi-inclusive DIS with identified pions and kaons, and proton-proton collisions. These fits allow the extraction of pPDFs consistently at NLO [228]. In particular in this context, SIDIS with identified hadrons in the final state is of essential need in order to achieve a full flavour decomposition for the polarized parton distributions.

For all these reasons, counting on precision theoretical description for SIDIS is mandatory. In the fully-inclusive case the structure functions are well known at next-to-next-to-leading order (NNLO) in perturbative QCD, both for the unpolarized [229–231] and for the polarized ones [232]. For the unpolarized case, even the hard corrections at order $\mathcal{O}(\alpha_s^3)$ are available [233]. However, for semi-inclusive DIS, the QCD corrections are only known up to NLO both in the unpolarized [108, 111] and the polarized cases [111].

Nowadays, NNLO is the state of the art for many observables of interest. It is then natural to try to reach the same accuracy for the unpolarized SIDIS process. In an effort to analytically calculate corrections at this level of precision, one may start by analyzing the simpler case of the longitudinal component of the process, in order then to use the acquired experience to extend the calculation to the more difficult transverse one. Both components are essential to evaluate the ratio between the longitudinal and transverse photoabsortion cross sections $R \equiv \sigma_L/\sigma_T$,

which plays an important role in the extraction of pPDFs from the observed asymmetries (see for instance [234]). In such analyses, the semi-inclusive ratio R is customarily assumed to be equal to the inclusive one, which may not be always a good approximation.

In the following sections we present the first steps towards the computation of the longitudinal SIDIS structure function at NNLO accuracy. In particular, we focus on the contribution of those channels that open for the first time at this order. In section 4.2 we introduce the SIDIS structure functions and the cross section ratio. Their flavour decomposition structure is discussed in section 4.3. In section 4.4 we explain the main features of the computation of the new contributions to the longitudinal structure function at NNLO. In section 4.5 we present some phenomenological results and finally the conclusions are presented in section 4.6.

4.2 Semi-inclusive deep inelastic scattering

The cross section for the scattering of leptons on nucleons with the observation of a hadron H in the final state can be written, in lowest-order perturbation theory of electroweak interactions, as

$$\frac{d\sigma^H}{dx\,dy\,dz} = \frac{2\pi\, y\,\alpha^2}{Q^4} \sum_j L^{\mu\nu} W^H_{\mu\nu}, \tag{4.1}$$

where the leptonic tensor $L^{\mu\nu}$ is associated with the coupling of the exchanged photon to the leptons (we do not include processes mediated by Z and W bosons) while the hadronic tensor $W^H_{\mu\nu}$ describes the interaction of the photon with the target nucleon and the hadronization of partons into H. Here, x and y denote the usual DIS variables:

$$-q^2 = Q^2 = Sxy, \qquad x = Q^2/(2P\cdot q),$$

where q is the photon four-momentum, P the nucleon momentum and S the center-of-mass energy squared of the lepton-nucleon system. Besides, $z = P_H \cdot P/P \cdot q$ here is the scaling variable representing the momentum fraction taken by the hadron H. Since we concentrate in the current fragmentation region, cuts over z should apply (typically, $z > 0.1$)[1].

The unpolarized SIDIS structure functions (F_i^H) are defined in terms of the hadronic tensor. Besides terms that cancel after integrating over the azhimutal angle of the outgoing hadron,

[1]Due to the definition of z, the target fragmentation process [235, 236] is strictly $z = 0$.

one gets the usual DIS tensor: [237]

$$W^H_{\mu\nu} = \left(-g_{\mu\nu} + \frac{q_\mu q_\nu}{q^2}\right) F_1^H(x,z,Q^2) + \frac{\hat{P}_\mu \hat{P}_\nu}{P\cdot q} F_2^H(x,z,Q^2), \tag{4.2}$$

where $\hat{P}_\mu = P_\mu - \frac{P\cdot q}{q^2} q_\mu$. We have not taken into account those terms proportional to the polarized structure functions.

The spin-averaged SIDIS cross section for $Q^2 \gg M^2$ (M being the mass of the target nucleon), is then given by

$$\frac{d\sigma^H}{dx\,dy\,dz} = \frac{2\pi\alpha^2}{x\,y\,Q^2}\left[\left[1+(1-y)^2\right] 2x\,F_1^H + (1-y)\,2\,F_L^H\right]. \tag{4.3}$$

The longitudinal structure function is defined as $F_L^H = F_2^H - 2\,x\,F_1^H$ and vanishes at lowest order [238].

Defining the ratio

$$R^H = \frac{\sigma_L^H}{\sigma_T^H} = \frac{F_L^H}{2\,x\,F_1^H}, \tag{4.4}$$

where σ_L^H and σ_T^H are the semi-inclusive cross section for longitudinal and transversely polarized virtual photons respectively, Eq. (4.3) can be rewritten as

$$\frac{d\sigma^H}{dx\,dy\,dz} = \frac{2\pi\alpha^2}{x\,y\,Q^2} F_2^H \left[\left[2(1-y) + \frac{y^2}{1+R^H}\right]\right]. \tag{4.5}$$

4.3 The structure functions at next-to-next-to leading order

Assuming factorization, the SIDIS structure functions can be obtained as the convolution of parton distribution functions (PDFs) and fragmentation functions (FFs), describing the low-energy non perturbative behaviour, with short-distance coefficients that can be evaluated in

perturbation theory. In general we can write

$$F_k(x,z,Q^2,\mu_F^2,\mu_I^2,\mu_r^2) = \Bigg[\sum_{q_a,q_b} q_a \otimes C_k^{q_a,q_b} \otimes D_{q_b}^h + \sum_{q_a} q_a \otimes C_k^{q_a,g} \otimes D_g^h + \sum_{q_b} g \otimes C_k^{g,q_b} \otimes D_{q_b}^h + g \otimes C_k^{g,g} \otimes D_g^h \Bigg] (x,z,Q^2,\mu_F^2,\mu_I^2,\mu_r^2) \ , \quad (4.6)$$

where $k \in \{1, L\}$, the sums are understood to run over all possible quark and anti-quark flavours and $\otimes$ denotes the usual convolution,

$$(q \otimes C \otimes D^h)(x,z,Q^2,\mu_I^2,\mu_F^2,\mu_r^2) = \int_x^1 \frac{dy}{y} \int_z^1 \frac{d\omega}{\omega}\, q(y,\mu_I^2) C\left(\frac{x}{y}, \frac{z}{\omega}, \mu_r^2, \frac{Q^2}{\mu_I^2}, \frac{Q^2}{\mu_F^2}, \frac{Q^2}{\mu_r^2}\right) \times D^h(\omega,\mu_F^2) \ . \quad (4.7)$$

The coefficient functions C_k^{ij} (with i and j denoting the initial and hadronizing partons respectively) can be perturbatively calculated as a series in the strong coupling constant α_s,

$$C_k^{ij}\left(x,z,\mu_r^2,\frac{Q^2}{\mu_I^2},\frac{Q^2}{\mu_F^2},\frac{Q^2}{\mu_r^2}\right) = \sum_n \left(\frac{\alpha_s(\mu_r^2)}{4\pi}\right)^n C_k^{ij\,(n)}\left(x,z,\frac{Q^2}{\mu_I^2},\frac{Q^2}{\mu_F^2},\frac{Q^2}{\mu_r^2}\right) \ . \quad (4.8)$$

The renormalization scale μ_r represents the "hard-scale" at which the perturbative expansion is performed whereas the factorization scales μ_I and μ_F separate conceptually the perturbative regime from the non-perturbative one in the initial and final state part of the process respectively. The PDFs q and g, describing the momentum fraction distribution of the parton inside the struck hadron, and the FFs D_q^h and D_g^h, describing the fragmentation of the parton into an hadron h, are process independent distributions that can be extracted from data through global QCD analysis of reference processes. Although they cannot be obtained from first principles in perturbative QCD, it is possible to predict their dependence on the factorization scale $\mu_{I,F}$ once they are given at some reference scale μ_0 by solving the Dokshitzer-Gribov-Lipatov-Altarelli-Parisi (DGLAP) evolution equations [49, 50, 119, 120]. Their respective space-like

and time-like versions read

$$\frac{\partial}{\partial \log \mu_I^2} f_i(x,\mu_I^2) = \sum_j \left(P_{ij}\left(\mu_r^2, \frac{\mu_I^2}{\mu_r^2}\right) \otimes f_j(\mu_I^2) \right)(x) \tag{4.9}$$

$$\frac{\partial}{\partial \log \mu_F^2} D_{f_i}^h(z,\mu_F^2) = \sum_j \left(P_{ji}^T\left(\mu_r^2, \frac{\mu_F^2}{\mu_r^2}\right) \otimes D_{f_j}^h(\mu_F^2) \right)(z)\,. \tag{4.10}$$

Here the sum runs over all possible $f_j = q_j,\ \bar{q}_j,\ g$. The space-like and time-like splitting functions, P_{ij} and P_{ji}^T respectively, are perturbative calculable functions. In the space-like case, for example, the expansion in $\alpha_s(\mu_r)$ can be written as

$$\begin{aligned}
P_{ij}\left(x,\mu_r^2,\frac{\mu_r^2}{\mu_I^2}\right) =& \sum_n a_s^{n+1}\left(\mu_r^2,\frac{\mu_r^2}{\mu_I^2}\right) P_{ij}^{(n)}(x) \\
=& a_s(\mu_r^2)P_{ij}^{(0)}(x) + a_s^2(\mu_r^2)\left(P_{ij}^{(1)}(x) + \beta_0 P_{ij}^{(0)}(x)\log\left(\frac{\mu_r^2}{\mu_I^2}\right)\right) \\
&+ a_s^3(\mu_r^2)\left(P_{ij}^{(2)}(x) + 2\beta_0 P_{ij}^{(1)}(x)\log\left(\frac{\mu_r^2}{\mu_I^2}\right)\right. \\
&\left.+ \left\{\beta_1 \log\left(\frac{\mu_r^2}{\mu_I^2}\right) + \beta_0^2 \log^2\left(\frac{\mu_r^2}{\mu_I^2}\right)\right\} P_{ij}^{(0)}(x)\right) + \dots \\
=& \sum_n a_s^{n+1}(\mu_r^2)\left(P_{ij}^{(n)}(x) + \sum_{m=1}^{n} \log^m\left(\frac{\mu_r^2}{\mu_I^2}\right) \sum_{k=0}^{n-m} A_{k,m}^{n+1} P_{ij}^k(x)\right)\,,
\end{aligned} \tag{4.11}$$

where $a_s = \alpha_s/4\pi$ and β_i are the usual expansion coefficients of the QCD beta function $\beta(a_s) = -a_s^2 \sum_{i=0}^{\infty} \beta_i\, a_s^i$. The second equality was obtained by re-expanding $a_s(\mu_r^2, \mu_r^2/\mu_I^2)$ in terms of $a_s(\mu_r^2)$ (see Eq. (D.1)). The coefficients $A_{k,m}^{n+1}$ collect the beta terms coming from this expansion and they will be of use for further discussion in Appendix D. For the sake of notation and simplicity, we can proceed by setting all scales equal, $\mu_I^2 = \mu_F^2 = \mu_r^2 = Q^2$ without loss of information. A sketch on how it is possible to recover all scale dependences is given in Appendix D for a specific case.

Eqs. (4.9) for the PDFs and (4.10) for the FFs are each $2N_f + 1$ integro-differential coupled equations, with N_f being the number of active massless flavours. It is customary to rewrite the quark sector into flavour singlet combinations

$$q_S \equiv \frac{1}{N_f}\sum_i^{N_f}(q_i + \bar{q}_i), \qquad D_S^h \equiv \frac{1}{N_f}\sum_i^{N_f}(D_{q_i}^h + D_{\bar{q}_i}^h), \tag{4.12}$$

which evolve together with g and D_g^h respectively according to

$$\frac{\partial}{\partial \log Q^2}\begin{pmatrix} q_S \\ g \end{pmatrix} = \begin{pmatrix} P_{qq} & P_{qg} \\ P_{gq} & P_{gg} \end{pmatrix} \otimes \begin{pmatrix} q_S \\ g \end{pmatrix}, \qquad \frac{\partial}{\partial \log Q^2}\begin{pmatrix} D_S^h \\ D_g^h \end{pmatrix} = \begin{pmatrix} P_{qq}^T & P_{gq}^T \\ P_{qg}^T & P_{gg}^T \end{pmatrix} \otimes \begin{pmatrix} D_S^h \\ D_g^h \end{pmatrix}, \tag{4.13}$$

and three non-singlet combinations for PDFs and for FFs

$$q_{ns,\,ik}^{\pm} = q_i \pm \bar{q}_i - (q_k \pm \bar{q}_k) \qquad D_{ns,\,ik}^{h,\,\pm} = D_{q_i}^h \pm D_{q_i}^h - (D_{q_k}^h \pm D_{\bar{q}_k}^h) \tag{4.14}$$

$$q_i^v = q_i - \bar{q}_i \qquad D_{q_i}^{h,\,v} = D_{q_i}^h - D_{\bar{q}_i}^h \tag{4.15}$$

which evolve independently with P_{ns}^+, P_{ns}^-, P_{ns}^v, $P_{ns}^{T,\,+}$, $P_{ns}^{T,\,-}$, $P_{ns}^{T,\,v}$ and decouple the remaining $2N_f - 1$ equations. All splitting functions are known up to NNLO [71, 122–124, 155]. For a detailed discussion on the NNLO evolution see Chapter 2.

As it is done in the literature for the totally inclusive case [48, 230], the structure functions in Eq. (4.6) can be explicitly written as functions of non-singlet and singlet PDFs and FFs combinations. This is especially relevant at NNLO since different diagrammatic contributions to the flavour combinations are made manifest. In the DIS inclusive case, for example, it is common to write the structure functions separating the "non-singlet" (NS) from the "singlet" (S) contributions $C_k^{\rm NS}$ and $C_k^{\rm S}$ which at $\mathcal{O}(a_s^2)$ start to differ from each other [230]:

$$F_k^{\rm DIS}(x,Q^2) = \sum_j \left(C_k^{{\rm DIS},\,q_j} \otimes q_j + C_k^{{\rm DIS},\,\bar{q}_j} \otimes \bar{q}_j\right) + C_k^{{\rm DIS},\,g} \otimes g \tag{4.16}$$

$$= \sum_j e_{q_j}^2 C_k^{\rm NS} \otimes q_j^{\rm NS}(x,Q^2) + \left(\sum_j e_{q_j}^2\right)\left[C_k^{\rm S} \otimes q_S + C_k^{{\rm DIS},\,g} \otimes g\right](x,Q^2)\,, \tag{4.17}$$

where $k \in \{1, L\}$, e_{q_j} are the electromagnetic charges of quarks and all sums run over the active flavours. The flavour combination $q_j^{\rm NS}$ is defined as

$$q_j^{\rm NS} \equiv \frac{1}{N_f}\sum_{k=1}^{N_f} q_{ns,\,jk}^+ = (q_j + \bar{q}_j) - \frac{1}{N_f}\sum_{k=1}^{N_f}(q_k + \bar{q}_k) \tag{4.18}$$

and therefore evolves with P_{ns}^+ whereas q_S was defined in (4.12) and evolves according to (4.9). The equality between (4.16) and (4.17) is a direct consequence of the charge conjugation symmetry $C_k^{{\rm DIS},\,q_i} = C_k^{{\rm DIS},\,\bar{q}_i}$ when the considered incoming vector is a photon. In fact we can

distinguish between NS diagrammatic contributions and "pure-singlet" (PS) ones and write

$$C_k^{\mathrm{DIS},\,q_i} = C_k^{\mathrm{DIS},\,\bar{q}_i} = e_{q_i}^2 C_k^{\mathrm{NS}} + \frac{1}{N_f}\left(\sum_j e_{q_j}^2\right) C_k^{\mathrm{PS}} \,. \tag{4.19}$$

In this case one defines NS contributions to be the ones where either on the left side or on the right side of the cut diagrams the struck parton is directly connected to the incoming quark through a quark line (e.g. at NNLO C^2 or BC in Fig. 4.1). On the other hand, PS contributions generate from cut diagrams where on both sides of the cut the struck parton is separated by gluon lines from the incoming quark (e.g. at NNLO A^2 in Fig. 4.1). Inserting Eq. (4.18) in (4.16) one obtains (4.17) with $C_k^{\mathrm{S}} = C_k^{\mathrm{NS}} + C_k^{\mathrm{PS}}$. Charge conjugation breaking terms proportional to $e_i \sum_j e_j$ vanish at each order either due to their colour structure or due to Furry's theorem, which means that (4.19), and therefore (4.17), are all-order valid equalities.

In the semi-inclusive case, the identification of a final state hadron complicates the above described diagrammatic contribution's separation since $C_k^{q_i,\,q_i} \neq C_k^{q_i,\,\bar{q}_i} \neq C_k^{q_i,\,q_j}$. In particular non vanishing terms proportional to $e_i e_j$ start to appear at NNLO due to contributions where the convolution with different FFs for quark and anti-quark spoils Furry's theorem: for example the $q_1 \otimes C_k^{q_1,\,q_2,\,(AC)} \otimes D_{q_2}^h$ and $q_1 \otimes C_k^{q_1,\,\bar{q}_2,\,(AC)} \otimes D_{\bar{q}_2}^h$ terms generating from the interference term AC in Fig 4.1 do not vanish in the sum since in general $D_{q_2}^h \neq D_{\bar{q}_2}^h$ although $C_k^{q_1,\,q_2,\,(AC)} = -C_k^{q_1,\,\bar{q}_2,\,(AC)}$. By introducing the corresponding time-like "non-singlet" combinations

$$D_{q_j}^{h,\,\mathrm{NS}} \equiv \frac{1}{N_f}\sum_{k=1}^{N_f} D_{ns,\,ik}^{h,\,+} = (D_{q_j}^h + D_{\bar{q}_j}^h) - \frac{1}{N_f}\sum_{k=1}^{N_f}(D_{q_k}^h + D_{\bar{q}_k}^h) \,, \tag{4.20}$$

we can express the semi-inclusive structure functions (4.6) as

$$\begin{aligned} F \;=\; & (q_S, g) \otimes \begin{pmatrix} \mathcal{C}^{S,D_S} & \mathcal{C}^{S,g} \\ \mathcal{C}^{g,D_S} & \mathcal{C}^{g,g} \end{pmatrix} \otimes \begin{pmatrix} D_S^h \\ D_g^h \end{pmatrix} \\ & + \sum_i^{N_f} q_i^{\mathrm{NS}} \otimes (\mathcal{C}_{q_i}^{\mathrm{NS},D_S}, \mathcal{C}^{q_i,g}) \otimes \begin{pmatrix} D_S^h \\ D_g^h \end{pmatrix} + \sum_j^{N_f} (q_S, g) \otimes \begin{pmatrix} \mathcal{C}_{q_j}^{S,D_{\mathrm{NS}}} \\ \mathcal{C}^{g,q_j} \end{pmatrix} \otimes D_{q_j}^{h,\,\mathrm{NS}} \end{aligned} \tag{4.21}$$

$$+\sum_{i,j}^{N_f} q_i^{\mathrm{NS}} \otimes \mathcal{C}^{\mathrm{NS}}_{q_i,q_j} \otimes D^{h,\,\mathrm{NS}}_{q_j} + \sum_{i}^{N_f} q_i^{v} \otimes \mathcal{C}^{\mathrm{v}}_{q_i,q_i} \otimes D^{h,\,v}_{q_i}$$
$$+\sum_{\substack{i,j \\ i\neq j}} q_i^{v} \otimes \mathcal{C}^{\mathrm{v}}_{q_i,q_j} \otimes D^{h,\,v}_{q_j} \tag{4.22}$$

where the index "k" and the dependencies on x, z and Q^2 were dropped in order to simplify the notation. The above formula is valid to all orders and the different coefficient functions $\mathcal{C}$ relate to the coefficient functions C in (4.8) according to the following equalities:

$$\mathcal{C}^{S,D_S} = \frac{1}{2}\sum_{i}^{N_f}\sum_{j}^{N_f}\left(C^{q_i,q_j} + C^{q_i,\bar{q}_j}\right) \qquad \mathcal{C}^{S,g} = \sum_{i}^{N_f} C^{q_i,g} \qquad \mathcal{C}^{g,D_S} = \sum_{j}^{N_f} C^{g,q_j} \qquad \mathcal{C}^{g,g} = C^{g,g}$$

$$\mathcal{C}^{\mathrm{NS},D_S}_{q_i} = \frac{1}{2}\sum_{j}^{N_f}\left(C^{q_i,q_j} + C^{q_i,\bar{q}_j}\right) \qquad \mathcal{C}^{q_i,g} = C^{q_i,g}$$

$$\mathcal{C}^{S,D_{\mathrm{NS}}}_{q_j} = \frac{1}{2}\sum_{i}^{N_f}\left(C^{q_i,q_j} + C^{q_i,\bar{q}_j}\right) \qquad \mathcal{C}^{g,q_j} = C^{g,q_j}$$

$$\mathcal{C}^{\mathrm{NS}}_{q_i,q_j} = \frac{1}{2}\left(C^{q_i,q_j} + C^{q_i,\bar{q}_j}\right) \qquad \mathcal{C}^{\mathrm{v}}_{q_i,q_j} = \frac{1}{2}\left(C^{q_i,q_j} - C^{q_i,\bar{q}_j}\right) \tag{4.23}$$

Here again we have dropped the index "k" and the dependencies x, z and Q^2 for readability. In a similar way as in (4.19), we can categorise the different contributions according to their electromagnetic charge dependences. Up to $\mathcal{O}(a_s^2)$ the coefficient functions C^{q_i,q_j} can be written as follows:

$$C^{q_i,q_i} = C^{\bar{q}_i,\bar{q}_i} = e_{q_i}^2 C^{\mathrm{NS}}_{qq} + \frac{1}{N_f}\left(\sum_i e_{q_i}^2\right) C^{\mathrm{PS}}_{qq} \qquad C^{q_i,\bar{q}_i} = C^{\bar{q}_i,q_i} = e_i^2(C^1_{q\bar{q}} - C^2_{q\bar{q}})$$
$$C^{q_i,q_j} = C^{\bar{q}_i,\bar{q}_j} \overset{i\neq j}{=} e_{q_i}^2 C^1_{qq\prime} + e_{q_j}^2 C^2_{qq\prime} + e_{q_i} e_{q_j} C^3_{qq\prime} \qquad C^{q_i,g} = C^{\bar{q}_i,g} = e_{q_i}^2 C_{qg}$$
$$C^{q_i,\bar{q}_j} = C^{\bar{q}_i,q_j} \overset{i\neq j}{=} e_{q_i}^2 C^1_{qq\prime} + e_{q_j}^2 C^2_{qq\prime} - e_{q_i} e_{q_j} C^3_{qq\prime} \qquad C^{g,q_i} = C^{g,\bar{q}_i} = e_{q_i}^2 C_{gq}$$
$$C^{g,g} = \frac{1}{N_f}\left(\sum_i e_{q_i}^2\right) C_{gg}\,. \tag{4.24}$$

At $\mathcal{O}(a_s^0)$ only the C^{NS}_{qq} differs from zero whereas the gluon-fusion contribution C_{gq} and the gluon-radiation term C_{qg} appear for the first time at NLO. They have been computed for both

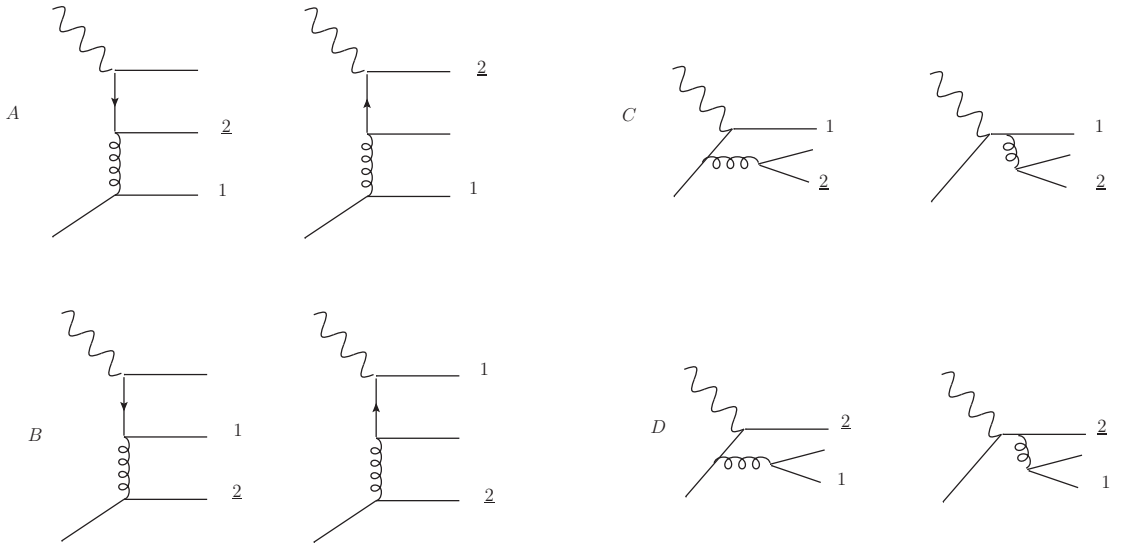

Figure 4.1: Diagram contributions to the sub-process $\gamma * + q \rightarrow q(1) + \text{“}q\text{”}(2) + \bar{q}$ (and $\gamma * + \bar{q} \rightarrow \bar{q}(1) + \text{“}\bar{q}\text{”}(2) + q$ if the arrows are inverted in group A and B). Particle “2” is assumed to be the one fragmenting in the semi-inclusive case.

F_1 and F_L up to $\mathcal{O}(a_s)$ in [108, 111]. The remaining coefficients $C_{qq}^{\rm PS}$, $C_{q\bar{q}}^{1,2}$, $C_{qq\prime}^{1,2,3}$, C_{gg} in (4.24) are non-zero for the first time at NNLO and they are generated at this order from the 2 to 3 diagrams of Fig. 4.1 and 4.3 [239]. Specifically :

- $C_{gg}^{(2)}$ takes contributions from squaring the diagrams in Fig. 4.3 and from the squared amplitudes generated by their interferences,
- B^2 in Fig. 4.1 is the only contribution to $C_{qq}^{\rm PS,\,(2)}$,
- $C_{q\bar{q}}^{1,\,(2)}$ is generated by A^2 and C^2 with fragmenting anti-quark (quark) of same flavour of the incoming quark (anti-quark) in Fig. 4.1,
- $C_{q\bar{q}}^{2,\,(2)}$ is generated by the interference term AC in Fig. 4.1 with fragmenting particle being an anti-quark (quark) of same flavour of the incoming quark (anti-quark),
- $C_{qq\prime}^{1,\,(2)}$ takes contributions only from C^2 in Fig. 4.1 when fragmenting and incoming quark or anti-quark are of different flavours,
- A^2 in Fig. 4.1 is the only contribution to $C_{qq\prime}^{2,\,(2)}$ when fragmenting and incoming quark or anti-quark are of different flavours,

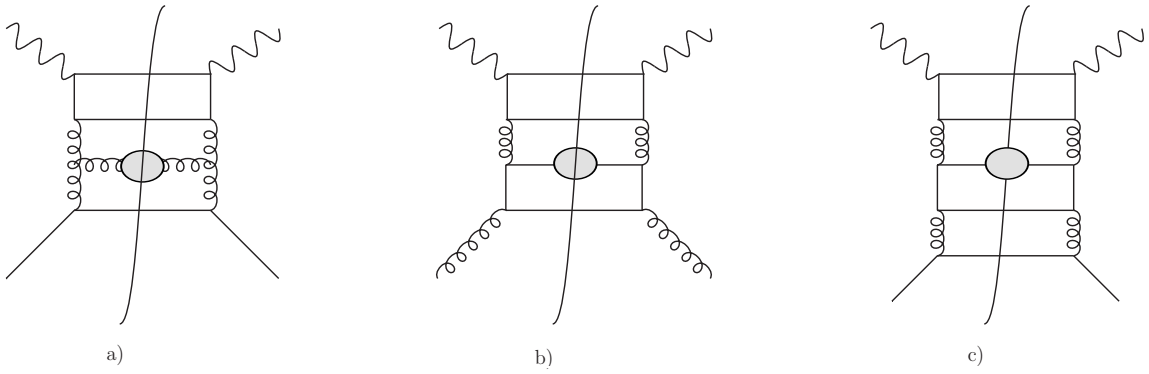

Figure 4.2: Cut diagrams proportional to $\sum_i \left(e_{q_i}^2\right)/N_f$. The grey blob indicates the fragmenting outgoing particle. a), b) contribute to the third order $C^{q_i,g,(3)}$ and $C^{g,q_i,(3)}$ respectively whereas c) contributes both to the fourth order $C^{q_i,\bar{q}_i,(4)}$ and to $C^{q_i,q_j,(4)}$.

- The interference term AC in Fig. 4.1 contributes to $C_{qq'}^{3,(2)}$ when fragmenting and incoming quark or anti-quark are of different flavours.

Moreover, the $\mathcal{O}(a_s^2)$ contribution to the C_{qq}^{NS} coefficient generates from loop and radiative corrections to the $\mathcal{O}(a_s^0)$ and $\mathcal{O}(a_s)$ diagrams together with the A^2, C^2, D^2, AD, BC contributions form Fig. 4.1 when the incoming quark (anti-quark) and the fragmenting quark (anti-quark) are of the same flavour. Contributions proportional to $\sum_i \left(e_{q_i}^2\right)/N_f$ will appear only starting from N^{3}LO for the coefficients $C^{q_i,g}$ and C^{g,q_i} whereas for C^{q_i,q_j} and $C^{q_i,\bar{q}_i}$ this will happen at N^{4}LO. An example of such contributions is given in Fig. 4.2.
As a last remark of this section, we want to stress the peculiarity of the $C_{qq'}^3$ coefficient. It generates from diagrams of the type that would vanish in the sum in the inclusive case. In SIDIS however, it isolates the "valence" combinations of PDFs and FFs when the incoming and the fragmenting quark or anti-quark are of different flavours. In fact, at NNLO $C_{qq'}^3$ is the only coefficient that contributes to the last line of Eq. (4.21).

4.4 Calculation of the new contributions to the longitudinal structure function

In the last section we have summarized the different NNLO contributions to the structure function that need to be calculated for a full $\mathcal{O}(a_s^2)$ result. We start by calculating the simplest corrections to the longitudinal structure function, namely the coefficients $C_{L,\,qq'}^{1,(2)}$, $C_{L,qq'}^{2,(2)}$, $C_{L,qq'}^{3,(2)}$

and $C^{(2)}_{L,\,gg\prime}$, whose definitions can be found in Eq. (4.24). As already discussed in Section 4.3, they represent two channels that appear for the first time at NNLO: $\gamma^* + q \to q + \bar{q}' + q'$ with fragmenting quark or anti-quark of different flavour of the incoming quark or anti-quark, and $\gamma^* + g \to q + \bar{q} + g$ with the fragmenting parton being the gluon g. From now on, we will indicate these two processes with qq' and gg respectively. Considering only qq' and gg channels, the structure function in (4.6) can be written using Eqs. (4.23) and (4.24) as

$$
\begin{aligned}
F^{(2)}_{L,(qq'+gg)}(x,z,Q^2) = a_s^2(Q^2)\Bigg\{ \sum_i^{N_f} e_{q_i}^2 \Bigg[\Bigg(q_i^{\mathrm{NS}} + q_S \Bigg) \otimes C^{1,(2)}_{L,qq\prime} \otimes \Bigg(\sum_{\substack{j \\ j\neq i}}^{N_f} \Big(D^{h,\mathrm{NS}}_{q_j} \Big) + (N_f - 1) D^h_S \Bigg) \\
+ \Bigg(\Big(\sum_{\substack{j \\ j\neq i}}^{N_f} q_j^{\mathrm{NS}} \Big) + (N_f - 1) q_S \Bigg) \otimes C^{2,(2)}_{L,qq\prime} \otimes \Big(D^{h,\mathrm{NS}}_{q_i} + D^h_S \Big) + \frac{1}{N_f} g \otimes C^{(2)}_{L,\,gg} \otimes D^h_g \Bigg](x,z) \\
+ \sum_i^{N_f} \sum_{\substack{j \\ j\neq i}}^{N_f} e_{q_i} e_{q_j} \Bigg[q_i^v \otimes C^{3,(2)}_{L,qq\prime} \otimes D^{h,\,v}_{q_j} \Bigg](x,z) \Bigg\}
\end{aligned}
\tag{4.25}
$$

Since no lower order diagrams are present for those channels, no loop corrections and no distributions appear at this level of accuracy. This simplifies the calculation considerably. Hereinafter the main highlights of our calculation are presented.

In order to regularize the divergences that appear at the intermediate stages of the computation we use dimensional regularization [240, 241], i.e., we work in a d-dimensional space, with $d = 4 - 2\epsilon$. All quarks are considered massless.

The diagrams contributing to qq' and gg channel are shown in Figs. 4.1 and 4.3. We compute the squared amplitudes for each channel with the MATHEMATICA packages FEYNARTS [242] and FEYNCALC [243]. When summing over the gluon helicities we only take into account the physical ones:

$$
\sum_\lambda \varepsilon_\mu(p,\lambda)\varepsilon^*_\nu(p,\lambda) = -g_{\mu\nu} + \frac{n_\mu\, p_\nu + n_\nu\, p_\mu}{n \cdot p}\,, \tag{4.26}
$$

with n an auxiliar vector ($n^2 = 0$). The explicit dependence on n drops out due to gauge invariance. The same result is obtained by working in a covariant gauge and thus taking external ghosts lines into account.

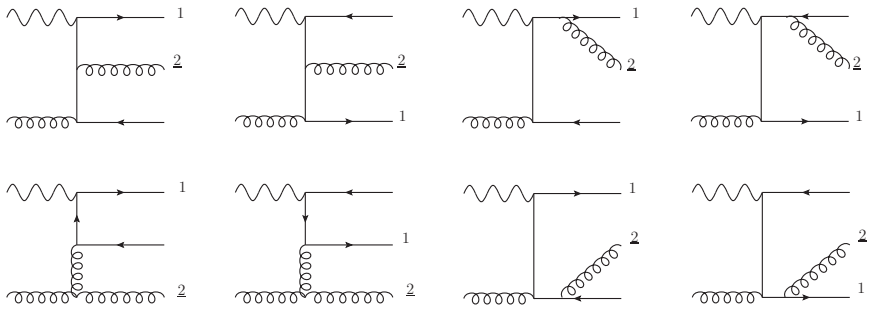

Figure 4.3: Contributing diagrams to the gg channel ($\gamma^* + g \to q(1) + \bar{q} +$ "g"(2)). As for before, particle "2" is assumed to be the one fragmenting.

Since the phase space integration has to be performed over the momenta of the unobserved partons (for instance, quark-antiquark pair for the gg channel), we decide to work in the center of mass frame of these two outgoing partons. In this frame, we still have the chance to choose which one of the remaining momenta defines the z-axis [244]. This choice defines three different sets of kinematic variables. While the set with the photon's momentum (q) along the z-axis is not useful, since the photon is not massless, the other two sets are convenient for parametrizing different terms of the computation. For all the sets available, we can define

$$2\,q\,\cdot\,k_h = \frac{Q^2}{x}\left[1 - x - z - (1-x)(1-z)\,y\right]\,, \tag{4.27}$$

with k_h being the momentum of the hadronizing parton (gluon in the gg channel and q' or $\bar{q}'$ for the qq' channel), x and z the usual SIDIS variables.

At the end, the amplitude can be written in terms of just Q^2, x, z, y, and the polar and azimuthal angles of the pair of unobserved partons: θ and ϕ respectively. Then, we can obtain each one of the coefficients C_L^{jk} as the finite part of the *partonic structure function*, defined by

$$F_L^{jk} = \frac{1}{4\pi}\int d\Gamma\; P_L^{\mu\nu}\;\overline{|M^{jk}|^2}_{\mu\nu}, \tag{4.28}$$

where $d\Gamma$ is the d-dimensional phase-space and the longitudinal projector is

$$P_L^{\mu\nu} = \frac{8\,x^2}{Q^2} p^\mu\,p^\nu. \tag{4.29}$$

The d-dimensional phase-space can be written as [245]

$$\begin{aligned}\int d\Gamma &= \frac{1}{(4\pi)^{4-2\epsilon}} \frac{(s+Q^2)^{1-2\epsilon}}{\Gamma(1-2\epsilon)} (1-x)^{1-2\epsilon} z^{-\epsilon} (1-z)^{1-2\epsilon} \\ &\times \int_0^\pi d\theta \int_0^\pi d\phi \, (\sin\theta)^{1-2\epsilon} (\sin\phi)^{-2\epsilon} \int_0^1 dy \, [y(1-y)]^{-\epsilon} \, . \end{aligned} \tag{4.30}$$

All the angular integrals of Eq. (4.28) can be written, by means of partial fractioning, as

$$I(k,l,a,b,A,B,C) = \int_0^\pi d\theta \int_0^\pi d\phi \, \frac{(\sin\theta)^{1-2\epsilon} (\sin\phi)^{-2\epsilon}}{(a+b\,\cos\theta)^k (A+B\,\cos\theta + C\,\cos\phi\,\sin\theta)^l}. \tag{4.31}$$

These integrals need to be classified according to the relations their parameters satisfy: i) $a^2 = b^2$, ii) $A^2 = B^2 + C^2$, iii) both relations or iv) neither of them. Besides, the integrals of group ii) can be recasted in terms of those of group i). In some cases (in particular whenever an integral of type iv) appears, but also for some integrals of group i)) we can compute the angular integrals in 4 dimensions. Nevertheless, some of the integrals are divergent and we therefore need a d-dimensional computation. Since the integration over y does not introduce extra poles for the contributions studied in this chapter, we can expand the results of the angular integrations up to order 0 in ϵ.

Most of the angular integrals that we need can be found in Appendix C of [244]. We had to compute, however, some unknown ones that are presented in Appendix E for the sake of completeness. These new integrals have been computed in 4 dimensions and are valid for groups i) and iv) enumerated above.

Moreover, we need to perform the integration over y, after expanding the integrand up to order 0 in ϵ. It is important to notice that this integral is not straightforward. Instead, several changes of variables must be done and some terms must even be rewritten in a clever way to avoid the appearance of spurious divergences in the intermediate steps.

For instance, one of the terms that appear in our computation is

$$\begin{aligned}&\frac{1}{(q-k_h)^2(q-k_2)^2} = \\ &= \frac{1}{(Q^2+u)} \frac{2}{Q^2} I[0,1,a,b,\frac{Q^2+s-u}{Q^2}, \frac{Q^2+s-t-(t+u)\,\cos(\psi)}{Q^2}, -\frac{(t+u)\sin(\psi)}{Q^2}]\end{aligned}$$

$$= \frac{2\pi x^2}{Q^4(1-z)} \frac{\log\left(\frac{(x+z+y(1-x)(1-z))+\sqrt{(x+z+y(1-x)(1-z))^2-4xz}}{(x+z+y(1-x)(1-z))-\sqrt{(x+z+y(1-x)(1-z))^2-4xz}}\right)}{(1+(-1+x)y)\sqrt{((x+z+y(1-x)(1-z))^2-4xz)}}.$$

Here, k_2 is the momentum of one of the partons in the final state that do not hadronize. Written like that, it cannot be integrated. However, after the change of variable $y \to \frac{w-x-z}{(1-x)(1-z)}$, equation (4.32) becomes

$$\frac{1}{(q-k_h)^2(q-k_2)^2} = \frac{2\pi x^2}{Q^4} \frac{\log(4xz) - 2\log\left(w+\sqrt{w^2-4xz}\right)}{(w-x-1)\sqrt{w^2-4xz}}, \tag{4.32}$$

whose integral can be performed analytically.
At the end, we obtain the functions F_L^{jk} defined in (4.28). These contain collinear divergences, that appear as poles in ϵ (for these processes at NNLO, simple poles in ϵ). We factorize these divergences within the $\overline{\text{MS}}$ scheme, by subtraction of the quantities

$$\begin{aligned}
\tilde{F}_L^{qq'}(x,z) =& \frac{1}{\hat{\epsilon}}\left[C_L^{gq',(1)}(x,z)\otimes P_{gq}^{(0)}(x) + C_L^{qg,(1)}(x,z)\otimes P_{qg}^{T,(0)}(z)\right], \\
\tilde{F}_L^{gg}(x,z) =& \frac{1}{\hat{\epsilon}}\left[C_L^{qg,(1)}(x,z)\otimes P_{qg}^{(0)}(x) + C_L^{gq,(1)}(x,z)\otimes P_{gq}^{T,(0)}(z)\right],
\end{aligned} \tag{4.33}$$

where $P_{jk}^{(0)}$ are the unpolarized LO splitting functions and we define

$$\frac{1}{\hat{\epsilon}} = \left[-\frac{1}{\epsilon} + \gamma_E - \log(4\pi)\right], \tag{4.34}$$

with $\gamma_E = 0,5772...$ the Euler constant. The finite functions obtained after factorization are the coefficients C_L^{jk}. Given the length of these coefficients, we do not show them here, but available upon request at the authors of [J6].

4.5 Results

We analyze in this section the differences between the semi-inclusive and the inclusive cross section ratio and we show the relevance of the NNLO corrections we have computed. The behavior of the SIDIS ratio R is studied in the range $0.1 < z < 1$ for different x values. We rely on MSTW PDFs [178] and DSS fragmentation functions [77]. We fix all scales equal to Q and consider $N_f = 4$ active flavours.

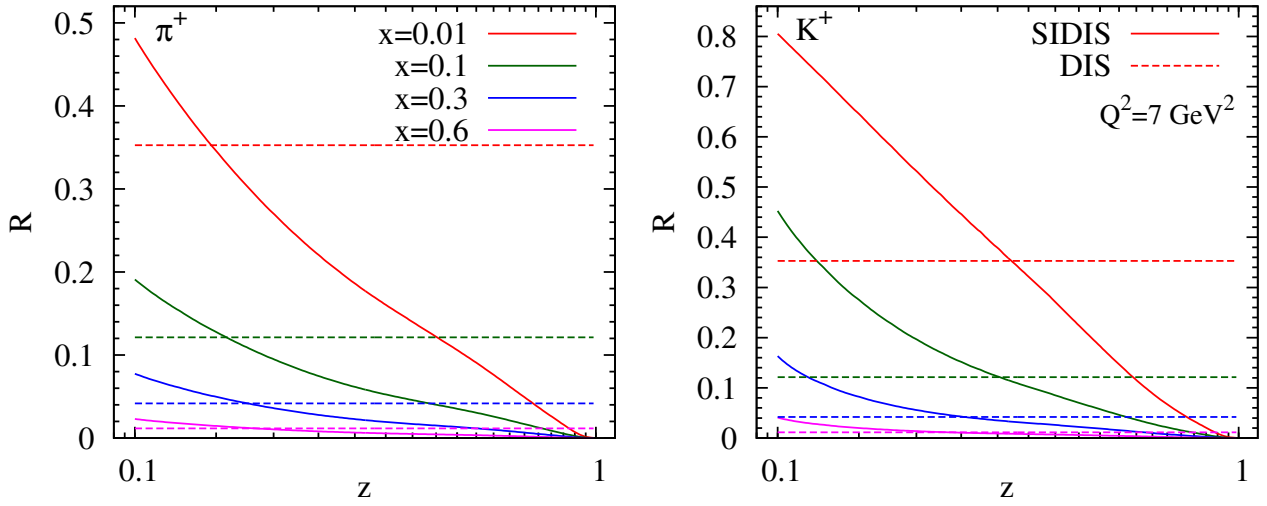

Figure 4.4: NLO longitudinal-transversal ratio at $Q^2 = 7\,\mathrm{GeV}^2$. The solid curves show the semi-inclusive case, with the observation of a π^+ (left side) and a K^+ (right side) in the final state, while the dashed ones shows the inclusive case.

In Fig 4.4 we show the semi-inclusive ratio R at NLO for $Q^2 = 7\,\mathrm{GeV}^2$ when a π^+ (left) or a K^+ (right) are observed in the final state. We compare it with the value of the fully-inclusive ratio also at NLO (dashed line), which does not depend on z. As we can see, the fully-inclusive and the semi-inclusive results may differ by a factor of two in the relevant kinematical region (and even more close to the edges). Thus, an accurate semi-inclusive description of R is crucial for phenomenological analyses and may not be, in general, approximated by the inclusive one. In Fig. 4.5 we present the predictions for the semi-inclusive R ratio including the contributions to the longitudinal structure function at NNLO considered in our work, at $Q^2 = 7\,\mathrm{GeV}^2$ and for different final-state hadrons. We should mention that NLO PDFs and FFs are used in order to fully appreciate the effect of the corrections introduced by the new coefficients.The inset plots show the ratio between the NNLO and the NLO computation presented in this chapter.
We can see that the corrections introduced by the NNLO contributions presented here turn out to be negative and, therefore, tend to considerably reduce the value of R with respect to the previous order. The corrections are specially sizeable for the low-z and high-z regions. This is likely due to the appearance of logarithmic terms introduced by the NNLO contributions and therefore only present in the numerator of the ratio R.
Due to the quark composition of kaons and protons, the contribution coming from $F^{(2)}_{L,qq'}$ is dominant for K^+ and K^-, for all x values analyzed. In fact, more than 80% of the new NNLO

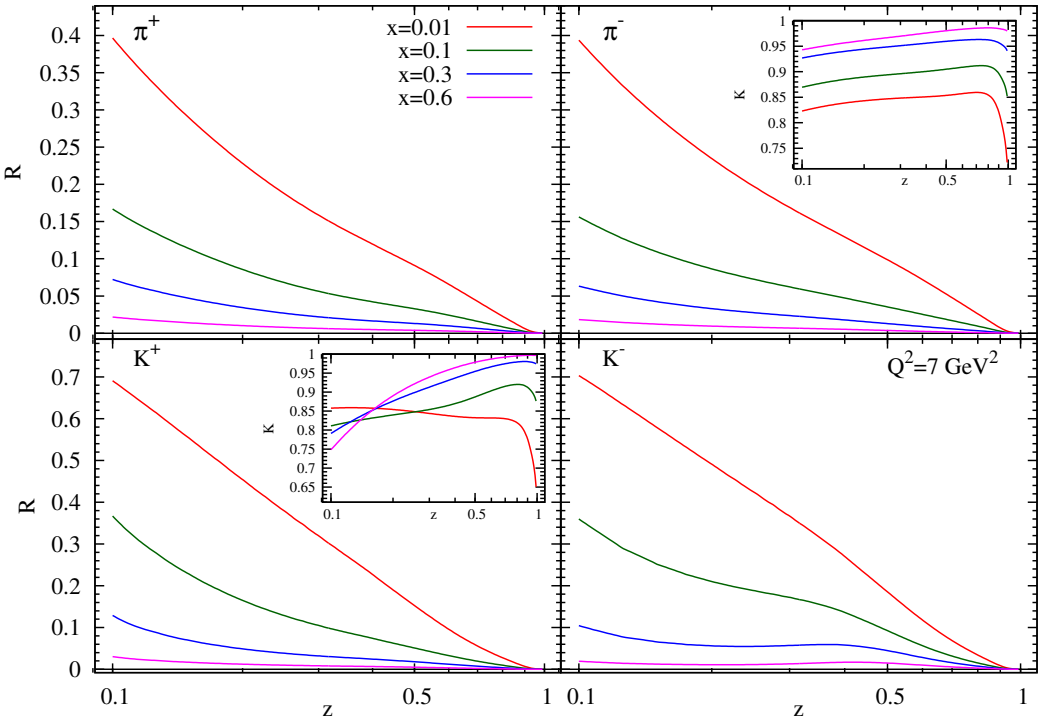

Figure 4.5: Longitudinal-transversal ratio computed taking into account the NNLO contributions considered in this chapter for different hadrons observed in the final state, at $Q^2 = 7\,\mathrm{GeV}^2$. The inset plots show the ratio between the NNLO and the NLO computation presented in this chapter.

correction arises from that channel. The situation is different for pions and in this case the corrections from qq' and gg channels turn out to be even of the same order for some kinematic regions.

Despite of including only a subset of contributions at NNLO, those in principle expected to be small due to their particular structure, the corrections to the longitudinal structure function turn out to be rather sizable, making the calculation of the full corrections even more mandatory.

4.6 Conclusions

In this chapter, we have discussed the results of [J6] where a first calculation of the $\mathcal{O}(\alpha_s^2)$ contributions to the SIDIS longitudinal structure function generated by partonic channels appearing for the first time at NNLO was presented together with an extensive discussion of the general aspects useful for the organization of the complete NNLO calculation.

We have started by studying the flavour decomposition of the full cross section. We have shown how to express both longitudinal and transversal structure functions in terms of usual singlet and non-singlet combinations of PDFs and FFs relevant in global analysis fits, thus exposing the flavour structure of the SIDIS cross section. For instance, one can notice that a specific contribution calculated here in this chapter, namely $C^3_{qq'}(2)$, isolates a particular "valence" flavor contribution, to which a NLO cross section would be insensitive. Along the way, we have given a summary of the different diagrammatic contributions to the partonic sub-processes in view of the full NNLO calculation. In the same spirit, a general recursive formula to reconstruct the dependence on both factorization scales involved in the SIDIS process at an arbitrary order in the strong coupling constant was derived.

In a second part, we have given details of our computation for the two channels treated in [J6]. In particular, the procedure to analytically calculate the phase space integrals has been discussed and a set of new angular integrals was presented. Although the calculated channels are a partial component of the full set of NNLO corrections to the cross section, we have discussed some phenomenological study done on the observable R as a theoretical investigation of the relevance of NNLO corrections to the cross section. It turns out that the small fraction of contributions calculated so far do exhibit sizeable corrections especially in the low-z and high-z region, likely due to the appearance of logarithms that are only present in the numerator.

Not only these observations are of theoretical interest, but stating whether or not this is also the case once all corrections up to NNLO are added is of great importance when it comes to extracting FFs from SIDIS data. As it is well know, including SIDIS data in a global analysis helps disentangling the different single flavour contributions to the fragmenting process. Even more at NNLO where the appearance of new channels discriminates specific new combinations of PDFs and FFs. Nonetheless, only with the full calculation available one can at the end asses their phenomenological relevance in the overall picture of a global analysis. With the precision of the FFs having been recently extended to NNLO and beyond in the context of electron-positron to pion only analysis, it is then natural to try to acquire the sort of "know how" needed to complete a NNLO calculation of the SIDIS process. In an attempt to attack this problem with an analytical approach, we have started by computing in [J6] the first simplest corrections to the longitudinal structure function as a playground where to explore and organize the future complete calculation. From a theoretical point of view, only with analytical results available one gathers useful insight in the structure of the perturbative series. A complete analytical calculation could in fact be relevant for further applications which go beyond PDFs and FFs

analyses. For instance, knowing the structure of sub-leading logarithms connected with precise phase-space configurations is an essential ingredient in order to extend resummation techniques to higher accuracy.

CHAPTER 5

Threshold resummation for polarized (semi-)inclusive deep inelastic scattering

We explore the effects of the resummation of large logarithmic perturbative corrections to double-longitudinal spin asymmetries for inclusive and semi-inclusive deep inelastic scattering in fixed-target experiments. We find that the asymmetries are overall rather robust with respect to the inclusion of the resummed higher-order terms. Significant effects are observed at fairly high values of x, where resummation tends to decrease the spin asymmetries. This effect turns out to be more pronounced for semi-inclusive scattering. We also investigate the potential impact of resummation on the extraction of polarized valence quark distributions in dedicated high-x experiments. This chapter is based on our published work [J2].

5.1 Introduction

Longitudinal double-spin asymmetries in inclusive and semi-inclusive deep inelastic scattering have been prime sources of information on the nucleon's spin structure for several decades. They may be used to extract the helicity parton distributions of the nucleon,

$$\Delta f(x,Q^2) \equiv f^+(x,Q^2) - f^-(x,Q^2) \ , \tag{5.1}$$

where f^+ and f^- are the distributions of parton $f = q, \bar{q}, g$ with positive and negative helicity, respectively, when the parent nucleon has positive helicity. x denotes the momentum fraction of the parton and Q the hard scale at which the distribution is probed. Inclusive polarized deep inelastic scattering (DIS), $\vec{\ell}\vec{p} \to \ell X$, offers access to the combined quark and antiquark distributions for a given flavor, $\Delta q + \Delta\bar{q}$, whereas in semi-inclusive deep inelastic scattering (SIDIS), $\vec{\ell}\vec{p} \to \ell h X$, one exploits the fact that a produced hadron h (like a π^+) may for instance have a quark of a certain flavor as a valence quark, but not the corresponding antiquark [246]. In this way, it becomes possible to separate quark and antiquark distributions in the nucleon from one another, as well as to better determine the distributions for the various flavors. HERMES [247] and recent COMPASS [234] measurements have marked significant progress concerning the accuracy and kinematic coverage of polarized SIDIS measurements. The inclusive measurements have improved vastly as well [248–253]. Some modern analyses of spin-dependent parton distributions include both inclusive and semi-inclusive data [254–257]. In addition, high-precision data for polarized SIDIS will become available from experiments to be carried out at the Jefferson Lab after the CEBAF upgrade to a 12 GeV beam [258]. Here the focus will be on the large-x regime.

A good understanding of the theoretical framework for the description of spin asymmetries in lepton scattering is vital for a reliable extraction of polarized parton distributions. In a recent paper [J1] we have investigated the effects of QCD threshold resummation on hadron multiplicities in SIDIS in the HERMES and COMPASS kinematic regimes. SIDIS is characterized by two scaling variables, Bjorken-x and a variable z given by the energy of the produced hadron over the energy of the virtual photon in the target rest frame. Large logarithmic corrections to the SIDIS cross section arise when the corresponding partonic variables become large, corresponding to scattering near a phase space boundary, where real-gluon emission is suppressed. This is typically the case for the presently relevant fixed-target kinematics. Threshold resummation addresses these logarithms to all orders in the strong coupling. In [J1] we found fairly significant resummation effects on the spin-averaged multiplicities. Since the spin-dependent cross section is subject to similar logarithmic corrections as the unpolarized one, it is worthwhile to explore the effects of resummation on the spin asymmetries. This is the goal of the work [J2] presented in this chapter. Our calculations is carried out both for inclusive DIS and for SIDIS. We note that previous work [259, 260] has addressed the large-x resummation for the inclusive spin-dependent structure function g_1, with a focus on the moments of g_1 and their Q^2-dependence. In this chapter we are primarily concerned with spin asymmetries and with

semi-inclusive scattering.

Our work will use the framework developed in [J1]. In Section 5.2, we briefly review the basic terms and definitions relevant for longitudinal spin asymmetries, and we describe the extension of threshold resummation to the polarized case. In Section 5.3 our phenomenological results are presented. We compare our resummed inclusive and semi-inclusive spin asymmetries with available HERMES, COMPASS and Jefferson Lab data. We also discuss the relevance of resummation for the extraction of $\Delta u/u$ and $\Delta d/d$ at large values of x.

5.2 Resummation for Longitudinal Spin Asymmetries in DIS and SIDIS

5.2.1 Leading and next-to-leading order expressions

We first consider the polarized SIDIS process $\vec{\ell}(k)\vec{p}(P) \to \ell(k')h(P_h)X$ with longitudinally polarized beam and target and with an unpolarized hadron in the final state. The corresponding double-spin asymmetry is given by a ratio of structure functions [247]:

$$A_1^h(x,z,Q^2) \approx \frac{g_1^h(x,z,Q^2)}{F_1^h(x,z,Q^2)}\,, \tag{5.2}$$

where $Q^2 = -q^2$ with q the momentum of the virtual photon, $x = Q^2/(2P\cdot q)$ is the usual Bjorken variable, and $z \equiv P\cdot P_h/P\cdot q$ the corresponding hadronic scaling variable associated with the fragmentation process.

Using factorization, the polarized structure function g_1^h, which appears in the numerator of Eq. (5.2), can be written as

$$2g_1^h(x,z,Q^2) \;=\; \sum_{f,f'=q,\bar{q},g} \int_x^1 \frac{d\hat{x}}{\hat{x}} \int_z^1 \frac{d\hat{z}}{\hat{z}}\, \Delta f\left(\frac{x}{\hat{x}},\mu^2\right) D_{f'}^h\left(\frac{z}{\hat{z}},\mu^2\right)\, \Delta\mathcal{C}_{f'f}\left(\hat{x},\hat{z},\frac{Q^2}{\mu^2},\alpha_s(\mu^2)\right), \tag{5.3}$$

where $\Delta f(\xi,\mu^2)$ denotes the polarized distribution function for parton f of Eq. (5.1), whereas $D_{f'}^h(\zeta,\mu^2)$ is the corresponding fragmentation function for parton f' going to the observed hadron h. The $\Delta\mathcal{C}_{f'f}$ are spin-dependent coefficient functions. We have set all factorization and renormalization scales equal and collectively denoted them by μ. In (5.3) $\hat{x}$ and $\hat{z}$ are the

partonic counterparts of the hadronic variables x and z. Setting for simplicity $\mu = Q$, we use the short-hand-notation

$$2g_1^h(x,z,Q^2) \equiv \sum_{f,f'=q,\bar{q},g} \left[\Delta f \otimes \Delta\mathcal{C}_{f'f} \otimes D_{f'}^h\right](x,z,Q^2) \tag{5.4}$$

for the convolutions in (5.3). A corresponding expression for the "transverse" unpolarized structure function $2F_1^h$ can be written by replacing the polarized parton distributions with the unpolarized ones, and using unpolarized coefficient functions which we denote here by $\mathcal{C}_{f'f}$.

The spin-dependent hard-scattering coefficient functions $\Delta\mathcal{C}_{f'f}$ in (5.3) can be computed in perturbation theory:

$$\Delta\mathcal{C}_{f'f} \,=\, \Delta C_{f'f}^{(0)} + \frac{\alpha_s(\mu^2)}{2\pi}\Delta C_{f'f}^{(1)} + \mathcal{O}(\alpha_s^2)\,. \tag{5.5}$$

At leading order (LO), we have

$$\Delta\mathcal{C}_{qq}(\hat{x},\hat{z}) \,=\, \Delta\mathcal{C}_{\bar{q}\bar{q}}(\hat{x},\hat{z}) \,=\, e_q^2\,\delta(1-\hat{x})\delta(1-\hat{z})\,, \tag{5.6}$$

with the quark's fractional charge e_q. All other coefficient functions vanish. The same result holds for the LO coefficient function for the spin-averaged structure function $2F_1^h$. Hence the asymmetry in Eq. (5.2) reduces to

$$A_1^h = \frac{\sum\limits_q e_q^2\left[\Delta q(x,Q^2)D_q^h(z,Q^2) + \Delta\bar{q}(x,Q^2)D_{\bar{q}}^h(z,Q^2)\right]}{\sum\limits_q e_q^2\left[q(x,Q^2)D_q^h(z,Q^2) + \bar{q}(x,Q^2)D_{\bar{q}}^h(z,Q^2)\right]}\,. \tag{5.7}$$

At next-to-leading order (NLO), Eq. (5.3) becomes

$$\begin{aligned} 2g_1^h(x,z,Q^2) \;=\; & \sum_q e_q^2\Big\{\Delta q(x,Q^2)D_q^h(z,Q^2) + \bar{q}(x,Q^2)D_{\bar{q}}^h(z,Q^2) \\ & + \frac{\alpha_s(Q^2)}{2\pi}\left[\left(\Delta q\otimes D_q^h + \Delta\bar{q}\otimes D_{\bar{q}}^h\right)\otimes\Delta C_{qq}^{(1)}\right. \\ & \left.\left. + (\Delta q + \Delta\bar{q})\otimes\Delta C_{gq}^{(1)}\otimes D_g^h + \Delta g\otimes\Delta C_{qg}^{(1)}\otimes(D_q^h + D_{\bar{q}}^h)\right](x,z,Q^2)\Big\}\,, \end{aligned} \tag{5.8}$$

where the symbol $\otimes$ denotes the convolution defined in Eqs. (5.3),(5.4). The explicit expres-

sions for the spin-dependent NLO coefficients $\Delta C^{(1)}_{f'f}$ have been derived in [111, 205]. The corresponding spin-averaged NLO coefficient functions $C^{(1)}_{f'f}$ may be found in [J1, 48, 108–111, 205].

In the case of *inclusive* polarized DIS, the longitudinal spin asymmetry A_1 is given in analogy with (5.2) by

$$A_1(x,Q^2) \approx \frac{g_1(x,Q^2)}{F_1(x,Q^2)} \,. \tag{5.9}$$

The inclusive structure functions g_1 and F_1 have expressions analogous to their SIDIS counterparts, except for the fact that they do not contain any fragmentation functions, of course. The unpolarized and polarized NLO coefficient functions for inclusive DIS may be found at many places; see, for example [48, 261].

5.2.2 Threshold resummation

As was discussed in [J1], the higher-order terms in the spin-averaged SIDIS coefficient function $\mathcal{C}_{qq}$ introduce large terms near the "partonic threshold" $\hat{x} \to 1$, $\hat{z} \to 1$. The same is true for the spin-dependent $\Delta\mathcal{C}_{qq}$. At NLO, choosing again for simplicity the scale $\mu = Q$, one has

$$\begin{aligned}\Delta C^{(1)}_{qq}(\hat{x},\hat{z}) \;\sim\; e_q^2 C_F \Bigg[&+ 2\delta(1-\hat{x}) \left(\frac{\ln(1-\hat{z})}{1-\hat{z}}\right)_+ + 2\delta(1-\hat{z}) \left(\frac{\ln(1-\hat{x})}{1-\hat{x}}\right)_+ \\ &+ \frac{2}{(1-\hat{x})_+(1-\hat{z})_+} - 8\delta(1-\hat{x})\delta(1-\hat{z}) \Bigg],\end{aligned} \tag{5.10}$$

where the "+"-distribution is defined as usual. The expression on the right-hand side is in fact identical to the one for the unpolarized coefficient function near threshold [J1]. At the kth order of perturbation theory, the coefficient function contains terms of the form $\alpha_s^k \delta(1-\hat{x}) \left(\frac{\ln^{2k-1}(1-\hat{z})}{1-\hat{z}}\right)_+$, $\alpha_s^k \delta(1-\hat{z}) \left(\frac{\ln^{2k-1}(1-\hat{x})}{1-\hat{x}}\right)_+$, or "mixed" distributions $\alpha_s^k \left(\frac{\ln^m(1-\hat{x})}{1-\hat{x}}\right)_+ \left(\frac{\ln^n(1-\hat{z})}{1-\hat{z}}\right)_+$ with $m+n = 2k-2$, plus terms less singular by one or more logarithms. Again, each of these terms will appear equally in the unpolarized and in the polarized coefficient function. The reason for this is that the terms are associated with emission of soft gluons [J1], which does not care about spin. Threshold resummation addresses the large logarithmic terms to all orders in the strong coupling. The resummation for the case of SIDIS was carried out in [J1]. Given these results and the equality of the spin-averaged and spin-dependent coefficient functions near threshold, it is relatively straightforward to perform the resummation for the polarized

case. Having the resummation for both g_1^h and F_1^h, we obtain resummed predictions for the experimentally relevant spin asymmetry A_1^h.

In [J1, 131, 199] threshold resummation for SIDIS was derived using an eikonal approach, for which exponentiation of the threshold logarithms is achieved in Mellin space. One takes Mellin moments of g_1^h separately in the two independent variables x and z [108, 262]:

$$\tilde{g}_1^h(N,M,Q^2) \equiv \int_0^1 dx x^{N-1} \int_0^1 dz z^{M-1}\, g_1^h(x,z,Q^2). \tag{5.11}$$

With this definition, Eq. (5.4) takes the form (again at scale $\mu = Q$)

$$2\tilde{g}_1^h(N,M,Q^2) \;=\; \sum_{f,f'=q,\bar{q},g} \Delta\tilde{f}^N(Q^2)\Delta\tilde{\mathcal{C}}_{f'f}(N,M,\alpha_s(Q^2))\tilde{D}_{f'}^{h,M}(Q^2)\,, \tag{5.12}$$

where the moments of the polarized parton distributions and the fragmentation functions are defined as

$$\begin{aligned} \Delta\tilde{f}^N(Q^2) &\equiv \int_0^1 dx x^{N-1}\Delta f(x,Q^2), \\ \tilde{D}_{f'}^{h,M}(Q^2) &\equiv \int_0^1 dz z^{M-1} D_{f'}^h(z,Q^2), \end{aligned} \tag{5.13}$$

and the double Mellin moments of the polarized coefficient functions are

$$\Delta\tilde{\mathcal{C}}_{f'f}\left(N,M,\alpha_s(Q^2)\right) \equiv \int_0^1 d\hat{x}\hat{x}^{N-1}\int_0^1 d\hat{z}\hat{z}^{M-1}\Delta\mathcal{C}_{f'f}\left(\hat{x},\hat{z},1,\alpha_s(Q^2)\right)\,. \tag{5.14}$$

Large $\hat{x}$ and $\hat{z}$ in $\Delta\mathcal{C}_{f'f}$ correspond to large N and M in $\Delta\tilde{\mathcal{C}}_{f'f}$, respectively.

The resummed spin-dependent coefficient function is identical to the spin-averaged one of [J1] and reads to next-to-leading logarithmic (NLL) accuracy in the $\overline{\text{MS}}$-scheme:

$$\Delta\tilde{\mathcal{C}}_{qq}^{\text{res}}(N,M,\alpha_s(Q^2)) = e_q^2 H_{qq}\left(\alpha_s(Q^2)\right)\exp\left[2\int_{\frac{Q^2}{\bar{N}\bar{M}}}^{Q^2}\frac{dk_\perp^2}{k_\perp^2}A_q\left(\alpha_s(k_\perp^2)\right)\ln\left(\frac{k_\perp}{Q}\sqrt{\bar{N}\bar{M}}\right)\right], \tag{5.15}$$

where $\bar{N} \equiv N\mathrm{e}^{\gamma_E}$, $\bar{M} \equiv M\mathrm{e}^{\gamma_E}$, with γ_E the Euler constant, and

$$A_q(\alpha_s) = \frac{\alpha_s}{\pi} A_q^{(1)} + \left(\frac{\alpha_s}{\pi}\right)^2 A_q^{(2)} + \dots \tag{5.16}$$

is a perturbative function. The coefficients required to NLL read

$$A_q^{(1)} = C_F, \quad A_q^{(2)} = \frac{1}{2} C_F \left[C_A \left(\frac{67}{18} - \frac{\pi^2}{6} \right) - \frac{5}{9} N_f \right], \tag{5.17}$$

where $C_F = 4/3$, $C_A = 3$ and N_f is the number of active flavors. Furthermore,

$$H_{qq}(\alpha_s) = 1 + \frac{\alpha_s}{2\pi} C_F \left(-8 + \frac{\pi^2}{3} \right) + \mathcal{O}(\alpha_s^2) \,. \tag{5.18}$$

The explicit NLL expansion of the exponent in (5.15) is given by [J1]

$$\int_{\frac{Q^2}{\bar{N}\bar{M}}}^{Q^2} \frac{dk_\perp^2}{k_\perp^2} A_q\left(\alpha_s(k_\perp^2)\right) \ln\left(\frac{k_\perp}{Q}\sqrt{\bar{N}\bar{M}}\right) \approx h_q^{(1)}\left(\frac{\lambda_{NM}}{2}\right) \frac{\lambda_{NM}}{2b_0\alpha_s(\mu^2)} + h_q^{(2)}\left(\frac{\lambda_{NM}}{2}, \frac{Q^2}{\mu^2}, \frac{Q^2}{\mu_F^2}\right), \tag{5.19}$$

where $\lambda_{NM} \equiv b_0\alpha_s(\mu^2)\left(\log\bar{N} + \log\bar{M}\right)$ and $h_q^{(1)}(\lambda)$ and $h_q^{(2)}\left(\lambda, \frac{Q^2}{\mu^2}, \frac{Q^2}{\mu_F^2}\right)$ are given in Eq. (3.32) The functions $h_q^{(1)}$, $h_q^{(2)}$ collect all leading-logarithmic and NLL terms in the exponent, which are of the form $\alpha_s^k \ln^n \bar{N} \ln^m \bar{M}$ with $n+m = k+1$ and $n+m = k$, respectively. Note that we have restored the full dependence on the factorization and renormalization scales in the above expression.

The polarized moment-space structure function $\tilde{g}_1^{h,\mathrm{res}}$ resummed to NLL is obtained by inserting the resummed coefficient function into in Eq. (5.12). To get the physical hadronic structure function $g_1^{h,\mathrm{res}}$ one needs to take the Mellin inverse of the moment-space expression. As in [J1], we choose the required integration contours in complex N, M-space according to the *minimal prescription* of [213], in order to properly deal with the singularities arising from the Landau pole due to the divergence of the perturbative running strong coupling constant α_s at scale Λ_{QCD}. Moreover, we match the resummed $g_1^{h,\mathrm{res}}$ to its NLO value, *i.e.* we subtract the $\mathcal{O}(\alpha_s)$ expansion from the resummed expression and add the full NLO result:

$$g_1^{h,\mathrm{match}} \equiv g_1^{h,\mathrm{res}} - g_1^{h,\mathrm{res}}\Big|_{\mathcal{O}(\alpha_s)} + g_1^{h,\mathrm{NLO}} \,. \tag{5.20}$$

The final resummed and matched expression for the spin asymmetry A_1^h is then given by

$$A_1^{h,\mathrm{res}}(x,z,Q^2) \equiv \frac{g_1^{h,\mathrm{match}}(x,z,Q^2)}{F_1^{h,\mathrm{match}}(x,z,Q^2)} \,. \tag{5.21}$$

Similar considerations can be made for inclusive DIS, where again the resummation for g_1 proceeds identically to that of F_1 in moment space. Only single Mellin moments of the structure function have to be taken:

$$\tilde{g}_1(N,Q^2) \equiv \int_0^1 dx x^{N-1}\, g_1(x,Q^2). \tag{5.22}$$

The threshold resummed coefficient function is the same as in the spin-averaged case and is discussed for example in [J1]. We note that the outgoing quark in the process $\gamma^* q \to q$ remains "unobserved" in inclusive DIS. At higher orders this is known to generate Sudakov *suppression* effects [263] that counteract the Sudakov enhancement associated with soft-gluon radiation from the initial quark. This is in contrast to SIDIS, where the outgoing quark fragments and hence is "observed", so that both the initial and the final quark contribute to Sudakov enhancement. As a result, resummation effects are generally larger in SIDIS than in DIS, for given kinematics.

5.3 Phenomenological results

We now analyze numerically the impact of threshold resummation on the semi-inclusive and inclusive DIS asymmetries A_1^h and A_1. Given that the resummed exponents are identical for the spin-averaged and spin-dependent structure functions, we expect the resummation effects to be generally very modest. On the other hand, it is also clear that the effects will not cancel identically in the spin asymmetries: Even though the resummed exponents for g_1 and F_1 are identical in Mellin-moment space, they are convoluted with different parton distributions and hence no longer give identical results after Mellin inversion. Moreover, the matching procedure also introduces differences since the NLO coefficient functions are somewhat different for g_1 and F_1. It is therefore still relevant to investigate the impact of resummation on the spin asymmetries. We will compare our results to data sets from HERMES [247] and COMPASS [234, 249]. In addition, we present some results relevant for measurements at the Jefferson Laboratory [250–252], in particular those to be carried out in the near future after the CEBAF upgrade to 12 GeV [258].

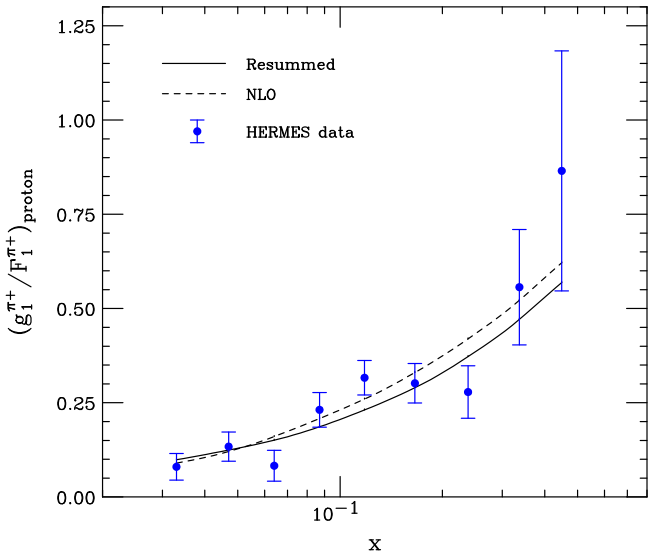

Figure 5.1: Spin asymmetry for semi-inclusive π^+ production off a proton target. The data points are from [247] and show statistical errors only. The $\langle x \rangle$ and $\langle Q^2 \rangle$ values were taken accordingly to the HERMES measurements.

For our calculations we use the NLO polarized parton distribution functions of [254, 255] and the unpolarized ones of [264]. Our choice of the latter is motivated by the fact that this set was also adopted as the baseline unpolarized set in [254, 255], so that the two sets are consistent in the sense that the same strong coupling constant is used. Additionally, in the case of SIDIS we choose the "de Florian-Sassot-Stratmann" [77] NLO set of fragmentation functions. In this work, we choose to focus only on pions in the final state. Resummation effects for other hadrons will be very similar. The factorization and renormalization scales are set to Q.
Figures 5.1 and 5.2 present comparisons of our resummed calculations with HERMES data [247] for semi-inclusive (π^+) and inclusive DIS, respectively, both off a proton target at $\sqrt{s} \approx 7.25$ GeV. The error bars show the statistical uncertainties only. For the SIDIS asymmetry, we integrate the numerator and the denominator of Eq. (5.2) separately over a region of $0.2 < z < 0.8$. We plot the theoretical results at the average values of x and Q^2 of each data point and connect the points by a line. The figures show the NLO (dashed lines) and the resummed-matched (solid lines) results. As one can see, the higher-order effects generated by resummation are indeed fairly small, although not negligible. They are overall more significant for SIDIS, which is expected due to the additional threshold logarithms in SIDIS (see discussion at the

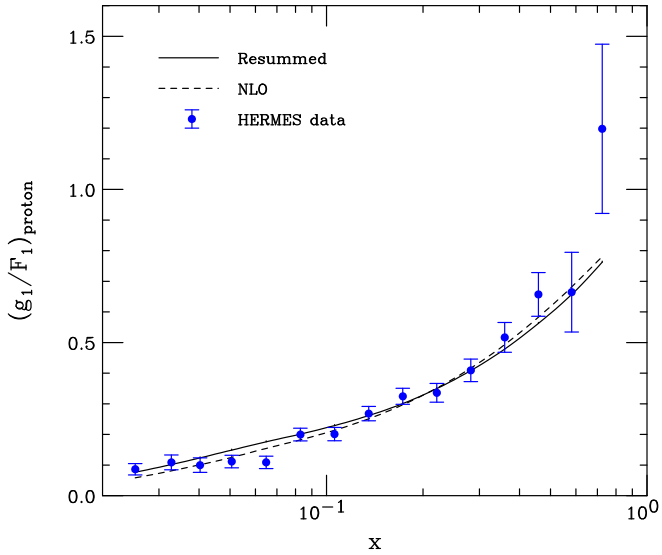

Figure 5.2: Spin asymmetry for inclusive polarized DIS off a proton target. The data points are from [248] and show statistical errors only. The $\langle x \rangle$ and $\langle Q^2 \rangle$ values were taken accordingly to the HERMES measurements.

end of Sec. 5.2.2). We expect the resummed results to be most reliable at rather high values of $x \gtrsim 0.2$ or so [J1]. In this regime, there is a clear pattern that resummation tends to decrease the spin asymmetries compared to NLO, more pronounced so for SIDIS. In other words, higher-order corrections enhance the spin-averaged cross section somewhat more strongly than the polarized one.

Figures 5.3 and 5.4 show similar comparisons to the SIDIS and DIS asymmetries measured by COMPASS [234, 249] with a polarized muon beam at $\sqrt{s} \approx$17.4 GeV. For COMPASS kinematics the effects of threshold resummation are overall somewhat smaller due to the fact that one is further away from partonic threshold because of the higher center-of-mass energy. However, the results remain qualitatively similar to what we observed for HERMES kinematics.

The inclusive *neutron* spin asymmetry is particularly interesting from the point of view of resummation, since it is known [250, 251] to exhibit a sign change at fairly large values of x. Near a zero of the polarized cross section resummation effects are expected to be particularly relevant. Figure 5.5 shows the asymmetry at NLO and for the NLL resummed case. For illustration we show the presently most precise data available, which are from the Hall-A Collaboration [250, 251] at the Jefferson Laboratory. In order to mimic the correlation of x

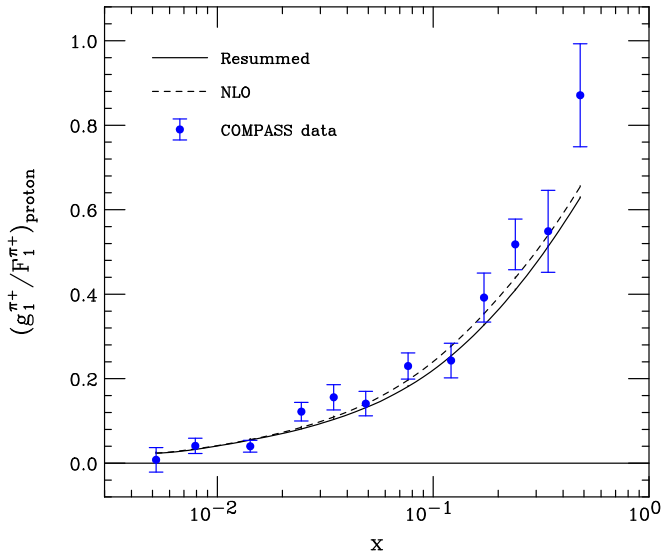

Figure 5.3: Same as Fig. 5.1 but comparing to the COMPASS measurements [234].

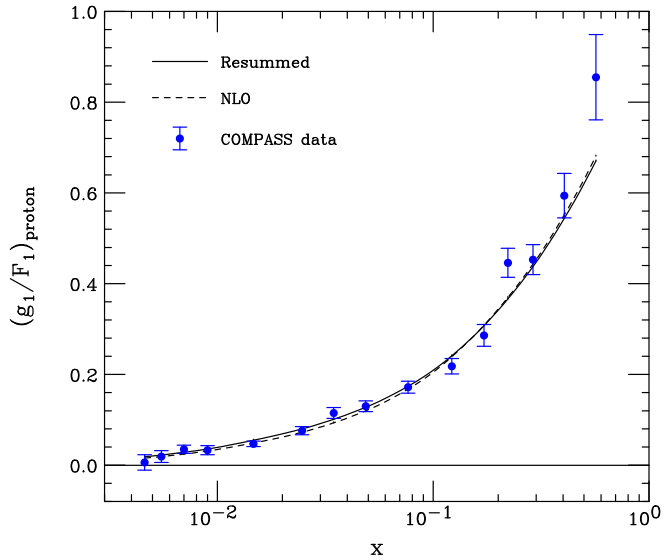

Figure 5.4: Same as Fig. 5.2 but comparing to the COMPASS measurements [249].

and Q^2 for the present Jefferson Lab kinematics, we choose $Q^2 = x \times 8$ GeV^2 in the theoretical calculation. As one can see, the effects of resummation are indeed more pronounced than for

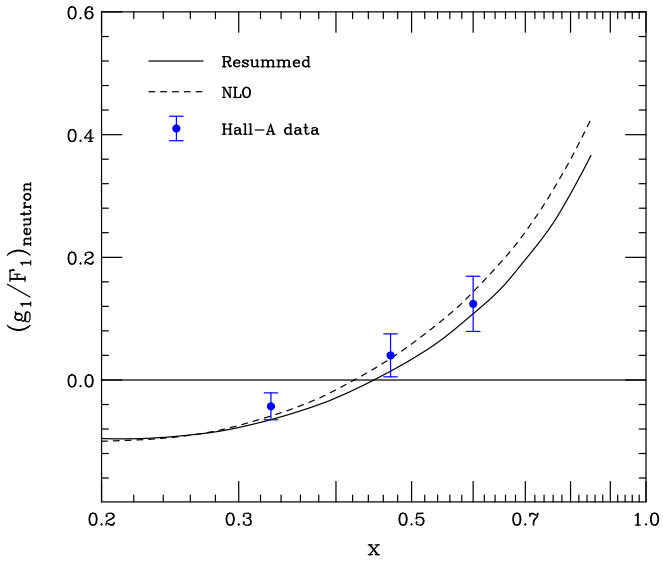

Figure 5.5: Spin asymmetry for inclusive polarized DIS off a neutron target. The data points are from [250, 251] and show statistical errors only. The Q^2 values in the theoretical calculation were chosen as $Q^2 = x \times 8$ GeV^2.

the inclusive proton structure functions considered in Figs. 5.2 and 5.4. Evidently the zero of the asymmetry shifts slightly due to resummation. On the other hand, the asymmetry is overall still quite stable with respect to the resummed higher order corrections.

The latter observation is quite relevant for the extraction of polarized large-x parton distributions from data for proton and neutron spin asymmetries in lepton scattering. For instance, to good approximation [250, 251] one may use the inclusive structure functions to directly determine the combinations $(\Delta u + \Delta\bar{u})/(u + \bar{u})$ and $(\Delta d + \Delta\bar{d})/(d + \bar{d})$. At lowest order, and neglecting the contributions from strange and heavier quarks and antiquarks, one has

$$\begin{aligned} R_u &\equiv \frac{\Delta u + \Delta\bar{u}}{u + \bar{u}}(x, Q^2) = \frac{4g_{1,\rm p} - g_{1,\rm n}}{4F_{1,\rm p} - F_{1,\rm n}}(x, Q^2)\,, \\ R_d &\equiv \frac{\Delta d + \Delta\bar{d}}{d + \bar{d}}(x, Q^2) = \frac{4g_{1,\rm n} - g_{1,\rm p}}{4F_{1,\rm n} - F_{1,\rm p}}(x, Q^2)\,, \end{aligned} \tag{5.23}$$

where the subscripts p,n denote a proton or neutron target, respectively. One may therefore determine $(\Delta u+\Delta\bar{u})/(u+\bar{u})$ and $(\Delta d+\Delta\bar{d})/(d+\bar{d})$ directly from experiment by using measured

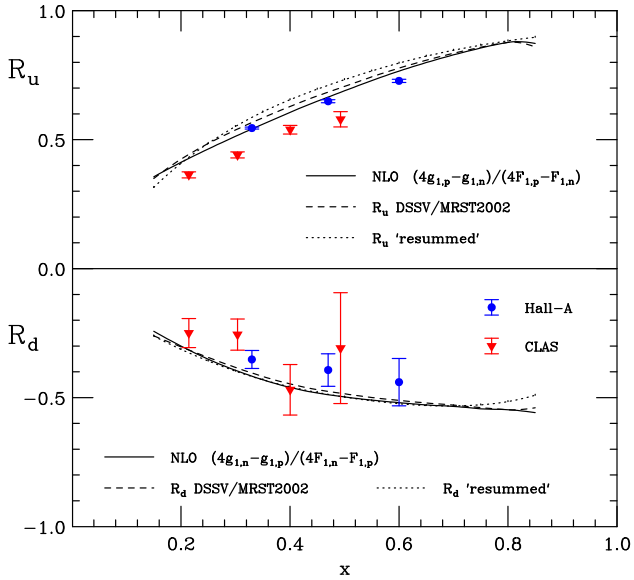

Figure 5.6: High-x up and down polarizations $(\Delta u + \Delta\bar{u})/(u + \bar{u})$ and $(\Delta d + \Delta\bar{d})/(d + \bar{d})$. The solid lines show the ratios of structure functions on the right-hand sides of Eq. (5.23), while the dashed lines show the actual parton distribution ratios as represented by the NLO sets of [254, 255] and [264]. The dotted lines show the expected shift of the distributions when resummation effects are included in their extraction, using Eq. (5.24). The Q^2 values in the theoretical calculation were chosen as $Q^2 = x \times 8$ GeV^2. We also show the present Hall-A [250, 251] and CLAS [252] data obtained from inclusive DIS measurements. Their error bars are statistical only.

structure functions $g_{1,\mathrm{p}}, g_{1,\mathrm{n}}, F_{1,\mathrm{p}}, F_{1,\mathrm{n}}$ in (5.23). Up to certain refinements required by the fact that measurements of the ratios $g_{1,\mathrm{p}}/F_{1,\mathrm{p}}$ and $g_{1,\mathrm{n}}/F_{1,\mathrm{n}}$ are more readily available than those of the individual structure functions, this is essentially the approach used by the Hall-A Collaboration (alternatively, one may also use the corresponding spin asymmetry for the deuteron instead of the neutron one [252]). In the following we explore the typical size of the corrections to the ratios due to higher orders. Figure 5.6 shows first of all the structure function ratios on the right-hand side of (5.23), computed at NLO using as before the polarized and unpolarized parton distribution functions of [254, 255] and [264], respectively (solid lines). We have again chosen $Q^2 = x \times 8$ GeV^2. Using (5.23), these ratios would correspond to the "direct experimental determinations" of R_u and R_d. The dashed lines in the figure show the actual ratios $(\Delta u + \Delta\bar{u})/(u + \bar{u})$ and $(\Delta d + \Delta\bar{d})/(d + \bar{d})$ as given by the sets of parton distribution

functions that we use. Any difference between the solid and dashed lines is, therefore, a measure of the significance of effects related to strange quarks and antiquarks, and to NLO corrections. As one can see, these have relatively modest size. Finally, we estimate the potential effect of resummation on R_u, R_d: Following [189, 210], we define 'resummed' quark (and antiquark) distributions by demanding that their contributions to the structure functions g_1, F_1 match those of the corresponding NLO distributions, which is ensured by setting

$$\tilde{q}^{N,\mathrm{res}}(Q^2) \equiv \frac{\tilde{\mathcal{C}}_q^{\mathrm{NLO}}(N,\alpha_s(Q^2))}{\tilde{\mathcal{C}}_q^{\mathrm{res}}(N,\alpha_s(Q^2))}\tilde{q}^{N,\mathrm{NLO}}(Q^2) \tag{5.24}$$

in Mellin-moment space. Here, $\tilde{\mathcal{C}}_q^{\mathrm{NLO}}$ and $\tilde{\mathcal{C}}_q^{\mathrm{res}}$ are the NLO and resummed quark coefficient functions for the inclusive structure function F_1, respectively. We match the resummed coefficient function to the NLO one by subtracting out its NLO contribution and adding the full NLO one, in analogy with (5.20). Equation (5.24) can be straightforwardly extended to the spin-dependent case. The ratios R_u, R_d for these 'resummed' parton distributions are shown by the dotted lines in Fig. 5.6. As one can see, they are quite close to the other results, indicating that resummation is not likely to induce very large changes in the parton polarizations extracted from future high-precision data. For illustration, we also show the Hall-A [250, 251] and CLAS [252] data in the figure, which have been obtained using parton-model relations for the inclusive structure functions, similar to (5.23). One can see that the error bars of the data are presently still larger than the differences between our various theoretical results. This situation is expected to be improved with the advent of the Jefferson Lab 12-GeV upgrade [258] or an Electron Ion Collider [265]. As is well-known, SIDIS measurements provide additional information on R_u, R_d, albeit so far primarily at lower x [247].

5.4 Conclusions

In this chapter we have presented the results of [J2]. There, we have investigated the size of threshold resummation effects on double-longitudinal spin asymmetries for inclusive and semi-inclusive deep inelastic scattering in fixed-target experiments. Overall, the asymmetries are rather stable with respect to resummation, in particular for the inclusive case. Towards large values of x, resummation tends to cause a decrease of the spin asymmetries, which is more pronounced in the semi-inclusive case and for asymmetries measured off neutron targets.

The relative robustness of the spin asymmetries bodes well for the extraction of high-x parton polarizations $(\Delta u + \Delta\bar{u})/(u + \bar{u})$ and $(\Delta d + \Delta\bar{d})/(d + \bar{d})$, which are consequently also rather robust. Nevertheless, knowledge of the predicted higher-order corrections should be quite relevant when future high-statistics large-x data become available. On the theoretical side, it will be interesting to study the interplay of our perturbative corrections with power corrections that are ultimately also expected to become important at high-x [198, 204, 259, 260, 266–269], although it appears likely that present data are in a window where the perturbative corrections clearly dominate. Finally, we note that related large-x logarithmic effects have also been investigated for the nucleon's light cone wave function [270], where they turn out to enhance components of the wave function with non-zero orbital angular momentum, impacting the large-x behavior of parton distributions. It will be very worthwhile to explore the possible connections between the logarithmic corrections discussed here and in [270].

Appendices

APPENDIX A

Basics of $\mathfrak{su}(N)$ Lie Algebra

In this appendix we will present a general idea of Lie groups and algebras without going too much into the mathematical details of group and representation theory. We will then focus our attention on $SU(N)$ groups and $\mathfrak{su}(N)$ algebras giving the practical instruments used in many non-Abelian gauge theories derivations, such as Casimir operators and quadratic Casimir operators. We refer to [271] and [272].

A.1 General aspects of Lie algebras and groups

If we consider gauge theories, the local symmetry transformations act on a set of quantum fields that satisfies the requirements given mathematically by the Lagrangian. In most of these theories, those transformations can be represented by continuously generated groups, meaning roughly that the group G contains elements arbitrarily close to the identity (called infinitesimal group elements), such that each element of G can be reached by sequential action of those infinitesimal elements. An infinitesimal element g can then be written as

$$g(\theta) = 1 + i\theta^a T^a + \mathcal{O}(\theta^2) \tag{A.1}$$

where θ^a are infinitesimal parameters and T^a are Hermitian operators called *generators* of the

symmetry group. Such a continuous group with this structure is called a *Lie Group*. The vector space $\mathfrak{g}$ in which the T^as live can be equipped with a binary and bilinear operation $[\cdot,\cdot] : \mathfrak{g} \times \mathfrak{g} \to \mathfrak{g}$ called the Lie product that satisfies two requirements:

- it is *alternating* on $\mathfrak{g}$

$$[T^a, T^a] = 0 \qquad \forall T^a \in \mathfrak{g} \tag{A.2}$$

- it satisfies the *Jacobi identity*

$$[T^a, [T^b, T^c]] + [T^b, [T^c, T^a]] + [T^c, [T^a, T^b]] = 0 \qquad \forall T^a, T^b, T^c \in \mathfrak{g}. \tag{A.3}$$

Such an algebraic structure is called *Lie algebra*. Since we normally work with $N \times N$ matrix representation of the Lie algebra, due to the associativity of the matrix product the Lie product becomes the well-known *commutator* operator (for more details refer to text book such as [273]). In this case the commutation relations of the generators T^a can be written as

$$\left[T^a, T^b\right] = i f^{abc} T^c \tag{A.4}$$

where the f^{abc} are called structure constants. The Jacobi identity can then be rewritten using the structure constants as

$$f^{ade} f^{bcd} + f^{bde} f^{cad} + f^{cde} f^{abd} = 0 \tag{A.5}$$

The connection between a Lie group and its algebra is provided by the *exponential map*

$$\begin{aligned} \exp :& \mathfrak{g} \longrightarrow G \\ & T^a \to U = \exp\{i T^a \theta_a\} \end{aligned} \tag{A.6}$$

where $U \in G$.

Another thing to be noticed is that the Lagrangian of a non-Abelian gauge theory depends only on the Lie algebra of the local symmetry. Thus, finding "the right way to express" the Lie algebra of the local symmetry is a crucial point in developing a theory. In rigorous terms we would say that we have to find the right *representation* of the Lie algebra (hence of the Lie group) that describes the reality that we see. To make this statement more clear let's bring up an example and take a symmetry transformation like the rotation of an object. The abstract 3D rotation group is defined, in mathematics, as the group of orthogonal 3×3 matrices with

$det = 1$ and denoted as $SO(3)$. However we can rotate every kind of object: shapes, vector spaces, fields, sets of numbers and so on. The explicit expressions of the operators performing the transformation will depend on the object that we are rotating. We will say that the different sets of operators are expressed in a particular representation of the abstract rotation symmetry group. In other words, the representation tells us how the rotation is performed on the specific object, while the rotation group gives the abstract concept of rotation. Or in a more abstract way, a representation of a Lie group G (or analogous for a Lie algebra $\mathfrak{g}$) is a map that associates each element of the abstract symmetry group (algebra) to a linear transformation acting on the "specific object" (formally speaking, acting on a vector space describing the object) in a homomorphic way.

When we construct a gauge theory, we will start by individuating from our observations the symmetry that we want our Lagrangian to have and then, according to the gauge principle, we will modify the expression of the Lagrangian in order for this symmetry to hold also locally. For most of today's gauge theories, the local symmetries are described by unitary transformations (which of course act on a set of fields). Thus we constrain our interest on Lie algebras with finite-dimensional Hermitian representation. The corresponding Lie group representation would be unitary and finite-dimensional. For our purposes we will also assume that the number of generators are finite, hence we will work with *compact* Lie algebras. Let's consider the simplest case when one of the T^a generators commutes with all the others. The group generated would be an Abelian group called $U(1)$ and the elements of it act on the fields as follows

$$\psi \to U\psi \qquad \text{with} \quad U = \exp\{i\theta\} \in G. \tag{A.7}$$

This group is well known to be the symmetry group of the quantum field theory of the electrodynamic interaction QED.

If a Lie algebra doesn't contain such commutating elements, it is called *semi-simple* and if, in addition, the Lie algebra can't be divided into two mutually commutating sets of generators, it is called *simple*. All simple, compact Lie algebras can be grouped in three infinite families (with just five exceptions) according to the characteristics of their corresponding generated Lie groups: the so-called *classical groups*. Those three families of classical groups are defined in terms of matrix representations and are:

1. *Unitary transformations of N-dimensional vectors.*

2. *Orthogonal transformations of N-dimensional vectors.*

3. *Symplectic transformations of of N-dimensional vectors.*

For the purposes of this thesis we will consider only the first family in which the $SU(N)$ groups are included. The pure phase transformation of A.7 is a unitary transformation which commutates with all other unitary transformations. If we subtract the corresponding $U(1)$ group to the other unitary groups, we obtain a simple Lie group called $SU(N)$.

A.2 $\mathfrak{su}(N)$ algebra

$SU(N)$ is the group of $N \times N$ unitary transformation U with $\det(U) = 1$. Its generators will be represented by Hermitian matrices t^a. As discussed before, all generators will be orthogonal to the generator of A.7. Thus, the generator of $SU(N)$ must be Hermitian traceless matrices

$$\mathrm{tr}[t^a] = 0. \tag{A.8}$$

There are $N^2 - 1$ independent Hermitian traceless matrices satisfying the above condition. Any finite set of $d \times d$-Hermitian matrices satisfying A.7 and A.4, is a d-dimensional representation of the $\mathfrak{su}(N)$ Lie algebra. Moreover, every such representation can be decomposed in a direct sum of *irreducible* representation by choosing a basis in which all representation matrices are block-diagonal. In QFT we work with irreducible representations. From now on, we will imply that a certain set of generators are expressed in an irreducible representation r by simply referring to them as t_r^a. For every irreducible representation, we have

$$\mathrm{tr}[t_r^a, t_r^b] = C(r)\delta^{ab}, \tag{A.9}$$

where $C(r)$ is a constant called *Casimir operator* which depends on the irreducible representation. This relation together with A.4 assures that the structure constants f^{abc} are totally antisymmetric for every irreducible representation since

$$f^{abc} = -\frac{i}{C(r)}\mathrm{tr}\left\{[t_r^a, t_r^b]t_r^c\right\}. \tag{A.10}$$

Using this property we can show, in analogy to the well know J^2 operator in the $\mathfrak{su}(2)$ group's algebra, that t_r^2 commutates with all other generators for every $\mathfrak{su}(N)$ algebra

$$\begin{aligned}[t^b, t^a t^a] &= (if^{bac}t^c)t^a + t^a(if^{bac}t^c)) \\ &= if^{bac}\{t^c, t^a\} = -if^{abc}\{t^c, t^a\} \\ &= 0.\end{aligned} \tag{A.11}$$

For a given irreducible representation we then have

$$t_r^a t_r^a = C_2(r) \cdot I_{d(r)} \tag{A.12}$$

where $I_{d(r)}$ is the $d(r) \times d(r)$-unit matrix ($d(r)$ is the dimension of the representation) and $C_2(r)$ is the so-called *quadratic Casimir constant*.

For every irreducible representation r we can define the associated *conjugate* representation $\bar{r}$ with matrices $t_{\bar{r}}^a$ by taking the conjugate of the infinitesimal transformation expressed in the representation r

$$\psi^* \to (1 - i\theta^a (t_r^a)^*)\psi^* = (1 + i\theta^a t_{\bar{r}}^a)\psi^* \tag{A.13}$$

where the relation between the matrices is $t_{\bar{r}}^a = -(t_r^a)^* = -(t_r^a)^T$.

Among all irreducible finite-dimensional representations of $\mathfrak{su}(N)$, two are of great interest for most QFT theories: the *fundamental* representation and the *adjoint* representation. The first one is also called the basic N-dimensional complex vector representation. It is a N-dimensional representation where the $N^2 - 1$ t_F^a are $N \times N$-Hermitian matrices. For $N > 2$ this representation is complex and the corresponding conjugate representation $\bar{F}$ is inequivalent. If we define $t_F^a \equiv \frac{\lambda^a}{2}$, for N=2 the λ^a are the usual Pauli matrices σ_i. For $N = 3$ they are called Gell-Mann matrices and are

$$\lambda^1 = \begin{pmatrix} 0 & 1 & 0 \\ 1 & 0 & 0 \\ 0 & 0 & 0 \end{pmatrix}, \quad \lambda^2 = \begin{pmatrix} 0 & -i & 0 \\ i & 0 & 0 \\ 0 & 0 & 0 \end{pmatrix}, \quad \lambda^3 = \begin{pmatrix} 1 & 0 & 0 \\ 0 & -1 & 0 \\ 0 & 0 & 0 \end{pmatrix}, \quad \lambda^4 = \begin{pmatrix} 0 & 0 & 1 \\ 0 & 0 & 0 \\ 1 & 0 & 0 \end{pmatrix},$$

$$\lambda^5 = \begin{pmatrix} 0 & 0 & -i \\ 0 & 0 & 0 \\ i & 0 & 0 \end{pmatrix}, \quad \lambda^6 = \begin{pmatrix} 0 & 0 & 0 \\ 0 & 0 & 1 \\ 0 & 1 & 0 \end{pmatrix}, \quad \lambda^7 = \begin{pmatrix} 0 & 0 & 0 \\ 0 & 0 & -i \\ 0 & i & 0 \end{pmatrix}, \quad \lambda^8 = \begin{pmatrix} 1 & 0 & 0 \\ 0 & 1 & 0 \\ 0 & 0 & -2 \end{pmatrix}. \tag{A.14}$$

The matrices satisfy the anticommutation relation

$$\left\{\lambda^a, \lambda^b\right\} \frac{4}{N}\delta^{ab} I_N + 2d^{abc} \tag{A.15}$$

where d^{abc} are totally symmetric. For $\mathfrak{su}(3)$ the only non zero f^{abc} and d^{abc} are

$$\begin{aligned} &\frac{1}{2}f^{123} = f^{147} = -f^{156} = f^{246} = f^{257} = f^{345} = -f^{367} = \frac{1}{\sqrt{3}}f^{458} = \frac{1}{\sqrt{3}}f^{678} = \frac{1}{2}, \\ &d^{146} = d^{157} = -d^{247} = d^{256} = d^{344} = d^{355} = -d^{366} = -d^{377} = \frac{1}{2}, \\ &d^{118} = d^{228} = d^{338} = -2d^{448} = -2d^{558} = -2d^{668} = -2d^{778} = -d^{888} = \frac{1}{\sqrt{3}}. \end{aligned} \tag{A.16}$$

The Casimir operator and the quadratic Casimir constant for the fundamental representation are

$$C(F) = \frac{1}{2} \equiv T_R, \qquad C_2(F) = \frac{N^2-1}{2N} \equiv C_F. \tag{A.17}$$

In this thesis we refer to the quadratic Casimir constant of the fundamental representation as C_F and to the Casimir operator of the fundamental representation as T_R according to the common convention used in many particle physics textbooks.

The representation to which the generators of the $\mathfrak{su}(N)$ algebra naturally belong is called the adjoint representation A. It is given by the $(N^2-1)\times(N^2-1)$-matrices with matrix elements given by the structure constants

$$(t_A^b)_{ac} = if^{abc}. \tag{A.18}$$

Since the structure constants are antisymmetric and real, $t_A^a = -(t_A^a)^*$. The adjoint representation is a real representation. The Casimir operator and the quadratic Casimir constant for the adjoint representation are

$$C(A) = C_2(A) \equiv C_A = N. \tag{A.19}$$

Another useful relation is the following

$$\mathrm{tr}\left[t_A^a t_A^b\right] = f^{abc}f^{bcd} = C_A\delta_{ab}. \tag{A.20}$$

Until now we have dealt with single objects which transform according to a representation. However, when we work with particle physics, we are interested in quantum states of more

particles together, which can each transform according to different irreducible representations of the $SU(N)$. Formally speaking, we are interested in the direct product of the different representations. Such a product is not in general an irreducible representation itself but can be decomposed into a direct sum of irreducible representations. For example, if we choose $N = 3$ and we take particles such as quarks and antiquarks, which transform according to the fundamental F and the conjugate of the fundamental representation $\bar{F}$ of $SU(3)$ respectively, we end up with different possible new particles corresponding to the different irreducible representation in which the product of the original representations can be decomposed:

$$q\bar{q} : \underline{3} \otimes \underline{3}^* = \underline{1} \oplus \underline{8}, \tag{A.21}$$

$$qqq : \underline{3} \otimes \underline{3} \otimes \underline{3} = \underline{1} \oplus \underline{8} \oplus \underline{8} \oplus \underline{10}, \tag{A.22}$$

$$qq : \underline{3} \otimes \underline{3} = \underline{3}^* \oplus \underline{6},$$

$$\dots$$

The numbers with a bottom bar refer to the dimensionality of the irreducible representation and the uppercase star indicates that it's the conjugate representation. The mathematical instrument thanks to which it is possible to systematically calculate the decomposition of products of irreducible representation into direct sums of irreducible representation is called *Young tableau*.

APPENDIX B

Mellin Transformation

A useful tool that is widely used in perturbative QCD is the Mellin transform. The direct and inverse transformations are defined in an integral form as follows

$$\begin{aligned} f^{(N)}(N) &= \int_0^1 dx x^{N-1} f(x), \\ f(x) &= \frac{1}{2\pi i} \int_{\mathcal{C}_N} dN x^{-N} f^{(N)}, \end{aligned} \tag{B.1}$$

where $\mathcal{C}_N$ is a contour in the complex plane. To perform the inverse transform, standard tools of the complex analysis (such as the residue theorem, the analytic continuations and so on) are needed. The $f^{(N)}$ is also referred in literature as the *Mellin moment* of the function $f(x)$. One of the most used properties of Mellin transforms is that in Mellin space the convolution of two functions $f(x) \otimes g(x)$ factorizes in the simple product of the two correspondent Mellin moments $f^{(N)} \cdot g^{(N)}$:

$$\begin{aligned} \int_0^1 dx x^{N-1} \int_x^1 \frac{dz}{z} f(z) g\left(\frac{x}{z}\right) &= \int_0^1 dx x^{N-1} \left[\int_0^1 dz \int_0^1 f(z) g(y) \delta(x - yz) \right] \\ &= \int_0^1 dz z^{N-1} f(z) \int_0^1 dy y^{N-1} g(y) = f^{(N)} \cdot g^{(N)}. \end{aligned} \tag{B.2}$$

As an example on how a typical calculation of a moment is made, we take the plus distribution $\frac{1}{(1-x)_+}$ and explicitly compute its Mellin moment:

$$\begin{aligned}\left(\frac{1}{(1-x)_+}\right)^{(N)} &= \int_0^1 \frac{x^{N-1}}{(1-x)_+} = \int_0^1 \frac{x^{N-1}-1}{1-x} = \sum_{j=0}^{\infty} \int_0^1 dx \left(x^{N-1}-1\right) x^j \\ &= \sum_{j=0}^{\infty} \left(\frac{1}{N+j} - \frac{1}{j+1}\right) = -\sum_{j=0}^{N-2} \frac{1}{j+1} \\ &= -\sum_{j=1}^{N-1} \frac{1}{j}. \end{aligned} \tag{B.3}$$

In Table B.1 we summarize the most important Mellin moments used throughout the work discussed in this thesis. The factor $\frac{-\pi^2}{6}$ in the third line is evaluated continuing analytically

$f(x)$	$f^{(N)}$
1	$\frac{1}{N}$
$\ln x$	$-\frac{1}{N^2}$
$\frac{\ln x}{1-x}$	$-\frac{1}{6}\pi^2 + \sum_{j=1}^{N-1} \frac{1}{j^2}$
$\ln(1-x)$	$-\frac{1}{N}\sum_{j=1}^{N} \frac{1}{j}$
$\delta(1-x)$	1
$\frac{1}{(1-x)_+}$	$-\sum_{j=1}^{N-1} \frac{1}{j}$
$\left(\frac{\ln(1-x)}{1-x}\right)_+$	$\sum_{k=1}^{N-1} \frac{1}{k} \sum_{j=1}^{k} \frac{1}{j}$

Table B.1: Mellin moments used throughout this thesis' work.

the series $\sum_{j=1}^{\infty} j^{-2}$ in the complex plane with the Riemann zeta function

$$\zeta(z) = \sum_{j=1}^{\infty} j^{-z}.$$

For $\Re(z) > 1$ the series converges and we have that $\zeta(2) = \frac{\pi^2}{6}$. The analytical continuation is also used to perform the inverse transformation of the moments. The resummation of threshold logarithms, for example, is made in Mellin space and the final result has to be brought back to the x-space. Hence, we have to be able to analytically continue in the complex plane the Mellin moments of plus distributions as the one shown in the two last lines of Table B.1. Let's start by defyining from the Γ-function the *digamma function* $\psi(z)$ as

$$\psi(z) = \frac{d}{dz} \ln \Gamma(z) = \frac{\Gamma'(z)}{\Gamma(z)}, \tag{B.4}$$

and the *polygamma function* of order m as

$$\psi^{(m)}(z) = \frac{d^m}{dz^m} \psi(x) = \frac{d^{m+1}}{dz^{m+1}} \ln \Gamma(z). \tag{B.5}$$

Let's consider now the partial sum $S_k(N)$ defined as

$$S_k(N) = \sum_{j=1}^{N} \frac{1}{j^k}. \tag{B.6}$$

For $k = 1$ it coincide with the N^{th} harmonic number defined by $H_N = \sum_{j=1}^{N} \frac{1}{j}$. The digamma function can be expressed in terms of the harmonic number as

$$S_1(N) = \sum_{j=1}^{N} \frac{1}{j} = H_N = \psi(N+1) + \gamma_E, \tag{B.7}$$

where γ_E is the Euler-Mascheroni constant defined by the relation

$$\lim_{N \to \infty} (H_N - \ln N) = \gamma_E \approx 0,577215. \tag{B.8}$$

For large values of N (i.e. for $x \to 1$ in the x-space), the moment of the simple plus distribution of the second last line in Table B.1 can be approximated as follows

$$\left(\frac{1}{(1-x)_+} \right)^{(N)} \xrightarrow[N \to \infty]{} -S_1(N) \to -\psi(N) \to -\left(\ln N + \gamma_E + \frac{1}{N} \right) = -\ln \bar{N} + \mathcal{O}\left(\frac{1}{N} \right), \tag{B.9}$$

where $\bar{N} = Ne^{\gamma_E}$. Using the relation below

$$\sum_{j=1}^{N} \frac{1}{j} \sum_{i=1}^{j} \frac{1}{i} = \frac{1}{2} \left(S_1^2(N) + S_2(N) \right), \tag{B.10}$$

we can also give the moment of the logarithmic plus distribution for large N:

$$\left(\left(\frac{\ln(1-x)}{1-x} \right)_+ \right)^{(N)} \xrightarrow[N\to\infty]{} \frac{1}{2} \left(S_1^2(N) + S_2(N) \right) \to \frac{1}{2} \left(\ln^2 \bar{N} + \frac{\pi^2}{6} \right) = \frac{1}{2} \ln^2 \bar{N} + \mathcal{O}(\ln \bar{N}). \tag{B.11}$$

As last point of this appendix, we observe that multiplying a function $f(x)$ by a factor x^i just shifts the variable $N \to N + i$ in the expression for $f^{(N)}$, e.g.

$$\left(x^2 \left(\frac{\ln(1-x)}{1-x} \right)_+ \right)^{(N)} = \sum_{k=1}^{N+1} \frac{1}{k} \sum_{j=1}^{k} \frac{1}{j}. \tag{B.12}$$

APPENDIX C

NLO Coefficient functions

In this appendix we present literature results for DIS and SIA coefficient functions useful for our discussion in Chapter 3.

C.1 DIS Coefficient Functions

The DIS coefficient functions up to NLO in the $\overline{\text{MS}}$ scheme are given by [48, 205, 261]

$$\begin{aligned}
\mathcal{C}_q^1(\hat{x}) =& e_q^2\delta(1-\hat{x}) + e_q^2\frac{\alpha_s}{2\pi}C_F\left[(1+\hat{x}^2)\left(\frac{\ln(1-\hat{x})}{1-\hat{x}}\right)_+ - \frac{3}{2}\frac{1}{(1-\hat{x})_+} - \frac{1+\hat{x}^2}{1-\hat{x}}\ln\hat{x} + 3\right.\\
&\left. - \left(-\frac{9}{2}+\frac{\pi^2}{3}\right)\delta(1-\hat{x})\right]\\
\mathcal{C}_q^L(\hat{x}) =& e_q^2\frac{\alpha_s}{2\pi}C_F\,2\hat{x}\\
\mathcal{C}_g^1(\hat{x}) =& e_q^2\frac{\alpha_s}{2\pi}C_F\left[\left(\hat{x}^2+(1-\hat{x})^2\right)\ln\left(\frac{1-\hat{x}}{\hat{x}}\right) - 1 + 4\hat{x}(1-\hat{x})\right]\\
\mathcal{C}_g^L(\hat{x}) =& e_q^2\frac{\alpha_s}{2\pi}C_F\left[4\hat{x}(1-\hat{x})\right]
\end{aligned} \tag{C.1}$$

where $j = q$, g and $\hat{x} = \xi/x$ and e_q is the fractional QED charge of the quark q. The definitions of x and ξ are given in Eqs. (3.5) and (3.6). These coefficients satisfy

$$\mathcal{C}_j^2(\hat{x}) = \mathcal{C}_j^1(\hat{x}) + \mathcal{C}_j^L(\hat{x})\,. \tag{C.2}$$

These coefficient functions are related to the coefficient functions h_i $(i = 1, 2, L)$ defined in [192] as follows

$$\mathcal{C}^1(\hat{x}) = 2h_1(\hat{x}) \quad \mathcal{C}^L(\hat{x}) = 2h_L(\hat{x}) \quad \mathcal{C}^2(\hat{x}) = \frac{h_2(\hat{x})}{\hat{x}} \tag{C.3}$$

so that

$$h_L = -h_1 + \frac{h_2}{\hat{x}}. \tag{C.4}$$

The structure function F_i^{AQ} $(i = 1, 2, L)$ presented in the same paper are connected to the ones defined in Eq. (3.11) by the following relations

$$\begin{aligned} F_1^{\mathrm{AQ}}(x_B, Q^2) &= \frac{\mathcal{F}_1^{\mathrm{TMC}}(x_B, Q^2)}{2} = F_1^{\mathrm{TMC}}(x_B, Q^2) \\ F_2^{\mathrm{AQ}}(x_B, Q^2) &= x_B \mathcal{F}_2^{\mathrm{TMC}}(x_B, Q^2) = F_2^{\mathrm{TMC}}(x_B, Q^2) \\ F_{L,}^{\mathrm{AQ}}(x_B, Q^2) &= \frac{\mathcal{F}_L^{\mathrm{TMC}}(x_B, Q^2)}{2} = \frac{F_L^{\mathrm{TMC}}(x_B, Q^2)}{2x_B} \end{aligned} \tag{C.5}$$

so that

$$F_L^{\mathrm{AQ}} = \frac{\rho^2}{2x_B} F_2^{\mathrm{AQ}} - F_1^{\mathrm{AQ}}, \tag{C.6}$$

where ρ is defined in Eq. (3.12).

C.2 SIA Coefficient Functions

The coefficient functions up to NLO for SIA in the $\overline{\mathrm{MS}}$ scheme are given by [48, 72, 109, 111]

$$\begin{aligned} \hat{\mathcal{C}}_q^1(\hat{z}) =& e_q^2 \delta(1-\hat{z}) + e_q^2 \frac{\alpha_s}{2\pi} C_F \left[(1+\hat{z}^2) \left(\frac{\ln(1-\hat{z})}{1-\hat{z}} \right)_+ - \frac{3}{2} \frac{1}{(1-\hat{z})_+} + 2\frac{1+\hat{z}^2}{1-\hat{z}} \ln \hat{z} + \frac{3}{2}(1-\hat{z}) \right. \\ & \left. + \left(\frac{2}{3}\pi^2 - \frac{9}{2} \right) \delta(1-\hat{z}) \right] \end{aligned}$$

$$
\begin{aligned}
\hat{\mathcal{C}}_q^L(\hat{z}) =& e_q^2 \frac{\alpha_s}{2\pi} C_F \\
\hat{\mathcal{C}}_g^1(\hat{z}) =& e_q^2 \frac{\alpha_s}{2\pi} C_F \, 2\left[\frac{1+(1-\hat{z})^2}{\hat{z}} \ln\left(\hat{z}^2(1-\hat{z})\right) - 2\frac{(1-\hat{z})}{\hat{z}}\right] \\
\hat{\mathcal{C}}_g^L(\hat{z}) =& e_q^2 \frac{\alpha_s}{2\pi} C_F \, \left[4\frac{(1-\hat{z})}{\hat{z}}\right] \,,
\end{aligned} \tag{C.7}
$$

where $j = q$, g and $\hat{z} = \xi_E/z$. The definitions of z and ξ_E are given in Eqs. (3.49) and (3.47). The listed coefficient functions are related by

$$
\hat{\mathcal{C}}_j^2(\hat{x}) = \hat{\mathcal{C}}_j^1(\hat{x}) + \hat{\mathcal{C}}_j^L(\hat{x}) \,. \tag{C.8}
$$

APPENDIX D

Reconstruction of scales for SIDIS

In this appendix we present a recursive method to calculate the structure of the dependence on the factorization and renormalization scales for the SIDIS process at any arbitrary fixed order in the strong coupling constant α_s. An all-order valid formula is then given for the first term in Eq. 4.21 as an example.

D.1 Reconstruction of scales

In order to reconstruct the full dependences on the factorization scales μ_F and μ_I at every order in perturbation theory, one can use a renormalization group approach similar to what was done in [169] for the totally inclusive DIS case or in Chapter 2 [J5] for the semi-inclusive electron-positron annihilation (SIA). In Chapter 2, an alternative method based on the mass factorization procedure was discussed in order to obtain the same results. We have extended both methods to the SIDIS case and found full agreement between them.
Hereinafter, we will review the extension of the renormalization group approach method to the SIDIS case in order to present a general recursive formula which can be utilize to reconstruct the scale dependence on the two factorization scales μ_I and μ_F at an arbitrary order in the strong coupling constant $a_s = \alpha_s/4\pi$. We are going to show the calculation only for the first term in Eq. 4.21 since it is the most complicated case due to its matrix structure. To simplify

the calculation we set the renormalization scale $\mu_r = \mu_F$ but keep $\mu_F \neq \mu_I \neq Q^2$. The reintroduction of the renormalization scale dependence can be easily achieved by re-expanding the result expressed as a function of $a_s(\mu_F^2)$ in terms of $a_s(\mu_r^2)$. The third order expansion of a_s reads [170]

$$\begin{aligned} a_s(\mu^2) = &\frac{a_s(\mu_0^2)}{X(\mu^2)} - \frac{a_s^2(\mu_0^2)}{X^2(\mu^2)}\left(\frac{\beta_1}{\beta_0}\log X(\mu^2)\right) \\ &+ \frac{a_s^3(\mu_0^2)}{X^3(\mu^2)}\left(\frac{\beta_1^2}{\beta_0^2}\Big(\log^2 X(\mu^2) - \log X(\mu^2) - 1 + X(\mu^2)\Big) + \frac{\beta_2}{\beta_0}\Big(1 - X(\mu^2)\Big)\right) + \dots . \end{aligned} \tag{D.1}$$

where $X(\mu^2) = 1 - \beta_0 \log(\mu_0^2/\mu^2)$, and μ_0 is a reference scale that in our case corresponds to μ_r. We denote

$$\begin{aligned} F_k^S(\mu_I^2, \mu_F^2) &= (q_S, g)(\mu_I^2) \otimes \begin{pmatrix} \mathcal{C}_k^{S,D_S} & \mathcal{C}_k^{S,g} \\ \mathcal{C}_k^{g,D_S} & \mathcal{C}_k^{g,g} \end{pmatrix} \left(a_s(\mu_F^2), L_I, L_M\right) \otimes \begin{pmatrix} D_S^h \\ D_g^h \end{pmatrix}(\mu_F^2) \\ &= \boldsymbol{q}(\mu_I^2) \otimes \boldsymbol{\mathcal{C}}_k^S\left(a_s(\mu_F^2), L_I, L_M\right) \otimes \boldsymbol{D}_S^h(\mu_F^2) \,, \end{aligned} \tag{D.2}$$

where $k \in \{1,\, L\}$, $L_I = \log(Q^2/\mu_I^2)$, $L_F = \log(Q^2/\mu_F^2)$ and the dependences on x and z were dropped for clarity in the notation. By taking the double Mellin transformation of the previous equation, we can further simplify the calculation. Since convolutions between functions are represented in Mellin space by simple multiplications between moments of them, we can then write

$$\tilde{F}_k^S(N, M, \mu_I^2, \mu_F^2, Q^2) = \tilde{\boldsymbol{q}}^N(\mu_I^2) \times \tilde{\boldsymbol{\mathcal{C}}}_k^S\left(N, M, \alpha_s(\mu_F^2), L_I, L_F\right) \times \tilde{\boldsymbol{D}}_S^{h,M}(\mu_F^2), \tag{D.3}$$

where the symbol $\times$ denotes the standard matrix multiplication and

$$\begin{aligned}
\tilde{F}_k^S(N, M, \mu_I^2, \mu_F^2, Q^2) &\equiv \int_0^1 dx x^{N-1} \int_0^1 dz z^{M-1} F_k^S(x, z, \mu_I^2, \mu_F^2, Q^2) \\
\tilde{\boldsymbol{q}}^N(\mu_I^2) &\equiv \int_0^1 dx x^{N-1} \boldsymbol{q}(x, \mu_I^2), \\
\tilde{\boldsymbol{D}}_S^{h,M}(\mu_F^2) &\equiv \int_0^1 dz z^{M-1} \boldsymbol{D}_S^h(z, \mu_F^2), \\
\tilde{\boldsymbol{\mathcal{C}}}_k^S\left(N, M, a_s(\mu_F^2), L_I, L_F\right) &\equiv \int_0^1 d\hat{x} \hat{x}^{N-1} \int_0^1 d\hat{z} \hat{z}^{M-1} \boldsymbol{\mathcal{C}}_k^S\left(\hat{x}, \hat{z}, a_s(\mu_F^2), L_I, L_F\right).
\end{aligned} \tag{D.4}$$

The dependence of each entry of the matrix $\tilde{\boldsymbol{\mathcal{C}}}_k^S$ on the factorization scales μ_I and μ_F can be expressed as

$$\begin{aligned}
\tilde{\mathcal{C}}_{k,ij}^{\mathrm{S}}\left(a_s(\mu_F^2), L_I, L_F\right) = \sum_{n=0}^{\infty} a_s^n(\mu_F^2) \Bigg(& \tilde{c}_{k,ij}^{(n,0,0)} + \sum_{\kappa=1}^{n} \tilde{c}_{k,ij}^{(n,\kappa,0)} L_I^\kappa + \sum_{l=1}^{n} \tilde{c}_{k,ij}^{(n,0,l)} L_F^l \\
& + \sum_{\kappa=1}^{n} \sum_{l=1}^{n-\kappa} \tilde{c}_{k,ij}^{(n,\kappa,l)} L_I^\kappa L_F^l \Bigg),
\end{aligned} \tag{D.5}$$

The coefficients $\tilde{c}_{k,ij}^{(n,0,0)}$ are the direct result of the perturbative calculation with $\mu_F^2 = \mu_I^2 = \mu_r^2 = Q^2$ while the $\tilde{c}_{k,ij}^{(n,\kappa,0)}$, $\tilde{c}_{k,ij}^{(n,0,l)}$, $\tilde{c}_{k,ij}^{(n,\kappa,l)}$ can be calculated order by order in a_s solving the renormalization group equations (RGEs) for the fatorization scales. They follow directly from the request that $\frac{\partial}{\partial \log \mu_I^2} \tilde{F}_k^S \stackrel{!}{=} 0$ and $\frac{\partial}{\partial \log \mu_F^2} \tilde{F}_k^S \stackrel{!}{=} 0$ and they read

$$\left(\Big[\frac{\partial}{\partial \log \mu_I^2} \Big] \delta_{im} + \tilde{P}_{im}^{Transp}(N, \mu_I^2) \right) \mathcal{C}_{k,mj}^S(N, M, a_s(\mu_F), L_I, L_F) = 0 \tag{D.6}$$

$$\left(\Big[\frac{\partial}{\partial \log \mu_F^2} + \beta(a_s) \frac{\partial}{\partial a_s} \Big] \delta_{mj} + \tilde{P}_{mj}^{T}(M, \mu_F^2) \right) \mathcal{C}_{k,im}^S(N, M, a_s(\mu_F), L_I, L_F) = 0\,. \tag{D.7}$$

Here $\tilde{P}_{im}^{Transp}(N, \mu_I^2)$ corresponds to the im entry of the matrix resulting from the trasposition

of

$$\tilde{\boldsymbol{P}}(N,\mu_I^2) \equiv \sum_{i=0}^{\infty} a_s^{i+1} \tilde{\boldsymbol{P}}^{(i)}(N,\mu_I^2) \equiv \sum_{i=0}^{\infty} a_s^{i+1} \begin{pmatrix} \tilde{P}_{qq}^{(i)} & \tilde{P}_{gq}^{(i)} \\ \tilde{P}_{qg}^{(i)} & \tilde{P}_{gg}^{(i)} \end{pmatrix} (N,\mu_I^2) \tag{D.8}$$

defined as the single Mellin transform of the matrix appearing in the first equation of (4.13). On the other side, $\tilde{P}_{mj}^{T}(M,\mu_I^2)$ represents the mj entry of the time-like $\tilde{\boldsymbol{P}}^{T}(M,\mu_I^2)$ matrix defined as the single Mellin transform of the matrix appearing in the second equation of (4.13).
Inserting Eq. (D.5) in (D.6) and (D.7) one is left with a system of linear equations in the coefficients $\tilde{c}_{k,ij}^{(n,\kappa,0)}$, $\tilde{c}_{k,ij}^{(n,0,l)}$ and $\tilde{c}_{k,ij}^{(n,\kappa,l)}$ which can be solved recursively order by order in a_s for every fixed value of κ and l once the results for $\kappa = 0$ and $l = 0$ are given. If we define $\tilde{\boldsymbol{c}}_k^{(n,\kappa,l)}$ to be the matrix with entries $\tilde{c}_{k,ij}^{(n,\kappa,l)}$, the formal solution for a fixed order $\mathcal{O}(a_s^n)$ can be recursively written as

$$\begin{aligned} \tilde{\boldsymbol{c}}_k^{(n,\kappa,0)} \overset{\kappa\neq 0}{=} & \frac{1}{\kappa} \sum_{w=\kappa-1}^{n-1} \tilde{\boldsymbol{P}}^{(n-w-1),\,Transp} \times \tilde{\boldsymbol{c}}_k^{(w,\kappa-1,0)} \\ & + \frac{1}{\kappa} \sum_{p=0}^{n-2} \sum_{q=0}^{\kappa-2} \left(\sum_{i=0}^{n-p-\kappa+q} A_{i,\,\kappa-q-1}^{n-p} \tilde{\boldsymbol{P}}^{(i),\,Transp} \right) \times \tilde{\boldsymbol{c}}_k^{(p,q,0)} \end{aligned} \tag{D.9}$$

$$\tilde{\boldsymbol{c}}_k^{(n,\kappa,l)} \overset{l\neq 0}{=} \frac{1}{l} \sum_{j=l-1+\kappa}^{n-1} \tilde{\boldsymbol{c}}_k^{(j,\kappa,l-1)} \times \left(\tilde{\boldsymbol{P}}^{T,(n-1-j)} - \mathbf{1}(j\,\beta_{n-1-j}) \right) , \tag{D.10}$$

where all dependences have been dropped to simplify the notation. The coefficients $\tilde{\boldsymbol{c}}_k^{(n,0,l)}$ are also given by the formula (D.10). All terms $\tilde{\boldsymbol{c}}_k^{(n,\kappa,l)}$ with $\kappa + l > n$ recursively generated by the above equations are obviously set to be equal zero. The coefficient $A_{i,\,\kappa-q-1}^{n-p}$, introduced in Eq. (4.11), appears in the last line of Eq. (D.9) since the space-like splitting functions showing in (D.6) are given as a function of μ_I. Nonetheless, one has to take great care when solving the system of equations (D.6) and (D.7) and re-expand $\tilde{P}_{im}^{Transp}(N,\mu_I)$ around the same $a_s(\mu_F)$ consistently with the one chosen in Eq. (D.5). As a consequence, Eqs. (D.9) and (D.10) can be correct only up to β_i terms neglected in the expansion of a_s (see Eq. (D.1)). To regain the expressions in the (x,z) space one has to formally perform a double Mellin inverse

$$\boldsymbol{\mathcal{C}}_k^S \left(\hat{x},\hat{z},a_s(\mu_F^2),L_I,L_F\right) = \int_{\mathcal{C}_N} \frac{dN}{2\pi i} \hat{x}^{-N} \int_{\mathcal{C}_M} \frac{dM}{2\pi i} \hat{z}^{-M} \tilde{\boldsymbol{\mathcal{C}}}_k^S \left(N,M,a_s(\mu_F^2),L_I,L_F\right) , \tag{D.11}$$

where $\mathcal{C}_N$ and $\mathcal{C}_M$ are contour chosen in the N and M complex moment space respectively. Assuming that for a fixed order $\mathcal{O}(a_s^n)$ the coefficient $\tilde{\boldsymbol{\mathcal{C}}}_k^{S,(n)}$ is integrable along the contours $\mathcal{C}_N$ and $\mathcal{C}_M$, we have that

$$\boldsymbol{c}_k^{(n,\kappa,l)}(\hat{x},\hat{z}) = \int_{\mathcal{C}_N} \frac{dN}{2\pi i}\hat{x}^{-N} \int_{\mathcal{C}_M} \frac{dM}{2\pi i}\hat{z}^{-M}\tilde{\boldsymbol{c}}_k^{(n,\kappa,l)}(N,M) \tag{D.12}$$

and the expressions (D.9) and (D.10) can be translated for the $\boldsymbol{c}_k^{(n,\kappa,l)}$ coefficients by symbolically dropping the "$\sim$" and substituting "$\times$" with "$\otimes$".

This procedure can be easily extended for the remaining lines of Eq. (4.21) by simply substituting the matrices $\tilde{\boldsymbol{P}}^{T,(i)}$ and $\tilde{\boldsymbol{P}}^{(i)}$ with the corresponding "non-singlet" scalar function $\tilde{P}^{T,+,(i)}$, $\tilde{P}^{T,v,(i)}$, $\tilde{P}^{+,(i)}$ or $\tilde{P}^{v,(i)}$ in (D.9) and (D.10). Here the symbol "$\sim$" denotes as before the single Mellin moment of the corresponding function. At the same time $\tilde{\boldsymbol{c}}_k^{(n,\kappa,l)}$ will represent each time a scalar function, a vector or a transposed vector accordingly to how the coefficient functions appear in (4.21).

APPENDIX E

Angular Integrals

We show below the results of some angular integrals needed for the computation of the SIDIS longitudinal structure functions, which are not available in the literature. The subscript 4 indicates that they have been computed in 4-dimensions. Except for the first three integrals (valid for every set of parameters) the results are only valid for $A^2 \neq B^2 + C^2$.

E.1 New Integrals

$$I_4[-4,0] = 2\pi\left(a^4 + 2a^2b^2 + \frac{b^4}{5}\right) \tag{E.1}$$

$$I_4[-3,0] = 2\pi a\left(a^2 + b^2\right) \tag{E.2}$$

$$I_4[-2,-1] = \frac{2}{3}\left(3\pi a^2 A + 2\pi abB + \pi Ab^2\right) \tag{E.3}$$

$$\tag{E.4}$$

$$
\begin{aligned}
I_4[-4,2] = & \frac{\pi}{3\left(B^2+C^2\right)^4\left(A^2-B^2-C^2\right)} \\
& \times \left\{A^2b^2\left(B^2+C^2\right)\left[36a^2\left(2B^4+B^2C^2-C^4\right)+b^2\left(-16B^4+84B^2C^2-15C^4\right)\right]\right. \\
& -12aAbB\left(B^2+C^2\right)^2\left[2a^2\left(B^2+C^2\right)+b^2\left(9C^2-4B^2\right)\right] \\
& +2\left(B^2+C^2\right)^2\left[3a^4\left(B^2+C^2\right)^2-18a^2b^2\left(B^4-C^4\right)-b^4\left(B^4+6B^2C^2-3C^4\right)\right] \\
& \left.-36aA^3b^3B\left(2B^4-B^2C^2-3C^4\right)+3A^4b^4\left(8B^4-24B^2C^2+3C^4\right)\right\} \\
& +\frac{\pi b}{2\left(B^2+C^2\right)^{9/2}}\log\left(\frac{A+\sqrt{B^2+C^2}}{A-\sqrt{B^2+C^2}}\right) \\
& \times\left\{-3Ab\left(B^2+C^2\right)\left(4a^2\left(2B^4+B^2C^2-C^4\right)-b^2C^2\left(C^2-4B^2\right)\right)\right. \\
& +4aB\left(B^2+C^2\right)^2\left(2a^2\left(B^2+C^2\right)+3b^2C^2\right)+12aA^2b^2B\left(2B^4-B^2C^2-3C^4\right) \\
& \left.+A^3b^3\left(-8B^4+24B^2C^2-3C^4\right)\right\} \qquad \text{(E.5)}
\end{aligned}
$$

$$
\begin{aligned}
I_4[-4,1] = & -\frac{\pi b}{12\left(B^2+C^2\right)^4} \\
& \times\left\{Ab\left(B^2+C^2\right)\left[72a^2\left(2B^4+B^2C^2-C^4\right)+b^2\left(8B^4+48B^2C^2-15C^4\right)\right]\right. \\
& -32aB\left(B^2+C^2\right)^2\left[3a^2\left(B^2+C^2\right)+b^2\left(B^2+3C^2\right)\right] \\
& -48aA^2b^2B\left(2B^4-B^2C^2-3C^4\right) \\
& \left.+3A^3b^3\left(8B^4-24B^2C^2+3C^4\right)\right\} \\
& +\frac{\pi}{8\left(B^2+C^2\right)^{9/2}}\log\left(\frac{A+\sqrt{B^2+C^2}}{A-\sqrt{B^2+C^2}}\right) \\
& \times\left\{6A^2b^2\left(B^2+C^2\right)\left(4a^2\left(2B^4+B^2C^2-C^4\right)-b^2C^2\left(C^2-4B^2\right)\right)\right. \\
& -16aAbB\left(B^2+C^2\right)^2\left(2a^2\left(B^2+C^2\right)+3b^2C^2\right) \\
& +\left(B^2+C^2\right)^2\left(8a^4\left(B^2+C^2\right)^2+24a^2b^2C^2\left(B^2+C^2\right)+3b^4C^4\right) \\
& +16aA^3b^3B\left(-2B^4+B^2C^2+3C^4\right) \\
& \left.+A^4b^4\left(8B^4-24B^2C^2+3C^4\right)\right\} \qquad \text{(E.6)}
\end{aligned}
$$

$$
\begin{aligned}
I_4[-3,2] = & \frac{\pi}{\left(B^2+C^2\right)^3\left(A^2-B^2-C^2\right)} \\
& \times \left\{2a^3B^6+6a^3B^4C^2+6a^3B^2C^4+2a^3C^6-6a^2AbB^5\right. \\
& -12a^2AbB^3C^2-6a^2AbBC^4+12aA^2b^2B^4+6aA^2b^2B^2C^2-6aA^2b^2C^4-6ab^2B^6 \\
& -6ab^2B^4C^2+6ab^2B^2C^4+6ab^2C^6-6A^3b^3B^3+9A^3b^3BC^2+4Ab^3B^5 \\
& \left.-5Ab^3B^3C^2-9Ab^3BC^4\right\} \\
& +\frac{3\pi b}{2\left(B^2+C^2\right)^{7/2}}\log\left(\frac{A+\sqrt{B^2+C^2}}{A-\sqrt{B^2+C^2}}\right) \\
& \times \left\{2a^2B^5+4a^2B^3C^2+2a^2BC^4-4aAbB^4-2aAbB^2C^2+2aAbC^4\right. \\
& \left.+2A^2b^2B^3-3A^2b^2BC^2+b^2B^3C^2+b^2BC^4\right\} \qquad \text{(E.7)} \\
I_4[-3,1] = & \frac{\pi b}{3\left(B^2+C^2\right)^3} \\
& \times \left\{18a^2B^5+36a^2B^3C^2+18a^2BC^4-18aAbB^4-9aAbB^2C^2+9aAbC^4\right. \\
& \left.+6A^2b^2B^3-9A^2b^2BC^2+2b^2B^5+8b^2B^3C^2+6b^2BC^4\right\} \\
& -\frac{\pi\left(-aB^2-aC^2+AbB\right)}{2\left(B^2+C^2\right)^{7/2}}\log\left(\frac{A+\sqrt{B^2+C^2}}{A-\sqrt{B^2+C^2}}\right) \\
& \times \left\{2a^2B^4+4a^2B^2C^2+2a^2C^4-4aAbB^3\right. \\
& \left.-4aAbBC^2+2A^2b^2B^2-3A^2b^2C^2+3b^2B^2C^2+3b^2C^4\right\} \qquad \text{(E.8)}
\end{aligned}
$$

Acknowledgments

In this last pages I would like to express my sincere gratitude to all people that have been essential in the accomplishment of my thesis. First of all, my most special thanks go to my supervisor Prof. Dr. Werner Vogelsang, who gave me the opportunity to work in such an amazing research group on many interesting projects. His professional and personal support has been a fundamental component to the writing of this thesis. Not only I am thankful for many helpful and clarifying discussions and for all the opportunities given me to attend summer schools and conferences, essential to my research activity, but also for the wonderful and welcoming working environment that he developed in his group. I am very happy to say that I will always remember my years in Tübingen as beautiful years of my life also because of the very nice atmosphere in our group.

I would like to thank my collaborator Dr. Marco Stratmann for his immense support during all my Ph.D. On top of many helpful discussions, he has always being supporting my research activity and giving me nice opportunities to speak about our projects in many relevant conferences.

Furthermore, I would like to thank Prof. Dr. Thomas Gutsche for stimulating discussions on Physiscs and for all nice life stories shared in front of a cup of coffee in our lunch breaks, and for being very helpful all time during my Ph.D.

I reserve a special thanks to Dr. Felix Ringer, who has been not only a fabulous office mate and multiple times co-worker but most of all a very good friend and a wonderful travelling companion. I am grateful for all professional and personal experiences shared with him and

for all his help during my Ph.D. Many thanks to Tom Kaufmann for the fruitful collaboration on different projects and for the nice time spent together with his lovely wife Ann-Katrin. I am grateful for their friendship and for their joyful and welcoming spirit. I'd also like to thank Martin and Franzi Lambertsen for the wonderful time spent together and for showing me a beautiful new part of Germany that I will never forget. I am thankful also for many stimulating Physics related discussions with Martin. Many thanks to Patriz Hiderer for fruitful discussions and for a very nice time in Tübingen and around the world travelling to conferences and summer schools.
Many thanks to my other collaborators Prof. Dr. Alberto Accardi, Prof. Dr. Daniel de Florian and Dr. Yamila Rotstein Habarnau. I want to specially thank Prof. Dr. Alberto Accardi and Prof. Dr. Daniel de Florian for their kind invitations respectively at Jefferson National Laboratory (Virginia, USA) and at Univeristy of Buenos Aires (Buenos Aires, Argentina).
Thanks to "Fondazione Cassa Rurale di Trento" for financially supporting part of my research activity.
I am grateful to Rodolfo Sassot, Andreas Vogt, Nobuo Sato, Zhong-Bo Kang, Ivan Vitev, Gunar Schnell, Joshua Davies, Peter Monaghan, Christian Weiss and Marco Traini for very useful communications.
I would like to thank Dr. Davide Campagnari for all useful discussions and for the very nice time spent in Tübingen.
Thanks to all the rest of the theoretical physics group in Tübingen, including Prof. Dr. Barbara Jäger, Dr. Giuseppe Burgio, Dr. Valery Lyubovitskij, Dr. Marc Schlegel, Dr. Julien Baglio, Ehsan Ebadati, Jan Heffner, Matthias Kesenheimer, Lukas Salfelder, Peter Vastag and Hannes Vogt, for many discussions and a nice working ambient. A special thanks to Sabine Werner, who patiently assisted me in all bureaucratic procedures during those years.
Finally, I would like to thank all people that are note directly related with my research activity but have been close to me in the years of my Ph.D. Thanks to all my old friends and new ones made along the way. Thanks to the "Big Family", to my sister Marica and to Fabrizio for always being there for me. Thanks to my beautiful girlfriend Ariele for coping with my awful temper during the writing of the thesis and for her loving support. And a very warm thanks to my two wonderful parents Sonia and Mariano, to whom I would like to dedicate this thesis. Although scattered around the world, they are always the closest companions of all my journeys and the best persons to share them with.
Grazie mamma e papà!

List of Figures

Bibliography

[1] Raymond Brock et al. "Handbook of perturbative QCD: Version 1.0". In: *Rev. Mod. Phys.* 67 (1995), pp. 157–248. DOI: 10.1103/RevModPhys.67.157.

[2] M. H. Seymour. "Quantum ChromoDynamics". In: *ArXiv:1010.2330* (Oct. 2010). arXiv: 1010.2330 [hep-ph].

[3] J. Chadwick and E. S. Bieler. "The Collisions of Alpha Particles with Hydrogen Nuclei". In: *The London, Edinburgh, and Dublin Philosophical Magazine and Journal of Science* XLII (1921), pp. 809–825.

[4] Hideki Yukawa. "On the Interaction of Elementary Particles". In: *Proc. Phys.-Math. Soc. Jpn.* 17 (1935), pp. 48–57.

[5] S. H. Neddermeyer and C. D. Anderson. "Note on the Nature of Cosmic Ray Particles". In: *Phys. Rev.* 51 (1937), pp. 884–886. DOI: 10.1103/PhysRev.51.884.

[6] J. C. Street and E. C. Stevenson. "New Evidence for the Existence of a Particle of Mass Intermediate Between the Proton and Electron". In: *Phys. Rev.* 52 (1937), pp. 1003–1004. DOI: 10.1103/PhysRev.52.1003.

[7] M. Conversi, E. Pancini, and O. Piccioni. "On the Disintegration of Negative Mesons". In: *Phys. Rev.* 71 (1947). [,579(1947)], pp. 209–210. DOI: 10.1103/PhysRev.71.209.

[8] C. M. G. Lattes et al. "Processes invloving charged mesons". In: *Nature* 159 (1947). [,42(1947)], pp. 694–697. DOI: 10.1038/159694a0.

[9] C. M. G. Lattes, G. P. S. Occhialini, and C. F. Powell. "Observations on the Tracks of Slow Mesons in Photographic Emulsions. 2". In: *Nature* 160 (1947). [,103(1947)], pp. 486–492. DOI: 10.1038/160486a0.

[10] Kazuhiko Nishijima. "Charge Independence Theory of V Particles". In: *Progress of Theoretical Physics* 13.3 (1955), pp. 285–304. DOI: 10.1143/PTP.13.285. URL: http://ptp.ipap.jp/link?PTP/13/285/.

[11] M. Gell-Mann. "The interpretation of the new particles as displaced charge multiplets". In: *Il Nuovo Cimento (1955-1965)* 4 (0 1956). 10.1007/BF02748000, pp. 848–866. ISSN: 1827-6121. URL: http://dx.doi.org/10.1007/BF02748000.

[12] M. Gell-Mann. "The Eightfold Way: a theory of strong ineractions symmetries". In: *Unpublished US Atomic Energy Technical Report* (1961).

[13] Y.Ne'eman. "Derivation of strong interactions from gauge invariance". In: *Nuclear Physics* 26 (1961), p. 222.

[14] Murray Gell-Mann. "A Schematic Model of Baryons and Mesons". In: *Phys. Lett.* 8 (1964), pp. 214–215. DOI: 10.1016/S0031-9163(64)92001-3.

[15] G. Zweig. "An SU(3) model for strong interaction symmetry and its breaking. Version 2". In: *DEVELOPMENTS IN THE QUARK THEORY OF HADRONS. VOL. 1. 1964 - 1978*. Ed. by D.B. Lichtenberg and Simon Peter Rosen. 1964, pp. 22–101. URL: http://inspirehep.net/record/4674/files/cern-th-412.pdf.

[16] G. Zweig. "An SU(3) model for strong interaction symmetry and its breaking. Version 1". In: (1964).

[17] Keith A. Brueckner. "Meson-Nucleon Scattering and Nucleon Isobars". In: *Phys. Rev.* 86 (1952), pp. 106–109. DOI: 10.1103/PhysRev.86.106.

[18] O. W. Greenberg. "Spin and Unitary-Spin Independence in a Paraquark Model of Baryons and Mesons". In: *Phys. Rev. Lett.* 13 (20 1964), pp. 598–602. DOI: 10.1103/PhysRevLett.13.598. URL: http://link.aps.org/doi/10.1103/PhysRevLett.13.598.

[19] M. Y. Han and Y. Nambu. "Three-Triplet Model with Double SU(3) Symmetry". In: *Phys. Rev.* 139 (4B 1965), B1006–B1010. DOI: 10.1103/PhysRev.139.B1006. URL: http://link.aps.org/doi/10.1103/PhysRev.139.B1006.

[20] V.V. Ezhela, S.B. Lugovsky, and O.V. Zenin. "Hadronic part of the muon g-2 estimated on the $\sigma_{tot}^{2003}(e^+e^- \rightarrow$hadrons) evaluated data compilation". In: *ArXiv: hep-ph/0312114* (2003). arXiv: hep-ph/0312114 [hep-ph].

[21] Chen-Ning Yang and Robert L. Mills. "Conservation of Isotopic Spin and Isotopic Gauge Invariance". In: *Phys. Rev.* 96 (1954), pp. 191–195. DOI: 10.1103/PhysRev.96.191.

[22] H. Fritzsch, Murray Gell-Mann, and H. Leutwyler. "Advantages of the Color Octet Gluon Picture". In: *Phys. Lett.* B47 (1973), pp. 365–368. DOI: 10.1016/0370-2693(73)90625-4.

[23] D. J. Gross and Frank Wilczek. "Asymptotically Free Gauge Theories. 1". In: *Phys. Rev.* D8 (1973), pp. 3633–3652. DOI: 10.1103/PhysRevD.8.3633.

[24] H. David Politzer. "Reliable Perturbative Results for Strong Interactions?" In: *Phys. Rev. Lett.* 30 (1973), pp. 1346–1349. DOI: 10.1103/PhysRevLett.30.1346.

[25] E. S. Abers and B. W. Lee. "Gauge Theories". In: *Phys. Rept.* 9 (1973), pp. 1–141. DOI: 10.1016/0370-1573(73)90027-6.

[26] L.D. Faddev and V.N. Popov. "Feynman Diagrams for the Yang-Mills field". In: *Phys.Lett.B* 25 (1967), p. 29.

[27] Felix Ringer. "Contributions of the Weak Gauge Bosons to Spin-Dependent Hard QCD Processes". MA thesis. Universität von Tübingen, 2011.

[28] T. van Ritbergen, J. A. M. Vermaseren, and S. A. Larin. "The Four loop beta function in quantum chromodynamics". In: *Phys. Lett.* B400 (1997), pp. 379–384. DOI: 10.1016/S0370-2693(97)00370-5. arXiv: hep-ph/9701390 [hep-ph].

[29] Siegfried Bethke. "The 2009 World Average of alpha(s)". In: *Eur. Phys. J.* C64 (2009), pp. 689–703. DOI: 10.1140/epjc/s10052-009-1173-1. arXiv: 0908.1135 [hep-ph].

[30] Francis. Halzen and Alan D. Martin. *Quarks and Leptons: an introductory course in modern particle physics*. John Wiley and son, 1984.

[31] Richard P. Feynman. "Very High-Energy Collisions of Hadron". In: *Phys. Rev. Lett.* 23 (1969), pp. 1415–1417.

[32] J. D. Bjorken and E. A. Paschos. "Inelastic Electron-Proton and γ^*-Proton Scattering and the Structure of the Nucleon". In: *Phys. Rev.* 185 (5 1969), pp. 1975–1982. DOI: 10.1103/PhysRev.185.1975. URL: http://link.aps.org/doi/10.1103/PhysRev.185.1975.

[33] G. Altarelli, R.K. Ellis, and G. Martinelli. "Large Perturbative Corrections to the Drell-Yann Process in QCD". In: *Nuclear Physics B* 157 (1979), pp. 461–497.

[34] C.G. Callan and David J. Gross. "High-Energy Electroproduction and the Constitution of the Electric Current". In: *Phys. Rev. Lett.* 22 (1969), pp. 156–159.

[35] Frank Close, Sandy Donnachie, and Graham Shaw. "Electromagnetic interactions and hadronic structure". In: *Camb. Monogr. Part. Phys. Nucl. Phys. Cosmol.* 25 (2007), pp. 1–499.

[36] J.D. Bjorken. "Asymptotic Sum Rules at Infinite Momentum". In: *Phys. Rev.* 179 (1969), pp. 1547–1553.

[37] W.B. Atwood. *Physics of Particle Detectors*. Tech. rep. SLAC summer institute on Particle Physics, 1979.

[38] R.K. Ellis, W.J. Stirling, and B.R. Webber. *QCD and Collider Physics*. Vol. 8. Camb.Monogr.Part.P
1996.

[39] J.C Collins and D.E. Soper. "Theorems of Perturbative QCD". In: *Ann.Rev.Nucl.Part.Sci.* 37 (1987), p. 383.

[40] J.C Collins, D.E. Soper, and G. Sterman. "Factorization of Hard Processes in QCD". In: *ArXiv: hep-ph/0409313* (2004).

[41] Sayipjamal Dulat et al. "New parton distribution functions from a global analysis of quantum chromodynamics". In: *Phys. Rev.* D93.3 (2016), p. 033006. DOI: 10.1103/PhysRevD.93.033006. arXiv: 1506.07443 [hep-ph].

[42] John C. Collins, Davison E. Soper, and George Sterman. "All-order factorization for Drell-Yan cross sections". In: *Physics Letters B* 134.34 (1984), pp. 263 –268. ISSN: 0370-2693. DOI: 10.1016/0370-2693(84)90684-1. URL: http://www.sciencedirect.com/science/article/pii/0370269384906841.

[43] F.D. Aaron et al. "Inclusive Deep Inelastic Scattering at High Q^2 with Longitudinally Polarised Lepton Beams at HERA". In: *ArXiv:1206.7007v1* (2012).

[44] T. Kinoshita. "Mass singularities of Feynman amplitudes". In: *J. Math. Phys.* 3 (1962), pp. 650–677. DOI: 10.1063/1.1724268.

[45] T. D. Lee and M. Nauenberg. "Degenerate Systems and Mass Singularities". In: *Phys. Rev.* 133 (1964). [,25(1964)], B1549–B1562. DOI: 10.1103/PhysRev.133.B1549.

[46] A. Zee, F. Wilczek, and S.B. Treiman. "Scaling Derivation for Neutrino Reactions in asymptotically Free Field Theories". In: *Phys. Rev. D* 10 (1974), pp. 2881–2891.

[47] W.J. Marciano. "Dimensional Regularization and Mass Singularities". In: *Phys. Rev.D* (1975), pp. 3861–3871.

[48] W. Furmanski and R. Petronzio. "Lepton - Hadron Processes Beyond Leading Order in Quantum Chromodynamics". In: *Z. Phys.* C11 (1982), p. 293. DOI: 10.1007/BF01578280.

[49] Guido Altarelli and G. Parisi. "Asymptotic Freedom in Parton Language". In: *Nucl. Phys.* B126 (1977), pp. 298–318. DOI: 10.1016/0550-3213(77)90384-4.

[50] V. N. Gribov and L. N. Lipatov. "Deep inelastic e p scattering in perturbation theory". In: *Sov. J. Nucl. Phys.* 15 (1972). [Yad. Fiz.15,781(1972)], pp. 438–450.

[51] G. Sterman. "Summation of large corrections to short distance hadronic cross-sections". In: *Nuclear Physics B* 281 (1987), p. 310.

[52] S. Catani and L. Trentadue. "Resummation of the QCD Perturbative Series for Hard Processes". In: *Nucl. Phys.* B327 (1989), pp. 323–352. DOI: 10.1016/0550-3213(89)90273-3.

[53] S. Catani and L. Trentadue. "Comment on QCD exponentiation at large x". In: *Nuclear Physics B* 353 (1991), pp. 183–186.

[54] F. Stefano and G. Ridolfi. "Renormalization Group Approach to Soft Gluon Resummation". In: *ArXiv: hep-ex/0209154* (2002).

[55] A. V. Manohar. "Deep inelastic scattering as $x \to 1$ using soft-collinear effective theory". In: *Phys. Rev. D* 68 (2003), p. 114019.

[56] Ahmad Idilbi and Xiang Dong Ji. "Threshold resummation for drell-yan process in soft-collinear effective theory". In: *Phys. Rev. D* 72 (2005), p. 054016.

[57] Paolo Bolzoni. "Sudakov resummation in QCD". PhD thesis. Universitá degli Studi di Milano, 2006.

[58] George F. Sterman. "Infrared divergences in perturbative QCD". In: *AIP Conf. Proc.* 74 (1981), pp. 22–40. DOI: 10.1063/1.33099.

[59] J. G. M. Gatheral. "Exponentiation of Eikonal Cross-sections in Nonabelian Gauge Theories". In: *Phys. Lett.* B133 (1983), pp. 90–94. DOI: 10.1016/0370-2693(83)90112-0.

[60] J. Frenkel and J. C. Taylor. "NONABELIAN EIKONAL EXPONENTIATION". In: *Nucl. Phys.* B246 (1984), pp. 231–245. DOI: 10.1016/0550-3213(84)90294-3.

[61] Matthias Aicher. "Threshold Resummation Effects on the Parton Distribution Function of the Pion and Time-Reversal-Odd Single-Spin Asymmetries". PhD thesis. Universität Regensburg, 2011.

[62] A. Bassetto et al. "Jet Multiplicity and Soft Gluon Factorization". In: *Nucl. Phys.* B207 (1982), pp. 189–204. DOI: 10.1016/0550-3213(82)90161-4.

[63] S. Albino et al. "Fully double-logarithm-resummed cross sections". In: *Nucl. Phys.* B851 (2011), pp. 86–103. DOI: 10.1016/j.nuclphysb.2011.05.014. arXiv: 1104.3018 [hep-ph].

[64] A. Bassetto, M. Ciafaloni, and G. Marchesini. "Jet Structure and Infrared Sensitive Quantities in Perturbative QCD". In: *Phys. Rept.* 100 (1983), pp. 201–272. DOI: 10.1016/0370-1573(83)90083-2.

[65] S. Albino et al. "Generalizing the DGLAP evolution of fragmentation functions to the smallest x values". In: *Phys. Rev. Lett.* 95 (2005), p. 232002. DOI: 10.1103/PhysRevLett.95.232002. arXiv: hep-ph/0503170 [hep-ph].

[66] Alfred H. Mueller. "Multiplicity and Hadron Distributions in QCD Jets. 2. A General Procedure for All Nonleading Terms". In: *Nucl. Phys.* B228 (1983), pp. 351–364. DOI: 10.1016/0550-3213(83)90329-2.

[67] P. J. Rijken and W. L. van Neerven. "Higher order QCD corrections to the transverse and longitudinal fragmentation functions in electron - positron annihilation". In: *Nucl. Phys.* B487 (1997), pp. 233–282. DOI: 10.1016/S0550-3213(96)00669-4. arXiv: hep-ph/9609377 [hep-ph].

[68] P. J. Rijken and W. L. van Neerven. "O (alpha-s**2) contributions to the longitudinal fragmentation function in e+ e- annihilation". In: *Phys. Lett.* B386 (1996), pp. 422–428. DOI: 10.1016/0370-2693(96)00898-2. arXiv: hep-ph/9604436 [hep-ph].

[69] P. J. Rijken and W. L. van Neerven. "O (alpha-s**2) contributions to the asymmetric fragmentation function in e+ e- annihilation". In: *Phys. Lett.* B392 (1997), pp. 207–215. DOI: 10.1016/S0370-2693(96)01529-8. arXiv: hep-ph/9609379 [hep-ph].

[70] Alexander Mitov and Sven-Olaf Moch. "QCD Corrections to Semi-Inclusive Hadron Production in Electron-Positron Annihilation at Two Loops". In: *Nucl. Phys.* B751 (2006), pp. 18–52. DOI: 10.1016/j.nuclphysb.2006.05.018. arXiv: hep-ph/0604160 [hep-ph].

[71] A. Vogt, S. Moch, and J. A. M. Vermaseren. "The Three-loop splitting functions in QCD: The Singlet case". In: *Nucl. Phys.* B691 (2004), pp. 129–181. DOI: 10.1016/j.nuclphysb.2004.04.024. arXiv: hep-ph/0404111 [hep-ph].

[72] S. Kretzer. "Fragmentation functions from flavor inclusive and flavor tagged e+ e- annihilations". In: *Phys. Rev.* D62 (2000), p. 054001. DOI: 10.1103/PhysRevD.62.054001. arXiv: hep-ph/0003177 [hep-ph].

[73] J. Binnewies, Bernd A. Kniehl, and G. Kramer. "Next-to-leading order fragmentation functions for pions and kaons". In: *Z. Phys.* C65 (1995), pp. 471–480. DOI: 10.1007/BF01556135. arXiv: hep-ph/9407347 [hep-ph].

[74] Bernd A. Kniehl, G. Kramer, and B. Potter. "Fragmentation functions for pions, kaons, and protons at next-to-leading order". In: *Nucl. Phys.* B582 (2000), pp. 514–536. DOI: 10.1016/S0550-3213(00)00303-5. arXiv: hep-ph/0010289 [hep-ph].

[75] S. Albino, B. A. Kniehl, and G. Kramer. "Fragmentation functions for light charged hadrons with complete quark flavor separation". In: *Nucl. Phys.* B725 (2005), pp. 181–206. DOI: 10.1016/j.nuclphysb.2005.07.010. arXiv: hep-ph/0502188 [hep-ph].

[76] M. Hirai et al. "Determination of fragmentation functions and their uncertainties". In: *Phys. Rev.* D75 (2007), p. 094009. DOI: 10.1103/PhysRevD.75.094009. arXiv: hep-ph/0702250 [hep-ph].

[77] Daniel de Florian, Rodolfo Sassot, and Marco Stratmann. "Global analysis of fragmentation functions for pions and kaons and their uncertainties". In: *Phys. Rev.* D75 (2007), p. 114010. DOI: 10.1103/PhysRevD.75.114010. arXiv: hep-ph/0703242 [HEP-PH].

[78] Daniel de Florian, Rodolfo Sassot, and Marco Stratmann. "Global analysis of fragmentation functions for protons and charged hadrons". In: *Phys. Rev.* D76 (2007), p. 074033. DOI: 10.1103/PhysRevD.76.074033. arXiv: 0707.1506 [hep-ph].

[79] Daniel de Florian et al. "Parton-to-Pion Fragmentation Reloaded". In: *Phys. Rev.* D91.1 (2015), p. 014035. DOI: 10.1103/PhysRevD.91.014035. arXiv: 1410.6027 [hep-ph].

[80] John C. Collins, Davison E. Soper, and George F. Sterman. "Factorization of Hard Processes in QCD". In: *Adv. Ser. Direct. High Energy Phys.* 5 (1989), pp. 1–91. DOI: 10.1142/9789814503266_0001. arXiv: hep-ph/0409313 [hep-ph].

[81] John C. Collins and Davison E. Soper. "Back-To-Back Jets in QCD". In: *Nucl. Phys.* B193 (1981). [Erratum: Nucl. Phys.B213,545(1983)], p. 381. DOI: 10.1016/0550-3213(81)90339-4.

[82] John C. Collins and Davison E. Soper. "Parton Distribution and Decay Functions". In: *Nucl. Phys.* B194 (1982), pp. 445–492. DOI: 10.1016/0550-3213(82)90021-9.

[83] M. Leitgab et al. "Precision Measurement of Charged Pion and Kaon Differential Cross Sections in e+e- Annihilation at s=10.52,Äâ,ÄâGeV". In: *Phys. Rev. Lett.* 111 (2013), p. 062002. DOI: 10.1103/PhysRevLett.111.062002. arXiv: 1301.6183 [hep-ex].

[84] J. P. Lees et al. "Production of charged pions, kaons, and protons in e^+e^- annihilations into hadrons at $\sqrt{s}$=10.54,Äâ,ÄâGeV". In: *Phys. Rev.* D88 (2013), p. 032011. DOI: 10.1103/PhysRevD.88.032011. arXiv: 1306.2895 [hep-ex].

[85] H. Aihara et al. "Pion and kaon multiplicities in heavy quark jets from e^+e^- annihilation at 29-GeV". In: *Phys. Lett.* B184 (1987), pp. 299–304. DOI: 10.1016/0370-2693(87)90586-7.

[86] H. Aihara et al. "Charged hadron inclusive cross-sections and fractions in e^+e^- annihiliation $\sqrt{s} = 29$ GeV". In: *Phys. Rev. Lett.* 61 (1988), p. 1263. DOI: 10.1103/PhysRevLett.61.1263.

[87] Xing-Qi Lu. "HEAVY QUARK JETS FROM E+ E- ANNIHILATION AT 29-GeV". PhD thesis. Johns Hopkins U., 1986. URL: http://wwwlib.umi.com/dissertations/fullcit?p8707273.

[88] K. Abe et al. "Production of pi+, K+, K0, K*0, phi, p and Lambda0 in hadronic Z0 decays". In: *Phys. Rev.* D59 (1999), p. 052001. DOI: 10.1103/PhysRevD.59.052001. arXiv: hep-ex/9805029 [hep-ex].

[89] D. Buskulic et al. "Inclusive pi+-, K+- and (p, anti-p) differential cross-sections at the Z resonance". In: *Z. Phys.* C66 (1995), pp. 355–366. DOI: 10.1007/BF01556360.

[90] P. Abreu et al. "pi+-, K+-, p and anti-p production in Z0 —> q anti-q, Z0 —> b anti-b, Z0 —> u anti-u, d anti-d, s anti-s". In: *Eur. Phys. J.* C5 (1998), pp. 585–620. DOI: 10.1007/s100529800989.

[91] R. Akers et al. "Measurement of the production rates of charged hadrons in e+ e- annihilation at the Z0". In: *Z. Phys.* C63 (1994), pp. 181–196. DOI: 10.1007/BF01411010.

[92] Manuel Epele et al. "Uncertainties in pion and kaon fragmentation functions". In: *Phys. Rev.* D86 (2012), p. 074028. DOI: 10.1103/PhysRevD.86.074028. arXiv: 1209.3240 [hep-ph].

[93] Nobuo Sato et al. "First Monte Carlo analysis of fragmentation functions from single-inclusive e^+e^- annihilation". In: *Phys. Rev.* D94.11 (2016), p. 114004. DOI: 10.1103/PhysRevD.94.114004. arXiv: 1609.00899 [hep-ph].

[94] Massimiliano Procura and Iain W. Stewart. "Quark Fragmentation within an Identified Jet". In: *Phys. Rev.* D81 (2010). [Erratum: Phys. Rev.D83,039902(2011)], p. 074009. DOI: 10.1103/PhysRevD.81.074009,10.1103/PhysRevD.83.039902. arXiv: 0911.4980 [hep-ph].

[95] Ambar Jain, Massimiliano Procura, and Wouter J. Waalewijn. "Parton Fragmentation within an Identified Jet at NNLL". In: *JHEP* 05 (2011), p. 035. DOI: 10.1007/JHEP05(2011)035. arXiv: 1101.4953 [hep-ph].

[96] Massimiliano Procura and Wouter J. Waalewijn. "Fragmentation in Jets: Cone and Threshold Effects". In: *Phys. Rev.* D85 (2012), p. 114041. DOI: 10.1103/PhysRevD.85.114041. arXiv: 1111.6605 [hep-ph].

[97] Francois Arleo et al. "Probing fragmentation functions from same-side hadron-jet momentum correlations in p-p collisions". In: *JHEP* 04 (2014), p. 147. DOI: 10.1007/JHEP04(2014)147. arXiv: 1311.7356 [hep-ph].

[98] Mathias Ritzmann and Wouter J. Waalewijn. "Fragmentation in Jets at NNLO". In: *Phys. Rev.* D90.5 (2014), p. 054029. DOI: 10.1103/PhysRevD.90.054029. arXiv: 1407.3272 [hep-ph].

[99] Tom Kaufmann, Asmita Mukherjee, and Werner Vogelsang. "Hadron Fragmentation Inside Jets in Hadronic Collisions". In: *Phys. Rev.* D92.5 (2015), p. 054015. DOI: 10.1103/PhysRevD.92.054015. arXiv: 1506.01415 [hep-ph].

[100] Zhong-Bo Kang, Felix Ringer, and Ivan Vitev. "Jet substructure using semi-inclusive jet functions in SCET". In: *JHEP* 11 (2016), p. 155. DOI: 10.1007/JHEP11(2016)155. arXiv: 1606.07063 [hep-ph].

[101] F. Abe et al. "Jet fragmentation properties of $\bar{p}p$ collisions at $\sqrt{s} = 1.8$ TeV". In: *Phys. Rev. Lett.* 65 (1990), pp. 968–971. DOI: 10.1103/PhysRevLett.65.968.

[102] Georges Aad et al. "Measurement of the jet fragmentation function and transverse profile in proton-proton collisions at a center-of-mass energy of 7 TeV with the ATLAS detector". In: *Eur. Phys. J.* C71 (2011), p. 1795. DOI: 10.1140/epjc/s10052-011-1795-y. arXiv: 1109.5816 [hep-ex].

[103] The ATLAS collaboration. "Jet Fragmentation in p+Pb Collisions". In: (2015).

[104] The ATLAS collaboration. "Measurement of two–particle correlations in ‚àös = 13 TeV proton–proton collisions at the LHC with the ATLAS detector". In: (2015).

[105] Serguei Chatrchyan et al. "Measurement of jet fragmentation into charged particles in *pp* and PbPb collisions at $\sqrt{s_{NN}} = 2.76$ TeV". In: *JHEP* 10 (2012), p. 087. DOI: 10.1007/JHEP10(2012)087. arXiv: 1205.5872 [nucl-ex].

[106] Benjamin Andreas Hess. "Measurement of hadron composition in charged jets from pp collisions with the ALICE experiment". In: *Proceedings, 2nd Conference on Large Hadron Collider Physics Conference (LHCP 2014): New York, USA, June 2-7, 2014*. 2014. arXiv: 1408.5723 [hep-ex]. URL: http://inspirehep.net/record/1312165/files/arXiv:1408.5723.pdf.

[107] Xianguo Lu. "Measurement of hadron composition in charged jets from pp collisions with the ALICE experiment". In: *Nucl. Phys.* A931 (2014), pp. 428–432. DOI: 10.1016/j.nuclphysa.2014.08.003. arXiv: 1407.8385 [hep-ex].

[108] Guido Altarelli et al. "Processes Involving Fragmentation Functions Beyond the Leading Order in QCD". In: *Nucl. Phys.* B160 (1979), pp. 301–329. DOI: 10.1016/0550-3213(79)90062-2.

[109] P. Nason and B. R. Webber. "Scaling violation in e+ e- fragmentation functions: QCD evolution, hadronization and heavy quark mass effects". In: *Nucl. Phys.* B421 (1994). [Erratum: Nucl. Phys.B480,755(1996)], pp. 473–517. DOI: 10.1016/S0550-3213(96)00498-1,10.1016/0550-3213(94)90513-4.

[110] Dirk Graudenz. "One particle inclusive processes in deeply inelastic lepton - nucleon scattering". In: *Nucl. Phys.* B432 (1994), pp. 351–376. DOI: 10.1016/0550-3213(94)90606-8. arXiv: hep-ph/9406274 [hep-ph].

[111] D. de Florian, M. Stratmann, and W. Vogelsang. "QCD analysis of unpolarized and polarized Lambda baryon production in leading and next-to-leading order". In: *Phys. Rev.* D57 (1998), pp. 5811–5824. DOI: 10.1103/PhysRevD.57.5811. arXiv: hep-ph/9711387 [hep-ph].

[112] F. Aversa et al. "QCD Corrections to Parton-Parton Scattering Processes". In: *Nucl. Phys.* B327 (1989), p. 105. DOI: 10.1016/0550-3213(89)90288-5.

[113] B. Jager et al. "Next-to-leading order QCD corrections to high p(T) pion production in longitudinally polarized pp collisions". In: *Phys. Rev.* D67 (2003), p. 054005. DOI: 10.1103/PhysRevD.67.054005. arXiv: hep-ph/0211007 [hep-ph].

[114] Daniel de Florian. "Next-to-leading order QCD corrections to one hadron production in polarized pp collisions at RHIC". In: *Phys. Rev.* D67 (2003), p. 054004. DOI: 10.1103/PhysRevD.67.054004. arXiv: hep-ph/0210442 [hep-ph].

[115] G. Curci, W. Furmanski, and R. Petronzio. "Evolution of Parton Densities Beyond Leading Order: The Nonsinglet Case". In: *Nucl. Phys.* B175 (1980), pp. 27–92. DOI: 10.1016/0550-3213(80)90003-6.

[116] W. Furmanski and R. Petronzio. "Singlet Parton Densities Beyond Leading Order". In: *Phys. Lett.* B97 (1980), pp. 437–442. DOI: 10.1016/0370-2693(80)90636-X.

[117] L. Baulieu, E. G. Floratos, and C. Kounnas. "Parton Model Interpretation of the Cut Vertex Formalism". In: *Nucl. Phys.* B166 (1980), pp. 321–339. DOI: 10.1016/0550-3213(80)90230-8.

[118] M. Stratmann and W. Vogelsang. "Next-to-leading order evolution of polarized and unpolarized fragmentation functions". In: *Nucl. Phys.* B496 (1997), pp. 41–65. DOI: 10.1016/S0550-3213(97)00182-X. arXiv: hep-ph/9612250 [hep-ph].

[119] L. N. Lipatov. "The parton model and perturbation theory". In: *Sov. J. Nucl. Phys.* 20 (1975). [Yad. Fiz.20,181(1974)], pp. 94–102.

[120] Yuri L. Dokshitzer. "Calculation of the Structure Functions for Deep Inelastic Scattering and e+ e- Annihilation by Perturbation Theory in Quantum Chromodynamics." In: *Sov. Phys. JETP* 46 (1977). [Zh. Eksp. Teor. Fiz.73,1216(1977)], pp. 641–653.

[121] J. Blumlein and V. Ravindran. "O (alpha**2(s)) Timelike Wilson Coefficients for Parton-Fragmentation Functions in Mellin Space". In: *Nucl. Phys.* B749 (2006), pp. 1–24. DOI: 10.1016/j.nuclphysb.2006.04.032. arXiv: hep-ph/0604019 [hep-ph].

[122] A. Mitov, S. Moch, and A. Vogt. "Next-to-Next-to-Leading Order Evolution of Non-Singlet Fragmentation Functions". In: *Phys. Lett.* B638 (2006), pp. 61–67. DOI: 10.1016/j.physletb.2006.05.005. arXiv: hep-ph/0604053 [hep-ph].

[123] S. Moch and A. Vogt. "On third-order timelike splitting functions and top-mediated Higgs decay into hadrons". In: *Phys. Lett.* B659 (2008), pp. 290–296. DOI: 10.1016/j.physletb.2007.10.069. arXiv: 0709.3899 [hep-ph].

[124] A. A. Almasy, S. Moch, and A. Vogt. "On the Next-to-Next-to-Leading Order Evolution of Flavour-Singlet Fragmentation Functions". In: *Nucl. Phys.* B854 (2012), pp. 133–152. DOI: 10.1016/j.nuclphysb.2011.08.028. arXiv: 1107.2263 [hep-ph].

[125] Valerio Bertone, Stefano Carrazza, and Emanuele R. Nocera. "Reference results for time-like evolution up to $\mathcal{O}(\alpha_s^3)$". In: *JHEP* 03 (2015), p. 046. DOI: 10.1007/JHEP03(2015)046. arXiv: 1501.00494 [hep-ph].

[126] Alfred H. Mueller. "On the Multiplicity of Hadrons in QCD Jets". In: *Phys. Lett.* B104 (1981), pp. 161–164. DOI: 10.1016/0370-2693(81)90581-5.

[127] Alfred H. Mueller. "Multiplicity and Hadron Distributions in QCD Jets: Nonleading Terms". In: *Nucl. Phys.* B213 (1983), pp. 85–108. DOI: 10.1016/0550-3213(83)90176-1.

[128] Alfred H. Mueller. "Square Root of alpha (Q**2) Corrections to Particle Multiplicity Ratios in Gluon and Quark Jets". In: *Nucl. Phys.* B241 (1984), pp. 141–154. DOI: 10.1016/0550-3213(84)90202-5.

[129] A. Vogt. "Resummation of small-x double logarithms in QCD: semi-inclusive electron-positron annihilation". In: *JHEP* 10 (2011), p. 025. DOI: 10.1007/JHEP10(2011)025. arXiv: 1108.2993 [hep-ph].

[130] C. H. Kom, A. Vogt, and K. Yeats. "Resummed small-x and first-moment evolution of fragmentation functions in perturbative QCD". In: *JHEP* 10 (2012), p. 033. DOI: 10.1007/JHEP10(2012)033. arXiv: 1207.5631 [hep-ph].

[131] Matteo Cacciari and Stefano Catani. "Soft gluon resummation for the fragmentation of light and heavy quarks at large x". In: *Nucl. Phys.* B617 (2001), pp. 253–290. DOI: 10.1016/S0550-3213(01)00469-2. arXiv: hep-ph/0107138 [hep-ph].

[132] J. Blumlein and V. Ravindran. "QCD threshold corrections to Higgs decay and to hadroproduction in l+ l- annihilation". In: *Phys. Lett.* B640 (2006), pp. 40–47. DOI: 10.1016/j.physletb.2006.07.029. arXiv: hep-ph/0605011 [hep-ph].

[133] S. Moch and A. Vogt. "Higher-order threshold resummation for semi-inclusive e+ e- annihilation". In: *Phys. Lett.* B680 (2009), pp. 239–246. DOI: 10.1016/j.physletb.2009.09.001. arXiv: 0908.2746 [hep-ph].

[134] A. Vogt. "Leading logarithmic large-x resummation of off-diagonal splitting functions and coefficient functions". In: *Phys. Lett.* B691 (2010), pp. 77–81. DOI: 10.1016/j.physletb.2010.06.010. arXiv: 1005.1606 [hep-ph].

[135] A. A. Almasy, N. A. Lo Presti, and A. Vogt. "Generalized threshold resummation in inclusive DIS and semi-inclusive electron-positron annihilation". In: *JHEP* 01 (2016), p. 028. DOI: 10.1007/JHEP01(2016)028. arXiv: 1511.08612 [hep-ph].

[136] P. Bolzoni, B. A. Kniehl, and A. V. Kotikov. "Gluon and quark jet multiplicities at N^3LO+NNLL". In: *Phys. Rev. Lett.* 109 (2012), p. 242002. DOI: 10.1103/PhysRevLett.109.242002. arXiv: 1209.5914 [hep-ph].

[137] Paolo Bolzoni, Bernd A. Kniehl, and Anatoly V. Kotikov. "Average gluon and quark jet multiplicities at higher orders". In: *Nucl. Phys.* B875 (2013), pp. 18–44. DOI: 10.1016/j.nuclphysb.2013.06.025. arXiv: 1305.6017 [hep-ph].

[138] Redamy Perez-Ramos and David d'Enterria. "Energy evolution of the moments of the hadron distribution in QCD jets including NNLL resummation and NLO running-coupling corrections". In: *JHEP* 08 (2014), p. 068. DOI: 10.1007/JHEP08(2014)068. arXiv: 1310.8534 [hep-ph].

[139] David d'Enterria and Redamy Pérez-Ramos. "α_s determination at NNLO*+NNLL accuracy from the energy evolution of jet fragmentation functions at low z". In: *Proceedings, 50th Rencontres de Moriond, QCD and high energy interactions: La Thuile, Italy, March 21-28, 2015*. 2015, p. 117. arXiv: 1505.02624 [hep-ph]. URL: http://inspirehep.net/record/1369101/files/arXiv:1505.02624.pdf.

[140] J. V. Guerrero et al. "Hadron mass corrections in semi-inclusive deep-inelastic scattering". In: *JHEP* 09 (2015), p. 169. DOI: 10.1007/JHEP09(2015)169. arXiv: 1505.02739 [hep-ph].

[141] Ekaterina Christova and Elliot Leader. "Problem of kinematic mass corrections for unpolarized semi-inclusive deep inelastic scattering". In: *Phys. Rev.* D94.9 (2016), p. 096001. DOI: 10.1103/PhysRevD.94.096001. arXiv: 1609.05816 [hep-ph].

[142] K. G. Chetyrkin, A. L. Kataev, and F. V. Tkachov. "Higher Order Corrections to Sigma-t (e+ e- —> Hadrons) in Quantum Chromodynamics". In: *Phys. Lett.* B85 (1979), pp. 277–279. DOI: 10.1016/0370-2693(79)90596-3.

[143] Michael Dine and J. R. Sapirstein. "Higher Order QCD Corrections in e+ e- Annihilation". In: *Phys. Rev. Lett.* 43 (1979), p. 668. DOI: 10.1103/PhysRevLett.43.668.

[144] William Celmaster and Richard J. Gonsalves. "An Analytic Calculation of Higher Order Quantum Chromodynamic Corrections in e+ e- Annihilation". In: *Phys. Rev. Lett.* 44 (1980), p. 560. DOI: 10.1103/PhysRevLett.44.560.

[145] S. Moch, J. A. M. Vermaseren, and A. Vogt. "The Longitudinal structure function at the third order". In: *Phys. Lett.* B606 (2005), pp. 123–129. DOI: 10.1016/j.physletb.2004.11.063. arXiv: hep-ph/0411112 [hep-ph].

[146] Wolfram Research. *Mathematica 10*. Champaign, Illinios, 2016.

[147] Maik Höschele et al. "MT: A Mathematica package to compute convolutions". In: *Comput. Phys. Commun.* 185 (2014), pp. 528–539. DOI: 10.1016/j.cpc.2013.10.007. arXiv: 1307.6925 [hep-ph].

[148] D Maitre. "HPL, a mathematica implementation of the harmonic polylogarithms". In: *Comput. Phys. Commun.* 174 (2006), pp. 222–240. DOI: 10.1016/j.cpc.2005.10.008. arXiv: hep-ph/0507152 [hep-ph].

[149] E. Remiddi and J. A. M. Vermaseren. "Harmonic polylogarithms". In: *Int. J. Mod. Phys.* A15 (2000), pp. 725–754. DOI: 10.1142/S0217751X00000367. arXiv: hep-ph/9905237 [hep-ph].

[150] E. G. Floratos, D. A. Ross, and Christopher T. Sachrajda. "Higher Order Effects in Asymptotically Free Gauge Theories: The Anomalous Dimensions of Wilson Operators". In: *Nucl. Phys.* B129 (1977). [Erratum: Nucl. Phys.B139,545(1978)], pp. 66–88. DOI: 10.1016/0550-3213(78)90367-X,10.1016/0550-3213(77)90020-7.

[151] D. A. Ross and Christopher T. Sachrajda. "Flavor Symmetry Breaking in anti-Quark Distributions". In: *Nucl. Phys.* B149 (1979), pp. 497–516. DOI: 10.1016/0550-3213(79)90004-X.

[152] Johannes Blumlein and Stefan Kurth. "Harmonic sums and Mellin transforms up to two loop order". In: *Phys. Rev.* D60 (1999), p. 014018. DOI: 10.1103/PhysRevD.60.014018. arXiv: hep-ph/9810241 [hep-ph].

[153] Johannes Blumlein. "Analytic continuation of Mellin transforms up to two loop order". In: *Comput. Phys. Commun.* 133 (2000), pp. 76–104. DOI: 10.1016/S0010-4655(00)00156-9. arXiv: hep-ph/0003100 [hep-ph].

[154] Johannes Blumlein. "Structural Relations of Harmonic Sums and Mellin Transforms up to Weight w = 5". In: *Comput. Phys. Commun.* 180 (2009), pp. 2218–2249. DOI: 10.1016/j.cpc.2009.07.004. arXiv: 0901.3106 [hep-ph].

[155] S. Moch, J. A. M. Vermaseren, and A. Vogt. "The Three loop splitting functions in QCD: The Nonsinglet case". In: *Nucl. Phys.* B688 (2004), pp. 101–134. DOI: 10.1016/j.nuclphysb.2004.03.030. arXiv: hep-ph/0403192 [hep-ph].

[156] Oleksandr Gituliar and Sven Moch. "Towards three-loop QCD corrections to the time-like splitting functions". In: *Acta Phys. Polon.* B46.7 (2015), pp. 1279–1289. DOI: 10.5506/APhysPolB.46.1279. arXiv: 1505.02901 [hep-ph].

[157] A. Vogt. "Efficient evolution of unpolarized and polarized parton distributions with QCD-PEGASUS". In: *Comput. Phys. Commun.* 170 (2005), pp. 65–92. DOI: 10.1016/j.cpc.2005.03.103. arXiv: hep-ph/0408244 [hep-ph].

[158] Stefano Catani et al. "Perturbative generation of a strange-quark asymmetry in the nucleon". In: *Phys. Rev. Lett.* 93 (2004), p. 152003. DOI: 10.1103/PhysRevLett.93.152003. arXiv: hep-ph/0404240 [hep-ph].

[159] O. V. Tarasov, A. A. Vladimirov, and A. Yu. Zharkov. "The Gell-Mann-Low Function of QCD in the Three Loop Approximation". In: *Phys. Lett.* B93 (1980), pp. 429–432. DOI: 10.1016/0370-2693(80)90358-5.

[160] S. A. Larin and J. A. M. Vermaseren. "The Three loop QCD Beta function and anomalous dimensions". In: *Phys. Lett.* B303 (1993), pp. 334–336. DOI: 10.1016/0370-2693(93)91441-O. arXiv: hep-ph/9302208 [hep-ph].

[161] M. Buza et al. "Charm electroproduction viewed in the variable flavor number scheme versus fixed order perturbation theory". In: *Eur. Phys. J.* C1 (1998), pp. 301–320. DOI: 10.1007/BF01245820. arXiv: hep-ph/9612398 [hep-ph].

[162] S. A. Larin, T. van Ritbergen, and J. A. M. Vermaseren. "The Large quark mass expansion of Gamma (Z0 —> hadrons) and Gamma (tau- —> tau-neutrino + hadrons) in the order alpha-s**3". In: *Nucl. Phys.* B438 (1995), pp. 278–306. DOI: 10.1016/0550-3213(94)00574-X. arXiv: hep-ph/9411260 [hep-ph].

[163] K. G. Chetyrkin, Bernd A. Kniehl, and M. Steinhauser. "Strong coupling constant with flavor thresholds at four loops in the MS scheme". In: *Phys. Rev. Lett.* 79 (1997), pp. 2184–2187. DOI: 10.1103/PhysRevLett.79.2184. arXiv: hep-ph/9706430 [hep-ph].

[164] Matteo Cacciari, Paolo Nason, and Carlo Oleari. "Crossing heavy-flavor thresholds in fragmentation functions". In: *JHEP* 10 (2005), p. 034. DOI: 10.1088/1126-6708/2005/10/034. arXiv: hep-ph/0504192 [hep-ph].

[165] L. N. Lipatov. "Small x physics in perturbative QCD". In: *Phys. Rept.* 286 (1997), pp. 131–198. DOI: 10.1016/S0370-1573(96)00045-2. arXiv: hep-ph/9610276 [hep-ph].

[166] Milton Abramowitz and Irene A. Stegun. *Handbook of Mathematical Functions, With Formulas, Graphs, and Mathematical Tables*. ninth Dover printing, tenth GPO printing. Dover Publications, Incorporated, 1974. ISBN: 0486612724.

[167] Johannes Blumlein and Andreas Vogt. "The Evolution of unpolarized singlet structure functions at small x". In: *Phys. Rev.* D58 (1998), p. 014020. DOI: 10.1103/PhysRevD.58.014020. arXiv: hep-ph/9712546 [hep-ph].

[168] J. Blumlein, V. Ravindran, and W. L. van Neerven. "On the Drell-Levy-Yan relation to O(alpha(s)**2)". In: *Nucl. Phys.* B586 (2000), pp. 349–381. DOI: 10.1016/S0550-3213(00)00422-3. arXiv: hep-ph/0004172 [hep-ph].

[169] W. L. van Neerven and A. Vogt. "NNLO evolution of deep inelastic structure functions: The Singlet case". In: *Nucl. Phys.* B588 (2000), pp. 345–373. DOI: 10.1016/S0550-3213(00)00480-6. arXiv: hep-ph/0006154 [hep-ph].

[170] S. Moch, J. A. M. Vermaseren, and A. Vogt. "The Quark form-factor at higher orders". In: *JHEP* 08 (2005), p. 049. DOI: 10.1088/1126-6708/2005/08/049. arXiv: hep-ph/0507039 [hep-ph].

[171] J. B. Gaffney and Alfred H. Mueller. "Alpha (Q**2) Corrections to Particle Multiplicity Ratios in Gluon and Quark Jets". In: *Nucl. Phys.* B250 (1985), pp. 109–142. DOI: 10.1016/0550-3213(85)90476-6.

[172] S. Albino et al. "Timelike Single-logarithm-resummed Splitting Functions". In: *Nucl. Phys.* B855 (2012), pp. 801–814. DOI: 10.1016/j.nuclphysb.2011.10.030. arXiv: 1108.3948 [hep-ph].

[173] L. A. Harland-Lang et al. "Parton distributions in the LHC era: MMHT 2014 PDFs". In: *Eur. Phys. J.* C75.5 (2015), p. 204. DOI: 10.1140/epjc/s10052-015-3397-6. arXiv: 1412.3989 [hep-ph].

[174] M. Epele, C. A. Garcia Canal, and R. Sassot. "Role of heavy quarks in light hadron fragmentation". In: *Phys. Rev.* D94.3 (2016), p. 034037. DOI: 10.1103/PhysRevD.94.034037. arXiv: 1604.08427 [hep-ph].

[175] P. Jimenez-Delgado, W. Melnitchouk, and J. F. Owens. "Parton momentum and helicity distributions in the nucleon". In: *J. Phys.* G40 (2013), p. 093102. DOI: 10.1088/0954-3899/40/9/093102. arXiv: 1306.6515 [hep-ph].

[176] Stefano Forte and Graeme Watt. "Progress in the Determination of the Partonic Structure of the Proton". In: *Ann. Rev. Nucl. Part. Sci.* 63 (2013), pp. 291–328. DOI: 10.1146/annurev-nucl-102212-170607. arXiv: 1301.6754 [hep-ph].

[177] Simon Albino. "The Hadronization of partons". In: *Rev. Mod. Phys.* 82 (2010), pp. 2489–2556. DOI: 10.1103/RevModPhys.82.2489. arXiv: 0810.4255 [hep-ph].

[178] A. D. Martin et al. "Parton distributions for the LHC". In: *Eur. Phys. J.* C63 (2009), pp. 189–285. DOI: 10.1140/epjc/s10052-009-1072-5. arXiv: 0901.0002 [hep-ph].

[179] J. F. Owens, A. Accardi, and W. Melnitchouk. "Global parton distributions with nuclear and finite-Q^2 corrections". In: *Phys. Rev.* D87.9 (2013), p. 094012. DOI: 10.1103/PhysRevD.87.094012. arXiv: 1212.1702 [hep-ph].

[180] Hung-Liang Lai et al. "New parton distributions for collider physics". In: *Phys. Rev.* D82 (2010), p. 074024. DOI: 10.1103/PhysRevD.82.074024. arXiv: 1007.2241 [hep-ph].

[181] Richard D. Ball et al. "Parton distributions for the LHC Run II". In: *JHEP* 04 (2015), p. 040. DOI: 10.1007/JHEP04(2015)040. arXiv: 1410.8849 [hep-ph].

[182] Alberto Accardi. "Large-x connections of nuclear and high-energy physics". In: *Mod. Phys. Lett.* A28.35 (2013), p. 1330032. DOI: 10.1142/S0217732313300322. arXiv: 1308.2906 [hep-ph].

[183] Serguei Chatrchyan et al. "Measurements of differential jet cross sections in proton-proton collisions at $\sqrt{s} = 7$ TeV with the CMS detector". In: *Phys. Rev.* D87.11 (2013). [Erratum: Phys. Rev.D87,no.11,119902(2013)], p. 112002. DOI: 10.1103/PhysRevD.87.112002,10.1103/PhysRevD.87.119902. arXiv: 1212.6660 [hep-ex].

[184] Georges Aad et al. "Measurement of inclusive jet and dijet production in pp collisions at $\sqrt{s} = 7$ TeV using the ATLAS detector". In: *Phys. Rev.* D86 (2012), p. 014022. DOI: 10.1103/PhysRevD.86.014022. arXiv: 1112.6297 [hep-ex].

[185] Roy J. Holt and Craig D. Roberts. "Distribution Functions of the Nucleon and Pion in the Valence Region". In: *Rev. Mod. Phys.* 82 (2010), pp. 2991–3044. DOI: 10.1103/RevModPhys.82.2991. arXiv: 1002.4666 [nucl-th].

[186] A. Courtoy. "Phenomenology of hadron structure — why low energy physics matters". In: *J. Phys. Conf. Ser.* 651 (2015), p. 012007. DOI: 10.1088/1742-6596/651/1/012007. arXiv: 1405.6567 [hep-ph].

[187] Jozef Dudek et al. "Physics Opportunities with the 12 GeV Upgrade at Jefferson Lab". In: *Eur. Phys. J.* A48 (2012), p. 187. DOI: 10.1140/epja/i2012-12187-1. arXiv: 1208.1244 [hep-ex].

[188] S. Alekhin, J. Blumlein, and S. Moch. "Parton Distribution Functions and Benchmark Cross Sections at NNLO". In: *Phys. Rev.* D86 (2012), p. 054009. DOI: 10.1103/PhysRevD.86.054009. arXiv: 1202.2281 [hep-ph].

[189] George F. Sterman and Werner Vogelsang. "Soft gluon resummation and PDF theory uncertainties". In: *QCD and weak boson physics in Run II. Proceedings, Batavia, USA, March 4-6, June 3-4, November 4-6, 1999*. 2000. arXiv: hep-ph/0002132 [hep-ph]. URL: http://alice.cern.ch/format/showfull?sysnb=2175873.

[190] A. D. Martin et al. "Uncertainties of predictions from parton distributions. 2. Theoretical errors". In: *Eur. Phys. J.* C35 (2004), pp. 325–348. DOI: 10.1140/epjc/s2004-01825-2. arXiv: hep-ph/0308087 [hep-ph].

[191] Nobuo Sato. "Threshold Resummation in Direct Photon Production". PhD thesis. Florida State University, 2014.

[192] Alberto Accardi and Jian-Wei Qiu. "Collinear factorization for deep inelastic scattering structure functions at large Bjorken x(B)". In: *JHEP* 07 (2008), p. 090. DOI: 10.1088/1126-6708/2008/07/090. arXiv: 0805.1496 [hep-ph].

[193] Howard Georgi and H. David Politzer. "Freedom at Moderate Energies: Masses in Color Dynamics". In: *Phys. Rev.* D14 (1976), p. 1829. DOI: 10.1103/PhysRevD.14.1829.

[194] Ingo Schienbein et al. "A Review of Target Mass Corrections". In: *J. Phys.* G35 (2008), p. 053101. DOI: 10.1088/0954-3899/35/5/053101. arXiv: 0709.1775 [hep-ph].

[195] S. Albino, B. A. Kniehl, and G. Kramer. "AKK Update: Improvements from New Theoretical Input and Experimental Data". In: *Nucl. Phys.* B803 (2008), pp. 42–104. DOI: 10.1016/j.nuclphysb.2008.05.017. arXiv: 0803.2768 [hep-ph].

[196] M. Soleymaninia et al. "Determination of pion and kaon fragmentation functions including spin asymmetries data in a global analysis". In: *Phys. Rev.* D88.5 (2013). [Addendum: Phys. Rev.D89,no.3,039901(2014)], p. 054019. DOI: 10.1103/PhysRevD.88.054019,10.1103/PhysRevD.89.039901. arXiv: 1306.1612 [hep-ph].

[197] S. Albino et al. "Resummation of soft gluon logarithms in the DGLAP evolution of fragmentation functions". In: *Phys. Rev.* D73 (2006), p. 054020. DOI: 10.1103/PhysRevD.73.054020. arXiv: hep-ph/0510319 [hep-ph].

[198] A. Accardi, T. Hobbs, and W. Melnitchouk. "Hadron mass corrections in semi-inclusive deep inelastic scattering". In: *JHEP* 11 (2009), p. 084. DOI: 10.1088/1126-6708/2009/11/084. arXiv: 0907.2395 [hep-ph].

[199] George F. Sterman and Werner Vogelsang. "Crossed Threshold Resummation". In: *Phys. Rev.* D74 (2006), p. 114002. DOI: 10.1103/PhysRevD.74.114002. arXiv: hep-ph/0606211 [hep-ph].

[200] Otto Nachtmann. "Positivity constraints for anomalous dimensions". In: *Nucl. Phys.* B63 (1973), pp. 237–247. DOI: 10.1016/0550-3213(73)90144-2.

[201] Jian-Wei Qiu. "Twist Four Contributions to the Parton Structure Functions". In: *Phys. Rev.* D42 (1990), pp. 30–44. DOI: 10.1103/PhysRevD.42.30.

[202] Edmond L. Berger. "SEMIINCLUSIVE INELASTIC ELECTRON SCATTERING FROM NUCLEI". In: *NPAS WORKSHOP ON ELECTRONUCLEAR PHYSICS WITH INTERNAL TARGETS, SLAC, JANUARY 5-8, 1987*. 1987, pp. 82–91.

[203] P. J. Mulders. "Current fragmentation in semiinclusive leptoproduction". In: *AIP Conf. Proc.* 588 (2001). [,75(2000)], pp. 75–88. DOI: 10.1063/1.1413147. arXiv: hep-ph/0010199 [hep-ph].

[204] L. T. Brady et al. "Next-to leading order analysis of target mass corrections to structure functions and asymmetries". In: *Phys. Rev.* D84 (2011). [Erratum: Phys. Rev.D85,039902(2012)], p. 074008. DOI: 10.1103/PhysRevD.84.074008,10.1103/PhysRevD.85.039902. arXiv: 1108.4734 [hep-ph].

[205] Daniel de Florian and Yamila Rotstein Habarnau. "Polarized semi-inclusive electroweak structure functions at next-to-leading-order". In: *Eur. Phys. J.* C73.3 (2013), p. 2356. DOI: 10.1140/epjc/s10052-013-2356-3. arXiv: 1210.7203 [hep-ph].

[206] S. Kretzer and M. H. Reno. "Target mass corrections to electroweak structure functions and perturbative neutrino cross-sections". In: *Phys. Rev.* D69 (2004), p. 034002. DOI: 10.1103/PhysRevD.69.034002. arXiv: hep-ph/0307023 [hep-ph].

[207] M. A. G. Aivazis, Frederick I. Olness, and Wu-Ki Tung. "Leptoproduction of heavy quarks. 1. General formalism and kinematics of charged current and neutral current production processes". In: *Phys. Rev.* D50 (1994), pp. 3085–3101. DOI: 10.1103/PhysRevD.50.3085. arXiv: hep-ph/9312318 [hep-ph].

[208] A. Vogt. "Next-to-next-to-leading logarithmic threshold resummation for deep inelastic scattering and the Drell-Yan process". In: *Phys. Lett.* B497 (2001), pp. 228–234. DOI: 10.1016/S0370-2693(00)01344-7. arXiv: hep-ph/0010146 [hep-ph].

[209] E. Gardi and R. G. Roberts. "The Interplay between Sudakov resummation, renormalons and higher twist in deep inelastic scattering". In: *Nucl. Phys.* B653 (2003), pp. 227–255. DOI: 10.1016/S0550-3213(03)00035-X. arXiv: hep-ph/0210429 [hep-ph].

[210] Gennaro Corcella and Lorenzo Magnea. "Soft-gluon resummation effects on parton distributions". In: *Phys. Rev.* D72 (2005), p. 074017. DOI: 10.1103/PhysRevD.72.074017. arXiv: hep-ph/0506278 [hep-ph].

[211] Georges Grunberg. "Large-x structure of physical evolution kernels in Deep Inelastic Scattering". In: *Phys. Lett.* B687 (2010), pp. 405–409. DOI: 10.1016/j.physletb.2010.03.036. arXiv: 0911.4471 [hep-ph].

[212] S. Schaefer, A. Schafer, and M. Stratmann. "Impact of higher order and soft gluon corrections on the extraction of higher twist effects in DIS". In: *Phys. Lett.* B514 (2001), pp. 284–292. DOI: 10.1016/S0370-2693(01)00809-7. arXiv: hep-ph/0105174 [hep-ph].

[213] Stefano Catani et al. "The Resummation of soft gluons in hadronic collisions". In: *Nucl. Phys.* B478 (1996), pp. 273–310. DOI: 10.1016/0550-3213(96)00399-9. arXiv: hep-ph/9604351 [hep-ph].

[214] N. Michel and M.V. Stoitsov. "Fast computation of the Gauss hypergeometric function with all its parameters complex with application to the Pöschl–Teller–Ginocchio potential wave functions". In: *Computer Physics Communications* 178.7 (2008), pp. 535–551. ISSN: 0010-4655. DOI: http://doi.org/10.1016/j.cpc.2007.11.007. URL: http://www.sciencedirect.com/science/article/pii/S0010465507004699.

[215] Y. Liang et al. "Measurement of R = sigma(L) / sigma(T) and the separated longitudinal and transverse structure functions in the nucleon resonance region". In: (2004). arXiv: nucl-ex/0410027 [nucl-ex].

[216] S. P. Malace et al. "Applications of quark-hadron duality in F(2) structure function". In: *Phys. Rev.* C80 (2009), p. 035207. DOI: 10.1103/PhysRevC.80.035207. arXiv: 0905.2374 [nucl-ex].

[217] F. D. Aaron et al. "Combined Measurement and QCD Analysis of the Inclusive e+-p Scattering Cross Sections at HERA". In: *JHEP* 01 (2010), p. 109. DOI: 10.1007/JHEP01(2010)109. arXiv: 0911.0884 [hep-ex].

[218] L. W. Whitlow et al. "Precise measurements of the proton and deuteron structure functions from a global analysis of the SLAC deep inelastic electron scattering cross-sections". In: *Phys. Lett.* B282 (1992), pp. 475–482. DOI: 10.1016/0370-2693(92)90672-Q.

[219] J. J. Aubert et al. "A Detailed Study of the Proton Structure Functions in Deep Inelastic Muon - Proton Scattering". In: *Nucl. Phys.* B259 (1985), p. 189. DOI: 10.1016/0550-3213(85)90635-2.

[220] A. Accardi et al. "New parton distributions from large-x and low-Q^2 data". In: *Phys. Rev.* D81 (2010), p. 034016. DOI: 10.1103/PhysRevD.81.034016. arXiv: 0911.2254 [hep-ph].

[221] P. Monaghan et al. "Moments of the longitudinal proton structure function F_L from global data in the Q^2 range 0.75-45.0 $(\mathrm{GeV}/c)^2$". In: *Phys. Rev. Lett.* 110.15 (2013), p. 152002. DOI: 10.1103/PhysRevLett.110.152002. arXiv: 1209.4542 [nucl-ex].

[222] W. Melnitchouk, R. Ent, and C. Keppel. "Quark-hadron duality in electron scattering". In: *Phys. Rept.* 406 (2005), pp. 127–301. DOI: 10.1016/j.physrep.2004.10.004. arXiv: hep-ph/0501217 [hep-ph].

[223] Johannes Blumlein and Avtandil Tkabladze. "Target mass corrections for polarized structure functions and new sum rules". In: *Nucl. Phys.* B553 (1999), pp. 427–464. DOI: 10.1016/S0550-3213(99)00289-8. arXiv: hep-ph/9812478 [hep-ph].

[224] M. E. Christy, J. Blumlein, and H. Bottcher. "Unfolding of target mass contributions from inclusive proton structure function data". In: (2012). arXiv: 1201.0576 [hep-ph].

[225] Sergey Alekhin et al. "The new ABMP16 PDF". In: (2016). arXiv: 1609.03327 [hep-ph].

[226] A. Accardi et al. "Constraints on large-x parton distributions from new weak boson production and deep-inelastic scattering data". In: *Phys. Rev.* D93.11 (2016), p. 114017. DOI: 10.1103/PhysRevD.93.114017. arXiv: 1602.03154 [hep-ph].

[227] Pedro Jimenez-Delgado and Ewald Reya. "Delineating parton distributions and the strong coupling". In: *Phys. Rev.* D89.7 (2014), p. 074049. DOI: 10.1103/PhysRevD.89.074049. arXiv: 1403.1852 [hep-ph].

[228] Daniel de Florian et al. "Evidence for polarization of gluons in the proton". In: *Phys. Rev. Lett.* 113.1 (2014), p. 012001. DOI: 10.1103/PhysRevLett.113.012001. arXiv: 1404.4293 [hep-ph].

[229] W. L. van Neerven and E. B. Zijlstra. "Order alpha-s**2 contributions to the deep inelastic Wilson coefficient". In: *Phys. Lett.* B272 (1991), pp. 127–133. DOI: 10.1016/0370-2693(91)91024-P.

[230] E. B. Zijlstra and W. L. van Neerven. "Order alpha-s**2 QCD corrections to the deep inelastic proton structure functions F2 and F(L)". In: *Nucl. Phys.* B383 (1992), pp. 525–574. DOI: 10.1016/0550-3213(92)90087-R.

[231] S. Moch and J. A. M. Vermaseren. "Deep inelastic structure functions at two loops". In: *Nucl. Phys.* B573 (2000), pp. 853–907. DOI: 10.1016/S0550-3213(00)00045-6. arXiv: hep-ph/9912355 [hep-ph].

[232] E. B. Zijlstra and W. L. van Neerven. "Order-α_s^2 corrections to the polarized structure function $g_1(x, Q^2)$". In: *Nucl. Phys.* B417 (1994). [Erratum: Nucl. Phys.B501,599(1997)], pp. 61–100. DOI: 10.1016/0550-3213(94)90538-X,10.1016/0550-3213(94)90135-X,10.1016/S0550-3213(97)00389-1,10.1016/j.nuclphysb.2007.03.002.

[233] J. A. M. Vermaseren, A. Vogt, and S. Moch. "The Third-order QCD corrections to deep-inelastic scattering by photon exchange". In: *Nucl. Phys.* B724 (2005), pp. 3–182. DOI: 10.1016/j.nuclphysb.2005.06.020. arXiv: hep-ph/0504242 [hep-ph].

[234] M. G. Alekseev et al. "Quark helicity distributions from longitudinal spin asymmetries in muon-proton and muon-deuteron scattering". In: *Phys. Lett.* B693 (2010), pp. 227–235. DOI: 10.1016/j.physletb.2010.08.034. arXiv: 1007.4061 [hep-ex].

[235] A. Daleo, C. A. Garcia Canal, and R. Sassot. "Order alpha(s)**2 corrections to one particle inclusive processes in DIS". In: *Nucl. Phys.* B662 (2003), pp. 334–358. DOI: 10.1016/S0550-3213(03)00334-1. arXiv: hep-ph/0303199 [hep-ph].

[236] A. Daleo and R. Sassot. "Next-to-leading order evolution of SIDIS processes in the forward region". In: *Nucl. Phys.* B673 (2003), pp. 357–384. DOI: 10.1016/j.nuclphysb.2003.09.007. arXiv: hep-ph/0309073 [hep-ph].

[237] J. Levelt and P. J. Mulders. "Quark correlation functions in deep inelastic semiinclusive processes". In: *Phys. Rev.* D49 (1994), pp. 96–113. DOI: 10.1103/PhysRevD.49.96. arXiv: hep-ph/9304232 [hep-ph].

[238] Curtis G. Callan Jr. and David J. Gross. "High-energy electroproduction and the constitution of the electric current". In: *Phys. Rev. Lett.* 22 (1969), pp. 156–159. DOI: 10.1103/PhysRevLett.22.156.

[239] A. Daleo, D. de Florian, and R. Sassot. "O(alpha**2(s)) QCD corrections to the electroproduction of hadrons with high transverse momentum". In: *Phys. Rev.* D71 (2005), p. 034013. DOI: 10.1103/PhysRevD.71.034013. arXiv: hep-ph/0411212 [hep-ph].

[240] C. G. Bollini and J. J. Giambiagi. "Dimensional Renormalization: The Number of Dimensions as a Regularizing Parameter". In: *Nuovo Cim.* B12 (1972), pp. 20–26. DOI: 10.1007/BF02895558.

[241] Gerard 't Hooft and M. J. G. Veltman. "Regularization and Renormalization of Gauge Fields". In: *Nucl. Phys.* B44 (1972), pp. 189–213. DOI: 10.1016/0550-3213(72)90279-9.

[242] R. Mertig, M. Bohm, and Ansgar Denner. "FEYN CALC: Computer algebraic calculation of Feynman amplitudes". In: *Comput. Phys. Commun.* 64 (1991), pp. 345–359. DOI: 10.1016/0010-4655(91)90130-D.

[243] Thomas Hahn. "Generating Feynman diagrams and amplitudes with FeynArts 3". In: *Comput. Phys. Commun.* 140 (2001), pp. 418–431. DOI: 10.1016/S0010-4655(01)00290-9. arXiv: hep-ph/0012260 [hep-ph].

[244] W. Beenakker et al. "QCD Corrections to Heavy Quark Production in p anti-p Collisions". In: *Phys. Rev.* D40 (1989), pp. 54–82. DOI: 10.1103/PhysRevD.40.54.

[245] T. Matsuura, S. C. van der Marck, and W. L. van Neerven. "The Calculation of the Second Order Soft and Virtual Contributions to the Drell-Yan Cross-Section". In: *Nucl. Phys.* B319 (1989), pp. 570–622. DOI: 10.1016/0550-3213(89)90620-2.

[246] Leonid L. Frankfurt et al. "The Valence and Strange Sea Quark Spin Distributions in the Nucleon From Semiinclusive Deep Inelastic Lepton Scattering". In: *Phys. Lett.* B230 (1989), pp. 141–148. DOI: 10.1016/0370-2693(89)91668-7.

[247] A. Airapetian et al. "Quark helicity distributions in the nucleon for up, down, and strange quarks from semi-inclusive deep-inelastic scattering". In: *Phys. Rev.* D71 (2005), p. 012003. DOI: 10.1103/PhysRevD.71.012003. arXiv: hep-ex/0407032 [hep-ex].

[248] A. Airapetian et al. "Precise determination of the spin structure function g(1) of the proton, deuteron and neutron". In: *Phys. Rev.* D75 (2007), p. 012007. DOI: 10.1103/PhysRevD.75.012007. arXiv: hep-ex/0609039 [hep-ex].

[249] M. G. Alekseev et al. "The Spin-dependent Structure Function of the Proton g_1^p and a Test of the Bjorken Sum Rule". In: *Phys. Lett.* B690 (2010), pp. 466–472. DOI: 10.1016/j.physletb.2010.05.069. arXiv: 1001.4654 [hep-ex].

[250] X. Zheng et al. "Precision measurement of the neutron spin asymmetry A1**N and spin flavor decomposition in the valence quark region". In: *Phys. Rev. Lett.* 92 (2004), p. 012004. DOI: 10.1103/PhysRevLett.92.012004. arXiv: nucl-ex/0308011 [nucl-ex].

[251] X. Zheng et al. "Precision measurement of the neutron spin asymmetries and spin-dependent structure functions in the valence quark region". In: *Phys. Rev.* C70 (2004), p. 065207. DOI: 10.1103/PhysRevC.70.065207. arXiv: nucl-ex/0405006 [nucl-ex].

[252] K. V. Dharmawardane et al. "Measurement of the x- and Q**2-dependence of the asymmetry A(1) on the nucleon". In: *Phys. Lett.* B641 (2006), pp. 11–17. DOI: 10.1016/j.physletb.2006.08.011. arXiv: nucl-ex/0605028 [nucl-ex].

[253] M. Burkardt, C. A. Miller, and W. D. Nowak. "Spin-polarized high-energy scattering of charged leptons on nucleons". In: *Rept. Prog. Phys.* 73 (2010), p. 016201. DOI: 10.1088/0034-4885/73/1/016201. arXiv: 0812.2208 [hep-ph].

[254] Daniel de Florian et al. "Global Analysis of Helicity Parton Densities and Their Uncertainties". In: *Phys. Rev. Lett.* 101 (2008), p. 072001. DOI: 10.1103/PhysRevLett.101.072001. arXiv: 0804.0422 [hep-ph].

[255] Daniel de Florian et al. "Extraction of Spin-Dependent Parton Densities and Their Uncertainties". In: *Phys. Rev.* D80 (2009), p. 034030. DOI: 10.1103/PhysRevD.80.034030. arXiv: 0904.3821 [hep-ph].

[256] D. de Florian et al. "Global analysis of helicity PDFs: Past - present - future". In: (2011). arXiv: 1108.3955 [hep-ph].

[257] Elliot Leader, Aleksander V. Sidorov, and Dimiter B. Stamenov. "Determination of Polarized PDFs from a QCD Analysis of Inclusive and Semi-inclusive Deep Inelastic Scattering Data". In: *Phys. Rev.* D82 (2010), p. 114018. DOI: 10.1103/PhysRevD.82.114018. arXiv: 1010.0574 [hep-ph].

[258] Volker D. Burkert. "The JLab 12 GeV upgrade and the initial science program - Selected topics". In: *Proc. Int. Sch. Phys. Fermi* 180 (2012), pp. 303–332. DOI: 10.3254/978-1-61499-197-7-303. arXiv: 1203.2373 [nucl-ex].

[259] S. Simula et al. "Leading and higher twists in the proton polarized structure function g**p(1) at large Bjorken x". In: *Phys. Rev.* D65 (2002), p. 034017. DOI: 10.1103/PhysRevD.65.034017. arXiv: hep-ph/0107036 [hep-ph].

[260] M. Osipenko et al. "Global analysis of data on the proton structure function g(1) and extraction of its moments". In: *Phys. Rev.* D71 (2005), p. 054007. DOI: 10.1103/PhysRevD.71.054007. arXiv: hep-ph/0503018 [hep-ph].

[261] M. Gluck et al. "Next-to-leading order radiative parton model analysis of polarized deep inelastic lepton - nucleon scattering". In: *Phys. Rev.* D53 (1996), pp. 4775–4786. DOI: 10.1103/PhysRevD.53.4775. arXiv: hep-ph/9508347 [hep-ph].

[262] Marco Stratmann and Werner Vogelsang. "Towards a global analysis of polarized parton distributions". In: *Phys. Rev.* D64 (2001), p. 114007. DOI: 10.1103/PhysRevD.64.114007. arXiv: hep-ph/0107064 [hep-ph].

[263] Stefano Catani, Michelangelo L. Mangano, and Paolo Nason. "Sudakov resummation for prompt photon production in hadron collisions". In: *JHEP* 07 (1998), p. 024. DOI: 10.1088/1126-6708/1998/07/024. arXiv: hep-ph/9806484 [hep-ph].

[264] A. D. Martin et al. "Uncertainties of predictions from parton distributions. 1: Experimental errors". In: *Eur. Phys. J.* C28 (2003), pp. 455–473. DOI: 10.1140/epjc/s2003-01196-2. arXiv: hep-ph/0211080 [hep-ph].

[265] Elke C. Aschenauer, Rodolfo Sassot, and Marco Stratmann. "Helicity Parton Distributions at a Future Electron-Ion Collider: A Quantitative Appraisal". In: *Phys. Rev.* D86 (2012), p. 054020. DOI: 10.1103/PhysRevD.86.054020. arXiv: 1206.6014 [hep-ph].

[266] Elliot Leader, Aleksander V. Sidorov, and Dimiter B. Stamenov. "Impact of CLAS and COMPASS data on Polarized Parton Densities and Higher Twist". In: *Phys. Rev.* D75 (2007), p. 074027. DOI: 10.1103/PhysRevD.75.074027. arXiv: hep-ph/0612360 [hep-ph].

[267] Elliot Leader, Aleksander V. Sidorov, and Dimiter B. Stamenov. "Some Remarks on Methods of QCD Analysis of Polarized DIS Data". In: *Phys. Rev.* D80 (2009), p. 054026. DOI: 10.1103/PhysRevD.80.054026. arXiv: 0908.2390 [hep-ph].

[268] Johannes Blumlein and Helmut Bottcher. "QCD Analysis of Polarized Deep Inelastic Scattering Data". In: *Nucl. Phys.* B841 (2010), pp. 205–230. DOI: 10.1016/j.nuclphysb.2010.08.005. arXiv: 1005.3113 [hep-ph].

[269] A. Accardi and W. Melnitchouk. "Target mass corrections for spin-dependent structure functions in collinear factorization". In: *Phys. Lett.* B670 (2008), pp. 114–118. DOI: 10.1016/j.physletb.2008.10.036. arXiv: 0808.2397 [hep-ph].

[270] Harut Avakian et al. "Effect of Orbital Angular Momentum on Valence-Quark Helicity Distributions". In: *Phys. Rev. Lett.* 99 (2007), p. 082001. DOI: 10.1103/PhysRevLett.99.082001. arXiv: 0705.1553 [hep-ph].

[271] Michael E. Peskin and Daniel V. Schroeder. *An Introduction to quantum field theory.* Perseus Books, 1995.

[272] Antonio Pich. "The Standard Model of Electroweak Interactions". In: *ArXiv:1201.0537* (2012). arXiv: 1201.0537 [hep-ph].

[273] R.Gilmore. *Lie groups, Lie algebras, and Some of Their Application*. New York, US: Wiley Interscience, 1974.